

# **From DNA-Guided Chromophore Arrays to Light-Harvesting Polymers**

Inauguraldissertation  
der Philosophisch-naturwissenschaftlichen Fakultät  
der Universität Bern

vorgelegt von  
Christian Bernhard Winiger  
von Jona (SG)

Leiter der Arbeit  
Prof. Dr. R. Häner  
Departement Chemie und Biochemie der Universität Bern

# From DNA-Guided Chromophore Arrays to Light-Harvesting Polymers

Inauguraldissertation  
der Philosophisch-naturwissenschaftlichen Fakultät  
der Universität Bern

vorgelegt von  
Christian Bernhard Winiger  
von Jona (SG)

Leiter der Arbeit  
Prof. Dr. R. Häner  
Departement Chemie und Biochemie der Universität Bern

von der Philosophisch-naturwissenschaftlichen Fakultät angenommen

Bern, November 2014

der Dekan

## **I. Acknowledgment**

I would like to thank Prof. Dr. R. Häner for giving me the opportunity to do my PhD Thesis in his laboratory. The research group of Professor Häner, the Department of Chemistry and Biochemistry and the University of Bern provided a stimulating atmosphere for the development of my scientific and personal skills. I like to thank Prof. Dr. J. Hall and Prof. Dr. J.-L. Reymond for the appraisal of this thesis.

I especially thank Dr. Simon Langenegger for helpful and inspiring discussions! Many thanks to the current and past members of the Häner-research group for help and fun. I would like to thank Prof. Dr. G. Calzaferri for his wonderful work and help with the interpretation of the spectroscopic data and calculations.

The supporting services in-house (Ausgabe, facility management, MS-team, NMR-team and crystallography-team) and financial support of the Swiss National Science Foundation (SNF) and the University of Bern are gratefully acknowledged.

My special thanks go to my family! Thank you very much for supporting me during all the years of my education!



to my parents



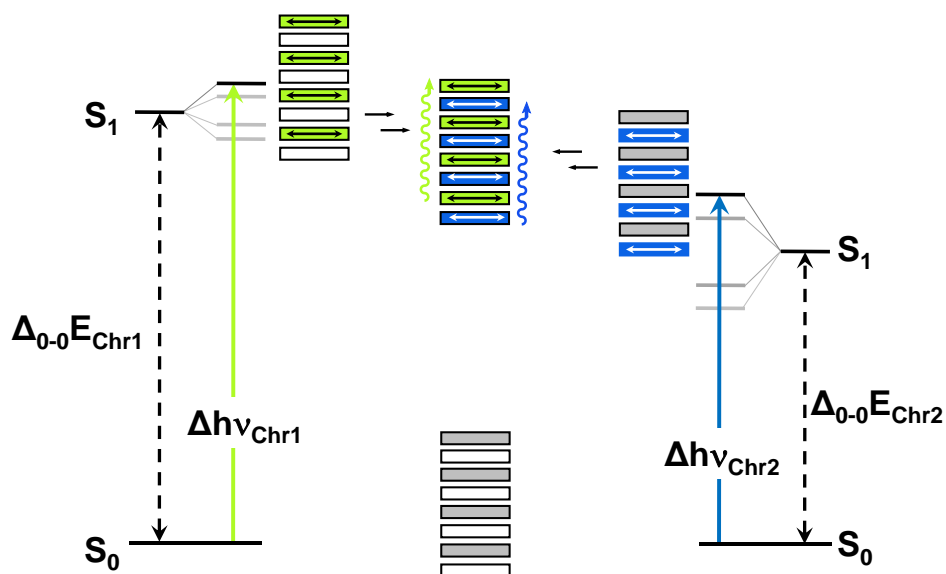
## II. Summary

The thesis is divided into four chapters. Chapters 1 and 2 focus on DNA guided chromophore arrays, chapter 3 and 4 highlight aspects of self-assembled chromophores which are linked by a flexible phosphate backbone.

In chapter 1, DNA guided arrays of a total of eight pyrene (electron rich aromatic molecule) or perylene-3,4,9,10-tetracarboxylic diimide (PDI, electron poor aromatic molecule) were realized. Upon designing systems with increasing numbers of pyrene-PDI interactions, it was found that each of these aromatic donor-acceptor interactions accounts for a stabilization of up to 7.4 °C per interaction. Different pyrene-PDI systems were probed and regularities for stability governed by the selective interaction of different chromophores were extracted. The data highlight the importance of the geometry of the building blocks and the sequential arrangement of the pyrenes and PDIs, which limits the generation of supramolecular arrangements with predictable stability from scratch.

Chapter 2 focuses on spectroscopic characteristics of aromatic chromophores (pyrene and PDI) in well-defined  $\pi$ -stacks. The formation of homo- and hetero aggregates of chromophores could both be well realized using DNA as guiding supramolecular polymer.

Both types of aggregates were found to show distinct H-aggregate character, indicating a strong coupling of identical chromophores with the respective nearest neighbour but most surprisingly also the next-nearest neighbour. Thus, alternating pyrene-PDI  $\pi$ -arrays were designed which exhibit two co-existing excitons at different energy levels in one and the same chromophore stack (Scheme II.1).



**Scheme II.1** Formation of alternating stacks of two different chromophores (green and blue, abbreviated as Chr1 and Chr2) show two co-existing excitons in one and the same chromophore stack at two different energy levels.

The work described in the first two chapters demonstrates plainly the power of DNA guided chromophore assembly. The formation of well-defined  $\pi$ -stacks of aromatic chromophores allows the study of characteristics and properties thereof which cannot be observed in the individual (monomeric) or randomly aggregated molecule.

In chapter 3, short oligoarenotides (3,6-dialkynylphenanthrene) which are linked by phosphodiester bonds are described. These short oligomers self-assemble to form long ( $\gg 1 \mu\text{m}$ ) linear 1-D polymers. The single aromatic compounds (phenanthrene, donor) assemble in a hydrophobicity driven face-to-face arrangement to yield long excitable  $\pi$ -arrays.

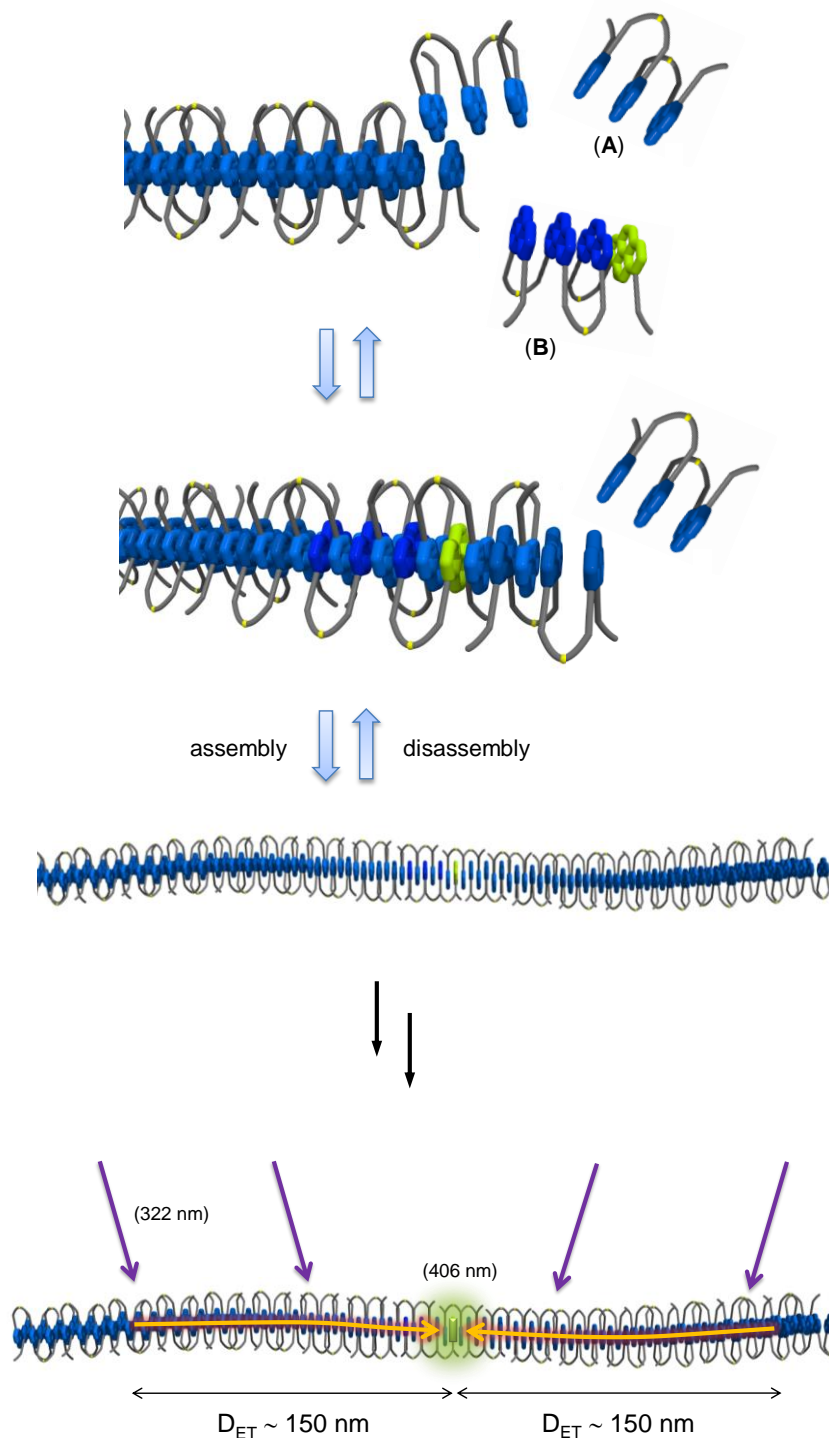
Doping of the polymers with minute amounts acceptor dialkynylpyrene results in very high pyrene fluorescence upon excitation of the donor-molecule – thus forming efficient water soluble light harvesting polymers. At higher pyrene contents ( $> 1\%$ ) the fluorescence quantum yield of the light harvesting polymers approximates the one of the monomeric pyrene building block ( $\phi_f^{Py} = 0.55$ ).

Most interestingly is that the quantum yield in arranged systems containing dialkynylphenanthrene and dialkynylpyrene is by far higher than the weighted sum of its individual components. Model considerations indicate that the energy is transferred in the polymer antenna with high efficiency over an average distance of approximately 150 nm (Scheme II.2). Quantum coherence mechanisms need to be considered to explain such an efficient long distance EET.

This work is an outstanding example to show the perennial issue in supramolecular chemistry: the design of well-arranged molecular systems - as only properly aligned molecules can fulfil outstanding tasks like the collection and the transfer of energy!

Chapter 4 describes the discovery of novel water soluble PDI J-aggregates. Six PDI molecules which are linked by phosphodiester bonds and are modified with short DNA parts form J-aggregates in aqueous solutions. In case of the covalent modification of the oligomers with one single nucleobase, the J-aggregate is formed in buffered saline and shows pronounced induced CD-signals of the J-band. PDI oligomers which are modified with longer DNA parts (6 bases) do only show J-aggregating character after the addition of spermine tetrahydrochloride which shields the charge of the DNA strand and prevents electrostatic repulsion within the formed structures.





**Scheme II.2** Schematic representation of the formation of the supramolecular polymer consisting of 3,6-dialkynylphenanthrene (donor, blue) and 1,8-dialkynylpyrene (acceptor, green). Excitation of the donor molecules at 322 nm results in very high pyrene fluorescence (406 nm). Rough estimations show that the energy transfer must occur over a distance of approximately 150 nm.



## III. Table of content

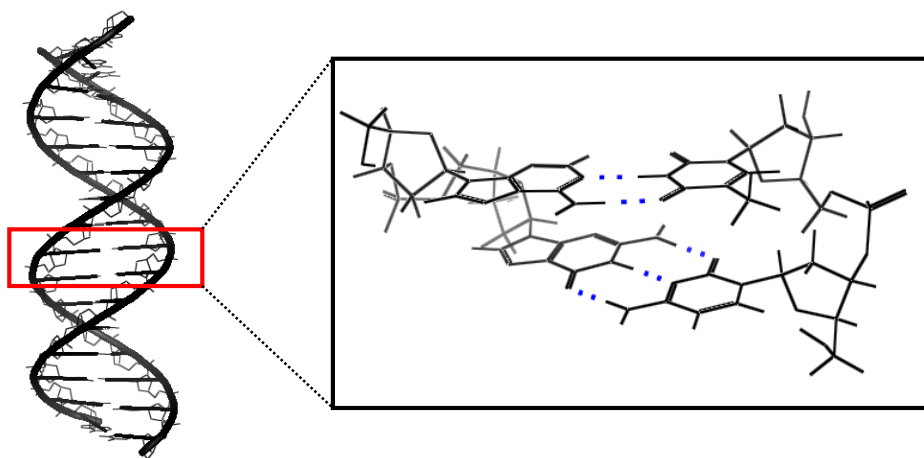
<b>I. Acknowledgment .....</b>	<b>2</b>
<b>II. Summary.....</b>	<b>6</b>
<b>III. Table of content .....</b>	<b>10</b>
<b>1.0. Introduction.....</b>	<b>13</b>
1.1. Unnatural DNA building blocks .....	13
1.2. Chromophores: from single molecules to functional systems – a DNA based approach 16	
<b>2.0. Characterization of selective aromatic interactions in DNA-guided hybrids.....</b>	<b>20</b>
2.1. Introduction .....	20
2.2. Aim of the work.....	23
2.3. Results and Discussion .....	23
2.3.1. Synthesis of duplexes and spectroscopic evaluation .....	23
2.3.2. Importance of electrostatic complementarity .....	26
2.3.3. Importance of aromatic donor and acceptor sequence .....	30
2.3.4. Impact of pyrene or PDI “dangling ends” .....	32
2.3.5. Impact of different aromatic donor and acceptor arrangements .....	33
2.3.6. Importance of the building block geometry .....	35
2.3.7. Impact on different pyrene geometries in the aromatic stack .....	38
2.3.8. Aromatic donor-acceptor sequence – an alternative approach .....	39
2.4. Summary, Conclusion and Outlook.....	42
<b>3.0. Observation of two independent H-couplings in a stack of multiple chromophores ...</b>	<b>45</b>
3.1. Introduction .....	45
3.1.1. Considerations of homo-H-aggregates .....	46
3.1.2. Considerations on hetero-H-aggregates .....	50

3.2. Aim of the work.....	51
3.3. Results and Discussion .....	51
3.3.1. Absorption spectra of the monomeric chromophores .....	51
3.3.1. Duplexes under investigation.....	52
3.3.2. Absorption spectra of the monomer chromophores in the aromatic stack .....	55
3.3.3. PDI and pyrene chromophores with nearest neighbour interactions .....	57
3.3.4. PDI and pyrene molecules with different distance $d$ toward each other .....	59
3.3.5. Relative angles of different interacting dipole moments .....	62
3.3.6. Increasing numbers of next-nearest PDI and pyrene interactions .....	63
3.3.7. Titration experiment of pyrene-pyrene interactions .....	68
3.3.8. Titration experiment of PDI-PDI interactions.....	69
3.3.9. Next-nearest neighbour interaction titration PDI-pyrene .....	70
3.3.10. General considerations on pyrene fluorescence and quenching by PDI – development of other alternating chromophore systems .....	72
3.4. Conclusion and Outlook .....	76
3.4.1. Observation of co-existing excitonic states in alternating chromophore stacks .....	76
3.4.2. Development of further antenna systems to simultaneously excite acceptor chromophores from co-existent excited states of alternating chromophore stacks .....	77
<b>4.0. Polymer light harvesting antenna with DNA like phosphate backbone.....</b>	<b>80</b>
4.1. Introduction .....	80
4.2. Aim of the work.....	82
4.3. Results and Discussion .....	82
4.3.1. Monomeric building blocks and assembled oligomers.....	82
4.3.2. AFM measurements of the supramolecular polymers .....	86
4.3.3. Fluorescence measurements of the light harvesting polymers .....	90
4.3.4. Dotting experiments using increasing concentrations of acceptor molecule <b>b</b> .....	91
4.3.4. Dotting experiments using increasing concentrations of donor oligomer <b>a</b> .....	93
4.3.5. Thermal stability of the supramolecular light harvesting polymers .....	95
4.3.6. Titration experiments using high concentrations of acceptor oligomer <b>b</b> .....	97
4.3.7. Polymer light harvesting antenna with pyrene monomer .....	99
4.3.8. Equilibrium between excimer and exciplex fluorescence.....	102
4.4. Conclusion and Outlook .....	114
4.4.1. Observation of long-distance EET in linear supramolecular antenna systems .....	114
4.4.2. Design of polymer light harvesting antenna systems .....	118

<b>5.0. Report on water-soluble J-aggregate forming PDI-oligomers and their interaction with pyrene-oligomers.....</b>	<b>119</b>
5.1. Introduction .....	119
5.2. Aim of the work.....	121
5.3. Results and Discussion .....	121
5.3.1. Oligomers containing enlarged PDI and pyrene stacks.....	121
5.3.2. Time dependent formation of PDI J-aggregates .....	123
5.3.3. J-aggregate formation inhibition by PDI-pyrene interaction .....	124
5.3.4. Spectroscopic characterization of oligomers with reduced DNA part.....	125
5.3.2. Interaction of PDI- and pyrene 3-mers.....	134
5.4. Conclusion and Outlook .....	138
<b>6.0. Experimental section.....</b>	<b>140</b>
<b>7.0. References .....</b>	<b>143</b>
<b>8.0. Appendix .....</b>	<b>150</b>
<b>9.0. Curriculum Vitae .....</b>	<b>166</b>
<b>10.0. List of Publications.....</b>	<b>167</b>

## 1.0. Introduction

The 1953 Nature publication by J.D. Watson and F.H.C. Crick is undoubtedly one of the most important publications in the history of science. In that publication J.D. Watson and F.H.C. Crick resolved the structure of double stranded DNA<sup>1</sup> based on X-ray data of Franklin, Wilkins, Gosling, Stokes and Wilson.<sup>2,3</sup> For the first time scientists had a model in hand how the structure of DNA looks like (Scheme 1.1). This discovery boosted the field of DNA-chemistry and had a great impact on life sciences in general.

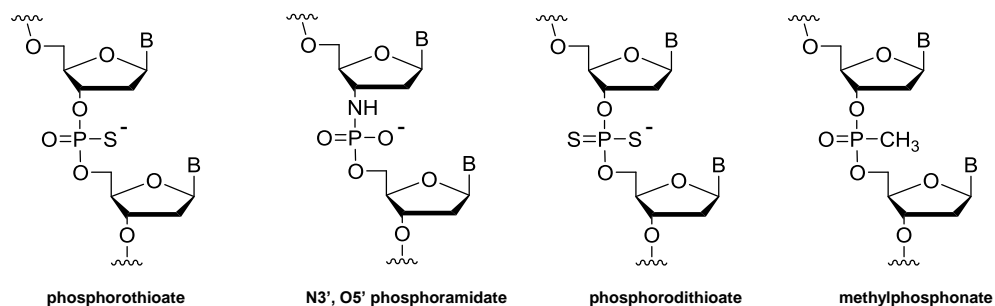


**Scheme 1.1** Left: double helical arrangement of the DNA. The model shows the staircase like  $\pi$ - $\pi$  arrangement of the purine and pyrimidine bases. Right: The H-bonding pattern between adenine and thymine (top, 2-H-bonds) and guanine and cytosine (bottom, 3-H-bonds) are shown.

### 1.1. Unnatural DNA building blocks

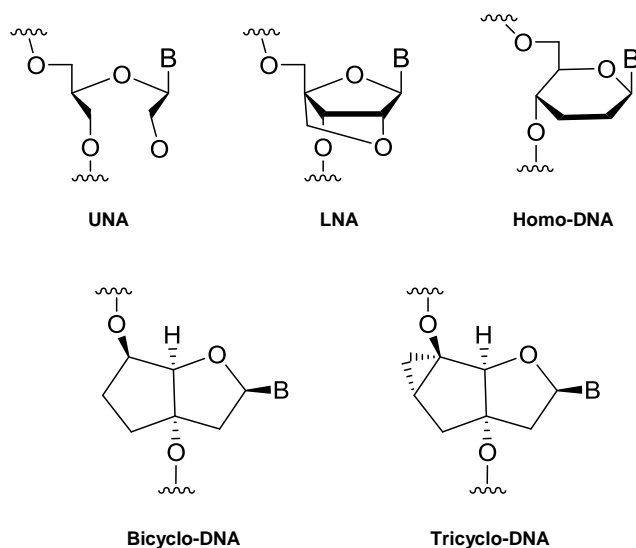
Almost 30 years later Caruthers and co-workers invented the solid phase synthesis of DNA.<sup>4,5</sup> This invention in 1981 had a big impact on biotechnology, biological chemistry, material sciences and related fields and speeded up the progress in science vastly<sup>6</sup>. Not only was it made possible to synthesize longer parts of DNA or RNA in a fast and cost-effective way – it was also made possible to use non-natural building blocks for the use in pharmaceutical research and other applications. Within this other applications the use of DNA for nanotechnology purposes became a widely used and familiar approach<sup>7-10</sup>. The easy chemical accessibility, the designable sequence paired with the well-defined and rigid structure makes DNA the perfect tool for building and assembling larger structures containing also non-natural parts. Pioneering work was performed by Eschenmoser et al. Eschenmoser and co-workers exchanged the ribose scaffold of the single

nucleotides by the hexapyranose moiety and tested the stability of these hybrids<sup>11-13</sup>. Modification of the phosphate backbone (Scheme 1.2) is an appropriate method to improve the stability of DNA and RNA against DNA-/RNAase activity.<sup>14-19</sup>



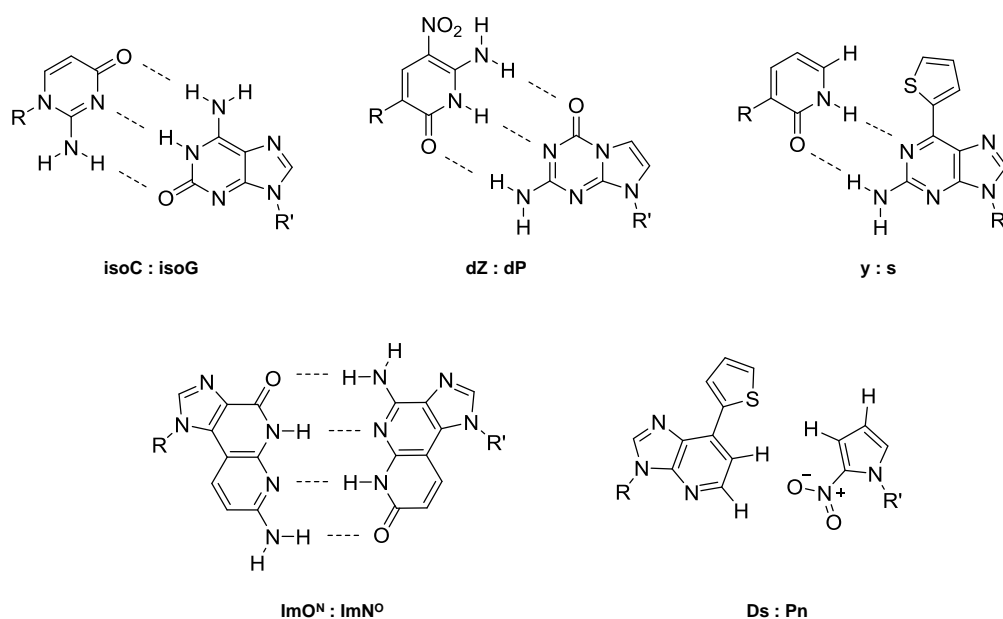
**Scheme 1.2** Selection of phosphate backbone modifications used in DNA chemistry. Taken from Ref<sup>14-19</sup>.

Altering of the sugar moiety in DNA aimed to preorganize the nucleobase and therefore stabilize (or destabilize) the double helix. Scheme 1.3 shows a selection of sugar modifications described in literature.



**Scheme 1.3** Selection of sugar modifications used in DNA chemistry. UNA<sup>20,21</sup>, LNA<sup>22,23</sup>, Homo-DNA<sup>24</sup>, Bicyclo-DNA<sup>25,26</sup> and Tricyclo-DNA<sup>27</sup>.

Further research was done to introduce nucleobases with altered H-bonding and steric patterns<sup>28-36</sup>. Figure 4 shows a selection thereof. Using non-standard nucleobases in DNA chemistry aims to build up bio-orthogonal information systems which can be used in transcription and translation to enrich the information content of natural DNA.



**Scheme 1.4** Selected base modifications to alter the H-bonding pattern: isoC : isoG<sup>31</sup>, dZ : dP<sup>37</sup>, y : s<sup>38,39</sup> and the ImO<sup>N</sup> : ImN<sup>O</sup> pair<sup>29</sup> and based on pure steric and hydrophobic considerations Ds : Pn<sup>40</sup>.

Kool et al. started work using enlarged nucleobases to test pairing and stability properties of DNA-double strands<sup>41-43</sup>. This work had an indispensable impact on the understanding of stability and properties of natural DNA. On the same time a completely new area of research was born. DNA-based nanotechnology henceforward makes use of unnatural building blocks incorporated into DNA to design new structures or functionalities. The aim, techniques, strategies and some results on this research will be highlighted in the next chapter of this introduction.

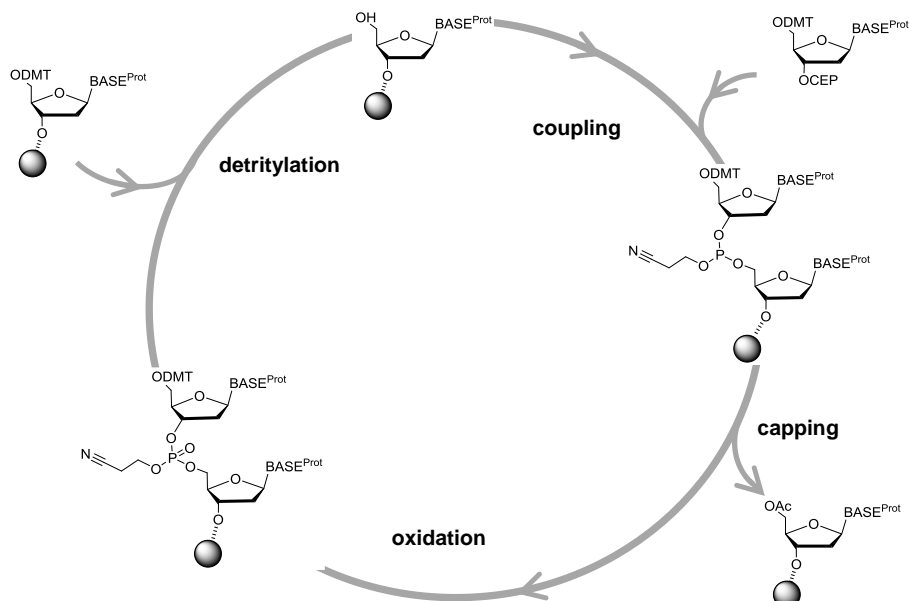


## **1.2. Chromophores: from single molecules to functional systems – a DNA based approach**

Organization of molecules and especially chromophores is a key requirement in nature and technology to design functional systems<sup>44-46</sup>. The structure of DNA, lipid bilayers or the folding of proteins are examples therefore. Another uppermost amazing natural example is given by the light harvesting complexes (LHC) in photosynthetic active plants and bacteria<sup>47</sup>. A well-defined arrangement of molecules and chromophores<sup>48</sup> in all these applications is indispensable as chromophoric complexes or ordered arrays thereof exhibit properties which are significantly different from those of the monomers<sup>49</sup>.

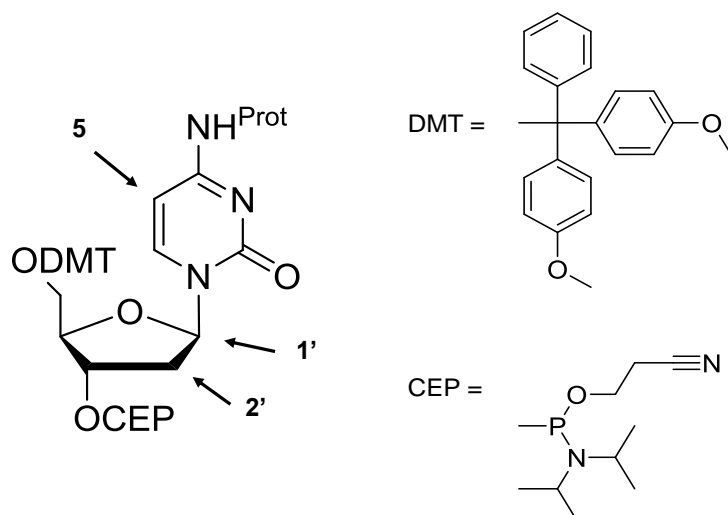
Using DNA as a well-defined and rigid scaffold for the arrangement of chromophores is an elegant and highly paid off method. The introduction of chromophores into oligonucleotides is achieved during or after the assembling of the oligonucleotide. Incorporation of functional molecules after the assembling process is also called post-synthetic modification and will not be discussed in this thesis. Many methods and protocols therefore exist<sup>50,51</sup> and find applications in DNA- and biotechnology.

The incorporation of modified or unnatural building blocks during the oligonucleotide synthesis makes it necessary to synthesize building blocks which are compatible with the oligonucleotide solid phase synthesis protocol (Scheme 1.5). In brief: A solid support is loaded with the first nucleoside of the sequence. Commercially available solid supports which are commonly used today are polystyrene beads or controlled pore glass (CPG) beads. Removal of the DMT (dimethoxytrityl) protecting group yields the free alcohol group. Subsequent coupling of the next nucleotide by activation of the phosphoramidite by tetrazole and reaction in AcN results in the corresponding dinucleotide. A capping step inactivates unreacted alcohol groups thus removes them from ongoing reaction. Oxidation with iodine solution (aq.) turns the phosphite-triester into the phosphate-triester. Repetition of this cycle synthesizes defined oligonucleotides with defined length and sequence. Molecules which were incorporated into an oligonucleotide strand during synthesis need to bear a cyanoethylphosphoramidite (CEP) on the one hydroxyl group of the molecule and a DMT-protecting group on the other (Scheme 1.6).

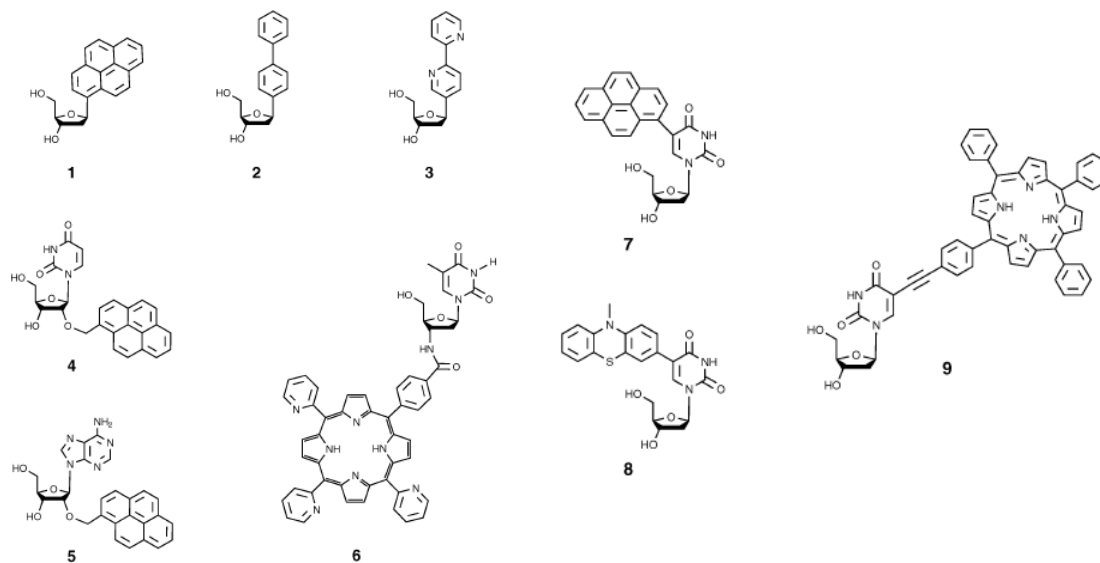


**Scheme 1.5** Solid phase synthesis of oligonucleotides. The four major steps are highlighted which are: detritylation (removal of the DMT protecting group), coupling of the next nucleobase, capping to remove unreacted species from the reaction pool and oxidation. Final cleavage from the solid support and fully deprotection is not shown.

Manifold possibilities exist to attach chromophores to nucleotides. Most prominent modifications include attachment at the 1' or 2' position of the ribose or the 5 position of the pyrimidine (marked with arrows in Scheme 1.6). Examples therefore are shown in Scheme 1.7.



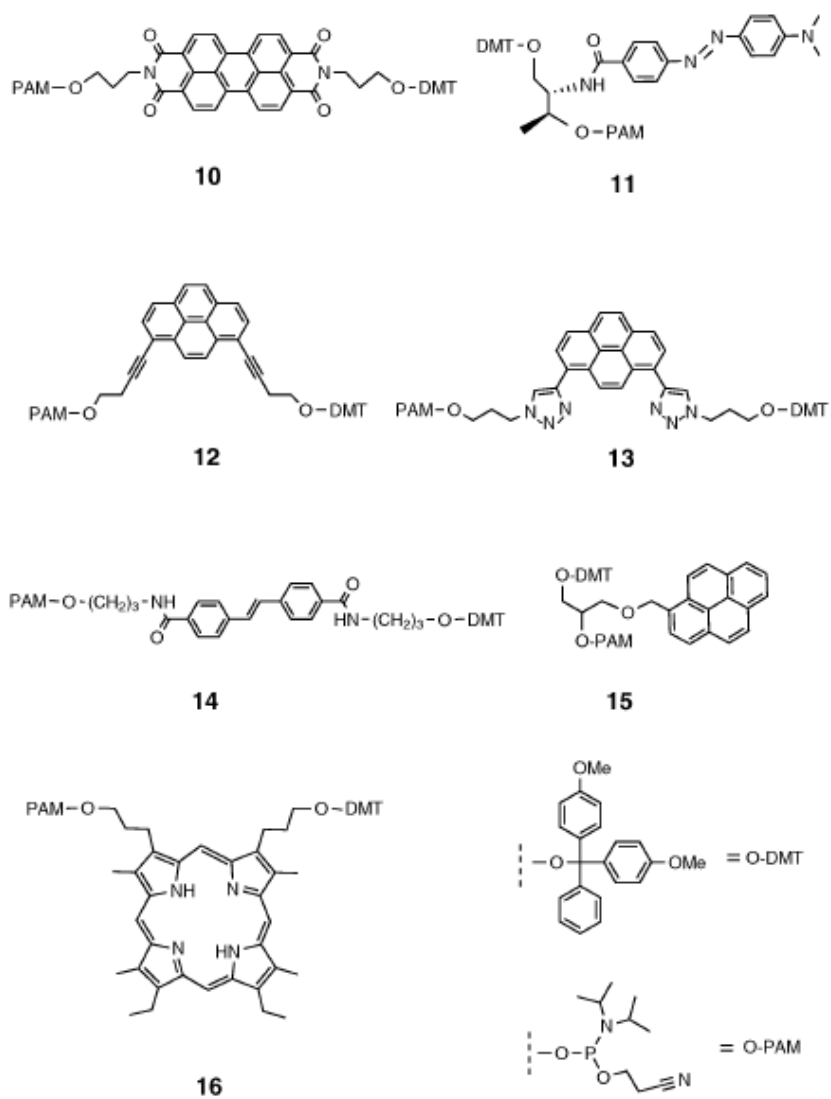
**Scheme 1.6** Commercially available nucleoside-phosphoramidite is shown. The DMT- and CEP protecting group as well as orthogonal base protecting groups are crucial for all building blocks used in the solid phase synthesis. Marked with arrows are the major sides for nucleoside modifications described in literature.



**Scheme 1.7** Sugar modified nucleotides **1-6** and base modified nucleotides **7-9** for studies in modified DNA according Ref <sup>52</sup>. Examples were taken from ref **1**<sup>53</sup>, **2** and **3**<sup>54</sup>, **4** and **5**<sup>55</sup>, **6**<sup>56</sup>, **7** and **8**<sup>57</sup>, **9**<sup>58</sup>.

Attaching the chromophores to the nucleobase or the 2' or 3' end of the sugar moiety leads to an arrangement of the chromophores in the major groove of the DNA/RNA depending on the side of attachment. The attachment of the chromophores at the 5'-position of the pyrimidine base takes an important role. Chemical substitution at this side is straight forward and allows a proper base pairing with the opposite strand in DNA<sup>49</sup>. An example where the nucleobase was replaced by aromatic compounds is represented by examples **1-3** in Scheme 1.7 and references <sup>54,59-61</sup>. In this case the aromatic base aligns along the natural base pair stack. Different pairs of electron rich aromatic molecules and electron poor aromatic molecules have been tested and recognition properties thereof have been evaluated in regard to stabilizing or destabilizing effects<sup>60</sup>.

Another class of modifications include non-nucleosidic building blocks as shown in Scheme 1.8. These modifications reduce the natural DNA part to the phosphate backbone and an enlarged aromatic molecule. Due to the extended aromatic system, the molecules have a strong tendency to stack within the DNA. Stilbene was used by Wu et Letsinger as loop replacements already in 1995<sup>62</sup>. Other building blocks followed as high-lighted by Lewis et al.<sup>63</sup> including porphyrine<sup>64</sup>, azo-benzene<sup>65</sup>, perylene<sup>63,66,67</sup>, phenanthrene<sup>68</sup>, pyrene<sup>69</sup>, phenanthroline<sup>70</sup> or tetrathiafulvalene<sup>71</sup>.



**Scheme 1.8** Selection (according Ref <sup>52</sup>) of non-nucleosidic building blocks used for DNA modification. Examples were taken from ref **10**<sup>72</sup>, **11**<sup>73</sup>, **12**<sup>74</sup>, **13**<sup>75</sup>, **14**<sup>62</sup>, **15**<sup>69</sup> and **16**<sup>64</sup>.

## 2.0. Characterization of selective aromatic interactions in DNA-guided hybrids

Work described in this chapter is published in:

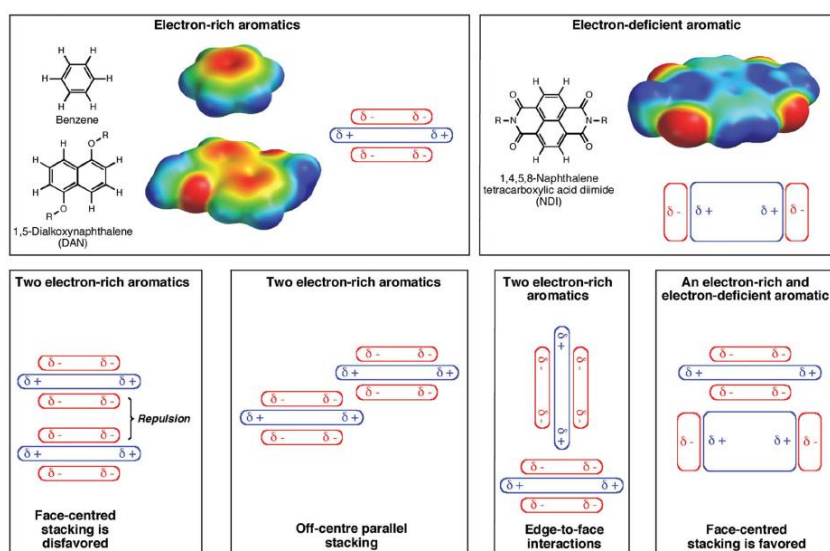
Influence of perylenediimide-pyrene supramolecular interactions on the stability of DNA-based hybrids: Importance of electrostatic complementarity

*C. B. Winiger, S.M. Langenegger, O. Khorev, R. Häner\**

*Beilstein J. Org. Chem.*, **2014**, *10*, 1589-1595 DOI: [10.3762/bjoc.10.164](https://doi.org/10.3762/bjoc.10.164)

### 2.1. Introduction

The stacking of aromatic molecules plays a crucial role in the molecular recognition process which is the key element of supramolecular chemistry and a common tool for the design of larger self-recognizing structures<sup>45,76</sup>. There exists many models and common accepted views on how aromatic interactions work. Nevertheless, the discussion on the detailed underlying mechanism of  $\pi$ - $\pi$  interactions is still controversially run among physical-, computational and organic chemists. Especially for larger systems the understanding is still poor and little experimental data available<sup>77</sup>. Conventional (and broadly accepted) considerations were introduced to the community in the early 1990s by Hunter and Sanders<sup>78,79</sup>. According to this model, an aromatic molecule is considered being a partially positive  $\sigma$ -scaffold with a sandwiched arrangement of negative charges represented by the  $\pi$ -electrons (Scheme 2.1).



**Scheme 2.1** Top: Schematically representation of electron rich and poor aromatic compounds with the respective electron density map. Bottom: Schematically representation of the favoured interactions of electron rich and poor aromatic compounds. Electron rich and electron poor aromatic compounds tend to form stabilized face-centred “donor-acceptor” complexes. Taken from Ref<sup>80</sup>.

Electron donating or electron withdrawing functional groups polarize the  $\pi$ -electron density of the aromatic core<sup>79,80</sup>. This favours a face-to-face stacking of electron deficient aromatic compounds with electron rich aromatic compounds. This special situation of the interaction of two aromatic molecules with different polarization is commonly been referred as being an “aromatic donor-acceptor” interaction<sup>80</sup>. Sanders and Hunter point out in their highly cited 1990 JACS paper that the “donor-acceptor” concept can be misleading as the stability of the stacking of aromatic compounds is highly dependent on the atoms in the regions of intermolecular contact which control the strength and geometry of interactions and not the overall molecular oxidation or reduction potentials<sup>79</sup>. Additionally, the term “electron donor-acceptor interaction” or “electron donor-acceptor complex” is – according to the IUPAC Gold Book - reserved for “charge-transfer complexes” or “Lewis adducts”<sup>81</sup>.

I will therefore use the terminology “electron deficient aromatic compound” and “electron rich aromatic compound” for aromatic molecules with polarized  $\pi$ -electrons and “aromatic donor-acceptor interactions” to define  $\pi$ - $\pi$  interactions thereof. On the other hand, the term “electron donor-acceptor interaction” is reserved for charge-transfer interactions of aromatic molecules.

In very general terms, face-to-face interactions of aromatic molecules are a result of solvophobicity, van der Waals interactions, electrostatic and charge transfer interactions.

Many research groups used aromatic  $\pi$ - $\pi$  interactions<sup>82-88</sup> and especially aromatic donor-acceptor interactions<sup>88</sup> and electron donor-acceptor interactions to design and build supra-molecular assemblies and functional systems. Recently Huc et al. presented  $\beta$ -sheet like foldamers based on arene-amide conjugates<sup>84,88</sup>. Iverson et al. build up alternating electron donor-acceptor foldamers making use of dialkoxynaphthalene (DAN) and naphthalenediimide (NDI)<sup>89</sup>. Matile et al. use aromatic interactions to prealign different bay-substituted NDI-compounds in self-sorting stacks to build up complex charge-transporting arrays<sup>90,91</sup>. Aromatic interactions play an important role in the synthesis of rotaxanes and catenanes to align the educts for synthesis<sup>92,93</sup>. A further example are the chemical cages and capsules prepared by M. Fujita, Misumi, Rebek, Cram or others<sup>94-98</sup>.

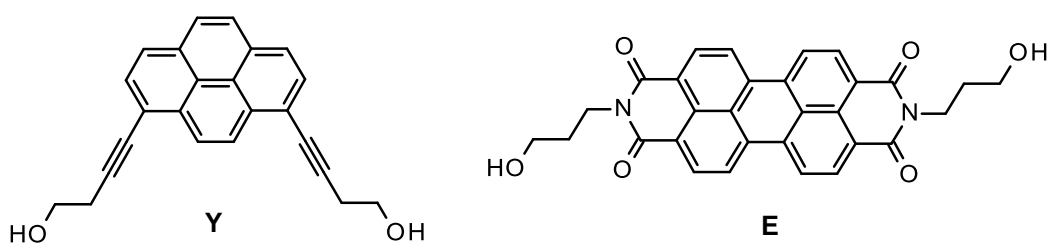
A major challenge in using aromatic interactions for the design of supramolecular assemblies or studying the properties and features of multiple chromophores is not only to define the exact number of stacked aromatic molecules but also the spacing and geometry within the stack<sup>95</sup>.

This issue can be perfectly addressed by using a molecular scaffold as for example DNA to arrange chromophores. Previous work from our group showed that the incorporation of aromatic non-nucleosidic molecules leads to an arrangement of these molecules within the stack of the natural DNA-structure<sup>99</sup>. The aromatic molecules stack in a face-to-face manner and due to optimal size act as a perfect base surrogate. Stabilization of the DNA duplex upon incorporation of covalently linked aromatic compounds was observed in case where the unnatural building block stacks either opposite an abasic site or has the chance to pair with another unnatural building block from the opposite DNA strand<sup>100,101</sup>. Incorporation of multiple chromophores into DNA showed that the stack of the unnatural chromophores adopt a DNA like helicity and does not disturb the all overall shape or stability of the natural DNA<sup>102</sup>. The incorporation of different pairs of chromophors has been reported (see below). Due to the well-defined positioning of the compounds toward each other, properties and characteristics thereof can be studied using spectroscopic methods. It was shown that DNA-mediated stacking of pyrene molecules leads to

an excimer fluorescence of the pyrenes<sup>103</sup>. The same was found using chrysene<sup>104</sup>. Similarly, the incorporation of pyrene and phenanthrenes into a DNA-duplex lead to the formation of an exciplex<sup>105</sup>. Based on these findings Langenegger et al. tried to elucidate how pyrenes and phenanthrenes preferentially interact with each other<sup>106</sup>. Bouquin et al. found in their research using pairs of pyrenes and perylenediimides (PDI) that the excimer fluorescence of pyrene is efficiently quenched by PDI. Furthermore, spectroscopic data suggests an alternating, zipper like arrangement of the pyrene and PDI units<sup>107</sup>. Based on this finding, the group of Prof. Häner developed a excimer controlled molecular beacon of pyrenes and PDI's using the quenching mechanism of alternating interaction of pyrenes and PDI's<sup>108-110</sup>.

The molecules under investigation for the following studies are the electron rich dialkynylpyrene (**Y**)<sup>74</sup> and the electron poor perylenediimide (PDI, **E**, Scheme 2.2). Both compounds have been studied previously in our research and research done by other groups<sup>111</sup>. Especially pyrene is an often used reporter molecule in DNA based material research as shown in Scheme 1.7.

Perylenediimides are a widely used class of molecules and have numerous potential applications. Due to the chemical robustness of PDI's, the photostability, outstanding optical and electronic properties, the dyes find applications as pigments, fluorescence sensors and n-semiconductors in organic electronics and photovoltaics<sup>111</sup>. In industrial and academic research, PDI molecules with their extended  $\pi$ -system are valuable molecules for the design of supramolecular architectures<sup>112-117</sup>. PDI is also often used in combination with DNA to align the PDI molecules in the defined scaffold<sup>118-125</sup>. Additionally, Li et al. used DNA like phosphorous polymers of PDI molecules to test the folding vs the assembling properties of these molecules in a concentration dependent way in organic solvents<sup>126</sup>.



**Scheme 2.2** Molecules under investigation in this section are the electron rich aromatic compound pyrene (**Y**) and the electron poor aromatic compound perylenediimide (PDI, **E**).

## 2.2. Aim of the work

Aromatic interactions are governed by electrostatics, van der Waals interactions and desolvation. Although that aromatic compounds have a tremendous impact on supramolecular chemistry, few general rules for stability and favourable interactions exists for larger aromatic systems. Based on our work in the last few years<sup>107,110</sup> it was suggested that pyrene and PDI molecules preferentially form alternating stacks within a DNA duplex and thereby stabilize the duplex. This could be explained by using the concept of electron poor and electron rich aromatic compounds and hypothesizing that aromatic donor chromophores preferentially interact with aromatic acceptor chromophores. In the following study we would like to formulate general rules which explain the selective interaction of the electron rich dialkynylpyrene molecule with the electron poor perylenediimide (PDI). We would like to rise general rules and predictions for the stability of a stack of multiple pyrenes and PDI's in different composition or sequence.

## 2.3. Results and Discussion

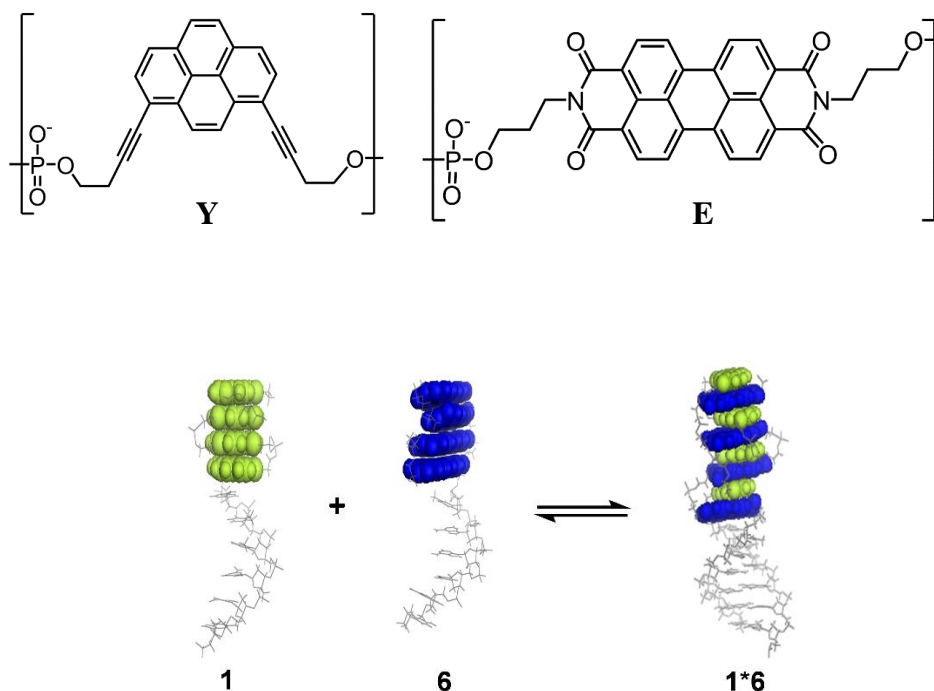
### 2.3.1. Synthesis of duplexes and spectroscopic evaluation

Mixed hybrids containing 6 natural bases and 4 unnatural building blocks of different sequences of pyrene and PDI were synthesized (Table 2.1). These oligomers were mixed in a way that double strands can be formed according to Watson-Crick base pairing (Scheme 2.3).

**Table 2.1** Sequences of the mixed DNA-oligoarenotide hybrids, whereby **Y** is the 1,6-dialkynylpyrene and **E** the perylenediimide

oligomer	sequence
1	5' GCG TTA YYY Y
2	5' YYY YTA ACG C
3	5' YEY YTA ACG C
4	5' EYE YTA ACG C
5	5' EEE YTA ACG C
6	5' EEE ETA ACG C
7	5' GCG TTA EEE E
8	5' YYY ETA ACG C
9	5' YEY ETA ACG C
10	5' YYY ETA ACG C





**Scheme 2.3** Representation of the hybridisation of oligomer **1** and oligomer **6**. Complementary DNA sequences lead to duplex formation and the alignment of the aromatic molecules, **Y** in green and **E** in blue.

Thereby the DNA strand acts as a supramolecular scaffold to align the chromophores which are covalently attached to the DNA strand. Flexible linkers between the molecules allow the chromophores of the opposite strands to interdigitate and arrange in hydrophobicity driven aromatic  $\pi$ -stacks. Absorption spectra of the single strands and the double stranded hybrids reveals information on the aromatic interactions and stacking properties in the scaffold. The absorption spectra of oligomer **1** shows a typical dialkynylpyrene absorption with two pronounced vibronic bands at 370 nm and 390 nm of the  $S_{0-1}$  transition (Figure 2.1). For PDI three pronounced vibronic bands are visible in the absorption spectra of oligomer **6** with an absorption maxima at 500 nm. Pronounced vibronic bands with higher energy (370 nm for pyrene and 500 nm for PDI) indicates a tight face-to-face stacking of the chromophores<sup>107,109,127</sup>. Formation of the double strand **1\*6** shows an altered absorption profile of the pyrene and the PDI molecules. The absorption band of the pyrene at 390 nm becomes more pronounced. The vibronic band of PDI at 500 nm is reduced compared to the vibronic band at lower energy and the shoulder of the third vibronic structure at 480 nm is reduced. The spectra resemble more a spectra of the monomeric chromophores, indicating that the tight stacks of pyrene and PDI molecules in the single strand are separated by alternating interdigitation of the pyrene and the PDIs. An elaborated view on absorption properties of hybrids with different supramolecular aromatic stacks will be presented in the Chapter 3.

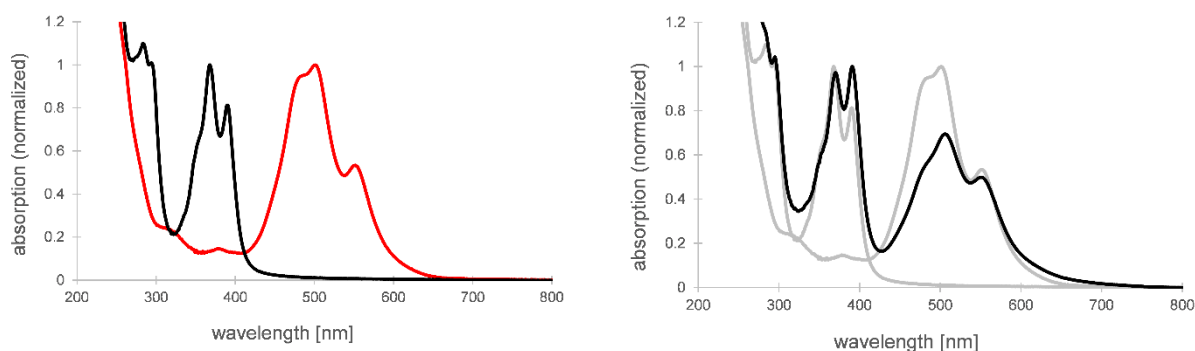
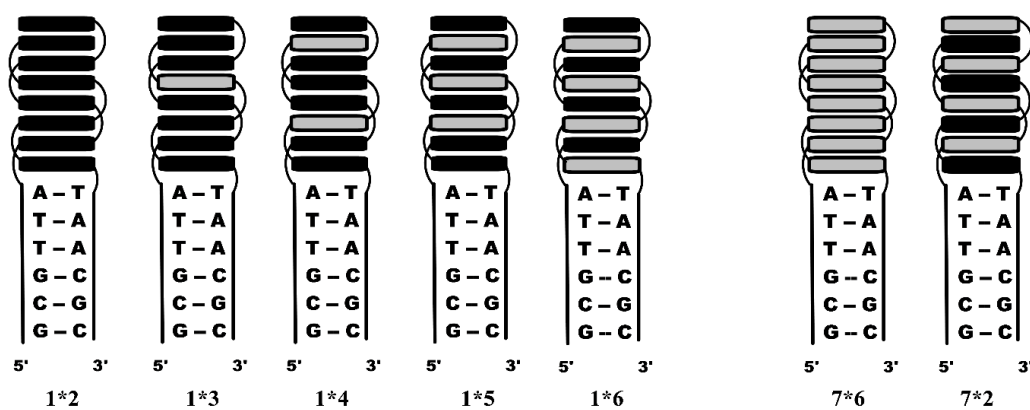


**Figure 2.1** Left: normalized absorption of oligomer **1** (black) and oligomer **6** (red). Right: normalized absorption of duplex **1\*6** (black) and the corresponding single strands in grey. Conditions: 2.5  $\mu$ M single strand, 10 mM sodium phosphate buffer, pH 7.2, 100 mM NaCl.

Double stranded hybrids were evaluated each of which contains a total of 8 chromophores in different sequences. The hybrids are shown in Scheme 2.4, whereby the black bars represent pyrene building blocks and the grey bars represent PDI building blocks. It must be mentioned that the exact sequence of alternating aromatic stacking can only be guessed as the first aromatic compound stacking on top of the DNA could belong to either of the two strands. Simple linker length and model DNA considerations let me conclude that stacking of the aromatic compound attached in the 5' end on top of the DNA is more probable. All the subsequent aromatic compounds are arranged in a zipper-like alternating manner. The melting temperature of each hybrid was determined. As the DNA strand of all hybrids is the same, the differences in melting temperature must originate from the modified aromatic stack part. Differences in melting temperature are therefore an indication of favourable interactions of different arrangements of the aromatic compounds.

### 2.3.2. Importance of electrostatic complementarity

All the duplexes were grouped in series to evaluate trends and properties thereof. A first series of hybrids consist of oligomer **1** which stays constant in each hybrid. The second strand contains different numbers of PDI molecules which in the duplex (**1\*2** – **1\*6**) results in different numbers of pyrene-PDI interactions (Scheme 2.4). Duplexes **7\*6** and **7\*2** are reference duplexes with only PDI interactions (**7\*6**) and fully alternating PDI-pyrene interactions (**7\*2**), similar to duplex **1\*6** but starting with pyrene on the DNA instead of PDI. The melting temperatures are summarized in Table 2.2 and graphically represented in Figure 2.2.



**Scheme 2.4** Representation of the hybrids containing different numbers of PDI (grey) molecules in the aromatic stack.

**Table 2.2** Sequences, measured  $T_m$  values and the number of aromatic donor-acceptor interactions of the duplexes under investigation. <sup>[a]</sup>Duplexes with a non-complementary DNA strand do not show a sigmoidal melting behaviour, thus, no  $T_m$  could be determined. Conditions: 2.5  $\mu$ M single strand, 10 mM sodium phosphate buffer, pH 7.2, 100 mM NaCl, ramp 0.3  $^{\circ}$ C/min, absorption was recorded at 260 nm, error  $\pm$  0.5  $^{\circ}$ C.

	Sequence	$T_m$ ( $^{\circ}$ C)	Number of aromatic donor-acceptor interactions
Ref	5' GCGTTA 3' CGCAAT	13.0	
<b>1</b> <b>2</b>	5' GCGTTA <b>YYYY</b> 3' CGCAAT <b>YYYY</b>	50.5	0
<b>1</b> <b>3</b>	5' GCGTTA <b>YYYY</b> 3' CGCAAT <b>YYEY</b>	54.5	2
<b>1</b> <b>4</b>	5' GCGTTA <b>YYYY</b> 3' CGCAAT <b>YEYE</b>	58.5	4
<b>1</b> <b>5</b>	5' GCGTTA <b>YYYY</b> 3' CGCAAT <b>YEEE</b>	61.0	6
<b>1</b> <b>6</b>	5' GCGTTA <b>YYYY</b> 3' CGCAAT <b>EEEE</b>	64.5	7
<b>7</b> <b>2</b>	5' GCGTTA <b>EEEE</b> 3' CGCAAT <b>YYYY</b>	66.5	7
<b>7</b> <b>6</b>	5' GCGTTA <b>EEEE</b> 3' CGCAAT <b>EEEE</b>	52.0	0
<b>1</b> <b>7</b>	5' GCGTTA <b>YYYY</b> 5' GCGTTA <b>EEEE</b>	- <sup>[a]</sup>	n/a
<b>2</b> <b>6</b>	3' CGCAAT <b>YYYY</b> 3' CGCAAT <b>EEEE</b>	- <sup>[a]</sup>	n/a

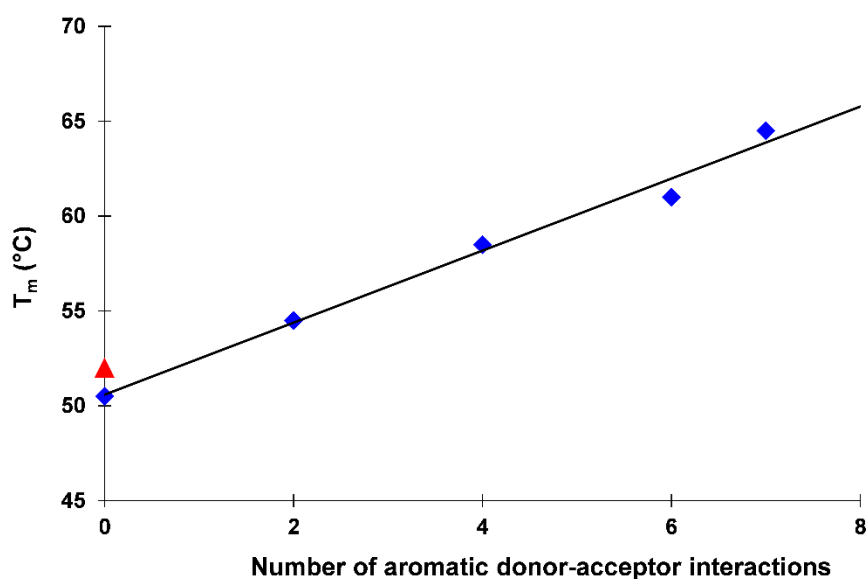


**Figure 2.2** A plot of melting temperature ( $T_m$ ) versus the number of pyrene-PDI interactions for duplexes presented in Scheme 2.4 and Table.  $T_m$  was recorded at 260 nm;  $R^2 = 0.987$ . The triangle represents the  $T_m$  of the control hybrid **7\*6**.

A reference oligonucleotide with only 6 natural bases and none unnatural building block has a melting temperature of 13 °C. Double strand **1\*6** bears for 7 pyrene-pyrene interactions (aromatic donor-donor interactions). This double strand has a melting temperature of 50.5 °C. This accounts for an additional 37.5 °C in melting temperature compared with the reference strand or in other words  $\Delta T_{m\ d-d} = 5.3$  °C per donor-donor interaction. A similar calculation can be done for duplex **7\*6** which has seven PDI-PDI interactions (aromatic acceptor-acceptor interactions) and melts at 52.0 °C. Each aromatic acceptor-acceptor interaction thus yields in additional  $\Delta T_{m\ a-a} = 5.5$  °C melting temperature in the duplex. From duplex **1\*6** the  $\Delta T_{m\ d-a}$  can be calculated which is 7.4 °C per interaction. For the reference duplex **7\*2** which also accounts for seven aromatic donor-acceptor interactions a  $\Delta T_{m\ d-a} = 7.6$  °C was calculated. The increase of thermal stability with increasing aromatic donor-acceptor interactions is rather linear in this series. Although it has to be mentioned that the arrangement of the chromophores in the  $\pi$ -stack and therefore the stability of the system is highly dependent on other factors like geometry in the interface DNA-aromatic molecules or solvation effects, for the above mentioned series a general trend in increasing thermal stability with increasing aromatic donor-acceptor interactions can be deduced. Comparing duplex **1\*2** with **7\*6**, only a slight difference in stability was found. According to theory the acceptor-acceptor interactions stabilize the system to a higher degree than donor-donor interactions<sup>128,129</sup>. Taking the experimental error into considerations the higher stability of duplex **7\*6** compared with **1\*2** is negligible.

No melting temperature was found in duplexes with non-complementary DNA parts (Table 2.2). Although that the unnatural aromatic part stabilizes the system to high degree, the DNA part is

essential for the alignment of the supramolecular stack and a proper orientation of the building blocks. This behaviour could also be seen in gel experiments (Figure 2.3). The electrophoretic mobility of relatively small (<1000 kbp), linear DNA strands is inversely proportional to their molecular weight<sup>130</sup>. Therefore polyacrylamide gel experiments are a reliable method to demonstrate the formation of double versus single stranded DNA structures.

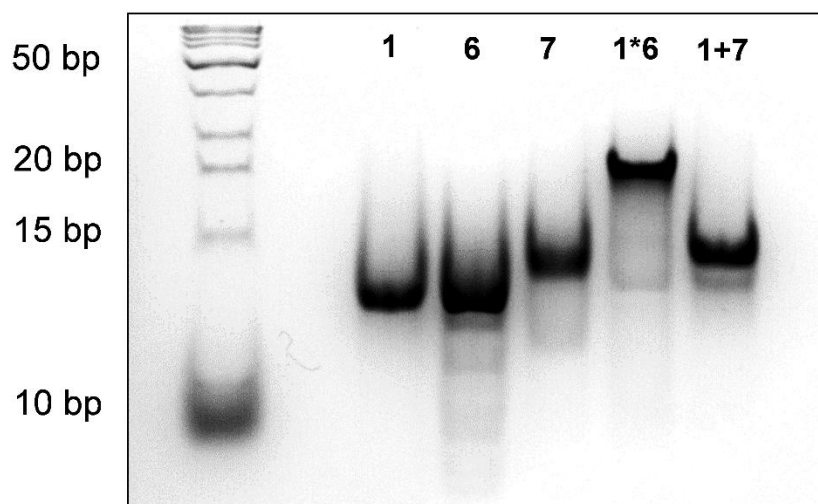


**Figure 2.3** PAGE experiment. All oligomers were used in a total amount of 150 pmol in 10 mM sodium phosphate buffer, 100 mM NaCl and 10% loading buffer, 20% polyacrylamide gel with a 10% loading gel, 1 h 40 min, 4 °C, 170 V, 6 mA, 2 W. Left lane: Ultra Short DNA ladder.

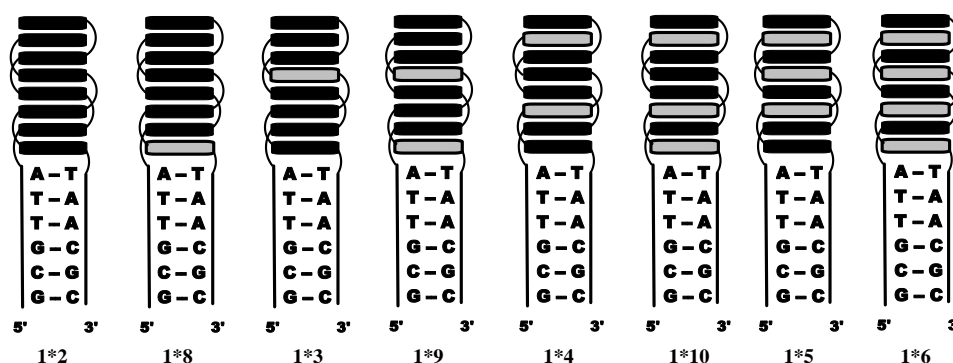
Oligomer single strands migrate with a speed of around 13 base pair double strand as indicated by the DNA ladder. Hybrid **1\*6** forms proper double strands and therefore migrates slower than the single strand. Oligomers with non-complementary DNA part as **1+7** migrate with the same speed as an oligomer single strand. This highlights the importance of the DNA sequence for the proper formation of duplexes.

## 2.3.3. Importance of aromatic donor and acceptor sequence

To achieve uneven numbers of aromatic donor-acceptor interactions duplexes were evaluated which have a PDI molecule stacking on top of the DNA (Table 2.3, Scheme 2.5). Melting temperatures of these duplexes are summarized in Table 2.3.

**Table 2.3** Sequence,  $T_m$  and number of donor-acceptor interactions of an additional set of hybrids. This set of hybrids has in common that the aromatic chromophore in the 5' end of the duplex is a PDI.

	Sequence	$T_m$ (°C)	Number of aromatic donor-acceptor interactions
Ref	5' GCGTTA 3' CGCAAT	13.0	
<b>1</b> <b>8</b>	5' GCGTTA <b>YYYY</b> 3' CGCAAT <b>EYYY</b>	58.6	1
<b>1</b> <b>9</b>	5' GCGTTA <b>YYYY</b> 3' CGCAAT <b>EY EY</b>	62.1	3
<b>1</b> <b>10</b>	5' GCGTTA <b>YYYY</b> 3' CGCAAT <b>EEYE</b>	65.6	5



**Scheme 2.5** Representation of the hybrids containing different numbers of PDI (grey) molecules in the aromatic stack at different position. This arrangement leads to duplexes containing 0 to 7 aromatic donor-acceptor interactions.

Graphical representation of the melting temperature plotted versus the number of aromatic donor-acceptor interactions shows again a linear increase with increasing aromatic donor-acceptor interactions. Surprisingly we see a higher stability in these duplexes where the PDI molecule stacks on top of the DNA (Figure 2.4).

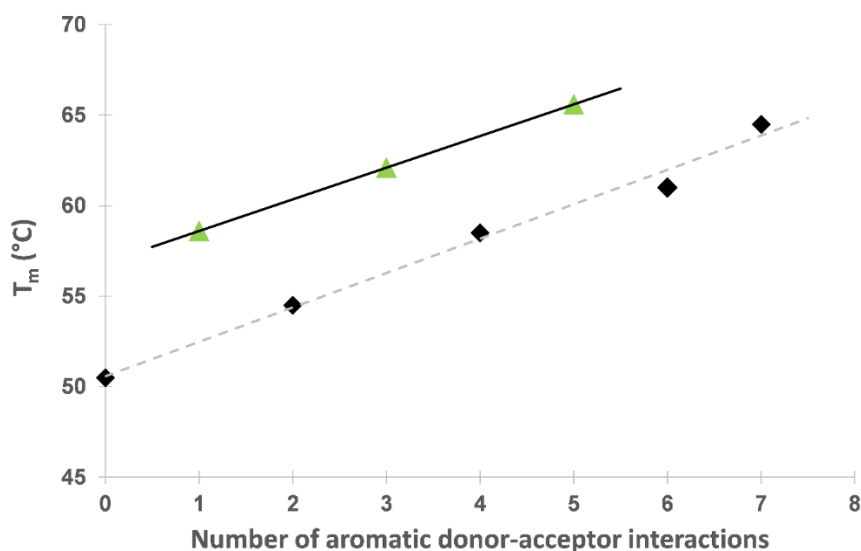


**Figure 2.4** Plot of the melting temperature ( $T_m$ ) versus the number of pyrene-PDI interactions for duplexes presented in Scheme 2.5 and Table 2.3. Condition as in Table 2.2. The melting temperature of the duplexes with 1, 3 and 5 donor-acceptor interactions are represented as green triangles.

Reasons therefore can either be explained by the better stacking abilities of the PDI molecule on top of the DNA or a favourable all-overall geometry of the stack which was induced by the stacking PDI. Stabilization of a DNA or RNA duplex due to stacking of a single additional base (overhang or dangling end) or an aromatic molecule is under intense investigation<sup>131-136</sup>. Predictions on how different dangling ends stabilize a duplex are difficult to achieve as parameters like solvation, electrostatics, geometry and size play a crucial role.

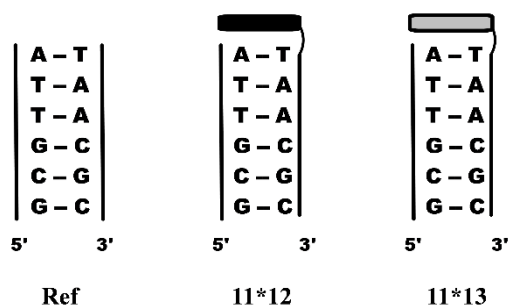


## 2.3.4. Impact of pyrene or PDI “dangling ends”

For the above mentioned set it was tested whether a pyrene or a PDI stacking on top of the DNA duplex has a bigger stabilizing effect (Table 2.4 and Scheme 2.6).

**Table 2.4** Sequence and  $T_m$  of short oligomer duplexes with pyrene (**11\*12**) or PDI (**11\*13**) “dangling end”

	Sequence	$T_m$ (°C)
Ref	5' GCGTTA 3' CGCAAT	13.0
<b>11</b> <b>12</b>	5' GCGTTA 3' CGCAAT Y	36
<b>11</b> <b>13</b>	5' GCGTTA 3' CGCAAT E	21



**Scheme 2.6** Representation of the short oligonucleotide duplexes with the pyrene (black) and PDI (grey) dangling end. The melting temperature of these two duplexes is compared with the melting temperature of a non-modified short DNA strand.

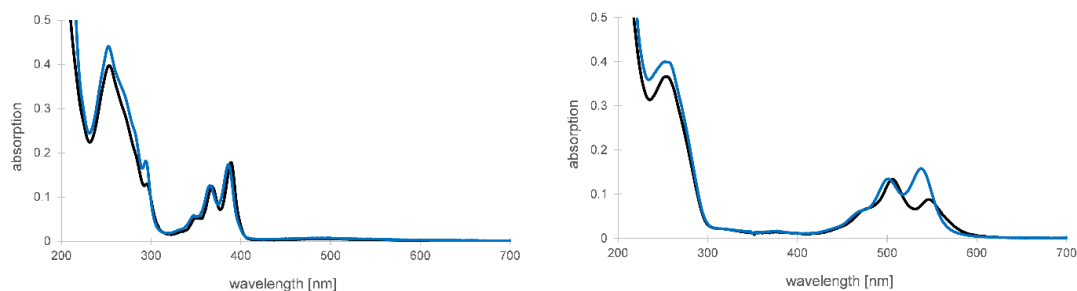


**Figure 2.5** Left: absorption of duplex **11\*12** Right: absorption of duplex **11\*13** at 20 °C (black) and 90 °C (blue). Conditions as in Table 2.2.

According to the melting temperature of duplexes **11\*12** and **11\*13** stacking of a pyrene on top of the DNA strand is more favourable than stacking of a PDI. The respective values for stabilization are:  $\Delta T_{m\text{pyrene}} = 23\text{ °C}$  and  $\Delta T_{m\text{PDI}} = 8\text{ °C}$ . It has to be pointed out that solvophobicity of the aromatic molecule toward the aqueous media does have a big effect on how the system is favourably stabilized. Additionally, the possibility exists that the dangling aromatic molecules are intercalated into the DNA-duplex and do not stack on top of the DNA.

UV/VIS measurement indicates that at least in duplex **11\*13** the hydrophobic effect results in the formation of higher ordered structures. At 20 °C the maximal absorption band is at 500 nm which is characteristic for PDI H-aggregates, thus dimers or multimers. At 90 °C the absorption maximum is at 540 nm which resembles the monomeric spectra. It is very likely that two duplexes stack top-on-top in a way that the PDI molecules stack in a face-to-face arrangement to shield the aromatic moiety from exposure to water. Similar systems were described by Lewis and co-workers<sup>72,116</sup>. It is therefore difficult to draw conclusions from the above experiments which could help to explain differences in the melting behaviour in duplexes in Figure 2.4.

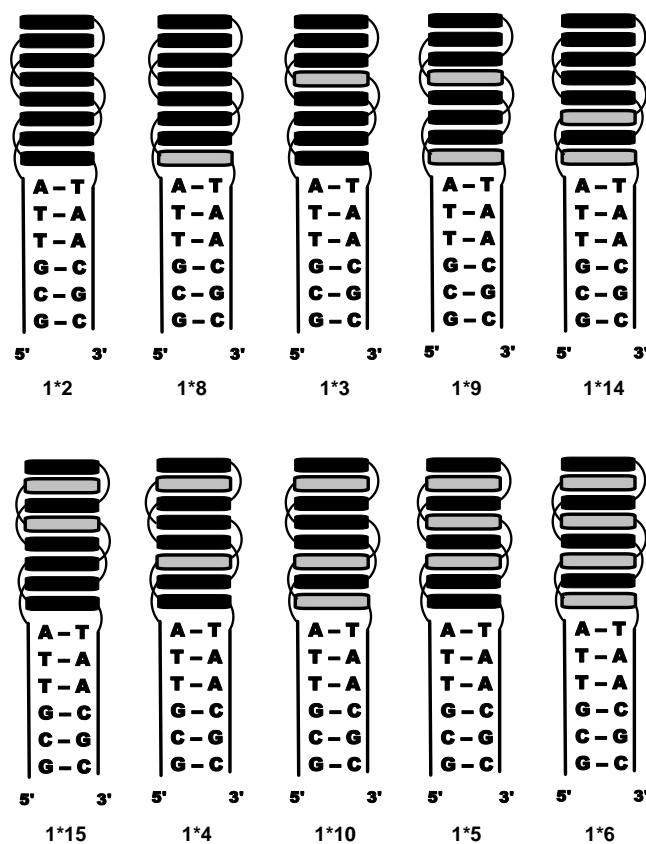
### 2.3.5. Impact of different aromatic donor and acceptor arrangements

Two further duplexes were measured. Both duplexes **1\*14** and **1\*15** contain two PDI molecules resulting in 3 and 4 aromatic donor-acceptor interactions respectively (Table 2.5). The melting behaviour of these two duplexes is compared to the series measured before and graphically represented in Figure 2.4. The duplexes have melting temperatures which indicate a thermal stability comparable to previously described duplexes. Interesting to see is, that duplex **1\*15** has the same number of aromatic donor-acceptor interactions as duplex **1\*4** but shows a much higher melting temperature which rather lays in accordance of duplexes **1\*8**, **1\*9** and **1\*10** (Figure 2.6). The comparison of duplexes **1\*15** and **1\*4** again indicates the importance of the overall geometry and the individual sequence of the  $\pi$ -stacks in the described hybrids. These hybrids have the same number of PDI molecules, the same number of aromatic donor-acceptor interactions and

the same aromatic compound stacking toward the DNA and pointing out to the water but nevertheless have a difference of the melting temperature of  $\Delta T_m = 5.6$  °C.

**Table 2.5** Sequences,  $T_m$  and number of donor-acceptor interactions of duplexes containing two times two **Y** or **E** in the complementary strand. Conditions as in Table 2.2

	Sequence	$T_m$ (°C)	Number of aromatic donor-acceptor interactions
Ref	5' GCGTTA 3' CGCAAT	13.0	
<b>1</b> <b>14</b>	5' GCGTTA <b>YYYY</b> 3' CGCAAT <b>EEYY</b>	63.6	3
<b>1</b> <b>15</b>	5' GCGTTA <b>YYYY</b> 3' CGCAAT <b>YYEE</b>	64.1	4



**Scheme 2.7** Schematically representation of duplexes containing different composition of the aromatic stack, yielding in different numbers of aromatic donor-acceptor interactions.

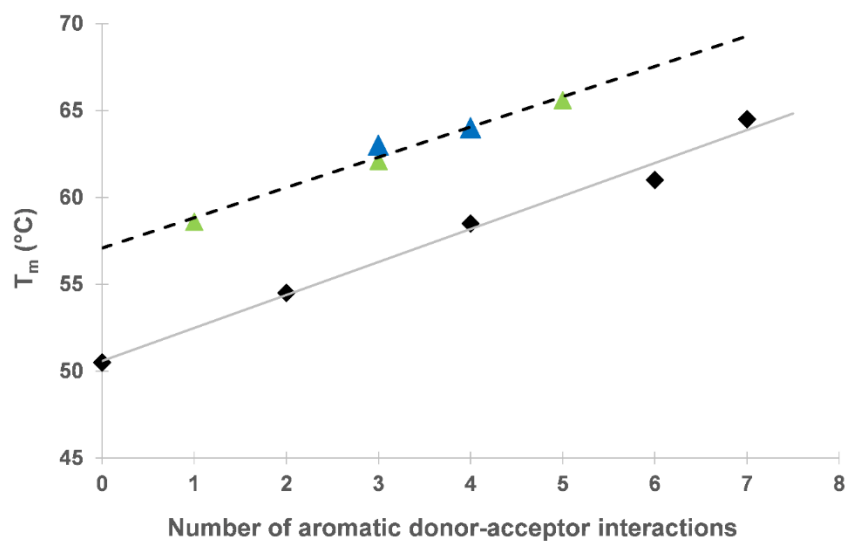
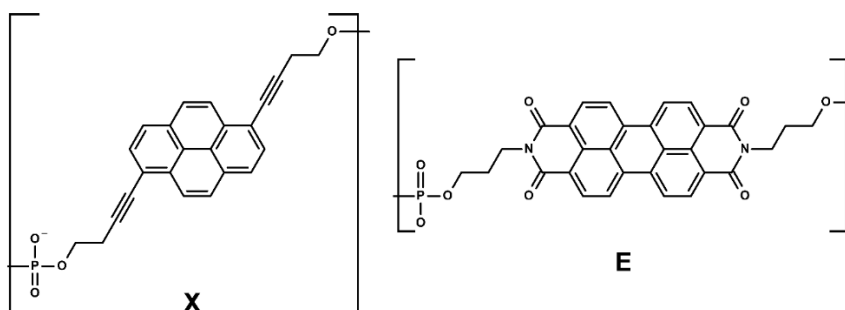


**Figure 2.6** Plot of the melting temperature ( $T_m$ ) versus the number of pyrene-PDI interactions for duplexes shown in Scheme 2.7. The data for duplex **1\*14** and **1\*15** are represented with the blue triangles, duplexes **1\*8**, **1\*9** and **1\*10** are shown with the green triangle.

### 2.3.6. Importance of the building block geometry

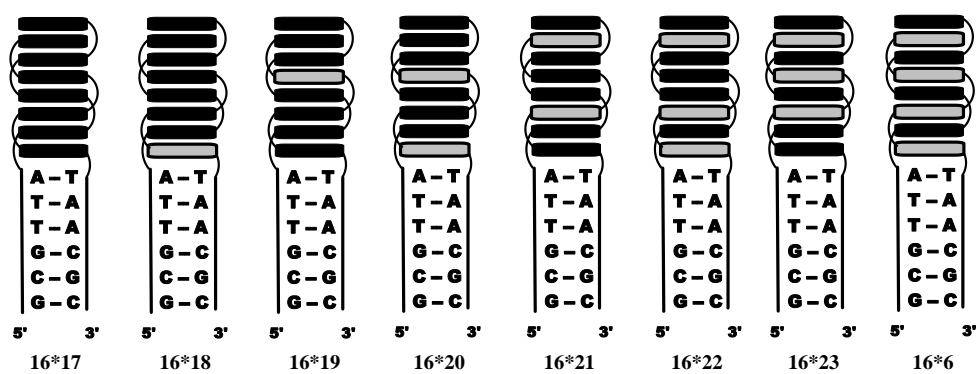
To address geometrical issues the kinked 1,8-dialkynylpyrene molecule used for the above studies was exchanged by the 1,6-dialkynylpyrene which – like the PDI – has a linear geometry (Scheme 2.8).



**Scheme 2.8** Chemical structure of the “linear” 1,6-dialkynylpyrene **X** and the PDI **E** used for the following study.

**Table 2.6** Sequences,  $T_m$  values and number of aromatic donor-acceptor interactions in duplexes containing **X** and **E**. Conditions as in Table 2.2.

	Sequence	$T_m$ (°C)	Number of aromatic donor-acceptor interactions
Ref	5' GCGTTA 3' CGCAAT	13.0	
16 17	5' GCGTTA <b>XXXX</b> 3' CGCAAT <b>XXXX</b>	52.7	0
16 18	5' GCGTTA <b>XXXX</b> 3' CGCAAT <b>EXXX</b>	60.5	1
16 19	5' GCGTTA <b>XXXX</b> 3' CGCAAT <b>XXEX</b>	56.0	2
16 20	5' GCGTTA <b>XXXX</b> 3' CGCAAT <b>EXEX</b>	67.3	3
16 21	5' GCGTTA <b>XXXX</b> 3' CGCAAT <b>XEXE</b>	64.0	4
16 22	5' GCGTTA <b>XXXX</b> 3' CGCAAT <b>EEXE</b>	75.8	5
16 23	5' GCGTTA <b>XXXX</b> 3' CGCAAT <b>XEEE</b>	65.8	6
16 6	5' GCGTTA <b>XXXX</b> 5' GCGTTA <b>EEEE</b>	75.7	7

**Scheme 2.9** Representation of the duplexes under investigation. Increasing aromatic donor-acceptor interactions from left to right. 1,6-dialkynylpyrene is shown in black, PDI in grey.

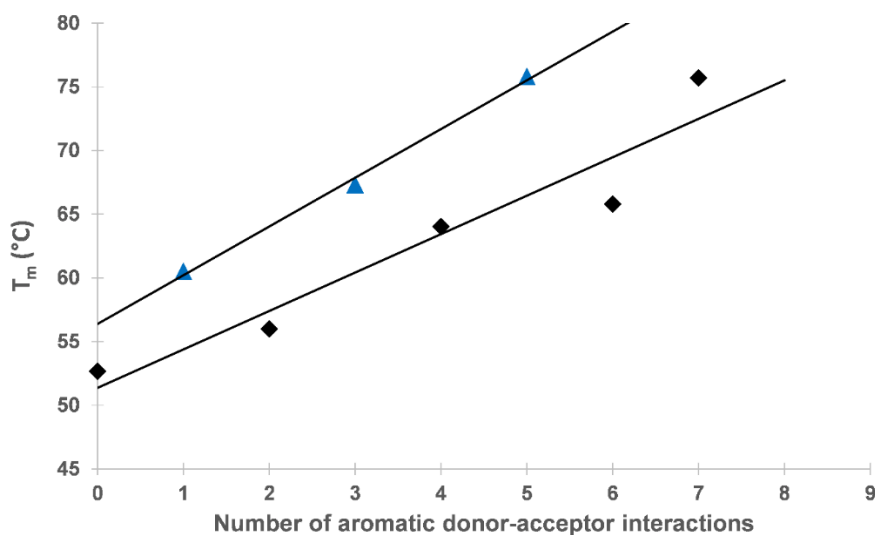


**Figure 2.7** Plot of the  $T_m$  vs the number of aromatic donor-acceptor interactions of the oligomers series containing pyrene **X** and PDI. Oligomers **16\*18**, **16\*20** and **16\*22** are shown in blue.

In duplexes using the 1,6-dialkynylpyrene we see the same melting pattern as in the experiment using the 1,8-dialkynylpyrene (Figure 2.4). Duplexes which possess a PDI molecule on top of the DNA stack show an increased thermal stability. As in Figure 2.4 we see the two same linear dependences of increasing thermal stability with increasing number of aromatic donor-acceptor interactions.

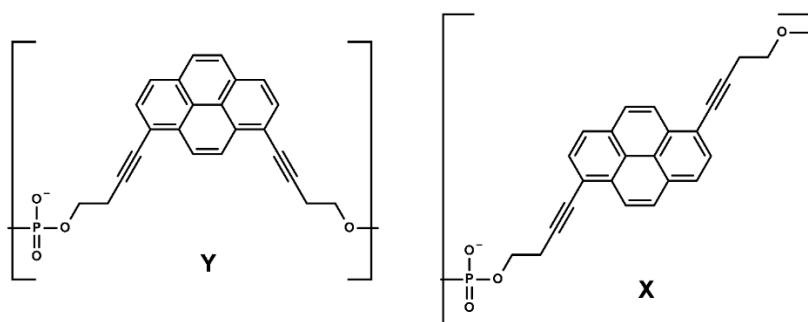
Additionally it was found that the hybrids with the 1,6-dialkynylpyrene geometry have a much higher melting temperature than duplexes with the 1,8-dialkynylpyrene. A duplex with a fully alternating pyrene-PDI sequence gains an additional 10 °C by using the 1,6-dialkynylpyrene. This accounts for  $\Delta T_{m \text{ d-a}} = 8.6$  °C per aromatic donor-acceptor interaction in the fully alternating hybrid **16\*6**.

## 2.3.7. Impact on different pyrene geometries in the aromatic stack

With the above synthesized oligomers three different hybrids consisting of pyrene-stacks with different geometry could be measured. Duplex **1\*2** consists of only 1,8-dialkynylpyrenes, duplex **16\*17** only has 1,6-dialkynylpyrene and duplex **16\*2** describes a hybrid with mixed 1,6-dialkynyl- and 1,8-dialkynylpyrene stacks (Table 2.7).

**Table 2.7** Sequences and  $T_m$  values of oligomer duplexes containing pyrenes. Thereby homo-duplexes of 1,8-dialkynylpyrene or 1,6-dialkynylpyrene as well as the hetero-duplex of a mixture of both is shown. Conditions as in Table 2.2.

	Sequence	$T_m$ (°C)
Ref	5' GCGTTA 3' CGCAAT	13.0
<b>1</b> <b>2</b>	5' GCGTTA <b>YYYY</b> 3' CGCAAT <b>YYYY</b>	50.5
<b>16</b> <b>17</b>	5' GCGTTA <b>XXXX</b> 3' CGCAAT <b>XXXX</b>	52.7
<b>16</b> <b>2</b>	5' GCGTTA <b>XXXX</b> 3' CGCAAT <b>YYYY</b>	53.7



The experiments shows a slight thermal stabilization of the mixed hybrid **16\*2** over hybrids **1\*2** and **16\*17**. The differences are minor compared to the stabilizing effect caused by the insertion of aromatic electron poor compounds. In duplex **16\*2** each pyrene-pyrene interaction accounts for  $\Delta T_{m\ X-Y} = 0.45$  °C compared to duplex **1\*2**.

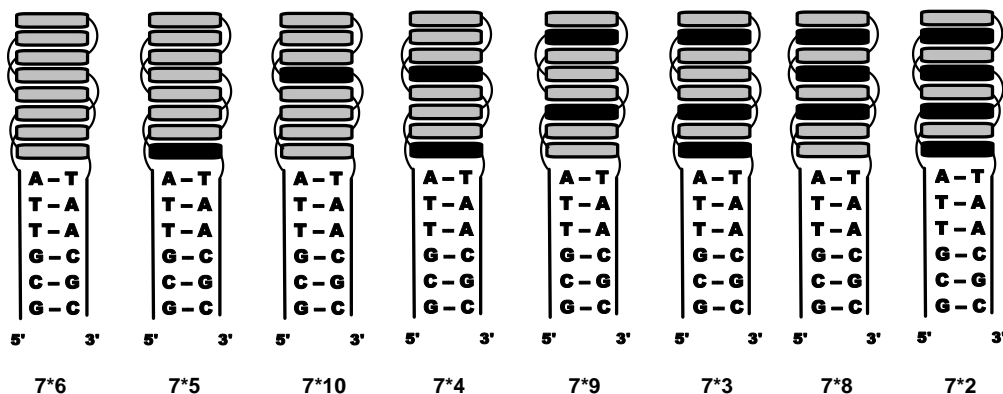
### 2.3.8. Aromatic donor-acceptor sequence – an alternative approach

With the above introduced sequences a series of duplexes has been measured with the same PDI-pyrene pattern but an inversed sequence compared to Scheme 2.5 (each PDI in Scheme 2.5 is replaced by a pyrene and vica versa). The series is depicted in Table 2.8 and Scheme 2.10.

**Table 2.8** Sequences,  $T_m$  values and number of aromatic donor-acceptor interactions of **Y** and **E** containing duplexes. Starting with a sequences with only PDIs more and more **Y** is incorporated into the duplex resulting in higher numbers of aromatic donor-acceptor interactions. Conditions as in Table 2.2.

	Sequence	$T_m$ (°C)	Number of aromatic donor-acceptor interactions
Ref	5' GCGTTA 3' CGCAAT	13.0	
<b>7</b> <b>6</b>	5' GCGTTA <b>EEEE</b> 3' CGCAAT <b>EEEE</b>	52.0	0
<b>7</b> <b>5</b>	5' GCGTTA <b>EEEE</b> 3' CGCAAT <b>YEEE</b>	48.7	1
<b>7</b> <b>10</b>	5' GCGTTA <b>EEEE</b> 3' CGCAAT <b>EEYE</b>	37.9	2
<b>7</b> <b>4</b>	5' GCGTTA <b>EEEE</b> 3' CGCAAT <b>YEYE</b>	47.1	3
<b>7</b> <b>9</b>	5' GCGTTA <b>EEEE</b> 3' CGCAAT <b>EY EY</b>	50.0	4
<b>7</b> <b>3</b>	5' GCGTTA <b>EEEE</b> 3' CGCAAT <b>Y Y EY</b>	59.8	5
<b>7</b> <b>8</b>	5' GCGTTA <b>EEEE</b> 3' CGCAAT <b>E Y Y Y</b>	58.8	6
<b>7</b> <b>2</b>	5' GCGTTA <b>EEEE</b> 3' CGCAAT <b>Y Y Y Y</b>	66.5	7





**Scheme 2.10** Oligomer hybrids under investigation. Increasing numbers of pyrene in the duplexes from left to right leads to an increasing number of aromatic donor-acceptor interactions.

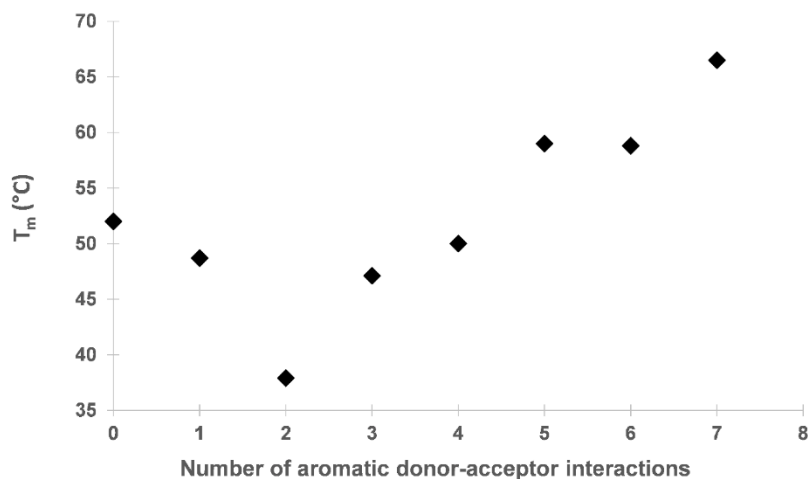


**Figure 2.8** Plot of  $T_m$  vs the number of aromatic donor-acceptor interactions. The data represents all the duplexes from Scheme 2.10.

Introduction of 1,8-dialkynylpyrene molecules into an aromatic  $\pi$ -stack of PDIs (duplex 7\*6) destabilizes the structure and leads to a lower melting temperature than in a stack consisting only of PDI molecules. After the incorporation of the second pyrene molecule a linear increase of thermal stability with increasing aromatic donor-acceptor interactions can be seen. Duplexes 7\*2 and 1\*6, both with the fully alternating pyrene-PDI sequence show the same melting temperature.

In the duplexes shown on top one of the two strands probed contained either four pyrene molecules or four PDI molecules but not mixed sequences. Further duplexes in which both of the strands contain both PDI and pyrene molecules were probed for their stability. The thermal stability is shown in Table 2.9. No conclusions on thermal stability in respect of number of

aromatic donor-acceptor interactions can be drawn from this series. Modification of each single strand with different chromophores and hybridization thereof leads to very diverse systems in respect to the angles of the chromophores and all overall geometry of the  $\pi$ -stack. This is most probably the case why no clear patterns for thermal stability could be concluded.

**Table 2.9** Sequence,  $T_m$  value and number of aromatic donor-acceptor interactions of duplexes which are not further discussed in this report. Characteristic for these duplexes is, that both single strands show combined sequences of pyrene and PDI molecules, whereas in the previous examples one of the two strand only contained **Y** or **E**. Conditions as in Table 2.2.

	Sequence	$T_m$ (°C)	Number of aromatic donor-acceptor interactions
Ref	5' GCGTTA 3' CGCAAT	13.0	
<b>24</b> <b>4</b>	5' GCGTTA <b>EEYY</b> 3' CGCAAT <b>YEYE</b>	49.5	4
<b>24</b> <b>14</b>	5' GCGTTA <b>EEYY</b> 3' CGCAAT <b>EEYY</b>	45.5	1
<b>24</b> <b>15</b>	5' GCGTTA <b>EEYY</b> 3' CGCAAT <b>YYEE</b>	55.0	6
<b>25</b> <b>4</b>	5' GCGTTA <b>YYEE</b> 3' CGCAAT <b>YEYE</b>	49.5	3
<b>25</b> <b>14</b>	5' GCGTTA <b>YYEE</b> 3' CGCAAT <b>EEYY</b>	49.5	6
<b>25</b> <b>15</b>	5' GCGTTA <b>YYEE</b> 3' CGCAAT <b>YYEE</b>	55.0	1

## 2.4. Summary, Conclusion and Outlook

A set of hybrid oligomers has been synthesized and various duplexes thereof were formed. The duplexes contain a DNA part which for all sequences stays constant and an enlarged covalently linked aromatic  $\pi$ - $\pi$  stacked part consisting of different sequences of 1,8-dialkynylpyrene and/or 1,6-dialkynylpyrene and PDI molecules. Thereby the dialkynylpyrene molecules are considered as being electron rich aromatic compounds and the PDI molecules are electron deficient aromatic compounds. The thermal stability of these duplexes has been evaluated. As the DNA part of all hybrids is the same, differences in the thermal stability must result from the different arrangement of the aromatic chromophores.

In different sets of double stranded hybrids it was found that the thermal stability correlates with the number of aromatic donor-acceptor interactions. Thus, the Hunter and Sanders 1990 introduced considerations on the interaction of polarized aromatic compounds have been successfully applied on a covalently linked, well defined, extended supramolecular assembly.

Further duplexes were found which show higher or lower thermal stability than predicted by the simple aromatic donor-acceptor consideration.

This indicates that many more parameters have to be taken into account to give a full overall picture. The parameters that could play a role are

- Attractive forces by aromatic donor-acceptor interaction
- Favourable/disfavourable aromatic donor-donor interactions
- Favourable/disfavourable aromatic acceptor-acceptor interactions
- Stacking of the first aromatic compound on top of the DNA
- Stacking of the last aromatic compound pointing toward the water
- The geometry of the building blocks and linkers

A mathematical evaluation of the above raised points has been performed. For each described duplex (duplexes with the 1,8-dialkynylpyrene geometry were used) the number of dues has been elucidated. Each of these dues has been assigned a certain value t-z which is an indication for the stabilization of the duplex by one of these dues in °C. The calculated  $T_m$  for each duplex is the sum of the different dues multiplied by the value [in °C] therefore:

$$T_m \text{ calculated} = \#DD * t + \#AA * u + \#DA * v + A_{DNA} * w + D_{DNA} * x + A_{water} * y + D_{water} * z$$

Whereby:

#DD is the number of donor-donor interactions

#AA is the number of acceptor-acceptor interactions

#DA is the number of donor-acceptor interactions

A<sub>DNA</sub> indicates whether an acceptor molecule stacks on the DNA and gets the value either 1 or 0

D<sub>DNA</sub> indicates whether a donor molecule stacks on the DNA and gets the value either 1 or 0

A<sub>water</sub> indicates whether an acceptor molecule points to the water and gets the value either 1 or 0

D<sub>water</sub> indicates whether a donor molecule points to the water and gets the value either 1 or 0

The difference between the calculated and the measured  $T_m$  is minimized using the least square method and by successively changing the values t-z. Thereby the measured  $T_m$  was reduced by the stability which accounts from the reference DNA part and which corresponds to 13 °C.

Table 2.10 Sequence of a selection of duplexes to demonstrate the principle of the matrix evaluation. The number of aromatic donor-donor (#DD), aromatic acceptor-acceptor (#AA) or aromatic donor-acceptor (#DA) interactions. Furthermore, the interaction of Y-DNA, E-DNA, Y-water or E-water is counted as either 0 or 1. The measured  $T_m$  (stability) was fitted by weighting each of these stability contributions.

	sequence	#DD	#AA	#DA	A_DNA	D_DNA	A_water	D_water	Tm
7*4	5' GCGTTAEEEE 3' CGCAATYEYE	0.000	4.000	3.000	0.000	1.000	1.000	0.000	47.500
1*2	5' GCGTTAYYYY 3' CGCAATYYYY	7.000	0.000	0.000	0.000	1.000	0.000	1.000	52.000
7*6	5' GCGTTAEEEE 3' CGCAATEEEEE	0.000	7.000	0.000	1.000	0.000	1.000	0.000	53.000
1*3	5' GCGTTAYYYY 3' CGCAATYYEY	5.000	0.000	2.000	0.000	1.000	0.000	1.000	55.000
7*3	5' GCGTTAEEEE 3' CGCAATYYEY	0.000	2.000	5.000	0.000	1.000	1.000	0.000	58.500
1*4	5' GCGTTAYYYY 3' CGCAATYEYE	3.000	0.000	4.000	0.000	1.000	0.000	1.000	60.000
1*5	5' GCGTTAYYYY 3' CGCAATYEEE	1.000	0.000	6.000	0.000	1.000	0.000	1.000	63.500
7*2	5' GCGTTAEEEE 3' CGCAATYYYY	0.000	0.000	7.000	0.000	1.000	1.000	0.000	63.500
1*6	5' GCGTTAYYYY 3' CGCAATEEEEE	0.000	0.000	7.000	1.000	0.000	0.000	1.000	66.000
1*10	5' GCGTTAYYYY 3' CGCAATEEYE	2.000	0.000	5.000	1.000	0.000	0.000	1.000	65.700

Thereby the following values for t-z were gained:

t = stabilization in [°C] for one donor-donor interaction	5.66
u = stabilization in [°C] for one acceptor-acceptor interaction	5.08
v = stabilization in [°C] for one donor-acceptor interaction	7.44
w = stabilization in [°C] for the interaction of an acceptor molecule with DNA	2.16
x = stabilization in [°C] for the interaction of a donor molecule with DNA	1.14
y = stabilization in [°C] for the interaction of an acceptor molecule with water	5.96
z = stabilization in [°C] for the interaction of a donor molecule with water	0.182

Using the above explained matrix all  $T_m$  values could be calculated within a reasonable accuracy ( $\pm 3^\circ\text{C}$ ) with the exception of duplexes **7\*5** and **7\*10**. These two duplexes were already in Figure 2.8 found to have a melting temperature different than what we would predict by simply using the donor-acceptor concept. The calculations indicate that the highest stabilization is observed between interactions of an electron rich aromatic compound with an electron poor aromatic compound. This calculated interaction accounts for  $\Delta T_m = 7.44^\circ\text{C}$ . The calculated interaction of two electron rich aromatic compounds account for  $\Delta T_m = 5.66^\circ\text{C}$  and the interaction for two electron poor aromatic compounds results in a calculated stability of  $\Delta T_m = 5.08^\circ\text{C}$  per interaction.

The calculated aromatic donor-donor interaction is slightly more favoured than the aromatic acceptor-acceptor interaction which is not in accordance with the theory<sup>79</sup>. An acceptor molecule stacking to the DNA stabilizes the DNA more than a donor aromatic compound stacking on the DNA (Figure 2.4). A huge calculated difference is found whether a donor or an acceptor molecule points toward the water. The calculations indicate that an acceptor molecule pointing to the water results in a much higher thermal stability of the hybrid. This finding is surprising on the first sight as it is not obvious from the graphs on top (Figure 2.4 and 2.8).

### 3.0. Observation of two independent H-couplings in a stack of multiple chromophores

Manuscript submitted

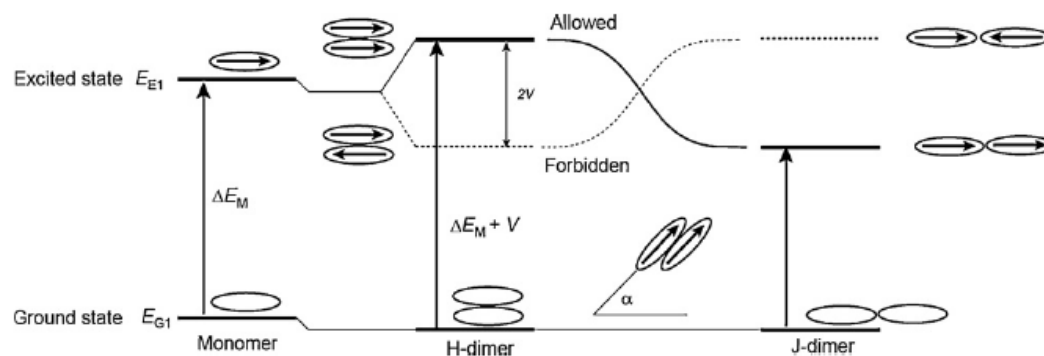
Co-existing excitonic states in alternating, DNA-assembled chromophore stacks

Christian B. Winiger, Simon M. Langenegger, Gion Calzaferri\* and Robert Häner\*

#### 3.1. Introduction

The appearance of excited states of multiple chromophores remains to be fascinating. Still more than 70 years after the pioneering contributions of Scheibe<sup>137</sup>, Davidov<sup>138</sup> and Kasha<sup>139</sup>, the topic is broadly discussed and reviewed in literature in great details. Some consequences and new aspects in multichromophore heteroaromatic stacks will be presented in the following chapter. The electronic transition in a monomer chromophore is represented by a ground and an excited state as shown in Scheme 3.1. A defined energy is used to bring the chromophores into the excited state. In the following considerations the first excited state is meant when speaking of the excited state.

*H. Asanuma et al. / Journal of Photochemistry and Photobiology C: Photochemistry Reviews 13 (2012) 124–135*



**Scheme 3.1** Representation of the excited monomer state and the representative excited dimer states dependent on the angle  $\alpha$  of the two dipole moments.  $\alpha < 54.7^\circ$  result in a J-aggregate whereas  $\alpha > 54.7^\circ$  result in an H-aggregate. In H-aggregates the excited state with higher energy is mostly allowed whereas in J-aggregates the excited state with lower energy is favoured. Taken from Ref. <sup>140</sup>

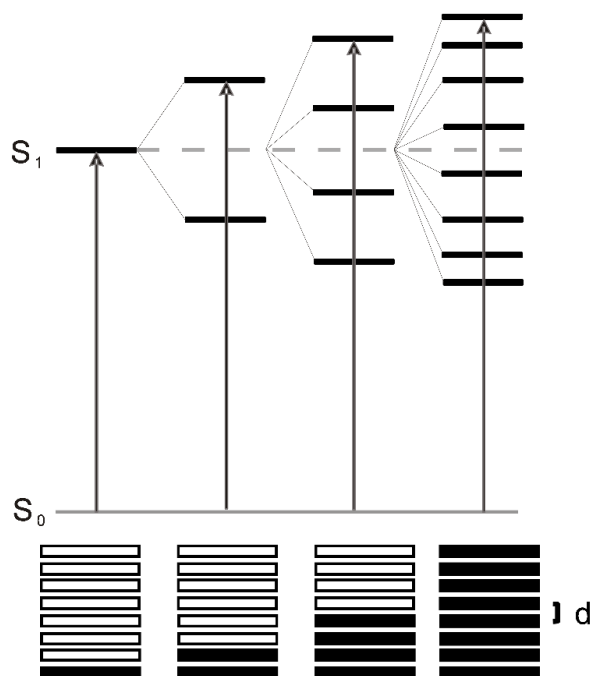
All chromophores have a dipole moment which is represented by the arrow. Forming a dimer with two identical chromophores the angle  $\alpha$  defines the relative orientation of the chromophores toward each other. In case of a  $90^\circ$  angle the dipole moments align as shown on the left side, in a  $0^\circ$  angle the chromophores adopt an arrangement as depicted in the right side of Scheme 3.1. In case of  $\alpha > 54.7^\circ$  we speak of H-dimers (or H-aggregates) whereas in situations  $\alpha < 54.7^\circ$  we

speaking of a J-dimer (or J-aggregate respectively). In both cases the excited energy state is split into two levels. In the case of the H-type arrangement the higher energy level is allowed whereas for the J-type arrangement the lower energy level is allowed. A deductive reasoning and mathematical calculations is given in reference<sup>140</sup>.

### 3.1.1. Considerations of homo-H-aggregates

For the considerations of this part of the thesis it is sufficient to give a more general introduction into relevant aspects of exciton theory. In the following parts the theory is only discussed for H-aggregates.

Interaction of two (identical) chromophores split the energy level of the excited state  $S_1$  into two corresponding excited energy levels. For  $N$  molecules in a stack, the excited energy level is split into  $N$  excited energy states (Scheme 3.2), whereby always the highest energy level is mostly allowed.



**Scheme 3.2** Representation of the splitting of the  $S_1$  level in  $N$  corresponding energy levels upon interaction of  $N$  molecules in an H-aggregate. The most favoured energy level for H-aggregates is shown.

The splitting of the excited energy levels can be calculated using equation [1] and the angle definitions as shown in Scheme 3.3.

$$\varepsilon(j, N) = E_e + 2\beta_c \cos\left(\frac{j}{N+1}\pi\right) \quad [1]$$

$$\beta_c = AD \frac{f}{\bar{\nu}} \frac{\kappa}{d^3} \frac{1}{n^2} \quad [2]$$

$$\kappa = 1 - 3\cos^2\theta \quad [3]$$

$$\text{or} \quad \kappa = (\sin\theta)^2 \cos\phi - 2(\cos\theta)^2 \quad [4]$$

whereby N is the number of interacting molecules

J is the numbering of states

$E_e$  is the reference energy which we choose as being the energy of the  $S_0$ - $S_1$  transition

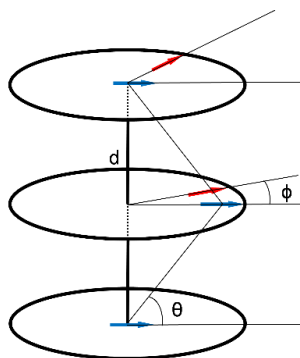
$\beta_c$  is the coulomb interaction (exciton interaction) in  $\text{cm}^{-1}$

f is the oscillator strength

$\bar{\nu}$  is the energy of the  $S_0$ - $S_1$  transition in  $\text{cm}^{-1}$

n is the refractive index which we set to 1.4

AD is equal to  $1.615 \times 10^{-18} \text{ m}^2 \text{ cm}^{-1}$



**Scheme 3.3** Representation of the interaction of three schematical chromophores. Indicated is the dipole moment (arrows). The relative orientation toward each other is represented by the angles  $\theta$  and  $\phi$ . The distance between the molecules is given by d.



$\theta$  defines the angles which arrange the chromophores into H- and J-aggregates. The angle  $\phi$  defines the in plane-rotation.  $f$  and  $\bar{v}$  which define  $\beta_c$  have to be determined spectroscopically.  $d$  is the distance of two chromophores which is set as being 3.5 Å as derived from crystal structures of polyaromatic hydrocarbons<sup>141,142</sup>.  $n$  was chosen as 1.4 which is around the refractive index of aromatic compounds i.e toluene.

A relative splitting pattern can be calculated by setting the reference energy  $E_e = 0$  (will be set to the energy of the  $S_0$ - $S_1$  transition for the absolute calculation) and setting  $\beta_c$  equal to 1.

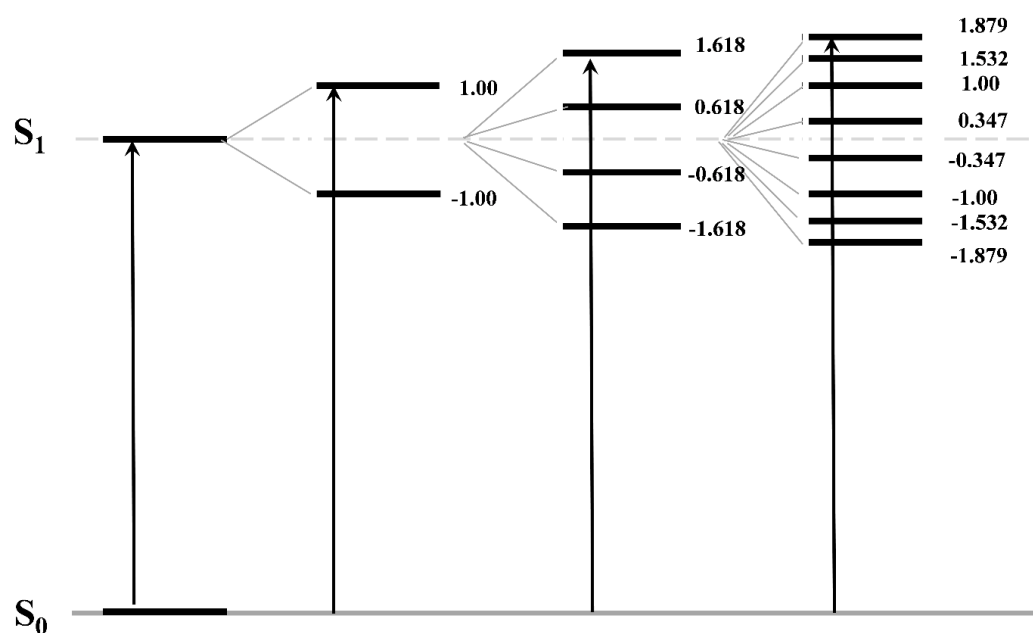
Calculation of the relative splitting pattern in stacks of 2, 4 and 8 chromophores using equation [1] with the above mentioned considerations results in the values in Table 3.1 which are graphically represented in Scheme 3.4.

**Table 3.1** Calculated relative energy levels for 2, 4 and 8 interacting chromophores

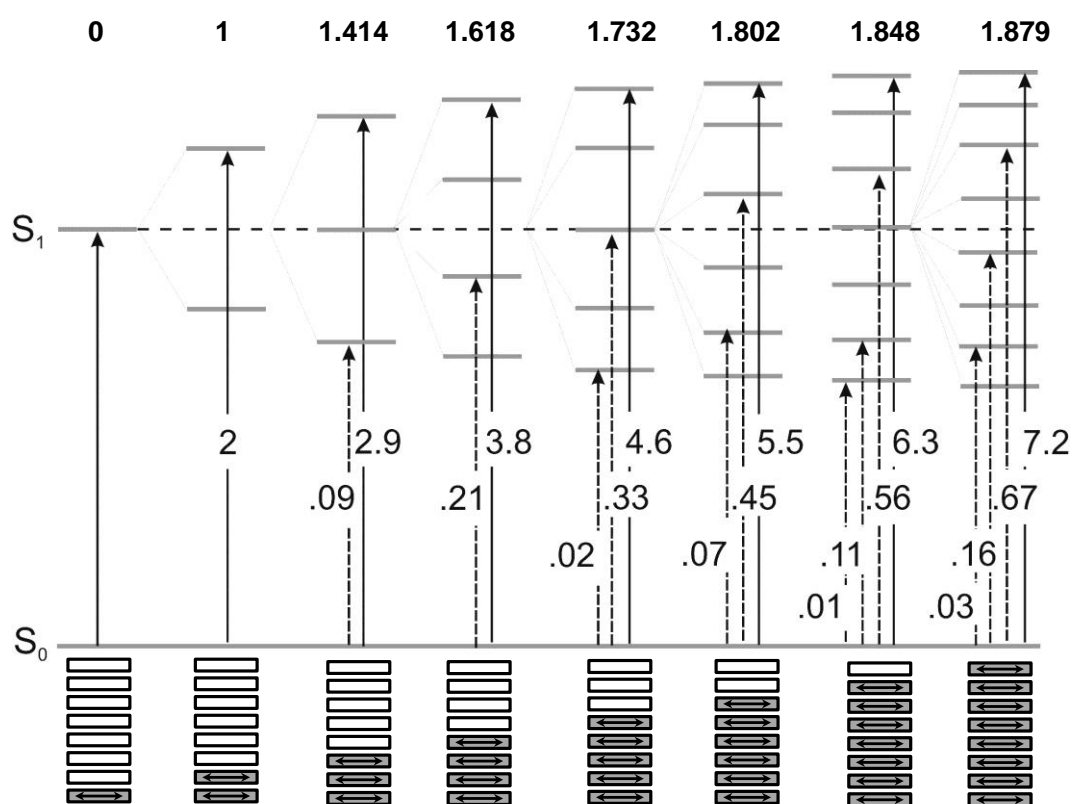
N/j	2	4	8
1	1	1.618	1.879
2	-1	0.618	1.532
3		-0.618	1
4		-1.618	0.347
5			-0.347
6			-1
7			-1.532
8			-1.879

The values of the ETDM (electronic transition dipole moment,  $M^2$ ) are further calculated using equation [5] and are graphically represented in Scheme 3.5 for systems with up to 8 interacting chromophores. The ETDMs represent the probability for the respective transition.

$$M(j) = \mu_a N \sum_{u=1}^N c(j, u) = \mu_a \sqrt{\frac{2}{N+1}} \sum_{u=1}^N \sin(j\pi \frac{u}{N+1}) \quad [5]$$



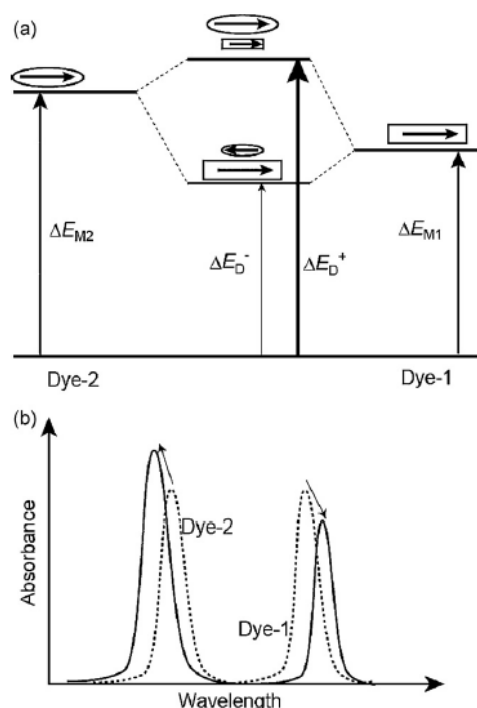
**Scheme 3.4** Representation of the calculated values of the relative exciton interaction. The uppermost excited state is strongly allowed whereas the lower states are either forbidden or weakly allowed. Values for the split exciton levels were obtained by using  $\beta_{(c,rel)} = 1$  and  $E_e$  equal to 0 (will later be set to the reference energy of the  $S_0$ - $S_1$  transition).



**Scheme 3.5** Representation of the calculated values of the relative exciton interaction and the corresponding ETDMs. The uppermost excited state is strongly allowed whereas the lower states are either forbidden or weakly allowed.

### 3.1.2. Considerations on hetero-H-aggregates

Hetero - H aggregates are formed when two or more different molecules stack in a face-to-face  $\pi$ - $\pi$  manner. The theory therefore predicts an energy splitting for the two dyes as shown in Scheme 3.6. Asanuma et al. derive mathematical considerations of the theory in their 2012 Journal of Photochemistry and Photobiology Review. They summarize: The absorption band for the dye with the longer wavelength is shifted hypochromically and bathochromically whereas the dye with the shorter band is shifted hyperchromically and hysochromically. “*These spectral changes relative to the isolated dyes become smaller when the gap of  $\lambda_{max}$  is larger, and thus two dyes behave like isolated ones. In contrast, maximum coherent interaction is expected with  $\Delta\lambda_{max} \cong 0$ . In this case, its spectroscopic behaviour should become similar to that of the homo H-dimer*”<sup>140</sup>. Asanuma et al. reported on hetero-H-aggregate which was characterized by one single sharp new absorption band which appeared after formation of the aggregate<sup>143</sup>. Elucidation of the detailed contributions of the interactions of multiple different chromophores is still a tricky task and predictions on energetic and spectroscopic aspects still difficult to achieve. Only few methodologies are available for a proper formation of hetero-H-aggregates and only few experiments are described in literature<sup>144</sup>. Detailed studies are important to gain further insight into this topic.



**Scheme 3.6** Theoretical considerations of the interaction of two chromophores forming a hetero-H-aggregate. The absorption band of the chromophore at higher energy is shifted hypsochromically (blueshift) whereas the chromophore at lower energy is shifted bathochromically (redshift). According to Ref <sup>140</sup>.

## 3.2. Aim of the work

The DNA assisted assembly of chromophores allows us to arrange chromophores in a well-defined way. Many different arrangements of dialkynylpyrene and PDI molecules were realized during the course of work. These hybrids features different sequences of pyrene and PDI molecules with dependent distances toward each other, thereby forming homo-H-aggregates in case of molecular stacks of same molecules and hetero-H-aggregates in case of different molecules interacting with each other. Dialkynylpyrenes and PDI's turned out to be the perfect molecules for interaction studies as their vibronic fine structure is well resolved. Furthermore, the absorption spectra of the transition under study ( $S_0$ - $S_1$ ) does not overlay between the pyrene and the PDI.

The obtained spectroscopic data of the hybrids is compared with derivations of the exciton theory. Thereby special focus was set on hetero-H-aggregates. Defined hetero-H-aggregates are rare in literature due to the difficulties of their preparation<sup>140,143</sup>. The exciton theory was expanded to these kinds of aggregates. The existing theories on hetero-H-aggregates are discussed controversial and new conclusions derived from the exciton theory are presented.

## 3.3. Results and Discussion

### 3.3.1. Absorption spectra of the monomeric chromophores

The spectra of mono-DMT-PDI in a 1:1 mixture of THF/ $H_2O$  and a spectra of 1,8-dialkynylpyrene diol in EtOH were used as reference spectra. The focus of this chapter is set on the  $S_0$ - $S_1$  transition of the respective molecule (Figure 3.1). The four vibronic fine structures of the PDI and the dialkynylpyrene are resolved with the maximal absorption of the PDI monomer at 526 nm and for dialkynylpyrene at 387 nm. From the monomer spectra the oscillator strength of PDI and dialkynylpyrene was calculated to be 0.76 for PDI and 0.49 for dialkynylpyrene.

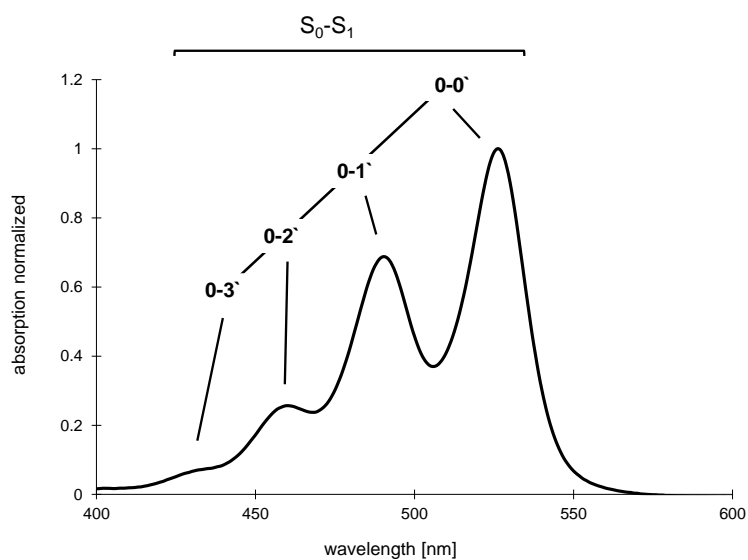


**Figure 3.1** Absorption trace of the PDI molecules (functionalized with the DMT protecting group) in a 1:1 mixture of THF and water. The spectra is normalized to the absorption of the 0-0' band.

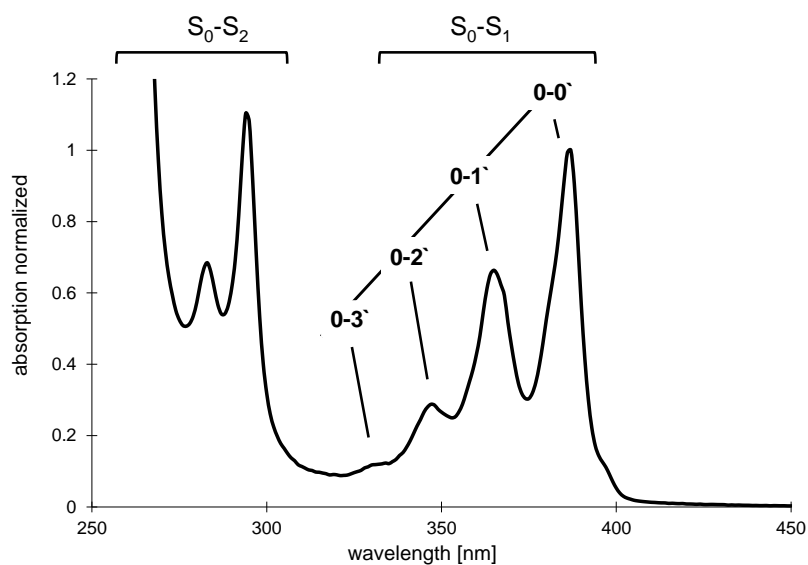


**Figure 3.2** Absorption spectra of pyrene diol in EtOH. The spectra is normalized to its 0-0' absorption band.

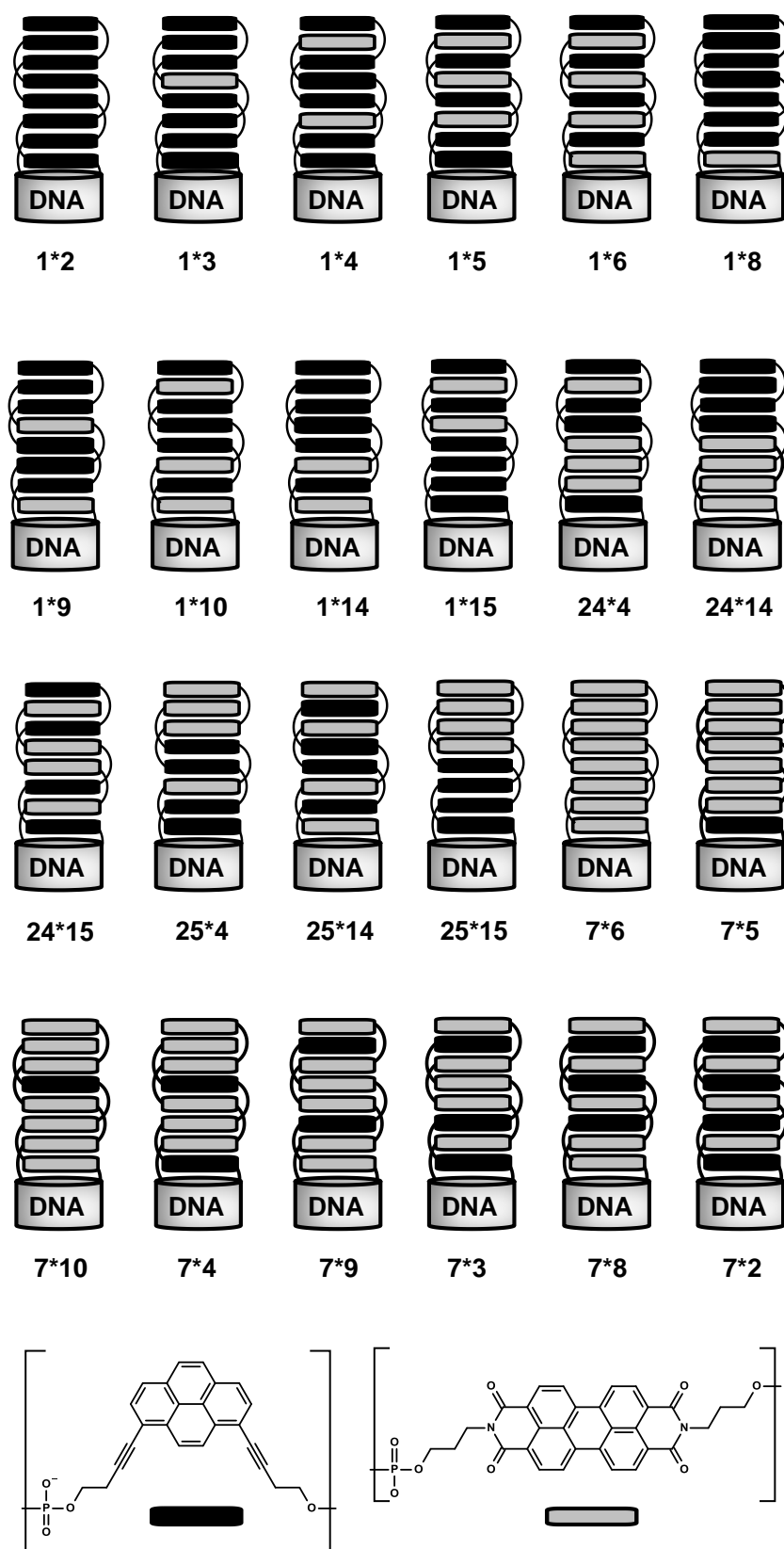
### 3.3.1. Duplexes under investigation

Duplexes under investigation are shown in Table 3.2 and Scheme 3.7.

### 3.0. Observation of two independent H-couplings in a stack of multiple chromophores

**Table 3.2** Sequence of the oligomers containing **Y** and **E**,  $T_m$  values and number of aromatic donor-acceptor interaction of the duplexes under investigation. Conditions same as in Table 2.2.

Ref	Sequence	$T_m$ (°C)	Number of aromatic donor-acceptor interactions
	5' GCGTTA 3' CGCAAT	13.0	
1 2	5' GCGTTA <b>YYYY</b> 3' CGCAAT <b>YYYY</b>	50.5	0
1 3	5' GCGTTA <b>YYYY</b> 3' CGCAAT <b>YYEY</b>	54.5	2
1 4	5' GCGTTA <b>YYYY</b> 3' CGCAAT <b>YEYE</b>	58.5	4
1 5	5' GCGTTA <b>YYYY</b> 3' CGCAAT <b>YEEE</b>	61.0	6
1 6	5' GCGTTA <b>YYYY</b> 3' CGCAAT <b>EEEE</b>	64.5	7
1 8	5' GCGTTA <b>YYYY</b> 3' CGCAAT <b>EYYY</b>	58.6	1
1 9	5' GCGTTA <b>YYYY</b> 3' CGCAAT <b>EYEY</b>	62.1	3
1 10	5' GCGTTA <b>YYYY</b> 3' CGCAAT <b>EYEE</b>	65.6	5
1 14	5' GCGTTA <b>YYYY</b> 3' CGCAAT <b>EYYY</b>	63.6	3
1 15	5' GCGTTA <b>YYYY</b> 3' CGCAAT <b>YYEE</b>	64.1	4
24 4	5' GCGTTA <b>EYYY</b> 3' CGCAAT <b>YEYE</b>	49.5	4
24 14	5' GCGTTA <b>EYYY</b> 3' CGCAAT <b>EYYY</b>	45.5	1
24 15	5' GCGTTA <b>EYYY</b> 3' CGCAAT <b>YEEE</b>	55.0	6
25 4	5' GCGTTA <b>YYEE</b> 3' CGCAAT <b>YEYE</b>	49.5	3
25 14	5' GCGTTA <b>YYEE</b> 3' CGCAAT <b>EYYY</b>	49.5	6
25 15	5' GCGTTA <b>YYEE</b> 3' CGCAAT <b>YEEE</b>	55.0	1
7 6	5' GCGTTA <b>EEEE</b> 3' CGCAAT <b>EEEE</b>	52.0	0
7 5	5' GCGTTA <b>EEEE</b> 3' CGCAAT <b>YEEE</b>	48.7	1
7 10	5' GCGTTA <b>EEEE</b> 3' CGCAAT <b>EYEE</b>	37.9	2
7 4	5' GCGTTA <b>EEEE</b> 3' CGCAAT <b>YEYE</b>	47.1	3
7 9	5' GCGTTA <b>EEEE</b> 3' CGCAAT <b>EYEY</b>	50.0	4
7 3	5' GCGTTA <b>EEEE</b> 3' CGCAAT <b>YYEY</b>	59.8	5
7 8	5' GCGTTA <b>EEEE</b> 3' CGCAAT <b>EYYY</b>	58.8	6
7 2	5' GCGTTA <b>EEEE</b> 3' CGCAAT <b>YYYY</b>	66.5	7



**Scheme 3.7** All duplexes depicted which are described in the following section.

### 3.3.2. Absorption spectra of the monomer chromophores in the aromatic stack

Duplex **1\*3** contains one PDI molecule embedded in a stack of 7 dialkynylpyrene molecules. The absorption spectra of this duplex is measured and the absorption of the PDI normalized to 1. The PDI absorption spectra of duplex **1\*3** is red-shifted compared to the monomer PDI molecule in THF/water (Figure 3.3). This red-shift could be explained by the different dielectric constant of the surrounding environment. For a spectra comparison the normalized absorption spectra of the monomer PDI molecule in THF/water mixture is 30 nm red-shifted to get a perfect overlay of the vibronic fine structures of the monomer PDI and the PDI absorption in the aromatic stack (Figure 3.4). In the stacked PDI a broadening of the absorption band is visible. The broadening is caused by the superposition of molecules experiencing minor different interaction with the pyrene environment which are larger than in a diluted homogeneous solution<sup>145</sup>. The  $S_1^{0-0}$ , the  $S_1^{0-1}$  and  $S_1^{0-2}$  vibronic structures are visible (the latter one as a very weak shoulder) whereas the  $S_1^{0-3}$  vibronic band is hidden.

In the same way the absorption of duplex **7\*10** was measured, the pyrene absorption normalized and compared with the absorption of the monomeric dialkynylpyrene (Figure 3.5). A shift of 5 nm to the pyrene absorption in duplex **7\*10** was extracted which leads to the maximal absorption at 387 nm. The vibronic transitions  $S_1^{0-0}$  and  $S_1^{0-1}$  are visible whereas the transitions  $S_1^{0-2}$  and  $S_1^{0-3}$  are hidden (Figure 3.6). The broadening of the pyrene absorption trace is quite pronounced.

The length of the electronic dipole moment was determined to be 0.19 nm for PDI and 0.13 nm for pyrene.<sup>146</sup>

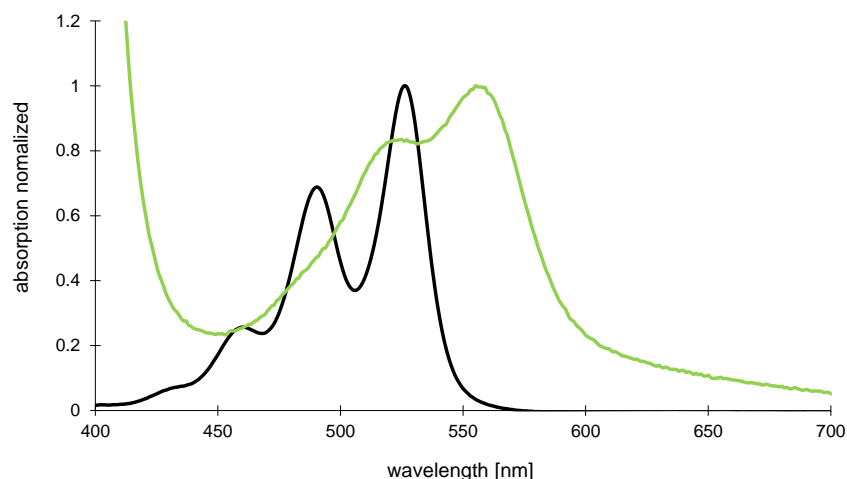


**Figure 3.3** Absorption of the PDI monomer (black) and a single incorporation of the PDI in a stack consisting of only pyrenes (duplex **1\*3**, green).



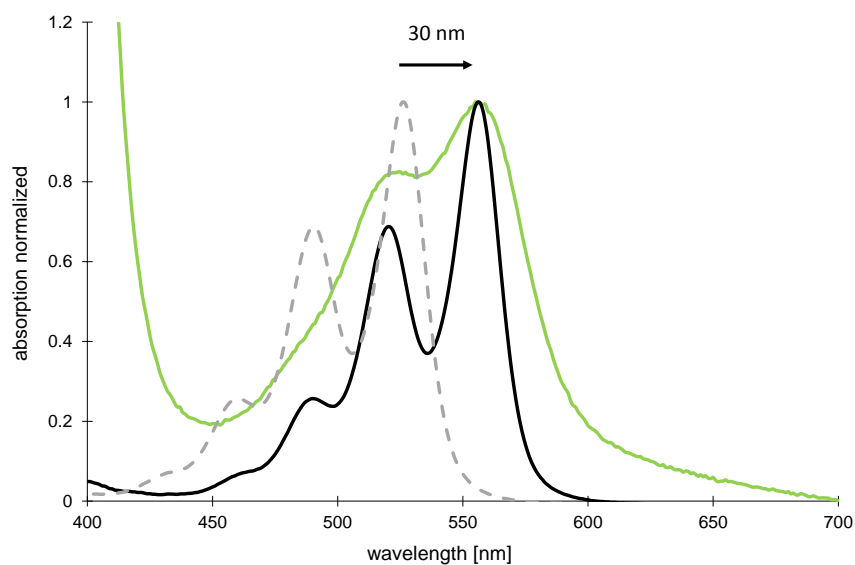


**Figure 3.4** Absorption of the PDI monomer (dotted) and the monomer spectra shifted by 30 nm (black). The Vibronic fine structures perfectly overlap the absorption of the PDI molecule incorporated into the DNA. The vibronic fine structure band of 0-3' is hidden.

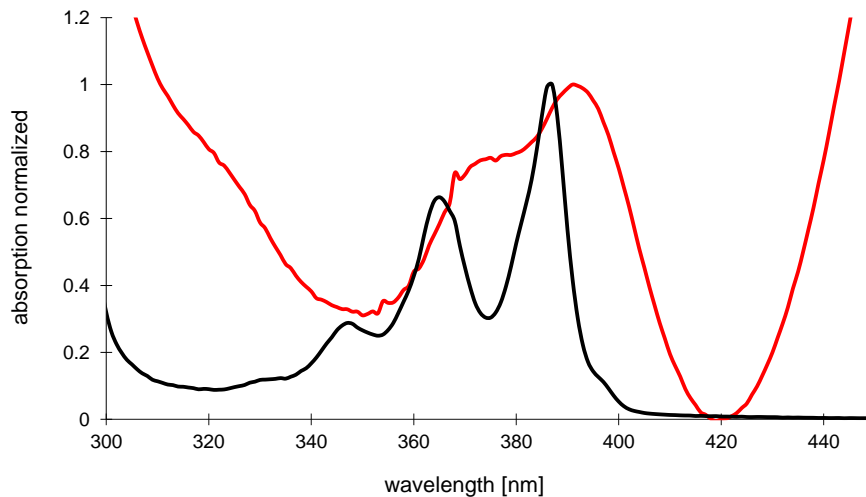


**Figure 3.5** Absorption of the pyrene monomer (black) and a single incorporation of the pyrene in a stack consisting of only PDIs (duplex 7\*10, red).

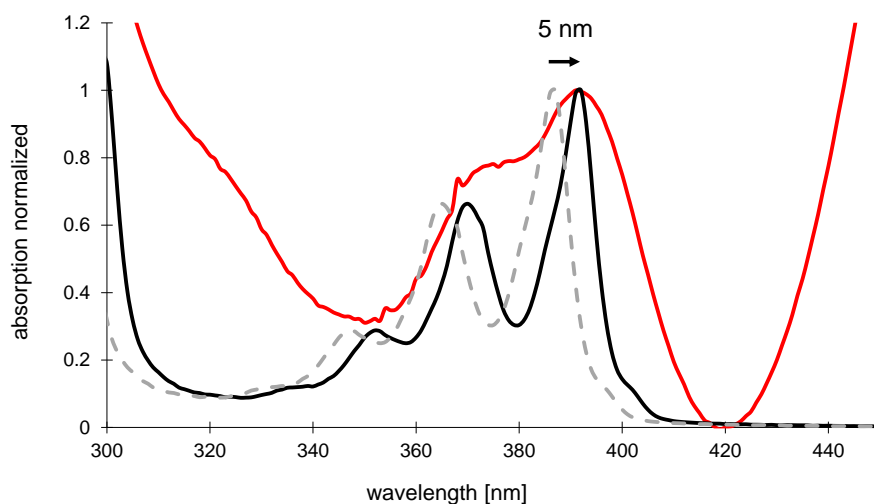


**Figure 3.6** Absorption of the pyrene monomer (dotted) and the monomer spectra shifted by 5 nm (black). The vibronic fine structures perfectly overlap the absorption of the pyrene molecule incorporated into the DNA. The vibronic fine structure of the absorption band 0-2' and 0-3' are hidden.

### 3.3.3. PDI and pyrene chromophores with nearest neighbour interactions

For all following measurements the absorption traces were normalized to 1 at their highest absorption. The absorption trace of 1 PDI molecule embedded in a stack of pyrene molecules is compared with stacks of 4, 7 and 8 adjacent PDI molecule (Figure 3.7). The same experiment was performed using duplexes which contain one dialkynylpyrene embedded in a stack of PDI molecules as well as 4, 7 and 8 adjacent dialkynylpyrene molecules in a stack (Figure 3.8). This represents a situation where we have a splitting of the energy levels into 4, 7 and 8 excited states. The respective absorption band in the spectra are shifted toward higher energy. In case of the PDI we see a shift of 45 nm (from 555 nm to 510 nm) in the case of the 4 PDI stack and a shift of 73 nm (from 555 nm to 482 nm) in the case of the 8 PDI stack. For the dialkynylpyrene these shifts account with 23 nm (from 391 nm to 368 nm) in the stack of 8 dialkynylpyrenes and an increased absorption of the band at 370 nm (shifted 21 nm) in the stack of 4 dialkynylpyrenes. The increased absorptivity at higher energy with increasing numbers of molecules in the stack is a clear indication for the formation of H-aggregates. The measured spectra meet the expectations predicted by the exciton theory (Scheme 3.8).

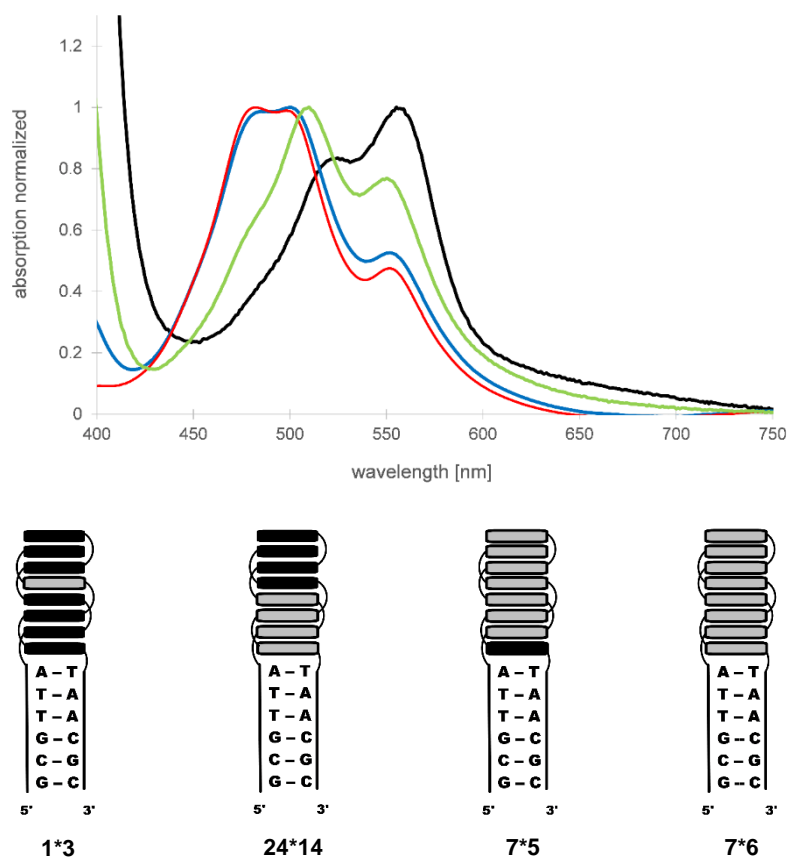
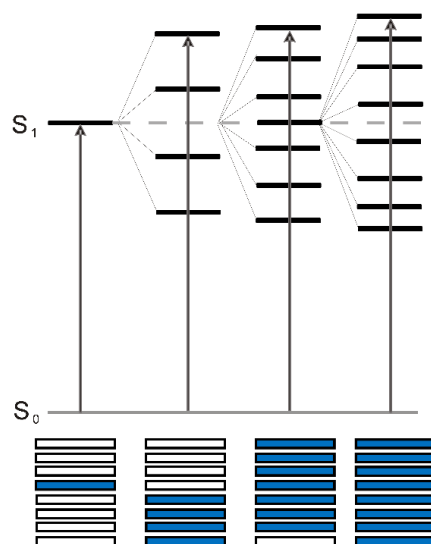


**Figure 3.7** Absorption and schematically representation of hybrids where 1 (black), 4 (green), 7 (blue) or 8 (red) PDI molecules are aligned in an aromatic stack (nearest neighbour interaction). An increasing blue-shift is visible upon interaction of an increasing amount of PDI molecules.



**Scheme 3.8** Graphical illustration of the energy levels in the above realized aromatic stacks. Interaction of up to 8 chromophores leads to the splitting of the  $S_1$  excited state into 8 energy levels. The absorption band is shifted toward higher energy (blue-shift).

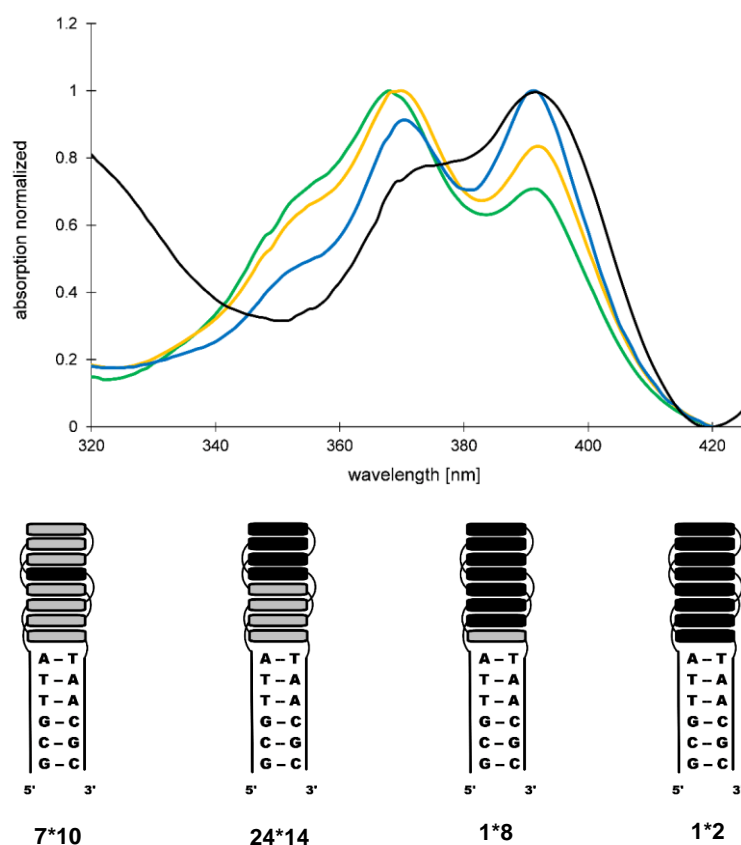


**Figure 3.8** Absorption and schematically representation of hybrids where 1 (black), 4 (blue), 7 (yellow) or 8 (green) pyrene molecules are aligned in an aromatic stack. An increasing blue-shift is visible upon interaction of an increasing number of pyrene molecules.

### 3.3.4. PDI and pyrene molecules with different distance $d$ toward each other

Further systems are evaluated to gain information on the exciton coupling in hetero  $\pi$  stacks and the coupling of molecules which are separated by other interdigitating molecules. Therefore the series in Figure 3.9 was evaluated. The absorption spectra of a single PDI molecule in a stack of dialkynylpyrenes was compared with different arrays whereby two PDI molecules are separated by either three, two or none pyrenes. The same experiment was performed with two dialkynylpyrene molecules separated by different numbers of PDIs. It thereby has to be mentioned that certain arrays (“sequences”) of chromophores could not have been realized with the oligomers synthesized. Apparent no duplex could be realized which contains only two adjacent PDI molecules (or two pyrene molecules). This molecular architecture was replaced by arrays which show a similar geometry i.e. duplex **24\*4**. Focusing on Figure 3.9 we see that the PDI molecules – even though that the molecules in the series are separated by dialkynylpyrene molecules – show H-aggregate character. This is an indication that the PDI molecules form excited states without directly stacking with each other. The formation of H-aggregate excited states is characterized by a blue-shift of the most intense absorption band compared to the monomeric PDI absorption band depicted in black in Figure 3.9.

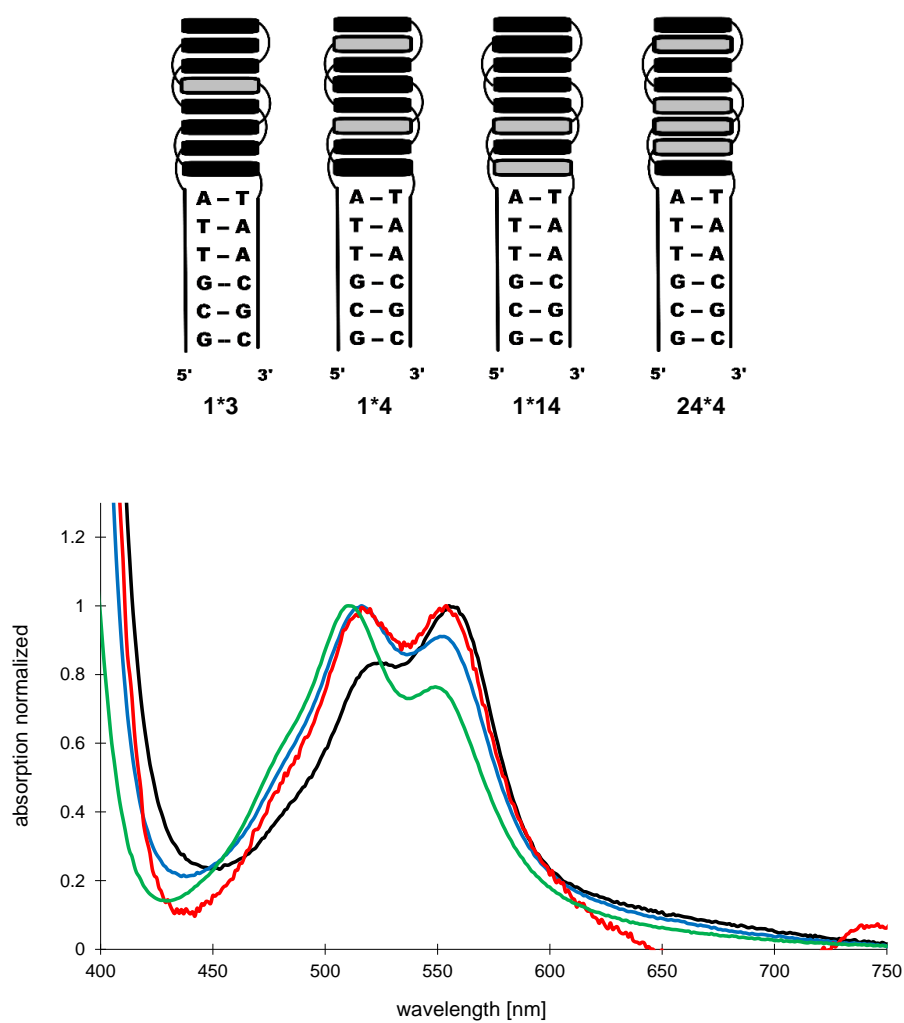


**Figure 3.9** 1\*3 (black), 1\*4 (red), 1\*14 (blue), and 24\*4 (green) to represent PDI molecules approaching themselves.

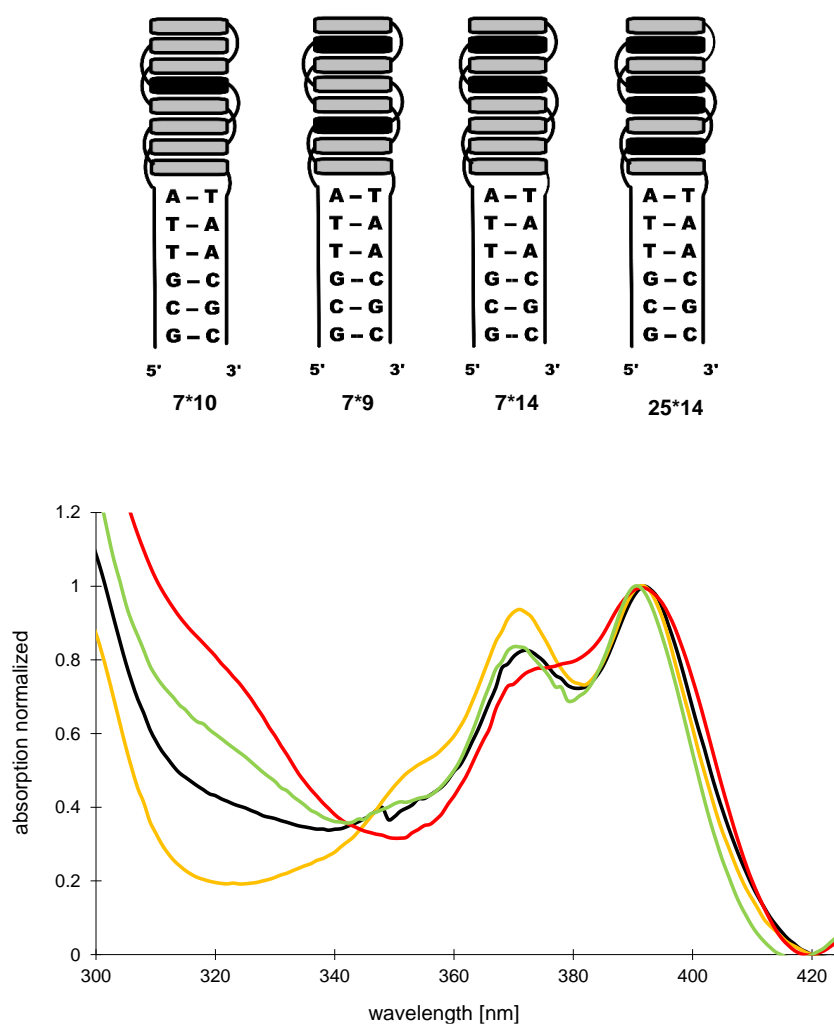
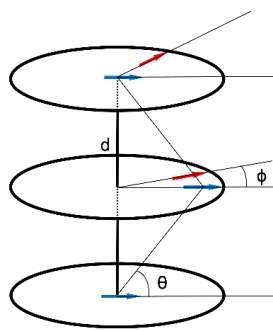


**Figure 3.10** 7\*10 (red), 7\*9 (black), 7\*14 (light green) and 25\*14 (orange) to represent pyrenes molecules approaching themselves.

### 3.3.5. Relative angles of different interacting dipole moments

It has to be mentioned at this point that certain geometries of arranged chromophores show different absorption spectra even though the distance of the chromophores between each other is the same. Exemplarily the two duplexes **1\*4** and **1\*9** or duplexes **1\*14** and **1\*15** are shown in Figure 3.11, whereby duplex **1\*9** is the only duplex measured which deviates strongly from theory and shows a total unpredictable absorption spectra. One explanation for deviating observation could be the relative orientation of the dipole moments (Scheme 3.9) toward each other<sup>147</sup>. In all the data shown in this chapter we assume (and the data confirms) an angle  $\theta$  which is not smaller than  $70^\circ$  and an angle  $\phi$  which is zero. Equations [2] and [4] correlate the angles with the exciton interaction. Different angles  $\theta$  and  $\phi$  would lead to an uncoupling of the chromophores and therefore from theory differentiating absorption spectra would be measured.



**Scheme 3.9** Representation of the interaction of three schematical chromophores. Indicated is the dipole moment (arrows). The relative orientation toward each other is represented by the angles  $\theta$  and  $\phi$ . The distance between the molecules is given by  $d$ .

All chromophores in our supramolecular stacks are linked by short flexible linkers which prealign the chromophores. Previous studies with extended aromatic stacks showed that the helicity of the DNA strand induces a helicity in the extended aromatic stack<sup>102</sup>. Similar twisting could lead to an uncoupling of the dipole moments of the molecules in our architectures. It has to be kept in mind that each duplex exhibits a different architecture and therefore a potentially different twisted arrangement. CD measurements could result in more information for the degree in exciton interaction of two or more molecules.

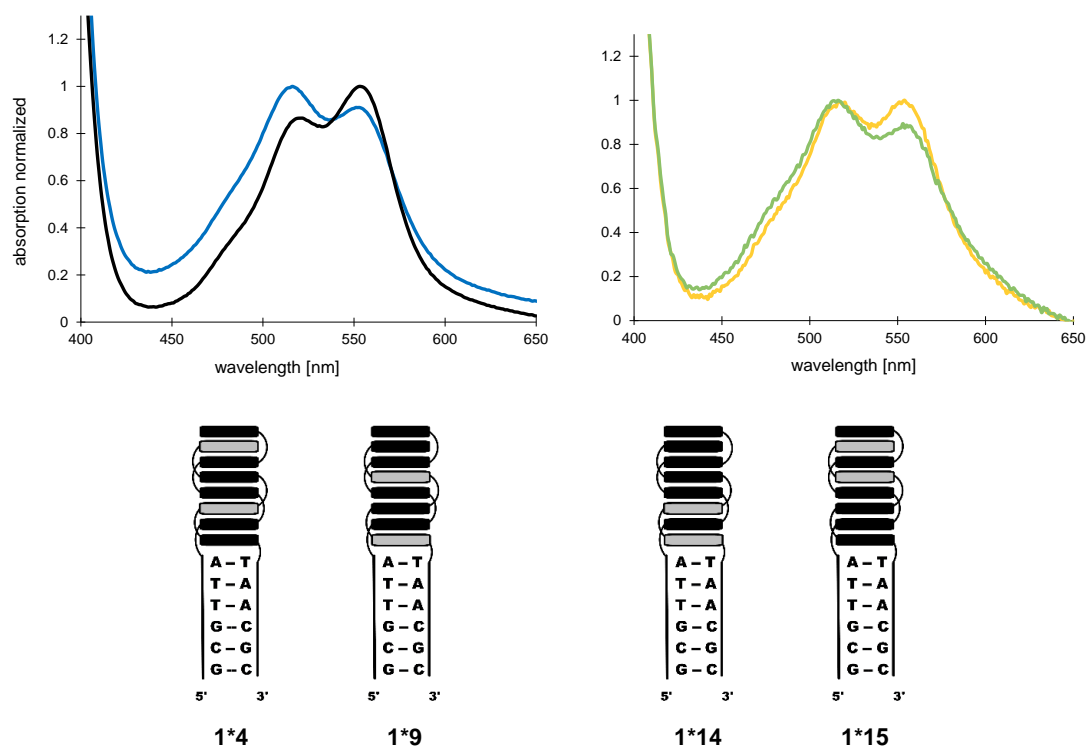


**Figure 3.11** Left: duplexes **1\*4** (blue) and duplex **1\*9** (black) and right duplex **1\*14** (yellow) and duplex **1\*15** (slight green).

### 3.3.6. Increasing numbers of next-nearest PDI and pyrene interactions

The above depicted results indicate that there is a substantial degree of H-coupling of molecules which do not interact directly. This effect is further investigated by measuring duplex systems containing stacks of dialkynylpyrenes whereby more and more PDI molecules were incorporated. Thereby the PDI molecules are always separated by interdigitating pyrene molecules (Figure 3.12). The same setup was also performed using stacks of PDI molecule and increasing amounts of dialkynylpyrenes (Figure 3.13).



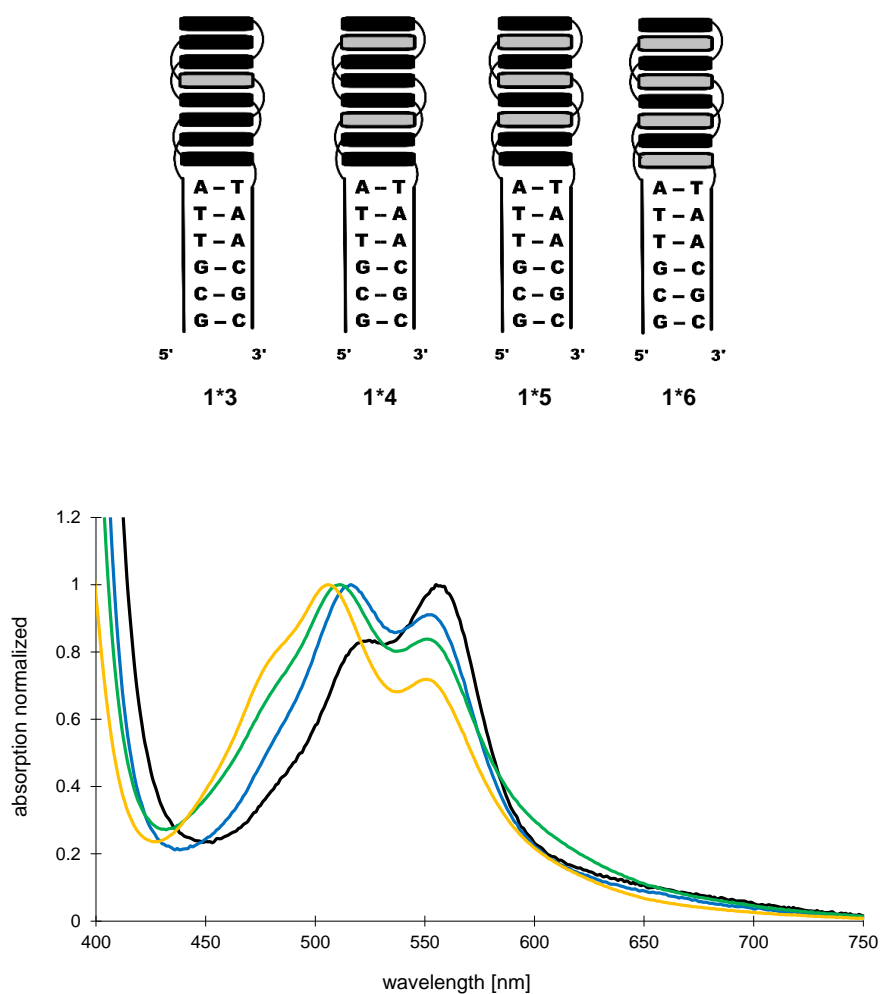


**Figure 3.12** Representation and absorption trace of duplexes **1\*3** (black), **1\*4** (blue), **1\*5** (green) and **1\*6** (yellow). Increasing numbers of next-nearest neighbour interactions shift the absorption spectra to higher energies.

The absorption spectra show an increasing amount of the blue-shifted absorption band which indicates an increasing amount of H-aggregate the more PDI molecules are inserted into the enlarged aromatic stack. The data strongly supports the hypothesis that within one aromatic stack all chromophores of the same nature interact with each other and form H-aggregates without being in direct contact with each other. This same behaviour could also be seen in the case where more and more pyrene molecules are inserted in a stack of PDI molecules.

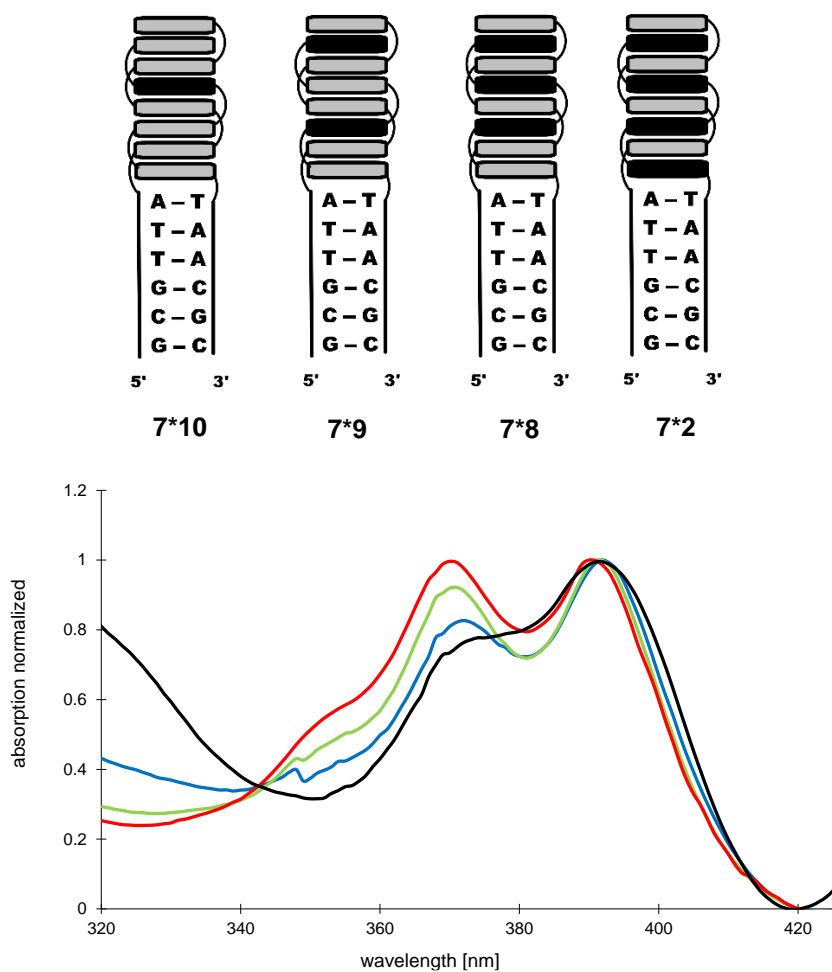
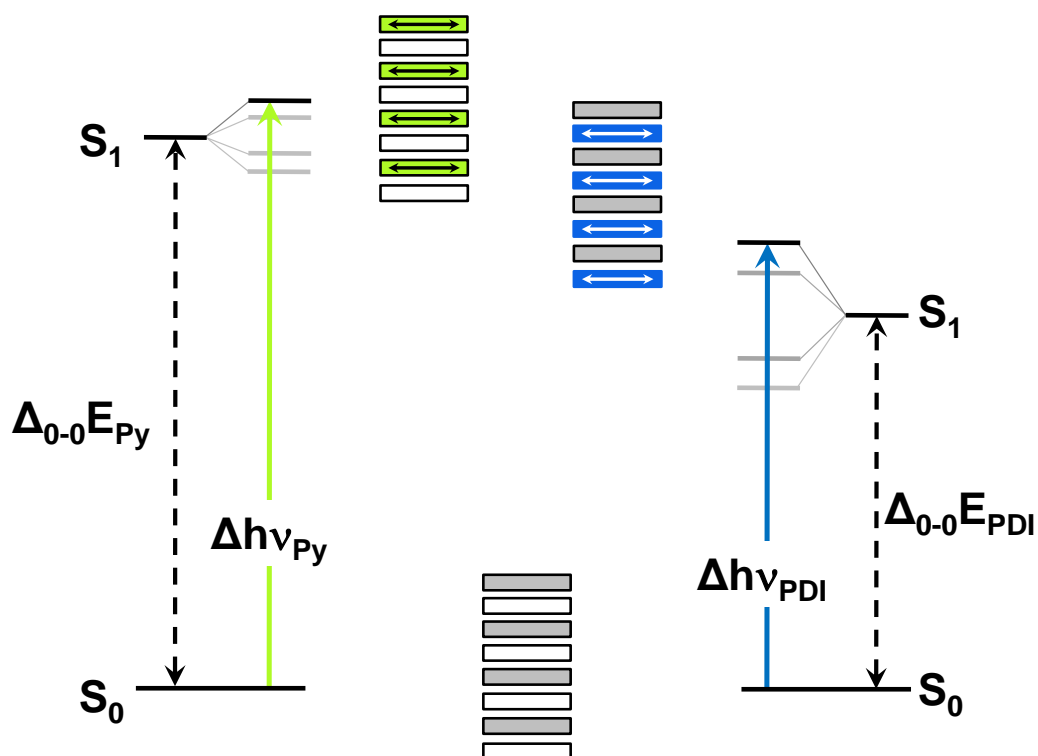


**Figure 3.13** Representation and absorption trace of duplexes **7\*10** (black), **7\*9** (blue), **7\*8** (green) and **7\*2** (red). Increasing numbers of next-nearest neighbour interactions shift the absorption spectra to higher energies.

The excitonic interaction increases in both setups until a system with alternating PDI-pyrene interactions is reached. In these alternating systems an independent excitonic coupling of the pyrene molecules is observed as well as an independent PDI coupling. This led to the conclusion that two H-excitons exist in the same volume but built by different chromophores at different energies.



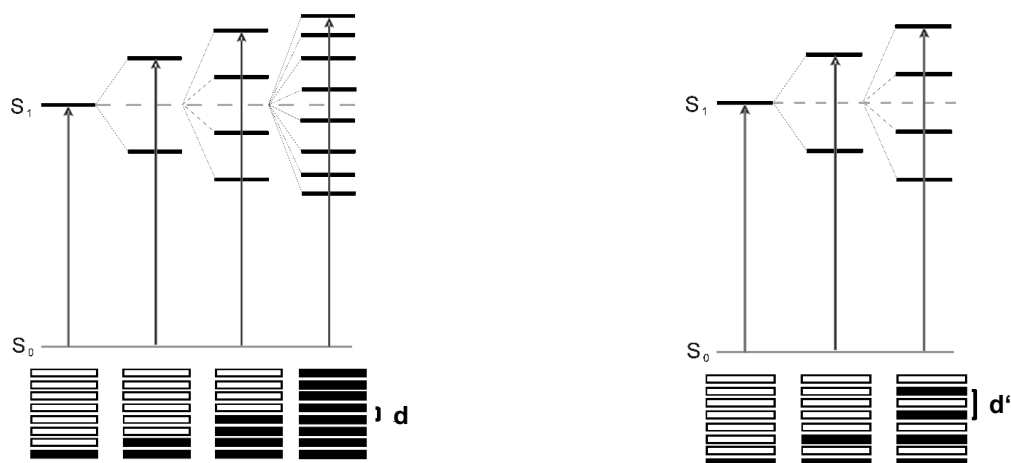
**Scheme 3.10** Representation of the two co-existing excited states within one alternating PDI-pyrene stack. The particular energy diagram is shown. The energy levels are not in scale.

The respective energy diagram would look like depicted in Scheme 3.10. The two independent H-excited states shown in green and blue exist in the same stack of aromatic molecules but do not interfere with each other.

The classical exciton theory could be adapted to explain the findings. Theoretical considerations of the exciton model consider chromophores which are in close contact. In the case of the alternating chromophore stacks the interacting molecules are separated by the distance of two aromatic molecules which is considered to be 0.7 nm. The respective exciton interaction  $\beta_c$  therefore change by the factor of  $\frac{1}{2^3} = \frac{1}{8}$ . The splitting for the arrangement with two, and 4 alternating stacked PDI chromophores is shown in Table 3.3 and Scheme 3.11.

**Table 3.3** Calculated and measured splitting of the highest excited energy levels for situations with 2, 4 and 8 interacting chromophores. Calculations by Prof. G. Calzaferri.

# chromophores interacting	nearest neighbour		Next-nearest neighbour	
	calculated [cm <sup>-1</sup> ]	measured [cm <sup>-1</sup> ]	calculated [cm <sup>-1</sup> ]	measured [cm <sup>-1</sup> ]
2	1596	1670	1020	1360
4	2600	1670	1650	1800
8	3000	2800	-	-

**Scheme 3.11** Left: Energy diagram of 1 to 8 chromophores interacting in a nearest neighbour manner. Right: 1 to 4 chromophore interacting in a next-nearest neighbour manner. For the next-nearest neighbour interaction, the distance  $d$  is doubled.

The H-aggregates in next-nearest neighbour situations develop in analogy to the classical exciton theory. This is a most logical and straight forward consideration of the classical exciton theory and explains the formation of H-aggregates in alternating stacked chromophore assemblies.

## 3.3.7. Titration experiment of pyrene-pyrene interactions

Titration experiments leading to duplexes **1\*2**, **1\*6**, **7\*2** and **7\*6** also show the development or the partial destruction of the H-aggregates in different situations with homo-aggregates or alternating hetero-aggregates. Due to the hydrophobic effect the aromatic molecules are already stacked face-to-face in a single stranded oligomer. After adding an oligomer with complementary DNA sequence the duplex is formed. Thereby the aromatic compounds stack in an alternating manner due to the rigidity of the linkers between the aromatic compounds. A schematic representation thereof could look like following (Figure 3.14):

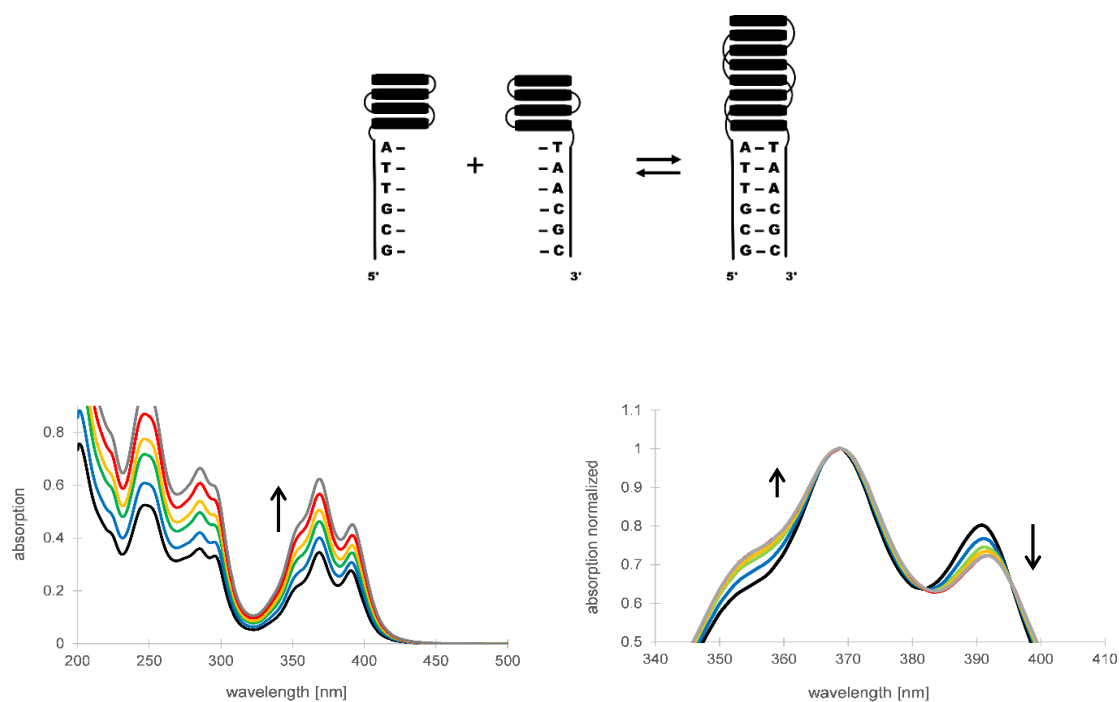


**Figure 3.14** Schematic representation (top) and absorption trace (bottom) of a titration experiment of two strands each containing four pyrenes (black). Bottom right: the absorption trace was normalized to 1.

Adding oligomer **2** to a solution containing oligomer **1** increases the fraction of stacks which form H-aggregates containing 8 dialkynylpyrene molecules. The development of a stronger H-aggregate is seen by the development of a more pronounced absorption band at 370 nm (reduction of intensity at 390 nm) and increase at 355 nm.

### 3.3.8. Titration experiment of PDI-PDI interactions

A similar titration experiment can be performed with two PDI containing oligomers. Thereby oligomer **6** was added in steps to a solution containing oligomer **7**.

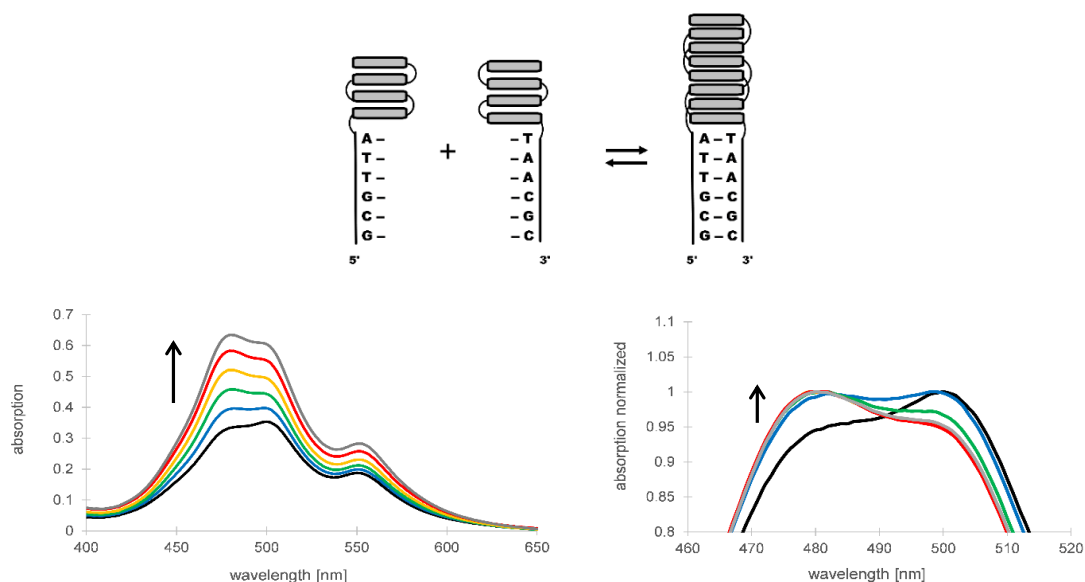


**Figure 3.15** Schematic representation (top) and absorption trace (bottom) of a titration experiment of two strands each containing four PDI molecules (grey). Bottom right: the absorption trace was normalized to 1.

The normalized spectra shows an increase of the absorption band at 482 nm. Whereas in the four PDI containing single strand the absorption at 482 nm shows a shoulder, the absorptivity increases steadily during the titration and lead finally to the most prominent absorption band in this area. Increase of the absorption at 550 nm is only minor in comparison with the increase at 500 nm and 482 nm which indicates that the PDI molecules form tight H-aggregates, thus have a blue shifted absorption. In the upper two titrations we looked at the formation of H-aggregates (increasing stack of the same molecules).

## 3.3.9. Next-nearest neighbour interaction titration PDI-pyrene

In the next two cases we focus on systems where we partially destroy H-aggregates by selectively interdigitate molecules of a different character which leads to H-aggregates with a larger distance  $d$ . Interdigitating the dialkynylpyrenes into the PDI molecules separated them to a distance of  $2d$  (Figure 3.16).

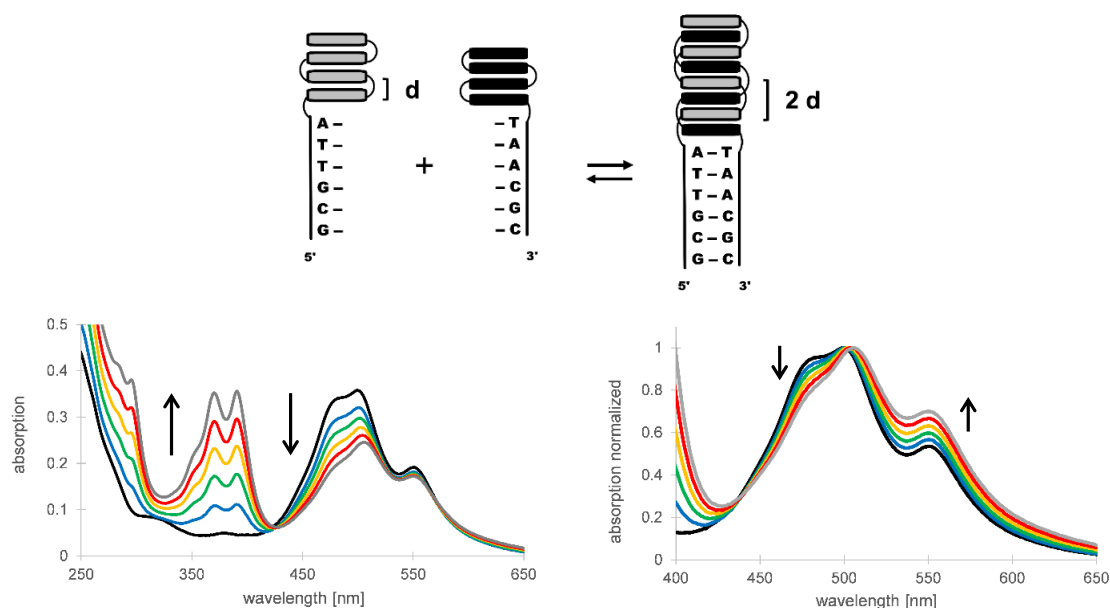


**Figure 3.16** Schematic representation (top) and absorption trace (bottom) of a titration experiment of a strand containing four pyrenes (black) to a DNA strand containing four PDIs (grey). Bottom right: the absorption trace was normalized to 1.

Addition of pyrene containing oligomer **2** leads to a linear increase of the absorption of the pyrene as well as a reduction of the absorption of PDI. The intensity of the band at 482 nm decreases until it remains a slight shoulder at equal quantities of PDI and pyrene containing strands. We assigned this band at 482 nm as a typical H-aggregate band (see titration experiment on top). The reduction of the absorption at 500 nm (respectively reduced in respect to the absorption band at 550 nm) is another sign for a reduced H-aggregate character caused by the separation of the PDI molecules by interdigitating pyrene molecules.

This exact result is also obtained by titration of a dialkynylpyrene containing oligomer **1** with PDI containing oligomer **6** (Figure 3.17). Increasing concentrations of PDI-oligomer added leads to a decreased pyrene absorption at 370 nm. At final equal concentrations of strand **1** and **6** the absorption intensity of the pyrene at 370 nm and 390 nm is the same. This titration experiments show in a simple and effective way the development of H-aggregates in stacks of pyrene, PDI and alternating systems.

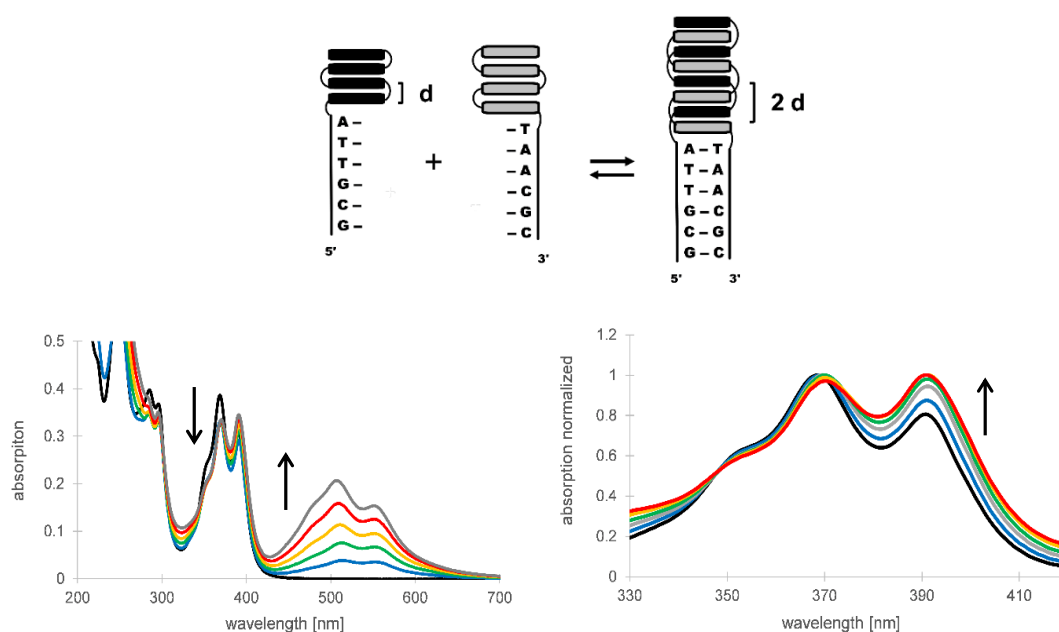


**Figure 3.17** Schematic representation (top) and absorption trace (bottom) of a titration experiment of a strand containing four PDIs (grey) to a DNA strand containing four pyrenes (black). Bottom right: the absorption trace was normalized to 1.



### 3.3.10. General considerations on pyrene fluorescence and quenching by PDI – development of other alternating chromophore systems

Pyrene molecules which form H-aggregated excited states show typical excimer fluorescence<sup>74,103</sup>. It was also reported by our group that PDI molecules can very efficiently quench the pyrene fluorescence<sup>107,110</sup>. It was assumed that the interdigitating PDI molecule prevents the formation of a pyrene excimer. This above shown data rise new questions on the interaction of molecules and their properties. The above stated H-exciton of non-aggregated molecules would also predict the formation of excited states (also excited dimers or excited multimers) independent whether the molecules under investigation are separated by further different molecules with different energies. This would draw the quenching mechanism of pyrenes and PDIs away from an “intercalating” one toward general EET quenching. Especially in PDI-pyrene systems the quenching mechanism is difficult to distinguish as the excimer fluorescence of the dialkynylpyrene perfectly overlays with the absorption of the PDI which theoretically could also lead to FRET quenching (Figure 3.18). Further systems which potentially could show a pyrene excimer fluorescence even though the pyrene molecules are separated by other molecules are currently under investigation in our laboratories<sup>148</sup>. Potentially interesting system for the investigation of these phenomena would contain molecules which show an excimer fluorescence where other molecules (i.e. PDI) does not absorb. A system which could meet these criteria could be dialkynylphenanthrenes and PDI molecules (Figure 3.18). The black line represents the absorption of the PDI molecules. It is seen that the absorption trace perfectly overlays the fluorescence of the pyrene excimer depicted in green. The red fluorescence of the dialkynylphenanthrene has its maximum at 400 nm where PDI only absorbs to a small extend.

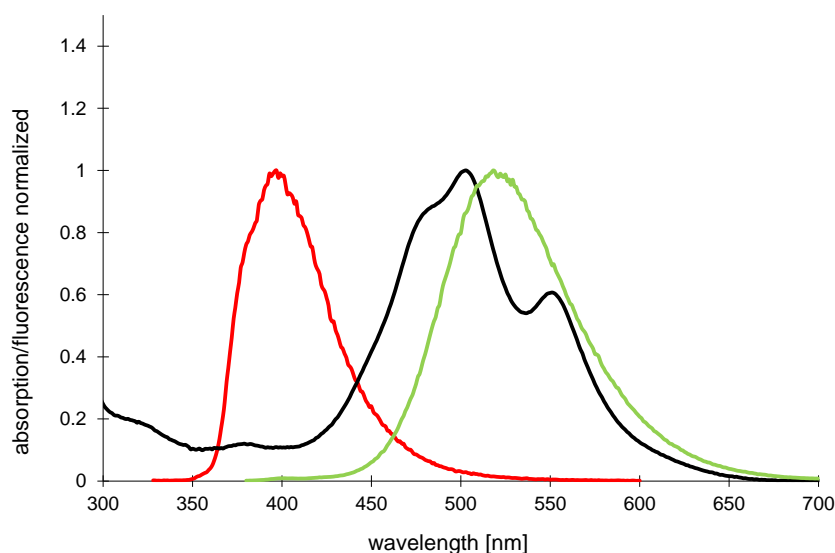
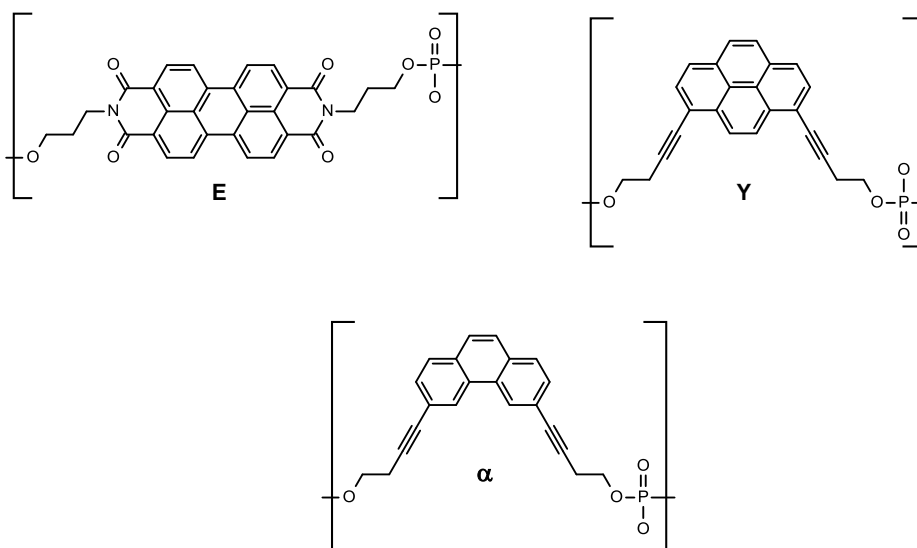


**Figure 3.18** Normalized absorption of PDI (black) and fluorescence of the 3,6-dialkynylphenanthrene (monomer, red) and fluorescence of 1,8-dialkynylpyrene (excimer, green). No clear excimer fluorescence of the phenanthrene was observed. The excimer fluorescence of the pyrene and the absorption of the PDI show a perfect overlap.

DNA molecules containing PDI or dialkynylphenanthrene or pyrene were synthesized (Table 3.4).

**Table 3.4** Sequence of DNA-PDI, DNA-dialkynylpyrene and DNA-dialkynylphenanthrene conjugates containing each 5 unnatural building blocks

oligomer	sequence
A(E5)	5' GAA GGA ACG TEE EEE ACA CTC GCA G 3'
P( $\alpha$ 5)	3' CTT CCT TGC A $\alpha\alpha$ $\alpha\alpha\alpha$ TGT GAG CGT C 5'
A(Y5)	5' GAA GGA ACG TYY YYY ACA CTC GCA G 3'
P( $\alpha$ 5)	3' CTT CCT TGC A $\alpha\alpha$ $\alpha\alpha\alpha$ TGT GAG CGT C 5'



The absorption trace of **P( $\alpha$ 5)\*A(E5)** as well as the fluorescence of **P( $\alpha$ 5)** after excitation at 318 nm is normalized and shown in Figure 3.19.

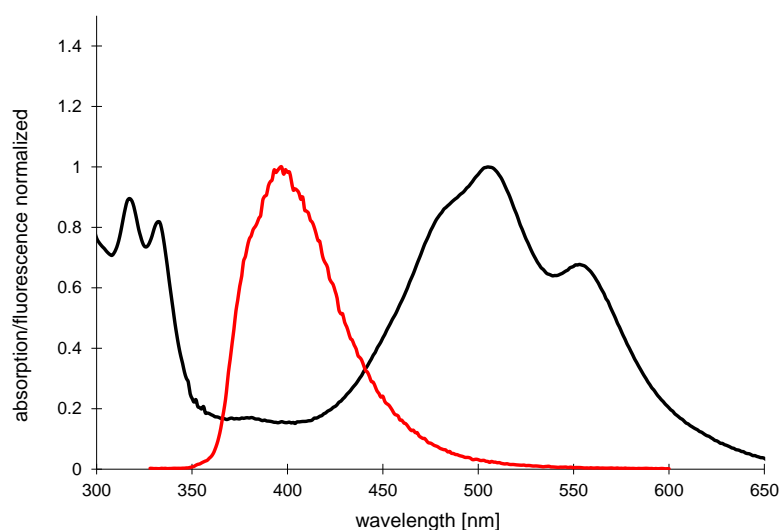


**Figure 3.19** Normalized absorption of  $P(\alpha 5)*A(E5)$  in black and fluorescence of  $P(\alpha 5)$  in red.

The fluorescence of the dialkynylphenanthrene (red curve) is situated between the absorption of the phenanthrene and the PDI. Temperature dependent fluorescence measurements show that the PDI strand  $A(E5)$  nevertheless quench the dialkynylphenanthrene fluorescence. Only at increasing temperatures – when the two DNA strands are melted – the fluorescence of the phenanthrene is restored (Figure 3.20).

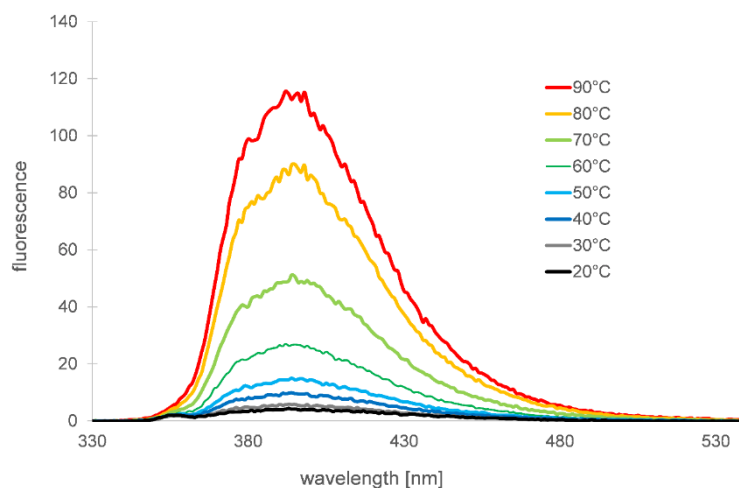


**Figure 3.20** Temperature dependent fluorescence of  $P(\alpha 5)$  and  $A(E5)$ . 2.5  $\mu\text{M}$  of each single strand, 10 mM sodium phosphate buffer, pH 7.2, 100 mM NaCl, ex. 322 nm.

Another situation is seen for duplex  $P(\alpha 5)*A(Y5)$ . Upon excitation at the phenanthrene absorption wavelength at 318 nm we mainly see pyrene excimer fluorescence. Melting of the

duplex by increased temperature lead to a decrease of the excimer fluorescence and a restoration of the phenanthrene fluorescence (Figure 3.21). An energy transfer from the phenanthrene molecules to the pyrene molecules takes place within the strand. The quantum yield of the total system is three times higher than the weighted sum of the quantum yields of its components – indicating a very efficient energy transfer which cannot be explained by a Förster based mechanism (Table 3.5). Even though that the dialkynylpyrene molecules are separated by phenanthrene units they show the excimer fluorescence. This is a strong indication that excimer fluorescence is possible in excited multimers which are not in direct contact to each other.

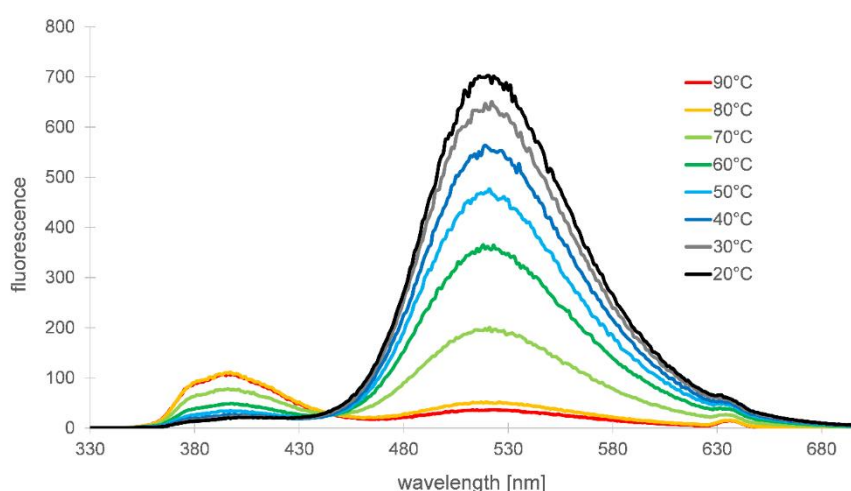


**Figure 3.21** Temperature dependent fluorescence of **P(α5)** and **A(Y5)**. 2.5 μM of each single strand, 10 mM sodium phosphate buffer, pH 7.2, 100 mM NaCl, ex. 322 nm.

**Table 3.5.** Absorption, fluorescence and measured quantum yield of molecules **P(α5)** and **A(Y5)** and the double strand formed thereof. Measured in 10 mM sodium phosphate buffer, pH 7.2, 100 mM NaCl, 20 °C. The weighted quantum yield is obtained by multiplying the quantum yield of **P(α5)** and **A(Y5)** with the respective absorption and dividing the result by the total absorption.

Oligomer	absorption at 318 nm	Fl. Integral 350-450 nm	Fl. Integral 350-450 nm	Quantum yield
<b>P(α5)</b>	0.145	9596		0.031
<b>A(Y5)</b>	0.036		15765	0.211
	weighted quantum yield of the single components			0.067
<b>P(α5)*A(Y5)</b>	0.158	1749		0.005
<b>P(α5)*A(Y5)</b>	0.158		59992	0.185
	quantum yield of the whole system			0.185

### 3.4. Conclusion and Outlook

#### 3.4.1. Observation of co-existing excitonic states in alternating chromophore stacks

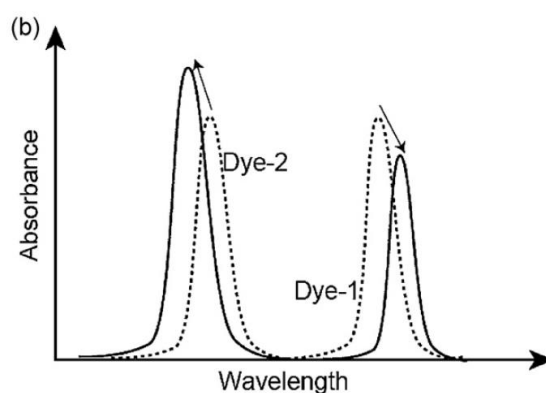
The absorption spectra of a series of DNA hybrids with an extended arenotide stack have been measured. Thereby the aromatic stack is assembled of two different kind of aromatic compounds in different sequences. This special architecture allows the design of multiple homo-, hetero- or mixed-stacks of chromophores.

The DNA-assisted formation of chromophore H-aggregates could be seen by UV/VIS spectrometry. The classical exciton theory was used to explain the findings in changes in the absorption spectra.

Increased H-stacking was observed when using hybrids with increasing numbers of the same chromophore in direct contact. Spectroscopically a blue-shift of the major absorption band of PDI of up to 73 nm was observed. For the pyrene this blue-shift account for 23 nm.

A blue-shift of the maximal absorption band was also observed in cases where two (or more) PDI molecules are aligned in a next-nearest neighbour situation (alternating stacking). Thereby the shift of the maximal absorption band was 41 nm (from 555 nm to 514 nm) in the case of two interacting PDI molecules and 49 nm (from 555 nm to 506 nm) in the case of 4 interacting PDI molecules – respectively 23 nm in the case of pyrene. The classical exciton theory could be adapted to explain these new findings.

Previous studies of Asanuma et al. on hetero aromatic stacks considered the formation of hetero H-excitons whereby the two different aromatic compounds interact with each other<sup>143,149</sup>. Thereby the chromophore at higher energy shows a blue-shift and hyperchromicity whereas the chromophore at lower energy shows a red-shift and hypochromicity.



**Scheme 3.12** Representation of the absorption changes upon interaction of two chromophores. According Ref <sup>140</sup>

The results of the aromatic arrays of PDI and dialkynylpyrene indicate that within one array of alternating aromatic molecules two independent excited states at two different energies exist in parallel.

Asanuma et al. pointed out in their 2012 *Journal of Photochemistry and Photobiology C Review* that the hyper- and hypsochromic shift respectively the hypo- and bathochromic shift become smaller the bigger the difference  $\Delta\lambda_{\max}$  of the two compounds is.

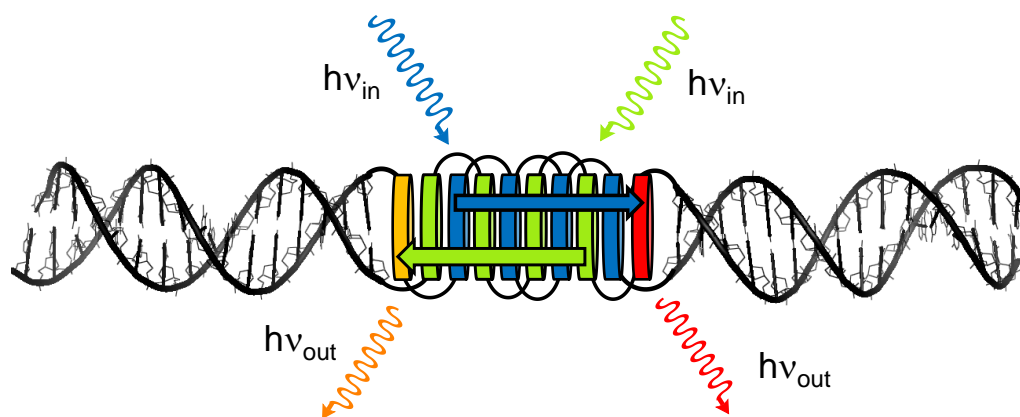
In the case of the dialkynylpyrene and the PDI the electronic transitions are well separated which could lead to an uncoupling of the two systems. Therefore the chromophores rather form homo-H- aggregates with the next-nearest neighbour instead of forming hetero-H-aggregates with the nearest neighbour.

It would be of uppermost interest to design systems which fluorescence of the excited states can be made visible even though they are separated by further molecules. Fluorescence measurements of DNA strands containing dialkynylphenanthrene and dialkynylpyrene indicate the formation of fluorescent pyrene excimers even though they are separated by phenanthrene building blocks (Figure 3.21).

Other systems which would be nice to test would make use of non-aromatic spacers between the molecules which form the excited multimers. Cyclohexyl building blocks used by Asanuma et al. would be molecules of choice.

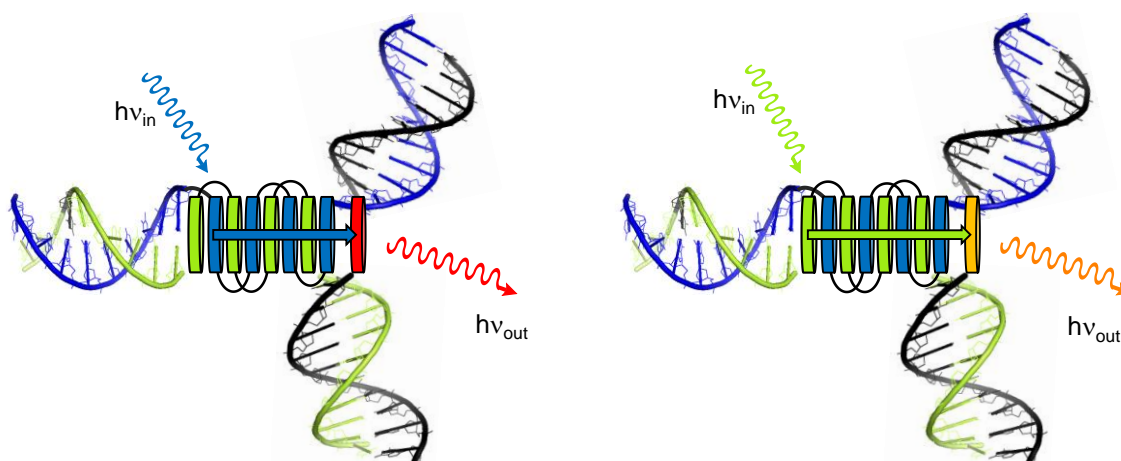
#### **3.4.2. Development of further antenna systems to simultaneously excite acceptor chromophores from co-existent excited states of alternating chromophore stacks**

Molecular antenna systems make use of a stack of collector molecules which collect light energy and transfer it to an acceptor molecule. Based on the above findings on co-existing excited states of alternating chromophore arrays, a DNA guided dual-antenna system could be designed. Stacks of two different chromophores (collector 1 and collector 2) could be assembled in a DNA duplex in alternating stacks. Two further chromophores (acceptor 1 and acceptor 2) could be assembled on either side of the alternating stack. Upon excitation of the collector 1 in the stack the energy is transferred to the acceptor molecule 1 at the one end of the stack. Excitation of the other chromophore (collector 2) leads to an excited state in the same volume but at the different energy and thus an excitation of acceptor chromophore 2 (Scheme 3.13). Thereby a design would be most wonderful in which the acceptor chromophore 1 is covalently linked to the collector molecule 2 and vice versa. This design would allow a very efficient detection of the assembling process and the formation of the dual-antenna system.



**Scheme 3.13** Illustration of a DNA duplex based molecular antenna system consisting of two independently excitable chromophore systems. The blue and the yellow chromophores are assembled in the first DNA single strand whereas the green and the red chromophores are assembled in the second. Formation of the double strand results in a dual antenna system whereby the red chromophore is excited upon excitation of the blue chromophore stack and the yellow chromophore is excited upon excitation of the green chromophore stack.

Other antenna systems described in literature could be adapted to use antenna systems with co-existing excited states. Chromophores could be assembled in a three-way junction according to published architectures<sup>150,151</sup>. Thereby the collector system could be assembled from two different chromophores in an alternating fashion. This collector system is assembled in one branch of the three-way junction (Scheme 3.14). The third strand of the junction contains the acceptor molecule.



**Scheme 3.14** Illustration of a DNA three way junction based antenna system consisting of two independently excitable chromophore systems. The acceptor chromophores (red and yellow) can be exchanged by hybridization of the respective DNA strand (black) with the three way junction.

Exchanging of the third strand (black) containing a different acceptor molecule could lead to a system which shows co-existing excited states at different energy levels and shows an energy transfer to different acceptor molecules.

Experiments with complementary oligonucleotides containing 5 dialkynylphenanthrene or 5 dialkynylpyrene show a very efficient energy transfer from phenanthrene to pyrene yielding pyrene excimer fluorescence. It can be quest that pheanthrenes and pyrenes interdigitate and by doing so form exited dimers with the next-nearest neighbour molecule.

The quantum yield of the duplex system is three times higher than the sum of the quantum yield of its components.

This design using dialkynylphenanthrene and dialkynylpyrene can be applied for the formation of extended polymeric light harvesting systems with increasing content of light absorbing phenanthrenes which transfer the energy to acceptor pyrene molecules – gaining an increasing quantum yield of the formed system.



## 4.0. Polymer light harvesting antenna with DNA like phosphate backbone

Work described in this chapter is published in:

Long Distance EET in Light-Harvesting Supramolecular Polymers\*\*

*Christian B. Winiger, Shaoguang Li, Ganesh R. Kumar, Simon M. Langenegger and Robert Häner\**

Angewandte Chemie Int. Ed, **2014**, 53, DOI:10.1002/anie.201407968

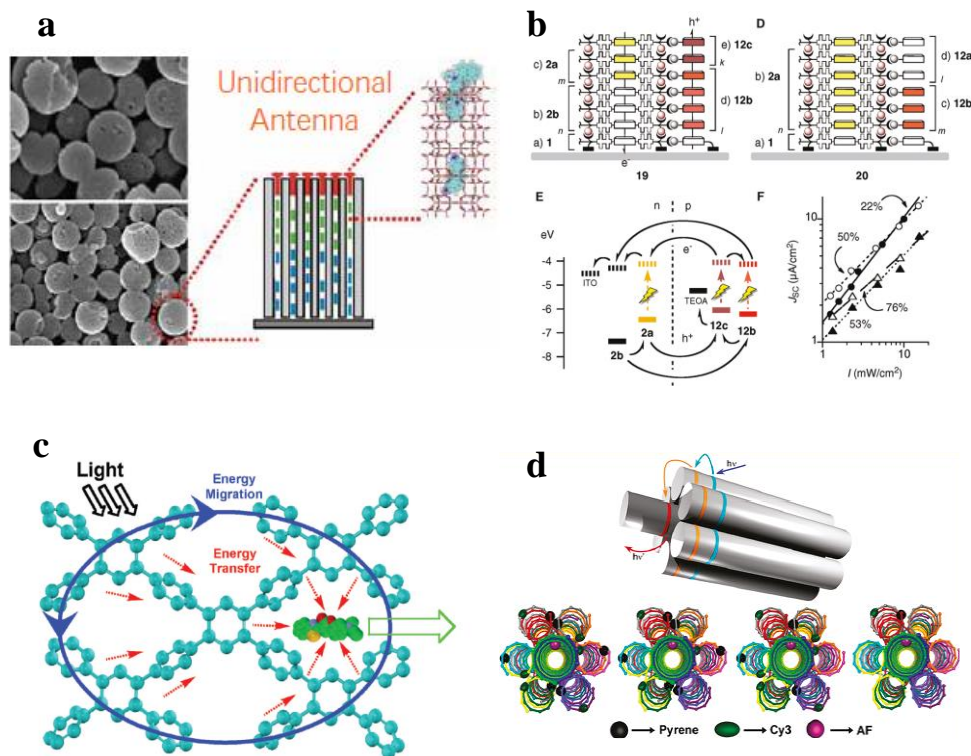
### 4.1. Introduction

In photosynthesis – a major biochemical process which enables life on earth - a proper arrangement of chromophores is indispensable. Photosynthetic active plants or some bacteria are responsible for the production of oxygen and sugar on earth using CO<sub>2</sub>, water and sunlight. To fulfil this prolific task sunlight is absorbed by special chromophores (mainly porphyrines and carotenoids) in the light harvesting complex (LHC) of the plant<sup>47</sup>. The chromophores are embedded in protein structures which align pigments and hold them in ideal positions to each other. A crystal structure which makes the positioning of the chromophores visible was published in 2005 in Nature<sup>152</sup>. The structure of the dimeric Photosystem II (PSII) shows among others the exact arrangement of a total of 35 chlorophyll a and 11 β-carotenoids. Only the defined positioning of the chromophores makes the efficient process photosynthesis possible.

In other natural light harvesting complexes – the chlorosomes of green sulphur and non-sulphur bacteria – the chromophores are arranged in a way that the aggregate is only controlled and stabilized by dye-dye interactions and not by the protein matrix. The exact arrangement of chromophores is still unknown and studies of the energy transfer within the chromophores is ongoing. Model compounds as for example the zinc chlorin are used to mimic molecules involved in the light harvesting process and relevant features and aspects are hoped to be elucidated<sup>153</sup>. Researchers around the world try to mimic the important process of photosynthesis and try to create artificial LHC with the aim of energy collection, transfer and energy conversion<sup>154-158</sup>.

Prominent examples of this research are highlighted (Scheme 4.1): Calzaferri et al. use zeolite to incorporate dye molecules which enables light collection and energy transfer along the structures. Furthermore, directionality of the energy transport process is given by a directed assembly of the chromophores within the zeolite. Jiang et al. specialized on covalent microporous polymers in which they insert chromophores which accept energy. Further approaches use solid surfaces for the assembling of the chromophores. The SOSIP approach from Matile et al. is mentioned<sup>90,91</sup> as an example. Matile et al. use surfaces to initiate polymerization of molecules with self-organizing properties. Lui et al. use heptamer bundles of DNA modified with pyrene, Cy 3 and alexa fluor 647 to generate a cascade of FRET-based energy transfer<sup>159</sup> reactions. Thereby the DNA acts as

a spacer and scaffold to align the chromophores in an optimal way. A similar approach was realized recently by Medintz et al.<sup>160</sup>



**Scheme 4.1** Selection of light harvesting systems described in literature. Different ways of arranging chromophores to functional systems are shown. a) using zeolite to incorporate chromophores b) surface initiated self-polymerization to form defined chromophore stacks c) microporous polymers and d) DNA-assembled chromophores. Examples are taken from Ref<sup>159,161-163</sup>

In 2012 Garo et al. introduced a DNA based light harvesting antenna<sup>158</sup> with a well-defined light harvesting  $\pi$ -array. Stacks of carboxyphenanthrene molecules were aligned with a carboxypyrene molecule within a DNA scaffold. The phenanthrene molecules act as light collecting molecules. The energy is transferred toward the pyrene molecule where phenanthrene and pyrene form an exciplex and the collected energy again is emitted. The emitted energy increases with increasing numbers of phenanthrene which collect light.

## 4.2. Aim of the work

Recent work in our group focused on the formation of DNA-like polymers consisting of heptamers of arenotide phosphates (1,8-dicarboxypyrene) as building blocks to form non-covalent long polymers. The polymers were up to 300 nm long and consist of a 1 D frame of molecules<sup>164,165</sup>. It was found that these polymers can adopt chirality which could be induced by chiral building blocks<sup>166,167</sup>. The stacking mode of the oligoarenotides was assigned depicting a face-to-face  $\pi$ - $\pi$  stacked manner<sup>168</sup>. It was found that the morphology of the formed polymers is highly dependent on the geometry of the underlying building blocks. Investigations with 3mers of 1,6-dialkynylpyrene showed the formation of sheet-like structures<sup>142</sup> whereas 3 mers or 6 mers of the 1,8-dialkynylpyrene showed linear polymers<sup>169</sup>.

In the following work a polymer light harvesting antenna was created trying to combine the features of the light harvesting DNA based antenna with approaches of the formation of linear polymeric  $\pi$ - $\pi$  stacks. Phenanthrenes were used as light collector molecules in analogy to the DNA based antenna. Therefore 3 mers of a 3,6-dialkynylphenanthrene were synthesized and the formation of supramolecular polymers was tested. 1,8-dialkynylpyrene acted as acceptor molecule. Previous work (see Chapter 3) showed a very efficient energy transfer from dialkynylphenanthrene to dialkynylpyrene with quantum yields which were significant higher than the sum of quantum yield of the individual components. Successful implementation of polymeric light harvesting antennas is a contribution for research toward the design of artificial light harvesting complexes (LHCs) and could lead to new insights into the energy transfer process in defined molecular assemblies and aggregates.

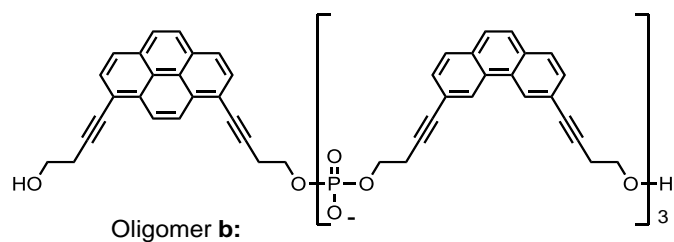
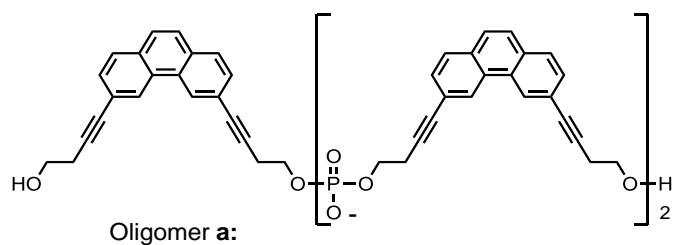
## 4.3. Results and Discussion

### 4.3.1. Monomeric building blocks and assembled oligomers

3,6-dialkynylphenanthrene phosphoramidites were synthesized according to adapted published procedures<sup>74</sup>. The 3,6-dibromophenanthrene for the Sonogashira coupling with the 3-butyne-1-ol was prepared in analogy to the procedure given in the literature<sup>68</sup> starting from 4,4'-dibromostilbene. Three 3,6-dialkynylphenanthrene building blocks were assembled on a DNA synthesizer using the standard protocol for DNA synthesis. A second multimer was assembled using three alkynylphenanthrenes and one dialkynylpyrene<sup>74</sup> (Table 4.1).

**Table 4.1** Oligomers synthesized and described in the following section.

	<b>sequence</b>
Oligomer <b>a</b>	5' <i>aaa</i>
Oligomer <b>b</b>	5' <i>Yaaa</i>



The absorption of the monomer building blocks in THF was measured (Figure 4.1). The phenanthrene building block absorbs between 310 nm and 340 nm where the pyrene does not show absorption. Thus, the phenanthrene building block can be almost selectively excited in further experiments.

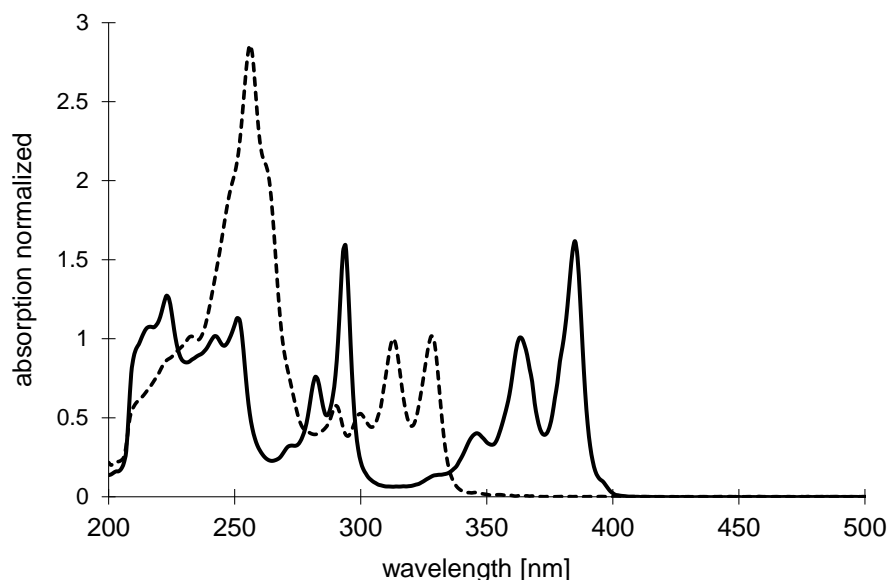


**Figure 4.1** Normalized absorption spectra of the 1,8-dialkynylpyrene (solid) and the 3,6-dialkynylphenanthrene (dashed) building block in THF.

UV absorption of oligomers **a** and **b** are shown in Figure 4.2. The blue line represents the absorption spectra of the phenanthrene 3mer with the absorption maxima at 314 nm and 329 nm. The black line shows the absorption of oligomer **b** with additionally the absorption maxima of pyrene at 365 nm and 386 nm. In the buffered aqueous solution the phenanthrene molecules show an aggregated absorption spectra with the phenanthrene maxima at 322 nm and 336 nm. Figure 4.3 shows the absorption spectra of 0.5  $\mu\text{M}$  of oligomer **a** in 10 mM sodiumphosphate buffer at 20  $^{\circ}\text{C}$  and 90  $^{\circ}\text{C}$ . Additionally we see a lower absorptivity at 20  $^{\circ}\text{C}$  in the area of 250 nm. Additionally the peak is shifted toward lower wavelength (hypsochromicity) and the peak is broadened. This indicates a tight H-like stacking of the chromophores at lower temperature.

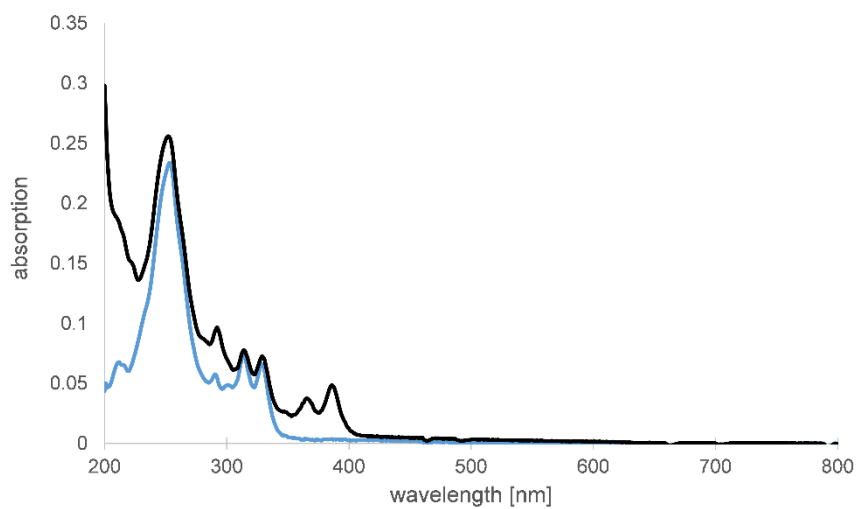


**Figure 4.2** Oligomer **a** (blue) and **b** (black) at 0.5  $\mu\text{M}$  in EtOH/H<sub>2</sub>O 1:1.

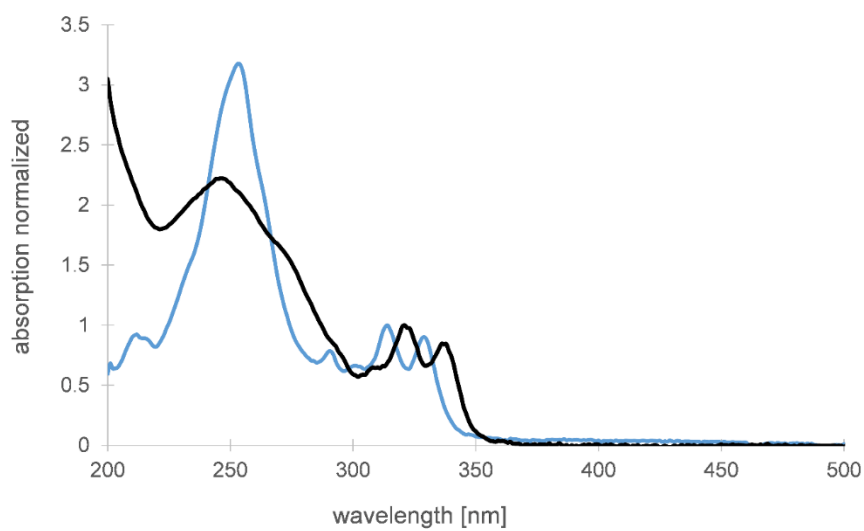


**Figure 4.3** Oligomer **a** at 0.5  $\mu\text{M}$  in 10 mM sodium phosphate buffer, pH 7.2 at 20 °C (black) and 90 °C (blue).

### 4.3.2. AFM measurements of the supramolecular polymers

The molecular antenna was assembled using 0.5  $\mu\text{M}$  of oligomer **a** and 0.5 nM of oligomer **b** in 10 mM sodium phosphate buffer. The oligomers self-assemble to form long linear polymers with length of more than 10  $\mu\text{m}$  (Figure 4.4).

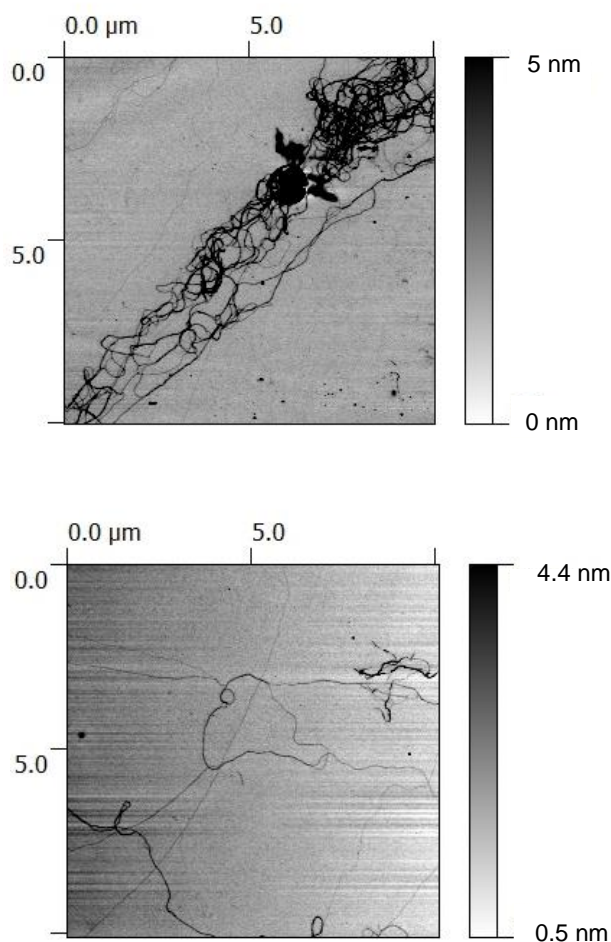


**Figure 4.4** AFM pictures of polymers consisting of 0.5  $\mu\text{M}$  of oligomer **a** and 0.5 nM of oligomer **b**.

The thickness of the polymers is found to be  $0.6 \pm 0.1$  nm in the case of the smallest size and up to 1.8 nm in the thicker polymers. 0.6 nm of measured polymer thickness corresponds to 2.4 nm in real height as elucidated in previous AFM studies of comparable polymers<sup>165</sup>. This thickness corresponds to the thickness of natural DNA<sup>170,171</sup>. In previous studies polymers consisting of polyarenes have been studied extensively by AFM, computational and spectroscopic methods<sup>165,168,172</sup>. A 1 dimensional extended face-to-face  $\pi$  stack of the arenes has been elucidated as structural motive.

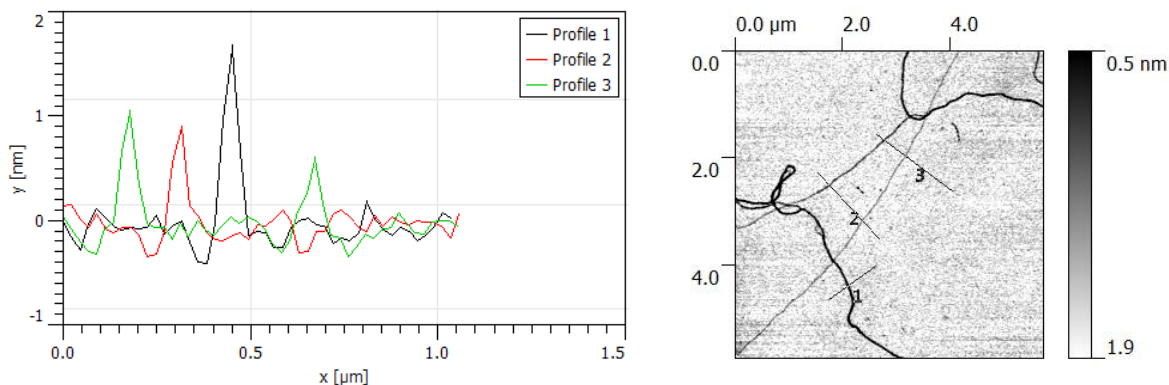


**Figure 4.5** AFM pictures of polymers consisting of 0.5  $\mu\text{M}$  of oligomer **a** and 0.5 nM of oligomer **b**. The cross sections at the indicated positions are depicted on the left.

The AFM studies of the phenanthrene polymer suggests for the smallest sized polymers a linear, one molecule thick  $\pi$ - $\pi$  array which can assemble to two or three strand thick assemblies. Branching points in the assembly of the higher polymers are visible. After these branching points the thickness of the polymers is the sum of the thickness of the two polymers before the branching point (Figure 4.6). The profiles have been extracted and the different heights are also visible from the shading of the polymers. The process of the formation of the light harvesting polymers is schematically shown in Scheme 4.2.



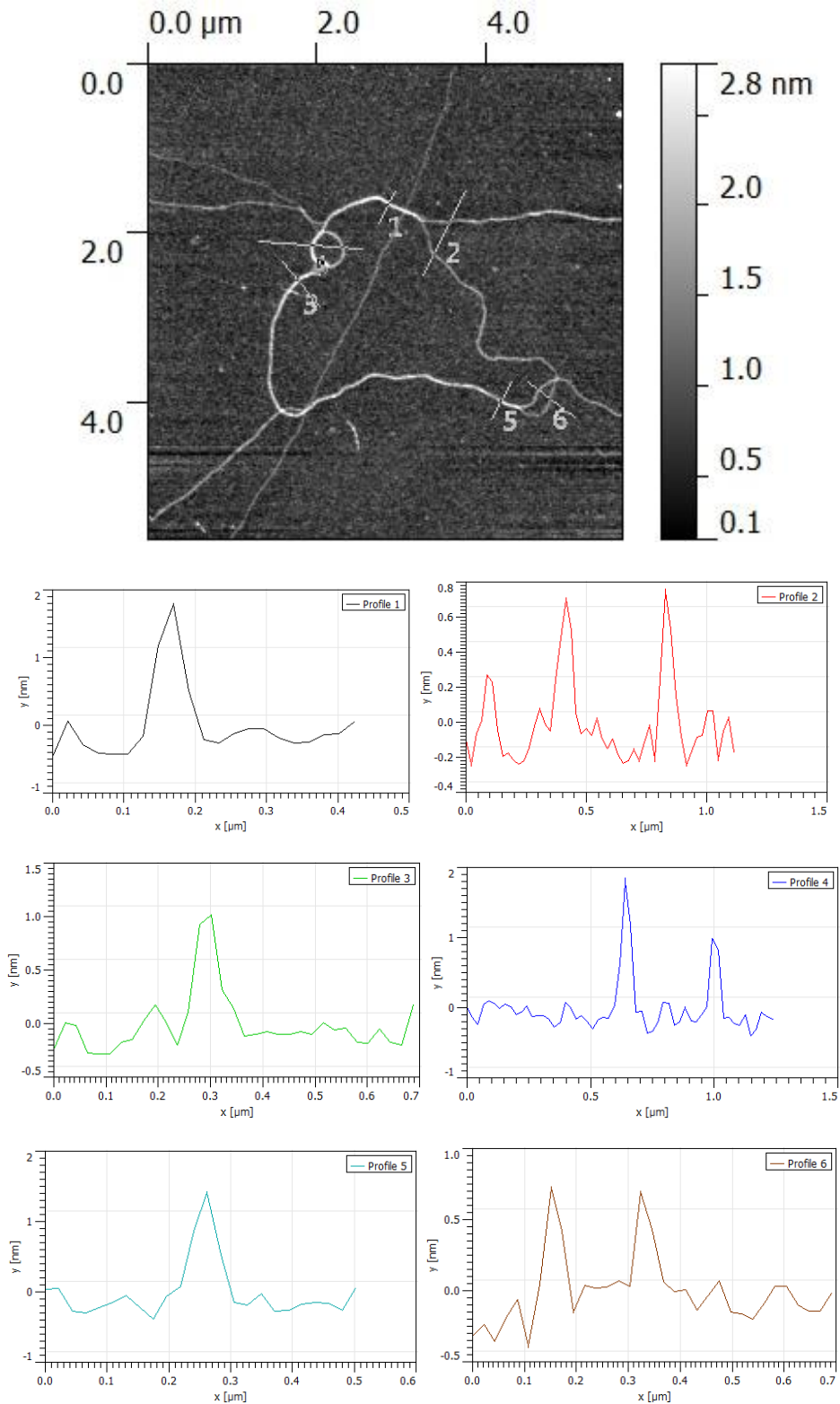
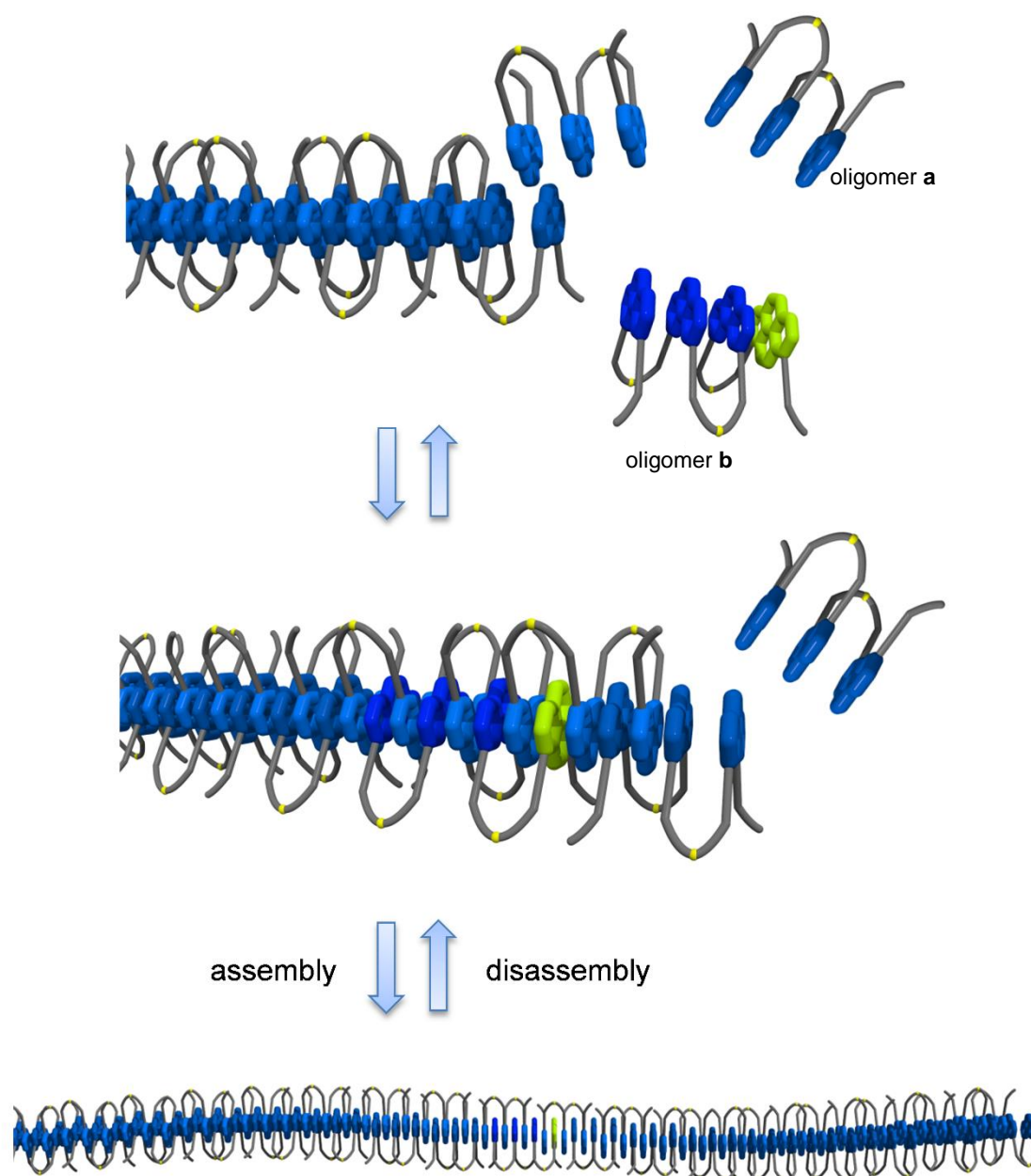


**Figure 4.6** AFM pictures of polymers consisting of 0.5 μM of oligomer **a** and 0.5 nM of oligomer **b**. The cross sections at the indicated positions are depicted. The different heights of the polymer is shown in the cross sections. The real height of the polymers has to be calculated from the raw data shown.



**Scheme 4.2** Graphical representation of the assembly and disassembly process of oligomer a and oligomer b. Graphics prepared by Simon M. Langenegger.

### 4.3.3. Fluorescence measurements of the light harvesting polymers

The fluorescence of 0.5  $\mu\text{M}$  of oligomer **a** is shown in Figure 4.7 (blue line). The addition of as little as 0.5 nM of oligomer **b** increases the fluorescence up to four fold.

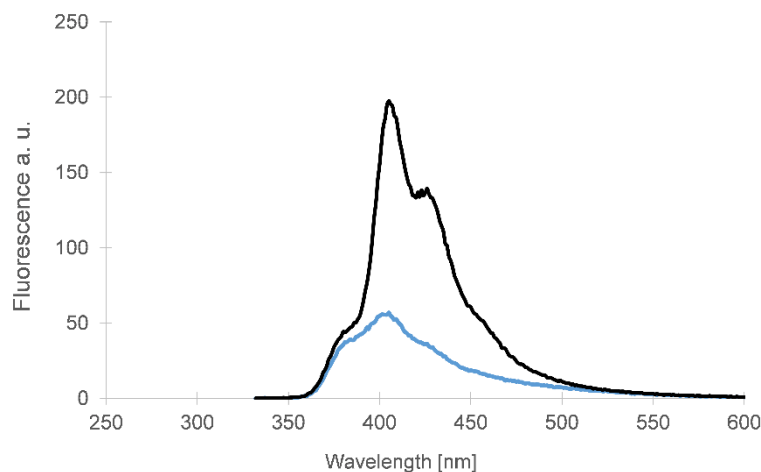


**Figure 4.7** Fluorescence of a solution of 0.5  $\mu\text{M}$  of oligomer **a** (blue) and a solution of 0.5  $\mu\text{M}$  of oligomer **a** and 0.5 nM of oligomer **b** (black). Both examples are measured in 10 mM sodium phosphate buffer, pH 7.2, ex 322 nm.

The solution of 0.5  $\mu\text{M}$  of oligomer **a** and 0.5 nM of oligomer **b** show at 20  $^{\circ}\text{C}$  and excitation at 322 nm a pyrene monomer fluorescence as depicted by the black line (Figure 4.8). Excitation of the same sample at the pyrene wavelength directly only yields in a very low pyrene fluorescence which is more than 100 times less than after the excitation at the phenanthrene molecule. This experiment indicates an efficient energy transfer from the phenanthrene molecules to the pyrene molecule which deals as a final energy acceptor and emits light.

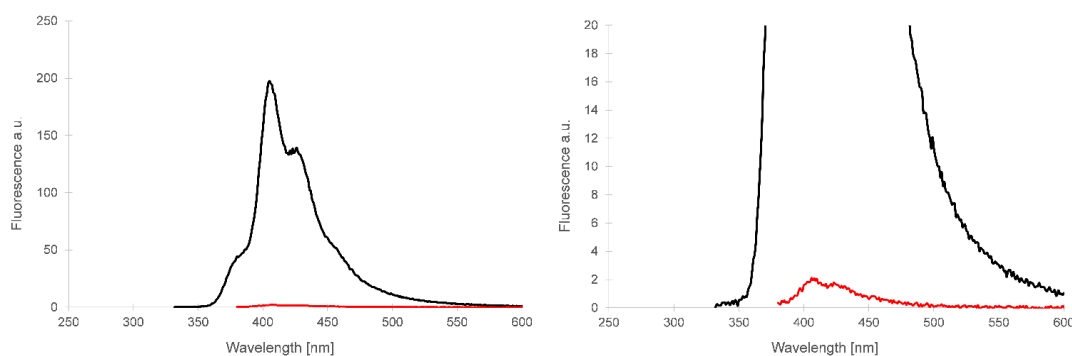


**Figure 4.8** Fluorescence of a solution of 0.5  $\mu\text{M}$  of oligomer **a** and 0.5 nM of oligomer **b**. The sample is measured in 10 mM sodium phosphate buffer, pH 7.2, ex 322 nm at phenanthrene (black) and ex 370 nm pyrene (red).

#### 4.3.4. Dotting experiments using increasing concentrations of acceptor molecule **b**

Polymers of the phenanthrene 3mer were titrated with pyrene-containing oligomer **b** starting with sub-per mille concentrations. The quantum yield of the system was calculated and plotted vs the amount of pyrene for each titration step (Figure 4.9 and Table 4.2). The quantum yield increases steadily and reaches a maximal permissible value of 0.54 which corresponds to the quantum yield of the dialkynylpyrene molecule when excited at the pyrene absorption directly. The energy transfer from the phenanthrene molecule to the pyrene molecule therefore is up to 100 %.

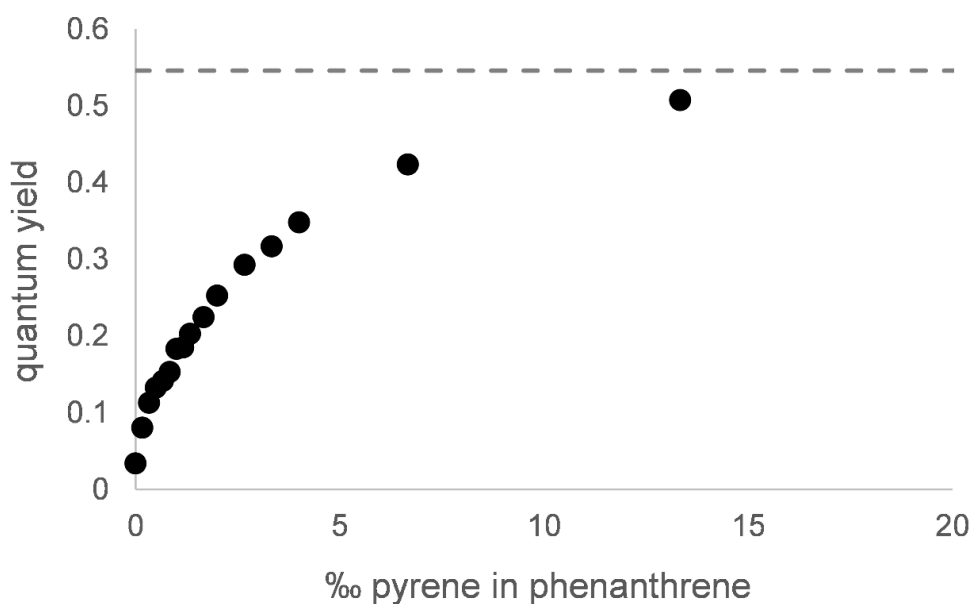


**Figure 4.9** Titration of a solution of 0.5  $\mu\text{M}$  of oligomer **a** is titrated with increasing amounts of oligomer **b**. The quantum yield (upon excitation at 322 nm) vs the % quantity of pyrene to phenanthrene is indicated. The grey dotted line represents the quantum yield of the pyrene monomer which is 0.54.

**Table 4.2** Concentration in nM and mol% of pyrene added to a solution of 0.5  $\mu\text{M}$  oligomer **a**. The measured absorption and the fluorescence is shown. The quantum yield was calculated.

conc. of <b>b</b> (nM)	mol% of pyrene	Absorption at 322 nm	Fluorescence (area under curve)	$\phi_f^A$
0.00	0.00	0.045	3047	0.034
0.25	0.17	0.044	7155	0.080
0.5	0.33	0.045	10115	0.113
0.75	0.50	0.046	12241	0.133
1.00	0.67	0.048	13652	0.141
1.25	0.83	0.049	14997	0.153
1.50	1.00	0.047	17297	0.183
1.75	1.17	0.047	17364	0.185
2.00	1.33	0.046	18538	0.203
2.50	1.67	0.046	20709	0.224
3.00	2.00	0.045	22861	0.252
4.00	2.67	0.044	25947	0.293
5.00	3.33	0.042	26629	0.317
6.00	4.00	0.045	31140	0.348
10.00	6.67	0.043	36815	0.424
20.00	13.33	0.045	45654	0.507

The titration performed is shown in Figure 4.10. 0.5  $\mu\text{M}$  of oligomer **a** is titrated with increasing amounts of oligomer **b** starting with 0.0005  $\mu\text{M}$ . The sample was always excited at 322 nm at the phenanthrene absorption and at 370 nm at the pyrene absorption. The fluorescence of the molecular antenna increased to 900 units when excited at 322 nm. Upon excitation at 370 nm the fluorescence only increases to 25 units. The increase of the fluorescence when excited at 370 nm is almost linear with increasing concentration. On contrary, the increase in fluorescence upon excitation at 322 nm follows a “law of diminishing return” and approaches a maximal permissive value.

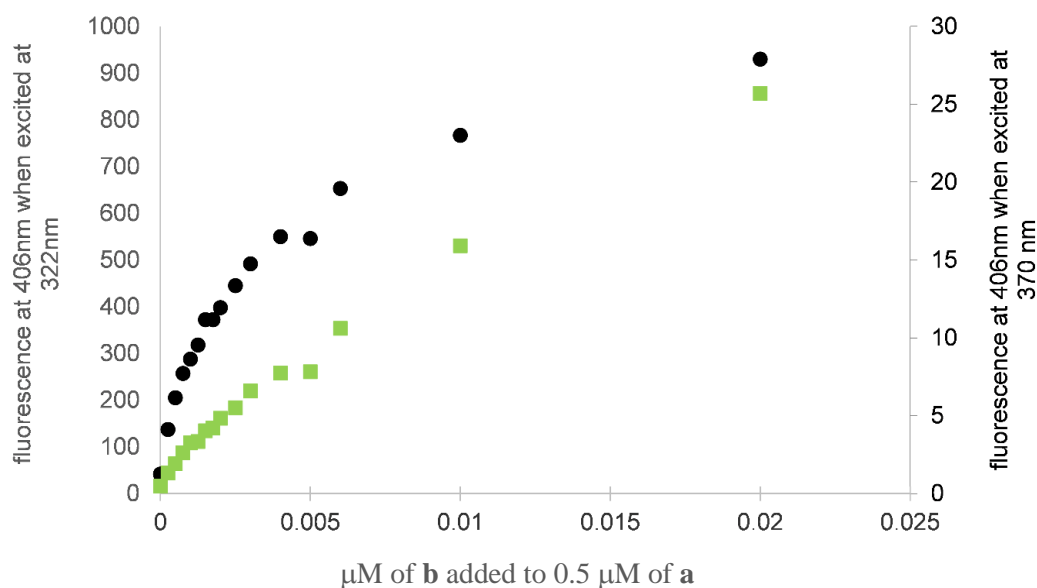


**Figure 4.10** Titration of oligomer **b** to a solution of 0.5  $\mu\text{M}$  of oligomer **a** in 10 mM sodium phosphate buffer. Excitation at 322 nm (black) and 370 nm (green), different axis scales.

A simple model can explain this behaviour. Each pyrene collects energy from adjacent phenanthrene molecules. The energy can be transported within the polymer only over a certain distance. If more and more pyrene molecules are inserted into the polymer they start to compete for the energy which results in a maximal permissive fluorescence that can be reached. On the other hand the fluorescence when excited at the pyrene directly increases linearly with the amount of pyrene added.

#### 4.3.4. Dotting experiments using increasing concentrations of donor oligomer **a**

Similar titration experiments can be performed by titrating a very small amount of oligomer **b** with increasing amounts of oligomer **a** (Figure 4.11). A reference titration was performed without oligomer **b** in solution (Figure 4.11, bottom).

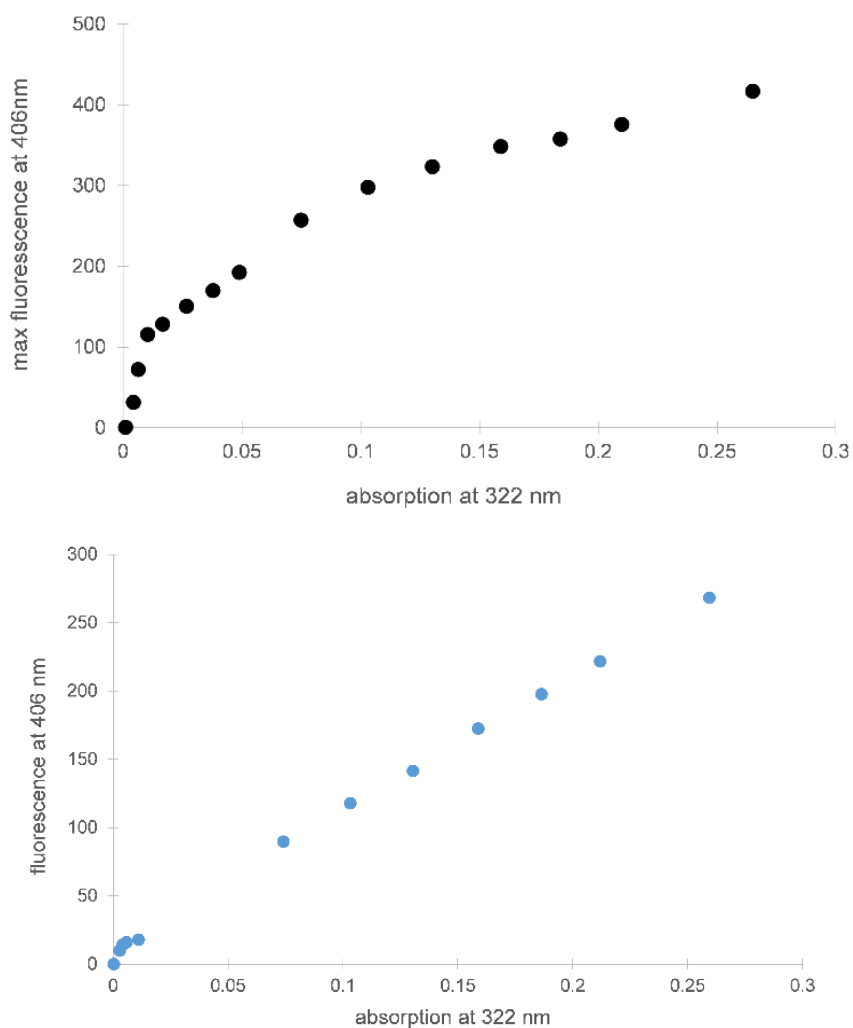


**Figure 4.11** Titration of oligomer **a** to a solution containing 0.5 nM oligomer **b** (top) or no oligomer **b** (bottom). The maximal fluorescence is plotted vs the absorption at 322 nm. Excitation at 322 nm.

A linear increase of fluorescence is observed when no oligomer **b** is in solution. Increasing amounts of phenanthrene results in a higher fluorescence from the phenanthrene. In the case where oligomer **b** is present in the solution the increase of fluorescence at the beginning is quite significant. The few phenanthrene molecules added efficiently build up a short light harvesting antenna which results in a high fluorescence. By adding more and more oligomer **a** to the system longer polymers are formed. The energy transfer within the polymer has to occur over longer distances and the gain of additional fluorescence becomes smaller. A pronounced kink is observed after addition of 0.15  $\mu\text{M}$  of oligomer **a**. This could be the ratio of oligomer **a** to oligomer **b** at which the distances between two pyrene molecules is ideal and corresponds to the length at which the energy transfer efficiency is maximal. Incorporation of more phenanthrene molecules results in longer polymers and additional phenanthrene molecules do not transport the energy efficient enough to the acceptor-pyrene.

At this ratio we do have one oligomer **a** on 300 oligomers **b** considering a statistical distribution. In other words, we have 300 x 3 phenanthrene molecules on 1 pyrene. Crystal structures of polyaromatic hydrocarbons showed a distance of the molecules of 3.4-3.5 Å (see also chapter: Observation of two independent H-couplings in a stack of multiple chromophores) in a face-to-face stacked manner. For the molecular antenna this would account for one pyrene molecule every 3150 Å or every 315 nm assuming again an ideal distribution. Further calculations of the energy transfer length are shown in the conclusion part.

#### 4.3.5. Thermal stability of the supramolecular light harvesting polymers

The molecular antenna shows a temperature dependent fluorescence (Figure 4.12). At low temperature we see the pyrene monomer fluorescence which indicates an efficient energy transfer from the phenanthrene molecules to the pyrene. At 90 °C the polymer is disassembled and shows a weaker fluorescence from the phenanthrene. The energy transfer from the phenanthrene to the pyrene is interrupted. A similar process is visible in the UV/VIS measurements. At 90 °C we see a pronounced hyperchromicity as well as a slight red-shift of the main absorption band at 250 nm. Additionally we see a blue-shift of the peaks at 322 nm and 336 nm. The spectra at 90 °C resembles the spectra of oligomer **a** in EtOH/water where we also see the spectra of the disassembled polymers. The hypochromicity and the blue-shift at lower temperature is an indication of H-aggregated stacking in buffered water at room temperature.

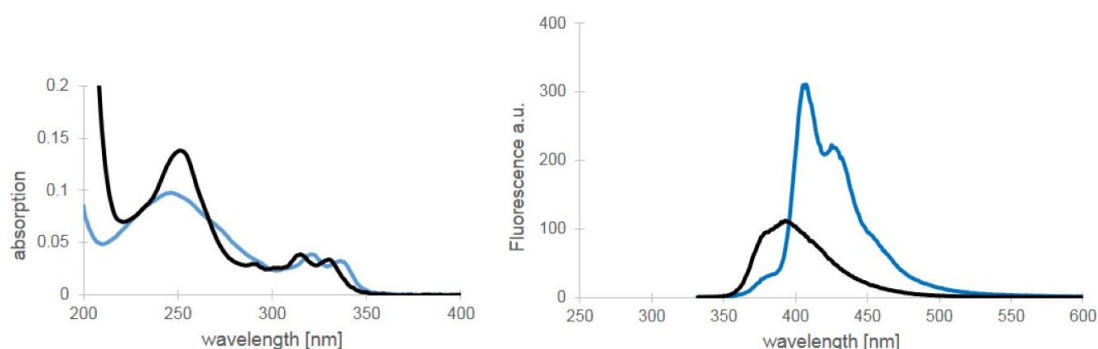


**Figure 4.12** UV absorption (left) and fluorescence (right) of a solution containing 0.5 μM of oligomer **a** and 0.5 nM of oligomer **b** measured at 20 °C (blue) and 90 °C (black). Excitation at 322 nm.

Temperature dependent fluorescence (Figure 4.13) and UV/Vis (Figure 4.14) measurements indicate the stability of the supramolecular polymer. The melting curves show a pronounced sigmoidal shape with hyperchromicity at higher temperatures. The cooling curves in the UV/VIS



as well the fluorescence melting experiment show that the polymers start to assemble below 50 °C. At this temperature the fluorescence starts to increase as the energy transfer within the assembled polymer takes place. The cooling curve is followed by a heating ramp which shows the temperature dependent melting of the polymers. The melting of the antenna is initiated above 40 °C. A pronounced hysteresis is visible.

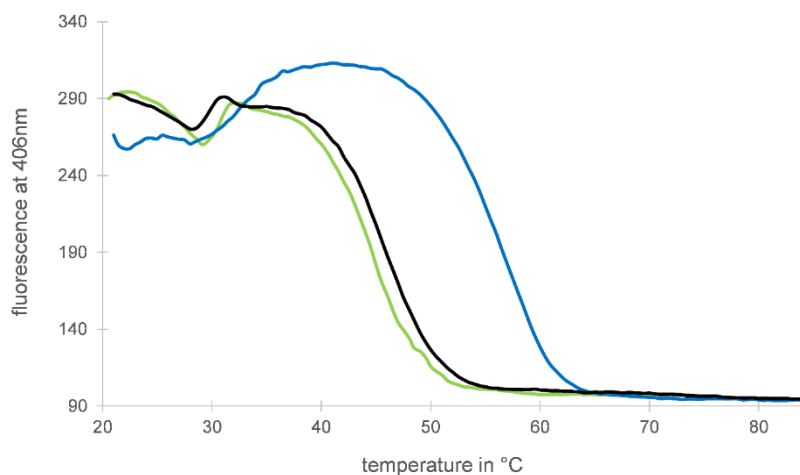


**Figure 4.13** Temperature dependent fluorescence measurement of a solution of 0.5  $\mu\text{M}$  of oligomer **a** and 0.5  $\mu\text{M}$  of oligomer **b**. Excitation at 322 nm, emission at 406 nm. The ramps were performed as cooling-heating-cooling ramps with 0.3 °C per min.

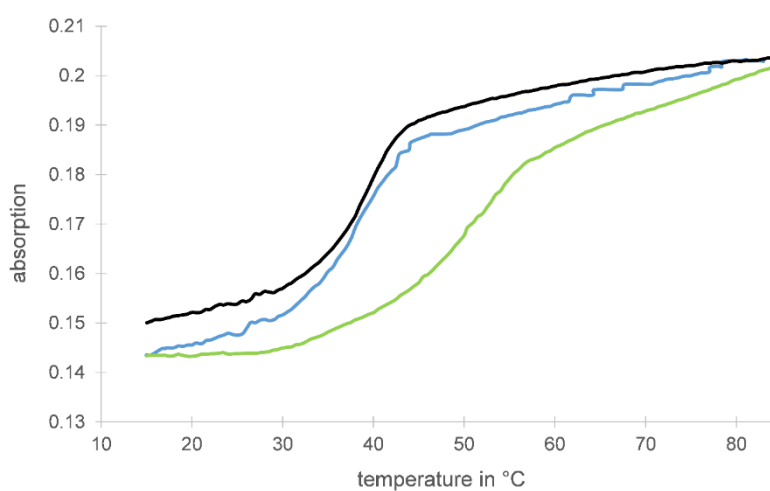


**Figure 4.14** Temperature dependent absorption measurement of a solution of 0.5  $\mu\text{M}$  of oligomer **a** and 0.5  $\mu\text{M}$  of oligomer **b**. Absorption was measured at 250 nm. The ramps were performed as cooling-heating-cooling ramps with 0.3 °C per min.

#### 4.3.6. Titration experiments using high concentrations of acceptor oligomer **b**

To 0.5  $\mu\text{M}$  of oligomer **a** concentrations of oligomer **b** were added in the range of 0.01  $\mu\text{M}$  up to 0.5  $\mu\text{M}$  (Figure 4.15). With increasing concentrations of oligomer **b** the chance that two or more of the pyrene molecules are in close proximity increases which results in a reduced pyrene monomer fluorescence and an increasing pyrene excimer fluorescence. The fluorescence of oligomer **b** alone is shown in Figure 4.16 at 20  $^{\circ}\text{C}$  and at 90  $^{\circ}\text{C}$ . A distinctive pyrene excimer fluorescence is visible which indicates an intermolecular aggregation of the pyrene molecules. Beside this, a shoulder at 430 nm is present which intensity increases at higher temperature and at 90  $^{\circ}\text{C}$  remains to be the only fluorescent band of the sample. The same fluorescent signal was observed in previous research in our group when in a DNA single strand one dialkynylpyrene and one dialkynylphenanthrene were incorporated<sup>173</sup>. This fluorescent signal is attributed to be the exciplex fluorescence of dialkynylpyrene and dialkynylphenanthrene (Figure 4.17).

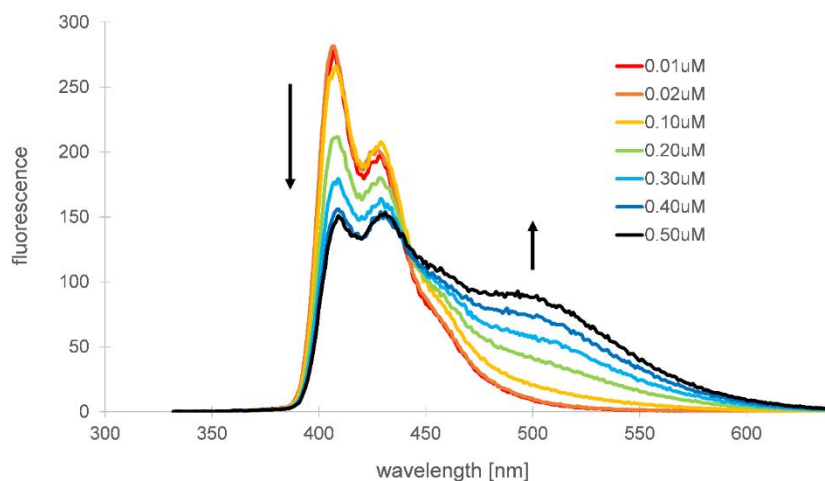


**Figure 4.15** A solution of 0.5  $\mu\text{M}$  of oligomer **a** in 10 mM sodium phosphate buffer was titrated with increasing amounts of oligomer **b**. Excitation at 322 nm. The fraction of excimer fluorescence is increasing with increasing concentration of oligomer **b**.

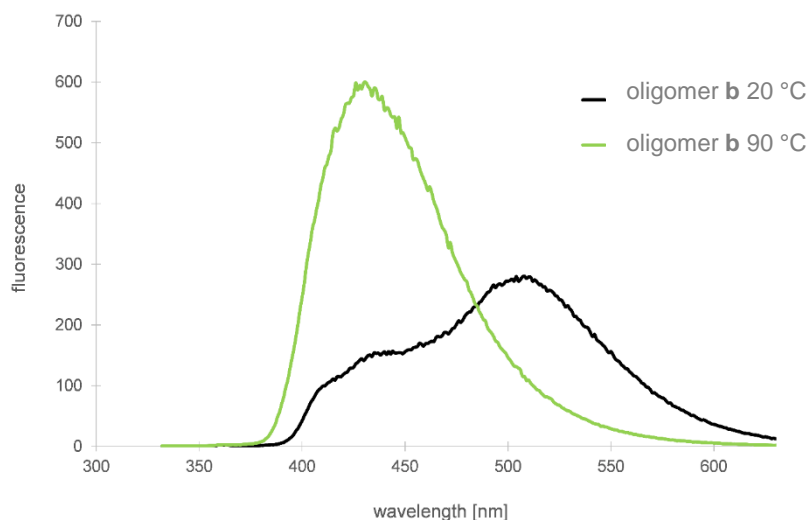


**Figure 4.16** Fluorescence spectra of 0.5  $\mu\text{M}$  of oligomer **b** in 10 mM sodium phosphate buffer at 20 °C (black) and 90 °C (green). At low temperature oligomer **b** starts to aggregate and forms the excimer fluorescence. Heating destroys the polymers and the excimer fluorescence disappears. Excitation at 322 nm.

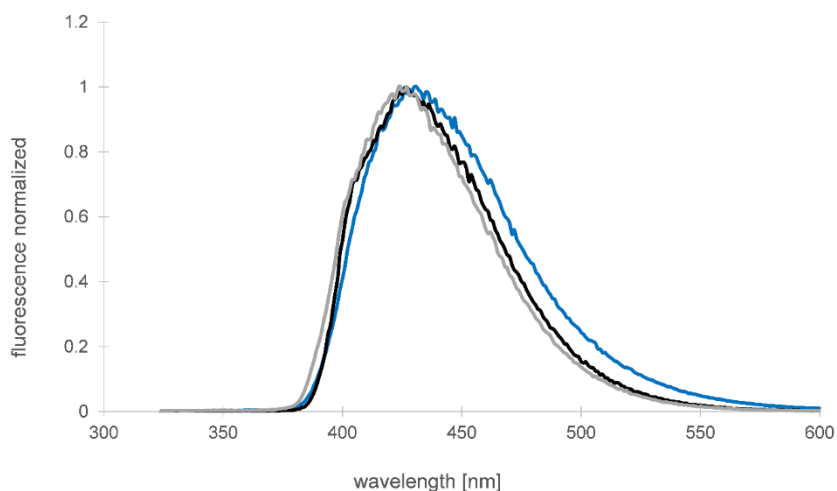


**Figure 4.17** Normalized fluorescence of oligomer **b** in 10 mM sodium phosphate buffer at 90 °C (blue) and oligomer **b** in EtOH (black) as well as the fluorescence trace of a DNA single strand containing one dialkynylpyrene and one dialkynylphenanthrene previously measured in our group by GK (grey).

Surprisingly enough, the exciplex fluorescence was never observed in the molecular antenna aggregated in buffered water for the above mentioned design of the antenna. This might have to do with geometrical reasons of the dialkynylphenanthren-dialkynylpyrene arrangement.

Nevertheless, there are indications that the dialkynylphenanthrene and the dialkynylpyrene form exciplexes in a deaggregated state of oligomer **b** as shown at higher temperatures or in mixtures containing higher amounts of EtOH (Figure 4.17). Further antenna systems with different acceptor molecules are discussed in the sections below (4.3.8.) to elucidate the characteristics of the exciplex formation.

#### 4.3.7. Polymer light harvesting antenna with pyrene monomer

The phenanthrene polymer is formed by using 0.5  $\mu\text{M}$  of oligomer **a** in 10 mM sodium phosphate buffer. Dialkynylpyrene diol was titrated to the solution (Figure 4.18). Also in this experiment we see a pronounced antenna effect and an efficient transfer of energy to the pyrene diol molecule. The pyrene diol intercalates into the phenanthrene polymer. It is assumed that the pyrene diol stacks in a face-to-face manner to the polymer as this would lead to the most efficient energy transfer but more detailed studies to elucidate the exact structure would be needed. The excitation of the pyrene molecule itself leads to a very low fluorescence which increases almost linearly with increasing pyrene-concentration (Figure 4.19).

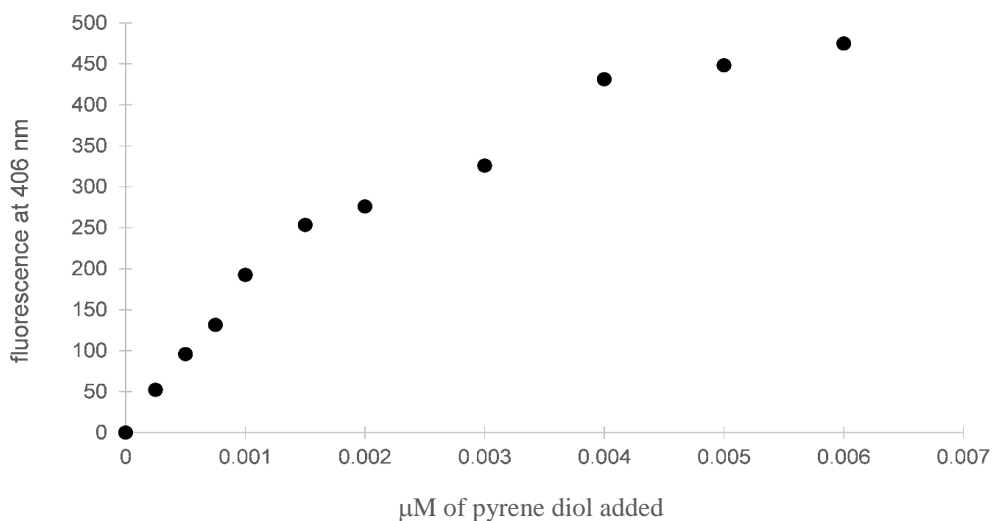


**Figure 4.18** Dialkynylpyrene diol was added to a solution of 0.5  $\mu\text{M}$  oligomer **a** in 10 mM sodium phosphate buffer. The fluorescence of the solution was measured upon excitation at 322 nm (phenanthrene).

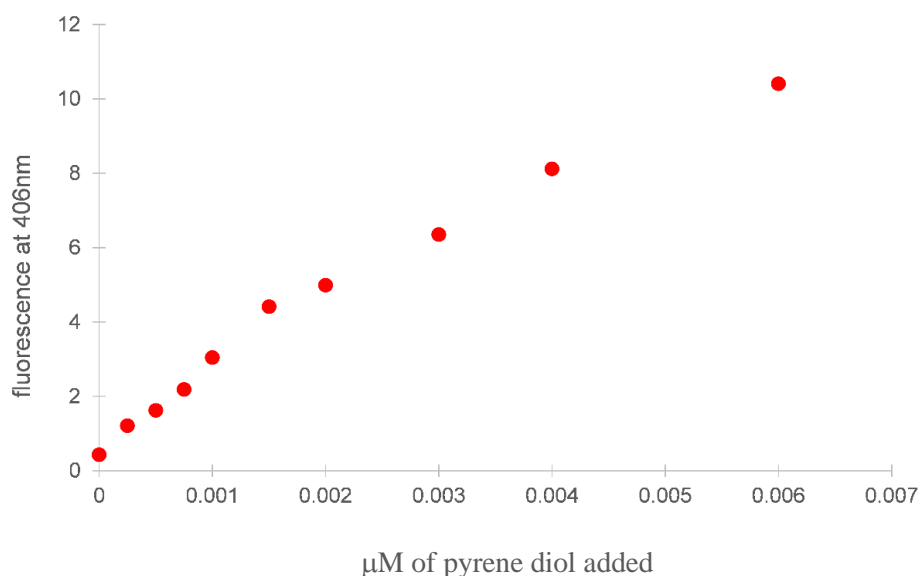


**Figure 4.19** Dialkynylpyrene diol was added to a solution of 0.5  $\mu\text{M}$  oligomer **a** in 10 mM sodium phosphate buffer. The fluorescence of the solution was measured upon excitation at 370 nm (pyrene).

Comparison of the two antenna systems with once oligomer **b** as an acceptor molecule and once with only the alkynylpyrene diol shows that they have almost the same transfer characteristics (Figure 4.20). Measurement of the fluorescence of both antenna systems with excitation at 370 nm (Figure 4.21) indicates that in both cases the same amount of acceptor molecule was added to the solution and that experimental errors are small (even though that very small concentrations and volumina had to be titrated). Excitation at the phenanthrene absorption at 322 nm shows a fluorescence up to 600 units. In both cases we see the fluorescence a maximal permisse value approaching which indicates a saturation of the polymer by energy absorbing pyrene. In the case of the dialkynylpyrene we see a fluorescence which is reduced by approximately one fifth compared with the antenna system where we use oligomer **b** as an energy acceptor molecule. The difference could be explained that the dialkynylpyrene shows a lower affinity to the polymer than the oligomer **b** which contains three dialkynylpheanthrenes and one dialkynylpyrene.

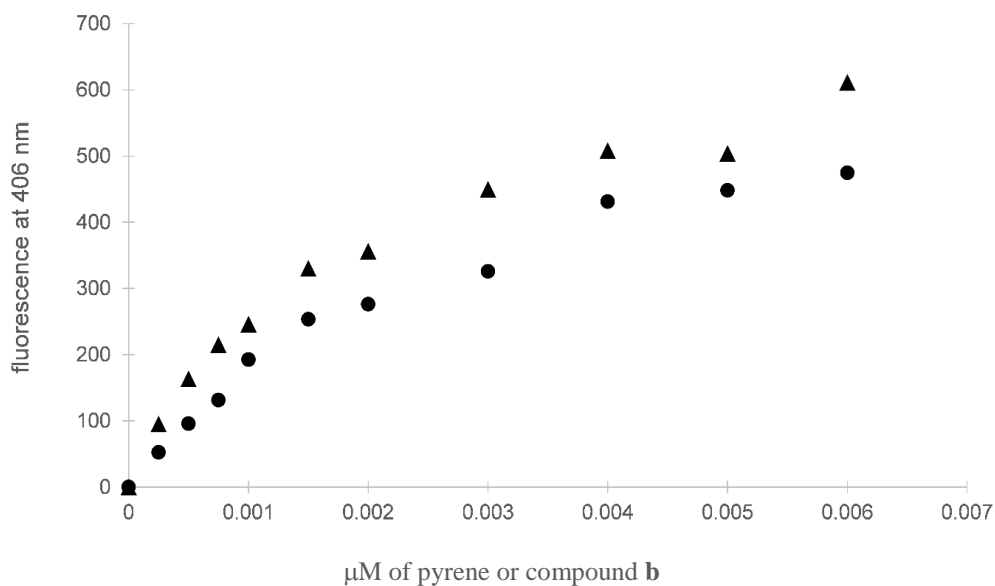


**Figure 4.20** To a solution of  $0.5 \mu\text{M}$  of oligomer **a** in  $10 \text{ mM}$  sodium phosphate amounts of pyrene diol (dots) or oligomer **b** (triangle) was added to reach the indicated concentrations. Excited at  $322 \text{ nm}$ . Comparison of the two experiments indicate that the pyrene diol is slightly less well incorporated into the polymer but acts also as a very efficient antenna acceptor.

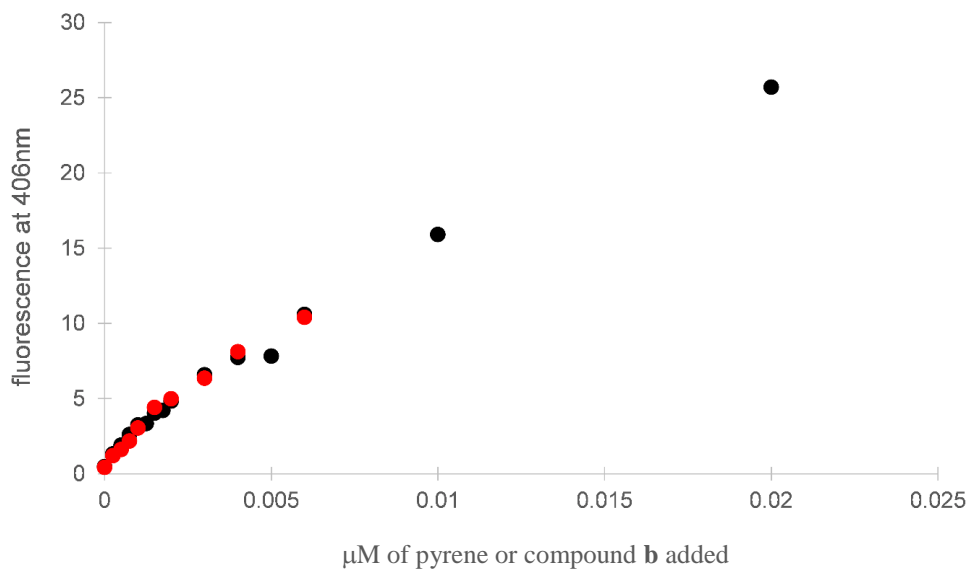


**Figure 4.21** To a solution of  $0.5 \mu\text{M}$  of oligomer **a** in  $10 \text{ mM}$  sodium phosphate amounts of pyrene diol (red dots) or oligomer **b** (black dots) was added to reach the indicated concentrations. Excited at  $370 \text{ nm}$ .

### 4.3.8. Equilibrium between excimer and exciplex fluorescence

In a further antenna system a different acceptor molecule is used which contains three covalently linked dialkynylpyrene molecules.

**Table 4.3** Sequence of oligomer **a** used as collector in the supramolecular antenna, oligomer **b** used as acceptor in the antennae (see data on top) and oligomer **c** used as an alternative acceptor molecule in the polymer antenna.

	sequence
oligomer <b>a</b>	5' <i>aaa</i>
oligomer <b>b</b>	5' <i>Yaaa</i>
oligomer <b>c</b>	5' <i>YYY</i>

Formation of polymers is shown by AFM at different concentrations of oligomer **a** and oligomer **c** (Figure 4.22).

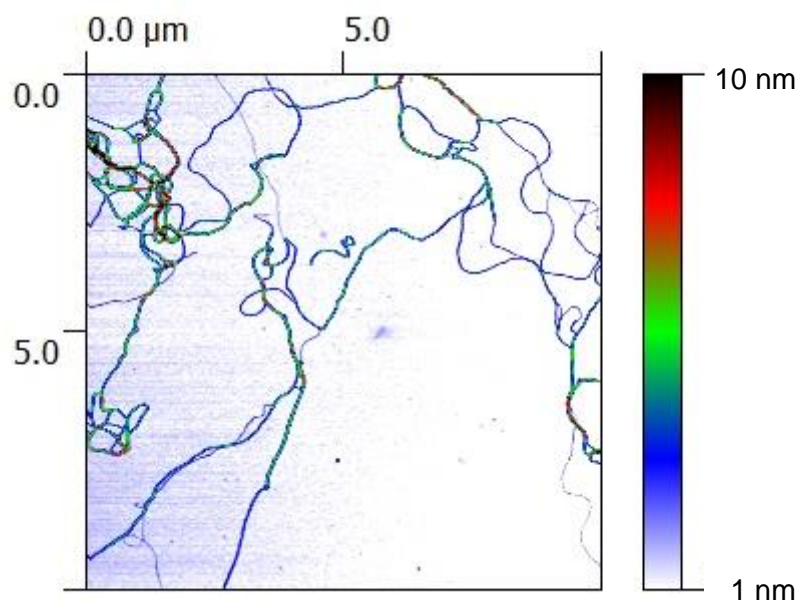


**Figure 4.22** AFM of a solution of 2  $\mu\text{M}$  oligomer **a** and 0.5  $\mu\text{M}$  of oligomer **c** in 10 mM sodium phosphate buffer.

0.5  $\mu\text{M}$  of oligomer **c** in 10 mM sodiumphosphate buffer shows an excimer fluorescence with a maxima at 522 nm after excitation at 370 nm, which is a characteristic for oligomers containing multiple **Y**<sup>74</sup>. The addition of 0.1  $\mu\text{M}$  of oligomer **a** shifts the fluorescence maxima to 491 nm and a reduced fluorescence is observed (Figure 4.23). Further addition of oligomer **a** increases the excimer fluorescence of the acceptor molecule until a maximal value is reached when the ratio of collector oligomer **a** and acceptor oligomer **c** is 1. Further addition of oligomer **a** did not enhance the fluorescence of the pyrene excimer when excited at the pyrene molecule.

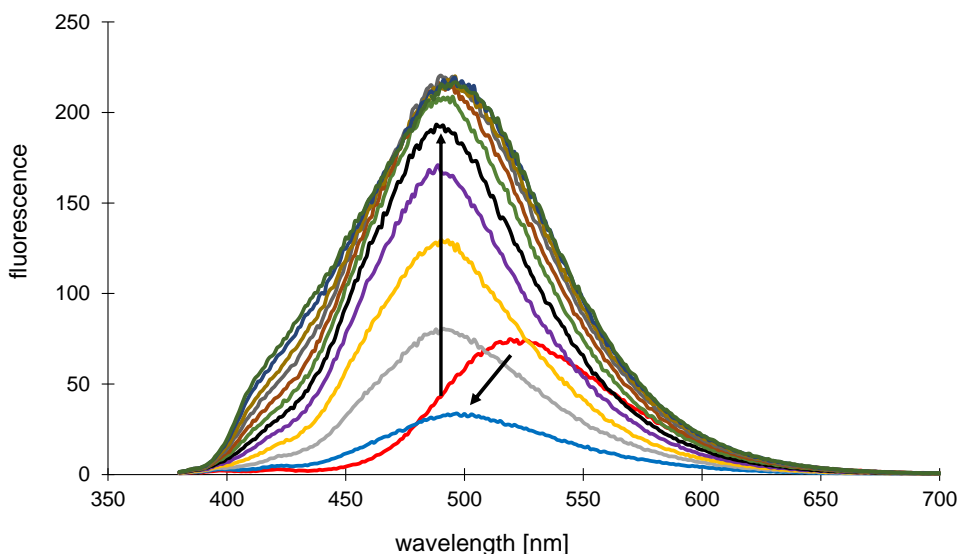


**Figure 4.23** To a solution of 0.5  $\mu\text{M}$  of oligomer **c** (red trace) in 10 mM sodium phosphate buffer, pH 7.2, oligomer **a** was added in 0.1  $\mu\text{M}$  steps up to 1.1  $\mu\text{M}$  (2.1 eq). Black line indicates the sample with a ratio of oligomer **a** to oligomer **c** of 1:1. Excitation at 370 nm. Arrows indicate the shift upon the first addition of 0.1  $\mu\text{M}$  of oligomer **a** (from red to blue trace) and subsequent increase upon further addition of oligomer **a**.

The same titration series was also excited at the pheanthrene absorption at 322 nm (Figure 4.24). Without addition of oligomer **a** the excimer fluorescence of the pyrene is quite weak as the absorption of the pyrene in the area of the 322 nm is minor. The pyrene excimer fluorescence is observed upon excitation at 322 nm. Addition of oligomer **a** also shifts the fluorescence of the excimer to lower wavelength and the fluorescence is increased. Further addition of phenanthrene 3 mer further increases the fluorescence steadily, showing a perfect antenna effect.



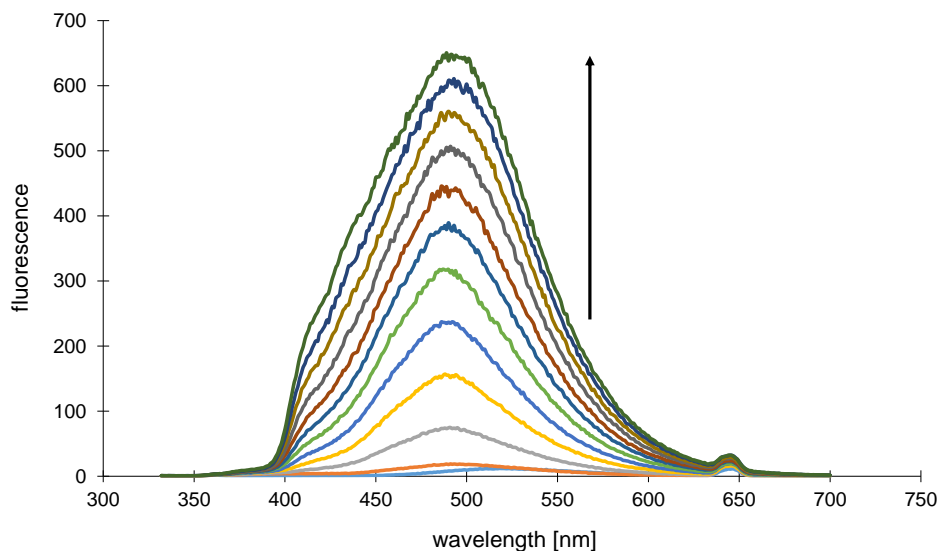


**Figure 4.24** To a solution of 0.5  $\mu\text{M}$  of oligomer **c** (slight blue trace) in 10 mM sodium phosphate buffer, pH 7.2, oligomer **a** was added in 0.1  $\mu\text{M}$  steps up to 1.1  $\mu\text{M}$  (2.1 eq). Excitation at 322 nm. The arrow indicates increasing fluorescence upon addition of increasing concentrations of oligomer **a**.

The shift of the excimer fluorescence can not be explained on details (Figure 4.25). A possible explanation could be the formation of static and flexible excimers by the dialkynylpyrene. In the solution with only oligomer **c** the pyrenes are loosely ordered and show an excimer which has the maximal fluorescence at 522 nm. After addition of the phenanthrene 3 mer the pyrenes are re-aligned to form static excimers with a well defined face-to-face geometry. This would result in a blue shifted fluorescence. Such static excimers have been described in literature<sup>174</sup>.

Previous findings in our group contradict this hypothesis as so far always the excimer at 522 nm was observed. This was the case in DNA-assisted assemblies of dialkynylpyrenes with two or more pyrenes as well as in polymeric dialkynylpyrene assemblies<sup>74,142</sup>. Especially in the DNA-guided assembly the interaction of the pyrene-molecules is considered as being quite static with a low degree of freedom for structural changes. Due to the unknown exact nature of the fluorescence signal with the maximal intensity at 491 nm I will name this exact type of fluorescence “pyrene-excimer-like” fluorescence in the following sections of this thesis. Visible from UV/VIS measurements is, that oligomer **c** alone forms a  $\pi$ - $\pi$  stacked H-aggregate which is characterized by a pronounced absorption-peak at 369 nm and a shoulder which is blue-shifted and appears at around 355 nm (Figure 4.26). The formation of mixed polymers of oligomers **c** and **a** results in an increased intensity of the pyrene absorption band at 390 nm which indicates an alternating phenanthrene-pyrene stacking (see also chapter Observation of two independent H-couplings in a stack of multiple chromophores).

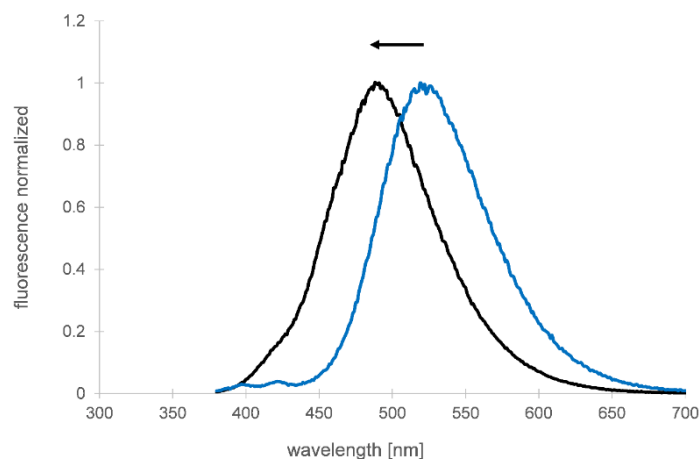


**Figure 4.25** Normalized fluorescence spectra of 1,8-dialkynylpyrene excimer fluorescence (oligomer **c**, blue trace) and observed fluorescence in the molecular antenna system (oligomer **a** and **c**, black).

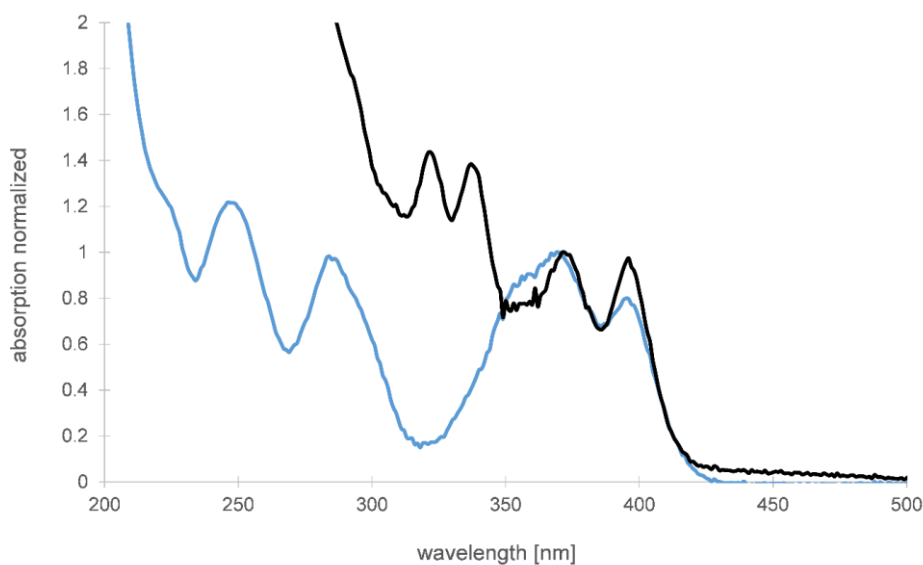


**Figure 4.26** Normalized absorption spectra of oligomer **c** (blue) and a 1:1 mixture of oligomer **a** and **c** (black) in 10 mM sodium phosphate. The higher absorption at 390 nm in mixed oligomers (black) indicates an alternating stacking of pyrene and pheanthrene i.e. a destacking of the tight pyrene-pyrene stack (blue).

Titration of 0.5  $\mu\text{M}$  of oligomer **c** with increasing concentrations of oligomer **a** shows the following pattern: The absorption of the pyrene stays constant as the concentration of pyrene is not changed during the titration experiment. Increasing concentrations of oligomer **a** are shown in the UV/VIS spectra (Figure 4.27). Fluorescence was measured upon excitation at 322 nm. Addition of up to 4 equivalents of oligomer **a** increases the fluorescence of the molecular antenna

(Figure 4.28). A fluorescent shoulder becomes more and more pronounced at 450 nm with increasing phenanthrene concentration. Fluorescence measurements of the phenanthrene itself shows a fluorescence maxima at 406 nm with a shoulder in the area of 380 nm<sup>175</sup>. The fluorescence of the molecular antenna using oligomers **a** and **c** shows a shape which is a composition of the excimer like fluorescence from the red curve in Figure 4.28 as well as an increasing amount of phenanthrene-pyrene exciplex fluorescence (Figure 4.17). Calculations show that the fluorescence of the titration experiment can be composed of these two kinds of fluorescence traces according to equation [5].

$$\text{calculated curve} = x * \text{"excimer"} + y * \text{"exciplex"} \quad [5]$$

Each curve was calculated and the differences between the calculated and the measured curve was minimized by altering the factors  $x$  and  $y$  of equation [5]. The differences of the two curves in the area between 500-650 nm accounted quite strongly in the least square method. Therefore the curves did not perfectly overlay in other areas. Shape complementarity was best by manually altering the factors  $x$  and  $y$  until the two curves overlay strongly. An example of the two aligning methods (least square vs manually alteration) is depicted in Figure 4.29.

In the calculated curve, a fraction  $x$  of excimer and a fraction  $y$  for exciplex of each curve is plotted versus the respective equivalents of oligomer **a** in the antenna. For the excimer, the red curve in Figure 4.28 is chosen to be  $x = 1$ . The exciplex fraction in the first curve is 0. For the next curve, the relative fraction of exciplex was calculated to be 1 (Figure 4.30 and Table 4.4).

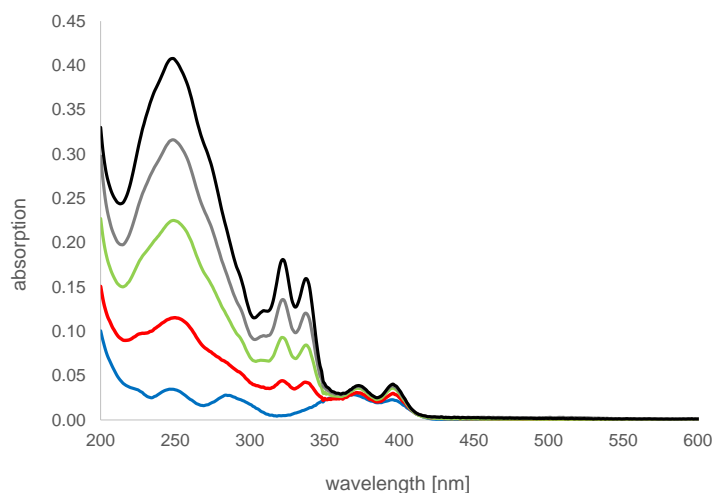


**Figure 4.27** Absorption trace of a titration of oligomer **a** in 0.5  $\mu\text{M}$  steps added to a solution of 0.5  $\mu\text{M}$  of oligomer **c** in 10 mM sodium phosphate.

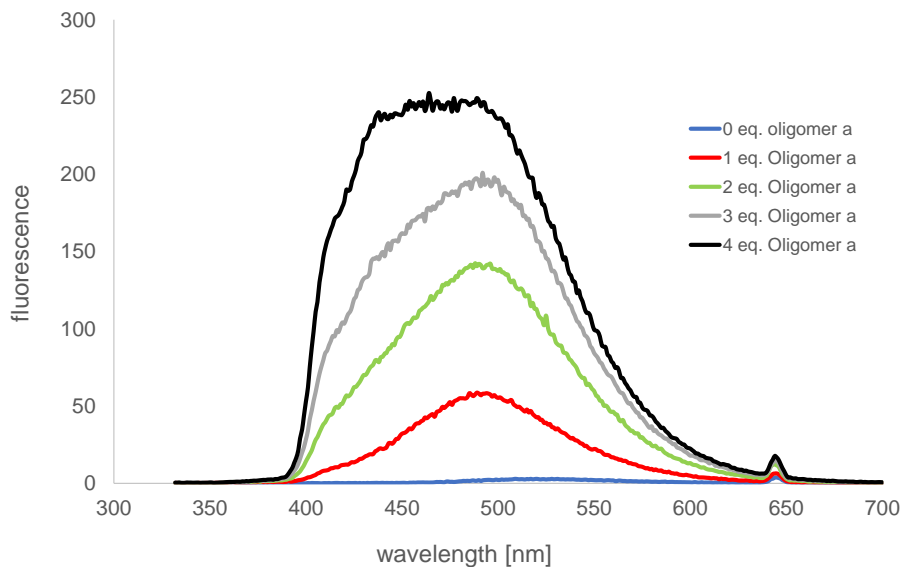


**Figure 4.28** Fluorescence of a titration of oligomer **a** in 0.5  $\mu\text{M}$  steps added to a solution of 0.5  $\mu\text{M}$  of oligomer **c** in 10 mM sodium phosphate. Excited at 322 nm.

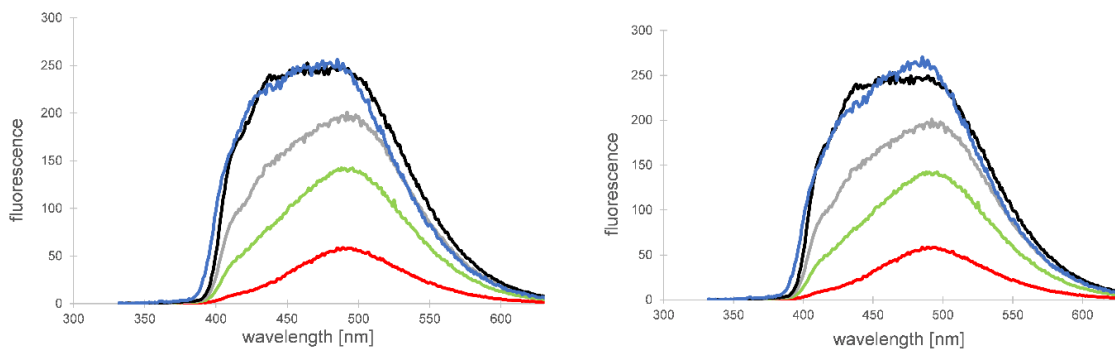


**Figure 4.29** Fluorescence of a titration of oligomer **a** in 0.5  $\mu\text{M}$  steps to a solution of 0.5  $\mu\text{M}$  of oligomer **c** in 10 mM sodium phosphate. Excited at 322 nm. The blue curve represents a fitted curve composed of a fraction “eximer” and “exciplex”. Left: the curve is fitted manually to get optimal geometrical overlay Right: the curve is fitted using least square method.

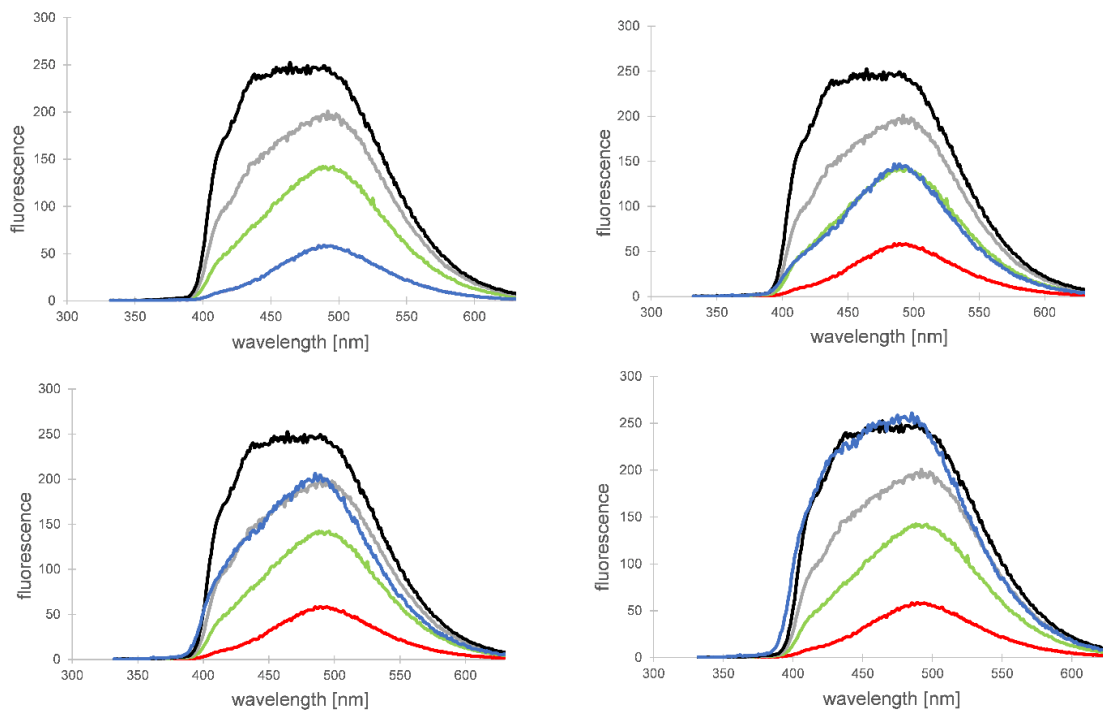


**Figure 4.30** Fluorescence of a titration of oligomer a in  $0.5 \mu\text{M}$  steps to a solution of  $0.5 \mu\text{M}$  of oligomer c in  $10 \text{ mM}$  sodium phosphate. Excited at  $322 \text{ nm}$ . The blue curve represents a fitted curve composed of a fraction “eximer” and “exciplex”. For each curve the fraction “eximer” and “exciplex” is extracted.

**Table 4.4** Relative fractions of excimer and exciplex contribution for each curve of the titration experiment. Values are derived by least square method.

	excimer	exciplex
curve 1	1	0
curve 2	2.4	1
curve 3	3.15	2.38
curve 4	3.7	4.76

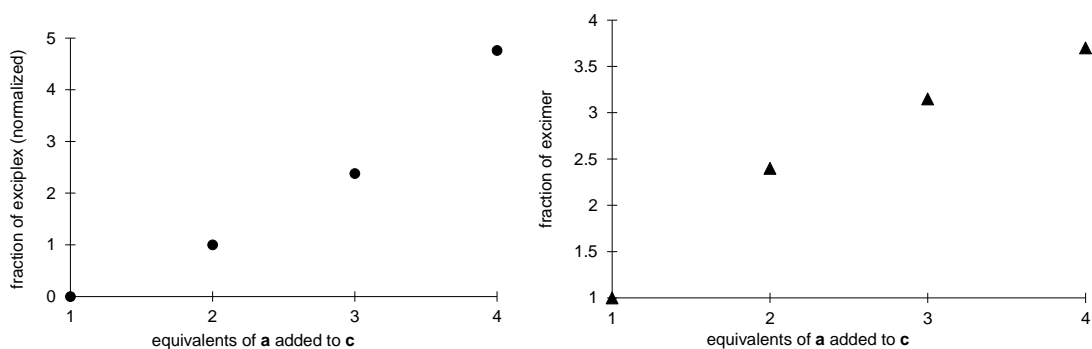


**Figure 4.31** Fraction of exciplex and excimer plotted against the equivalents of oligomer **a** added to a solution of oligomer **c**. The fraction of exciplex always gets more pronounced, whereas the fraction of excimer reaches a maximal permissible value.

It can be seen that the increase of the excimer fraction becomes less and less as more phenanthrene oligomer **a** is added to the solution. On the same time the fraction of exciplex increases. Titration of a solution of oligomer **a** with increasing amounts of oligomer **c** even better illustrates this effect (Figure 4.32). At very low concentrations of oligomer **c** almost only exciplex fluorescence is seen with a shoulder at around 405 nm. The fluorescence at 405 nm has monomeric character. Currently no explanation for this monomeric fluorescence is available.

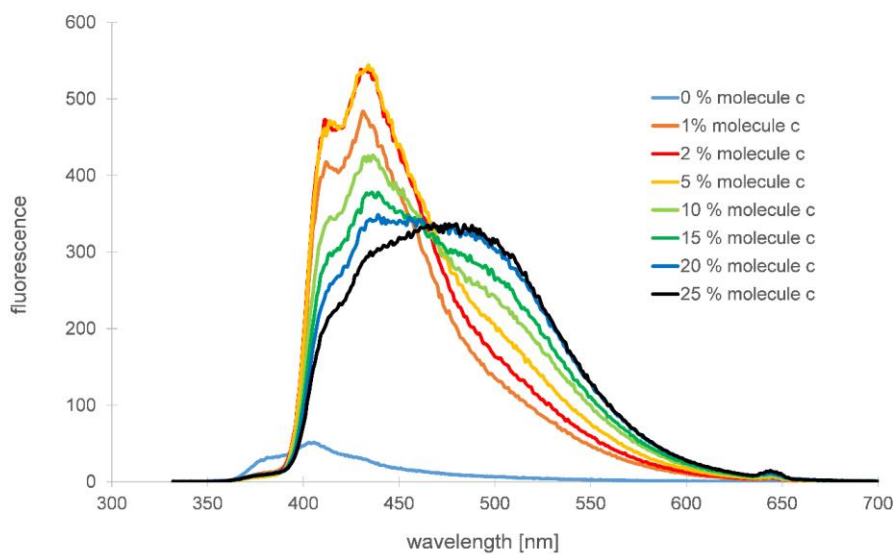


**Figure 4.32** Titration of low amounts of oligomer **c** to a solution of  $0.5 \mu\text{M}$  of oligomer **a**. The fraction of exciplex fluorescence decreases whereas the fraction of pyrene excimer fluorescence increases steadily.

The fluorescence of increasing amounts of oligomer **a** without acceptor molecule is shown in Figure 4.33.

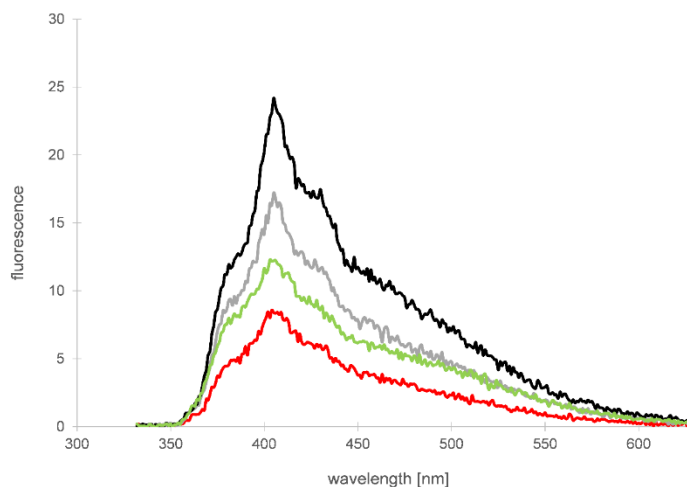


**Figure 4.33** Increase of the dialkynylphenanthrene fluorescence upon titration. Each step represents the addition of 0.5  $\mu\text{M}$  of oligomer **a**. Excitation at 322 nm, excitation slit width 2.5 nm.

Temperature dependent UV/VIS and fluorescent measurements have been carried out on a mixture of oligomer **a** and **c** in a ratio 1 to 1. At 90 °C the absorption spectra is shifted by 8 nm toward lower wavelength (Figure 4.35). A slightly higher absorption band of the  $S_0$ - $S_1$  transition of the pyrene is seen at higher temperature which indicates a closer stacking of the pyrene molecules respectively an unstacking at lower temperatures due to the alternating interaction with the phenanthrene. For the phenanthrene units we again see a hyperchromicity at the area of 250 nm upon melting. Fluorescence measurements at 20 °C show a pronounced pyrene excimer like fluorescence upon irradiation at 322 nm. After melting and excitation of the phenanthrene at 314 nm (new maximal absorption of phenanthrene) a very weak excimer like fluorescence was observed and a new fluorescent signal is observed below 400 nm. This fluorescence is attributed to the phenanthrene molecules at high temperature (Figure 4.34).

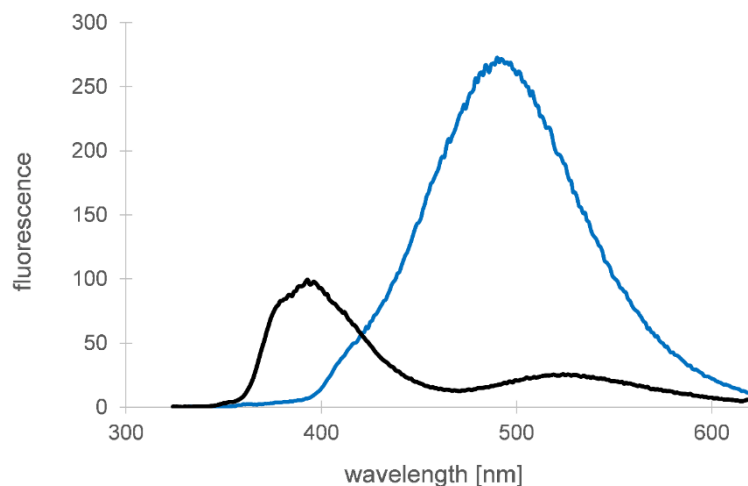


**Figure 4.34** Fluorescence of a solution containing each 0.5  $\mu\text{M}$  oligomer **a** and oligomer **c** in 10 mM sodium phosphate at 20  $^{\circ}\text{C}$  (blue) and 90  $^{\circ}\text{C}$  (black). Excitation at 322 nm, the energy transfer from the phenanthrene to the pyrene is interrupted upon heating and destruction of the polymer resulting in a sharp decrease of the fluorescence at 491 nm.

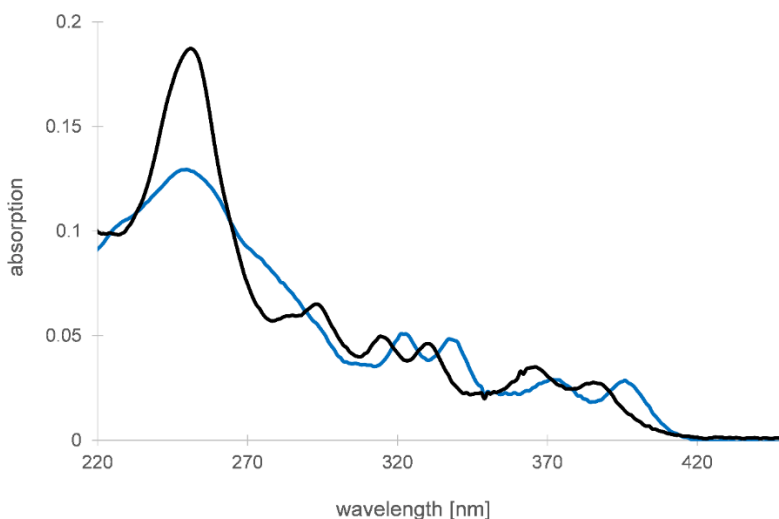


**Figure 4.35** UV/VIS absorption of a solution containing each 0.5  $\mu\text{M}$  oligomer **a** and oligomer **c** in 10 mM sodium phosphate at 20  $^{\circ}\text{C}$  (blue) and 90  $^{\circ}\text{C}$  (black).

A fluorescent melting experiment has been performed using the molecular antenna consisting of 0.5  $\mu\text{M}$  of oligomer **c** and 0.5  $\mu\text{M}$  of oligomer **a**. The antenna was excited at 322 nm (Figure 4.36) and 370 nm (Figure 4.37) at different temperatures. At 20  $^{\circ}\text{C}$  we see a pronounced pyrene excimer like fluorescent signal with a slight shoulder at 420 nm. This shoulder most probably comes from phenanthrene fluorescence as discussed above. Slight differences of the curve shapes at 20  $^{\circ}\text{C}$  in Figures 4.36 and 4.37 could be explained by kinetic effects (fast or slow cooling) of the polymer solutions. Basic experiments to get insight into the polymerisation kinetics of the polymers have been performed but will not be further discussed in this thesis<sup>176</sup>. Increasing the temperature steadily and upon excitation at 322 nm we first see a decrease of the fluorescent intensity at 420



nm which was on top indicated as being phenanthrene fluorescence which was not efficiently transferred to the pyrene molecules. At 50 °C a pure pyrene-excimer fluorescence is observed which then starts to melt as higher temperatures destroy the phenanthrene-pyrene polymer and prevents the transfer of energy in the polymer. Increasing phenanthrene fluorescence at 380-390 nm arises as a consequence thereof. Excitation at 370 nm results in the same excimer-like fluorescence with a shoulder at 420 nm. Melting of the polymers also reduces this shoulder but in contrary to the case when the samples are excited at 322 nm the fluorescence of the pyrenes does not decrease as the pyrene is excited directly.

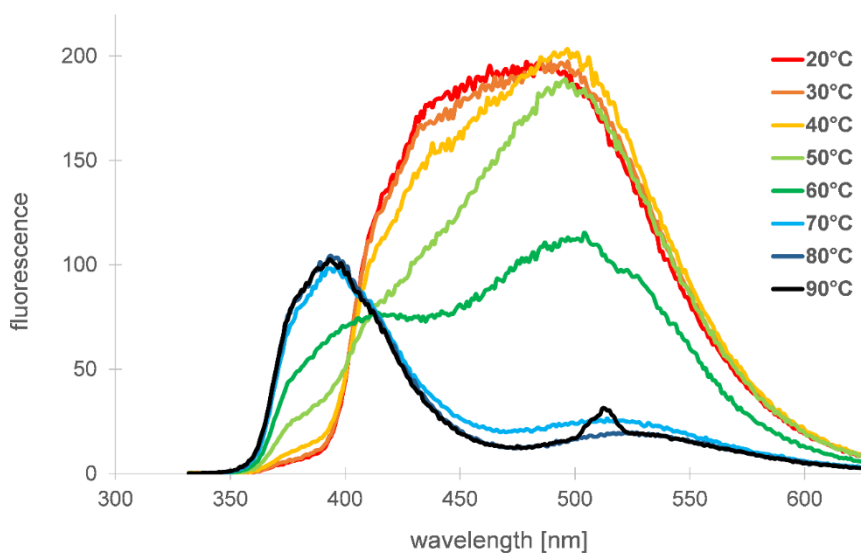


**Figure 4.36** Temperature dependent measurement of a molecular antenna composed of each 0.5  $\mu\text{M}$  oligomer **a** and oligomer **c** in 10 mM sodium phosphate. Excitation at 322 nm.

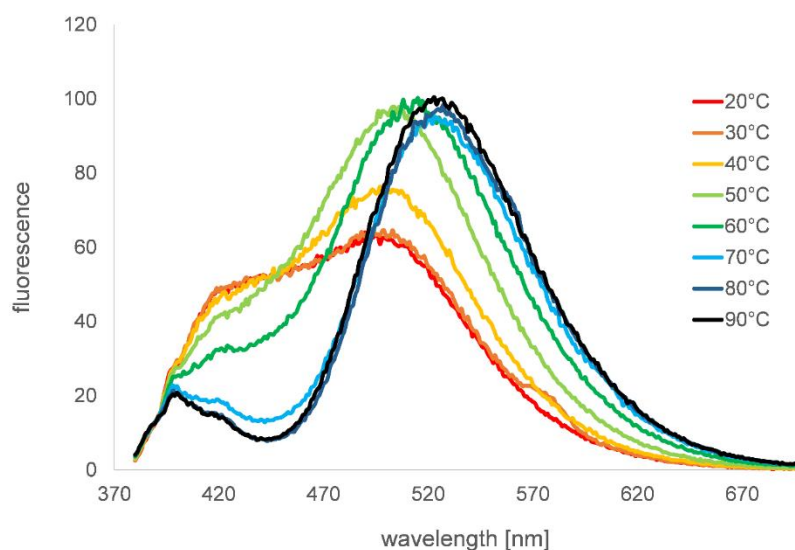


**Figure 4.37** Temperature dependent measurement of a molecular antenna composed of each 0.5  $\mu\text{M}$  oligomer **a** and oligomer **c** in 10 mM sodium phosphate. Excitation at 370 nm.

Upon excitation at 322 nm and measuring the emission at 490 nm a pronounced melting behaviour is visible. The melting behaviour of the molecular antenna consisting of 0.5  $\mu\text{M}$  of oligomer **c** and 2  $\mu\text{M}$  of oligomer **a** was measured. Polymerization was initiated at 64  $^{\circ}\text{C}$  with a sharp transition and a rapid increase of fluorescence. A huge hysteresis again is observed as the polymers melt at higher temperatures as they are formed. This is remarkable as the heating and cooling ramps were chosen to be 0.2  $^{\circ}\text{C}$  per min which is quite slow.

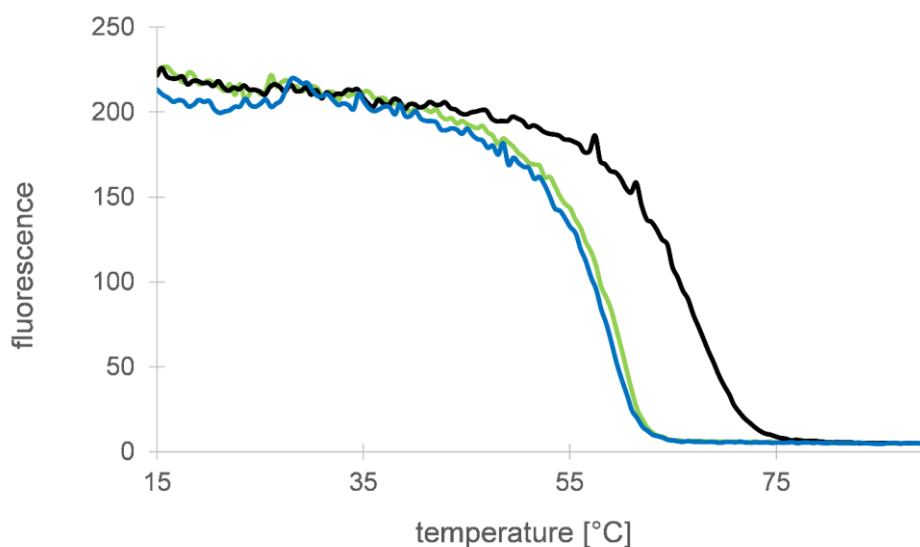


**Figure 4.38** Temperature dependent fluorescence measurement of a polymer antenna system composed of each 0.5  $\mu\text{M}$  of oligomer **a** and oligomer **c** in 10 mM sodium phosphate buffer. Excitation at 322 nm, emission at 491 nm. The experiment was performed in subsequent cooling-heating-cooling ramps with 0.2  $^{\circ}\text{C}$  per min.

## 4.4. Conclusion and Outlook

### 4.4.1. Observation of long-distance EET in linear supramolecular antenna systems

Dialkynylphenanthrene based linear polymers with light harvesting properties were investigated in combination with different dialkynylpyrene acceptor molecules.

- a) Using an acceptor molecule which consists of three dialkynylphenanthrene molecules and one dialkynylpyrene and mixing them in small quantities with the phenanthrene-polymer, pyrene monomer fluorescence is visible.
- b) Using dialkynylpyrene-diol as an acceptor molecule pyrene, monomer fluorescence is visible
- c) Using an acceptor molecule which consists of three pyrenes and mixing it in small quantities with the phenanthrene polymer results in dialkynylphenanthrene-dialkynylpyrene exciplex. Using the acceptor in higher quantities pyrene-excimer fluorescence is visible.
- d) For case a) information on the efficiency of the electronic energy transfer (EET) can be derived from the doping experiment (Figure 4.9). Polymers formed exclusively of oligomer **a** exhibit only weak fluorescence. Addition of  $0.5 \times 10^{-3}$  equivalents of oligomer **b**, which corresponds to a phenanthrene/pyrene ratio of approx. 6000 (indicated with arrow in Figure 4.39), results in a sharp increase in the quantum yield  $\phi_f$  (0.080). It can be assumed that, at this ratio, the pyrene accepts and emits the maximum possible amount of excitation energy. The energy absorbed by the phenanthrene molecules is transferred along the polymer over a certain distance to the pyrene acceptor where it is emitted. When the number of pyrenes, which are assumed to be statistically distributed over the polymer chain, increases, they are located more and more densely in the polymer. The quantum yield of the polymer grows with an increasing number of pyrenes and eventually approximates the value of 1,8-dialkynylpyrene monomer ( $\phi_f^{Py} = 0.55$ , dotted line in Figure 4.38). Together with the molecular distance separating face-to-face stacked polyaromatic compounds (0.35 nm), and assuming a random statistical distribution of pyrene acceptor molecules within the polymer, a rough estimation of the average distance of ET ( $D_{ET}$ ) can be made according to the equation below:  $N^{phe}$  = number of phenanthrene molecules per one pyrene,  $\phi_f^{Py}$  = quantum yield of 1,8-dialkynylpyrene monomer and  $\phi_f^A$  = quantum yield of phenanthrene polymers doped with  $0.5 \times 10^{-3}$  mol equivalents of pyrenes; the factor 0.5 addresses the fact that light is collected from both sides of the pyrene.

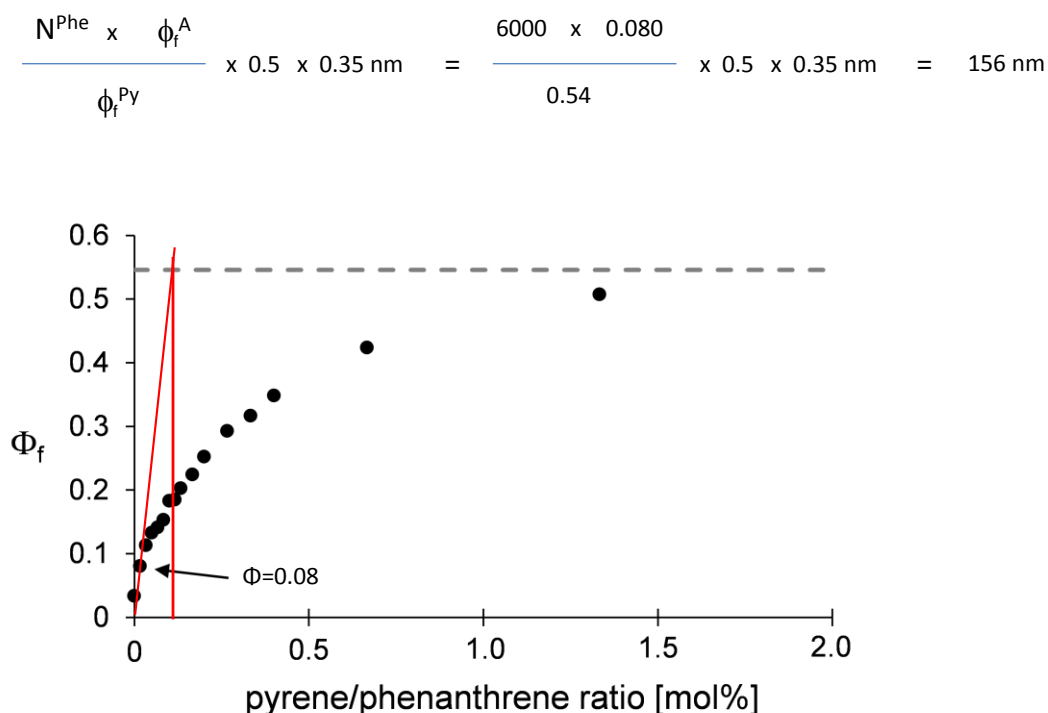


**Figure 4.39** Increasing amounts of oligomer **b** (indicated in mol%) are added to a solution of 0.5  $\mu\text{M}$  of oligomer **a**. The quantum yield (0.08) of the first added amount of oligomer **b** was used to calculate the ET-distance according to the above mentioned equation.

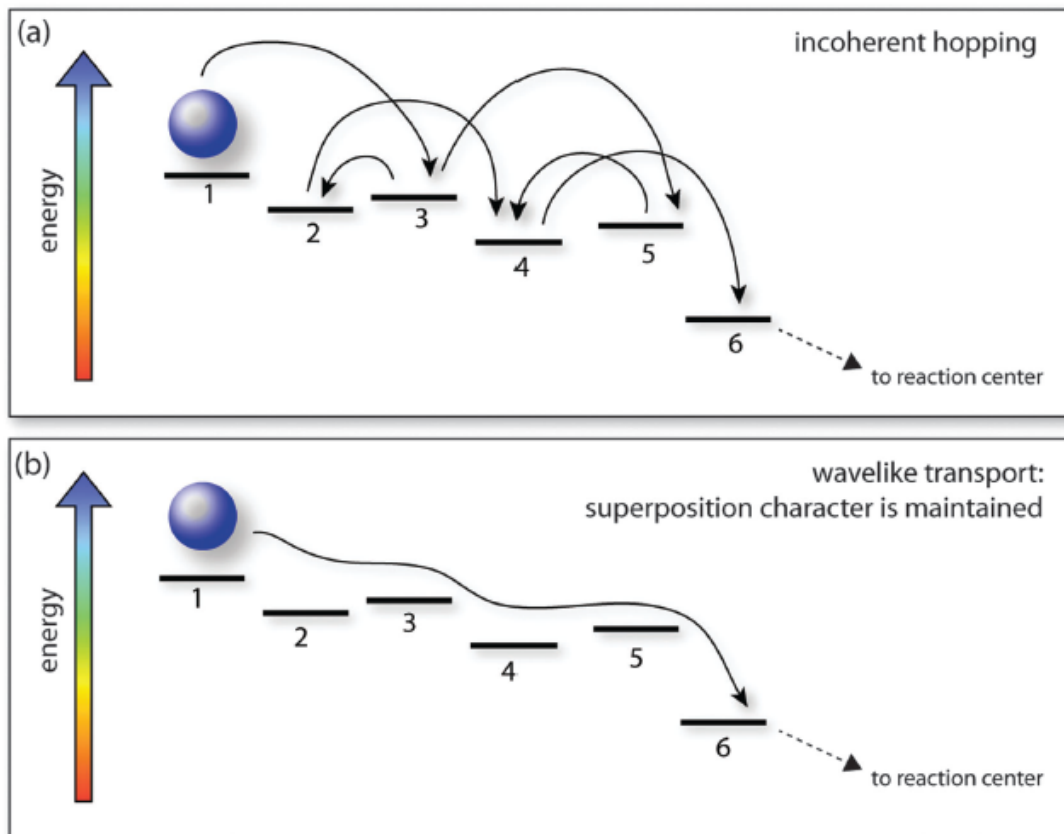
Such a long range energy transfer most probably does not rely on a classical EET (excitation energy transfer, i.e. Förster Resonance Energy Transfer FRET<sup>177</sup>) and other energy transfer mechanisms have to be taken into account. In classical EET in multichromophoric systems the excitation energy can be transferred by a series of EET hops over a reasonable long distance. The excited state lifetime is the limiting factor for excited energy transfer<sup>178</sup>. In FRET-based mechanisms the electronic coupling of two molecules (which are represented as a dipole-dipole interaction between electric dipole transition moments) is highly dependent on the distance between these two molecules. FRET based energy transfer efficiency  $E$  decreases with increasing distance  $R$  of the chromophores by:

$$E = \frac{1}{1+(R/R_0)^6} \quad [6]$$

Whereby  $R_0$  is the Förster radius of the chromophores – the critical molecular separation at which the energy transfer efficiency is 50 %<sup>179</sup>. Another prerequisite is a spectral overlap of the emission spectrum of the donor molecule and the absorption spectrum of the acceptor chromophore.

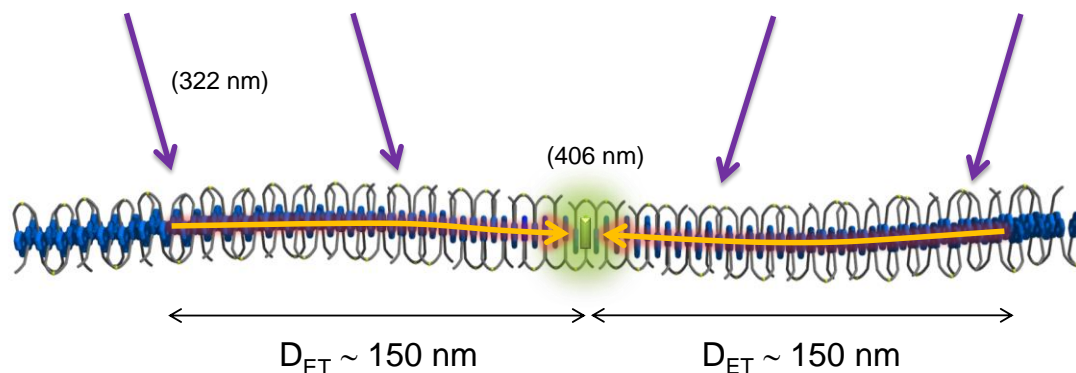
Quantum coherence was in the recent years found to play a prominent role in natural light harvesting processes of plants and photosynthetic active bacteria<sup>178,180-185</sup>. Scheme 4.3 depicts the difference between the classical EET whereby the excited state is always localized on one

particular molecule and coherent mechanisms. In an incoherent process, the excitation energy jumps randomly between the molecules losing energy at each step. In quantum coherence the excitonic states are considered to be super positioned and the excitation energy is shared among several molecules<sup>178</sup>.



**Scheme 4.3** Schematical representation of the energy transfer processes by incoherent hopping and according to a coherent mechanism. From Ref<sup>178</sup>.

Quantum coherence might be a way to explain the very efficient energy transfer in the above described light harvesting polymers (Scheme 4.4). Further investigations and calculations would be needed to further elucidate an exact theory of the system.



**Scheme 4.4** Representation of the light harvesting polymers of phenanthrene (blue) and one inserted pyrene (green). Excitation of the phenanthrene at 322 nm results in pyrene fluorescence (406 nm). Calculations show an energy transfer over distances of 150 nm. Scheme was prepared by S. Langenegger.

Adding acceptor oligomer **c** in low concentrations to the phenanthrene polymer shows a dialkynylphenanthrene-dialkynylpyrene exciplex. Increasing the concentration of the acceptor results in a pyrene excimer fluorescence. At high concentration of oligomer **c** it is plausible that the pyrenes form the excimer even though that the phenanthrene molecules interdigitate and separate the pyrene molecules from each other (see also chapter Observation of two independent H-couplings in a stack of multiple chromophores). At lower concentrations of **c** it is hypothesized that the excited states of the pyrenes superimpose with the excited states of the phenanthrene molecules and thereby form coherent excited states which are visible as exciplex fluorescence of the antenna system.

The use of dialkynylpyrene diol as acceptor molecule in very low concentrations (0.5 nM) and even lower encouraged us to try to use the phenanthrene polymer antenna as a sub nanomolar detection system for polyaromatic hydrocarbons. Using unmodified pyrene (CAS 129-00-0) as a potential acceptor molecule no antenna effect was observed which indicates that no intercalation of the pyrene molecule into the polymer antenna was possible. Using a diol-modified chrysene molecule<sup>104,186</sup> also did not incorporate into the polymer rather formed self-aggregates<sup>148</sup>. Nevertheless, I think that different selected molecules could act as acceptor molecules. Different cyanine dyes, perylene dyes or chrysene molecules with different linkers could be feasible candidates. Thereby polymer antennas could be generated with altering acceptor and differently emitting properties. The same could be performed with molecules with quenching properties. Preliminary experiments with naphthalenediimide monomers and three-mers thereof have been performed and showed quenching effects of the antenna. Different ratios of fluorescent and quenching acceptor molecules could be applied to study the energy transfer mechanism.

Time resolved fluorescence measurements could unravel the exact energy transfer mechanism and probably determine essential parameters like the coherence length in the polymers.

#### 4.4.2. Design of polymer light harvesting antenna systems

A next step would be to design light-harvesting polymers with absorption properties in the visible light. Appropriate molecules therefore would be perylene based chromophors<sup>146</sup>.

Using DNA modified collector oligomer **d** did not result in an antenna effect<sup>148</sup>. This is most probably due to higher solubility of the DNA modified molecule.

**Table 4.5** DNA modified acceptor molecules for molecular polymer antennas

molecule	sequence
<b>d</b>	5' GCG TTA <b>Yaa a</b>
<b>e</b>	5' <b>YYY</b> YTA ACG C
<b>f</b>	5' <b>EEE</b> ETA ACG C

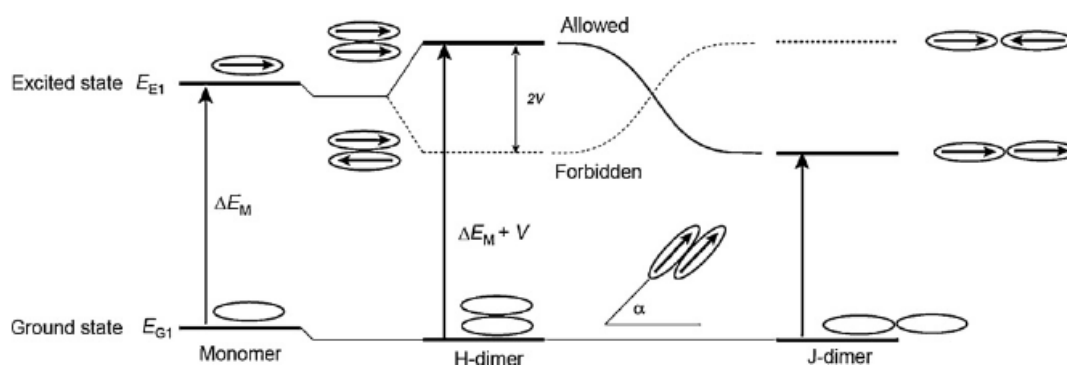
Increasing salt concentrations could help to build a polymer antenna with DNA modified acceptor molecules. This would open a complete new area of research: The DNA parts would allow to functionalize the antenna by addition of molecules which could undergo a FRET transfer, form excimers (i.e. oligomer **e**), quench the fluorescence (i.e. oligomer **f**) or in more sophisticated approaches use the energy for reactions or the generation of electrons.

Furthermore, the addition of a DNA-part to the acceptor molecule generates a kind of a head group. Unlike in the main part described example, the polymerization of the antenna could only propagate in one direction as the other end is shielded by the very hydrophilic DNA part. This directed antenna would probably allow more accurate time dependent measurements as the population of antenna molecules is more uniform.

## 5.0. Report on water-soluble J-aggregate forming PDI-oligomers and their interaction with pyrene-oligomers

### 5.1. Introduction

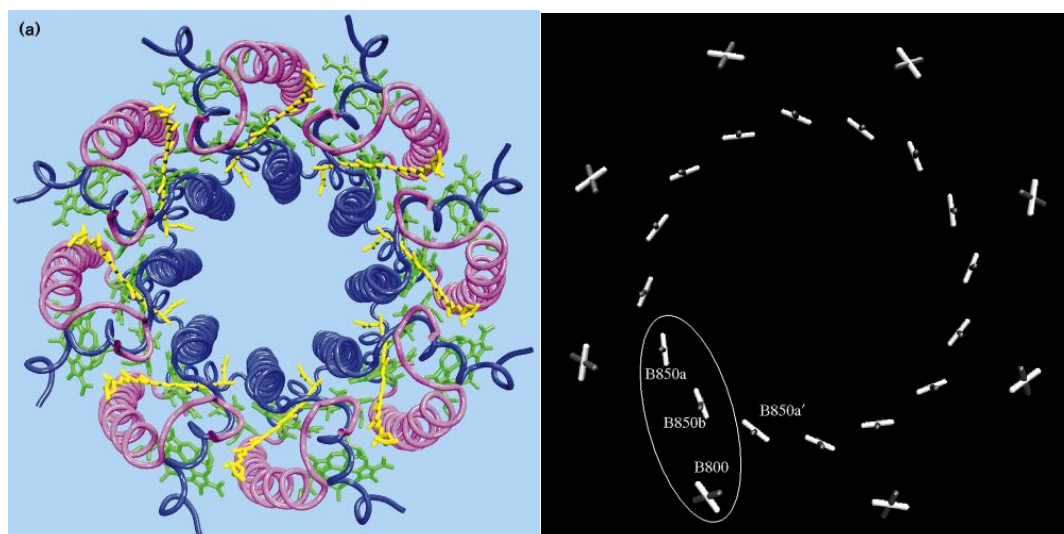
More than 70 years ago, Scheibe et al. and Jelly reported on unusual findings of pseudoisocyanine chloride (PIC chloride) in aqueous solutions<sup>187-189</sup>. The dyes showed an absorption spectra which was different from that in other solvents like ethanol. The absorption maximum was shifted to lower energies and at increasing concentration the band became more intense and sharper<sup>153</sup>. Nowadays, dye aggregates with a bathochromically shifted absorption band (compared to the monomer absorption, Scheme 5.1) are called Scheibe-aggregates or J-aggregates (J denotes Jelley).



**Scheme 5.1** Representation of the excited monomer state and the representative excited dimer states dependent on the angle  $\alpha$  of the two dipole moments.  $\alpha < 54.7^\circ$  result in a H-aggregate whereas  $\alpha > 54.7^\circ$  result in a J-aggregate. In H-aggregates the excited state with higher energy is mostly allowed whereas in J-aggregates the excited state with lower energy is favoured. Taken from Ref. <sup>140</sup>

Many more examples of J-forming dyes have been reported in the last few decades<sup>153,190,191</sup> among which the chlorophylls and bacteriochlorophylls take a prominent role. Chlorophylls and bacteriochlorophylls are derivatives of the tetrapyrrole macrocycle porphyrin and acts as natural light-harvesting system in nature (see also chapter “Soluble polymer light harvesting antenna with DNA like phosphate backbone”). In the light harvesting complex (LHC) 18 and 16 of the chlorophyll molecules are organized in a circular arrangement which affords a slipped stacking J-type arrangement<sup>192,193</sup>.





**Scheme 5.2** Arrangement of chlorophyll molecules in a J-type slipped arrangement. Left: protein structure (pink and blue) around the chromophores (green) is shown. Right: Electric dipole moment of the chlorophyll is shown representing two perfect circular structures. From Ref <sup>193</sup>.

This chromophore arrangement allows an efficient excitation energy transfer within the LHC<sup>192,194-196</sup>. Other than LH complexes of purple bacteria or plants, the dye molecules (up to 200 000 bacteriochlorophyll molecules per chlorosome) in the chlorosomes of green sulphur bacteria (*Chlorobi*) and green non-sulfur bacteria (*Chloroflexi*) are arranged and stabilized only by dye-dye interactions without protein matrix<sup>197</sup>. The exact arrangement of these chromophores in the aggregate are still under debate. But Oostergetel et al. and others suggested based on cryo-TEM studies also a slipped stack J-arrangement <sup>198,199</sup>.

Recently the group of Häner reported on 2 D nano-sheets in which a tight packing of pyrene molecules in a J-/H-type manner is observed<sup>142</sup>. Würthner et al. described in many publications the successful design of PDI molecules which form J-type aggregates. Bay substituted PDI molecules form H-bond mediated long rope-like supramolecular assemblies <sup>117,200</sup>. Substitution effects and resulting steric hindrance led to the design of functional PDI molecules with either H-aggregating or J-aggregating properties depending on the substitution <sup>113</sup>. Mixtures of both dye molecules showed self-sorting properties. Hetero aggregates of PDI and melamine derivatives form hydrogen-bonding motifs of the type ADA-DAD (A=H-bond acceptor and D=H-bond donor). Together with the  $\pi$ - $\pi$  interactions of the adjacent PDIs the mixture led to the formation of extended PDI-melamine networks with J-type absorption properties <sup>201</sup>. This research and reviews and book chapters point out the interest in designing specific PDI molecules <sup>153,202</sup> for the use in material science or organic molecular electronics.

## 5.2. Aim of the work

Our group reported on multiple incorporation of pyrene molecules into DNA<sup>203</sup>. Studies of hybrids with a reduced DNA part and increased number of arenes lead to the development of new functional material and give insight into current questions of supramolecular chemistry. Heptamers of dicarboxypyrenes with either none or one natural base were found to form long linear polymers<sup>83</sup>. PDI-DNA with a high PDI content in comparison to DNA was not reported so far. PDIs in water tend to form very stable aggregates which makes it difficult to control a defined arrangement of multiple PDI molecules in aqueous solution<sup>111</sup>.

The following study focuses on DNA-PDI hybrids with a high PDI content compared to DNA. Characteristics of their assembling properties in aqueous solution were investigated, also in respect to a co-assembling with polymers consisting of pyrenes.

## 5.3. Results and Discussion

### 5.3.1. Oligomers containing enlarged PDI and pyrene stacks

Starting from hybrids composed of 6 natural DNA bases and 4 covalently linked PDI building blocks (see Chapter 2 and 3) hybrids were synthesized composed of 6 PDI molecules and either 1 or 6 natural bases. A PDI-oligomer with only 6 PDI molecules and no nucleobases could not have been synthesized as the solubility in any solvent was too poor. A 3 mer of PDI molecules with no nucleobase was successfully synthesized. In addition to this, sequences with 6 pyrenes and a complementary DNA part to the PDI analogues was synthesized (Table 5.1).

## 5.0. Report on water-soluble J-aggregate forming PDI-oligomers and their interaction with pyrene-oligomers

**Table 5.1** Oligomer sequences used in the present study, whereby **E** is PDI, **Y** is 1,8-dialkynylpyrene and **X** is the 1,6-dialkynylpyrene.

	sequence	comments
I	5' GCG TTA EEE EEE	
II	5' EEE EEE TAA CGC	
III	5' YYY YYY TAA CGC	
IV	5' GCG TTA YYY YYY	
V	5' EEE EEE G	
VI	5' EEE EEE C	
VII	5' EEE EEE T	
VIII	5' EEE EEE A	
IX	5' YYY YYY C	
X	EEE	
XI	XXX	kind gift from M. Vybornyi

Absorption of oligomer **I** as an example of a PDI-DNA hybrid with an extended PDI moiety which shows a shape of H-aggregated PDI with an absorption maxima at 481 nm is shown in Figure 5.1. Similarly, the absorption of oligomer **III** shows an absorption trace with high intensity at 370 nm indicating a tight H-stacking of the pyrene molecules (Figure 5.2).

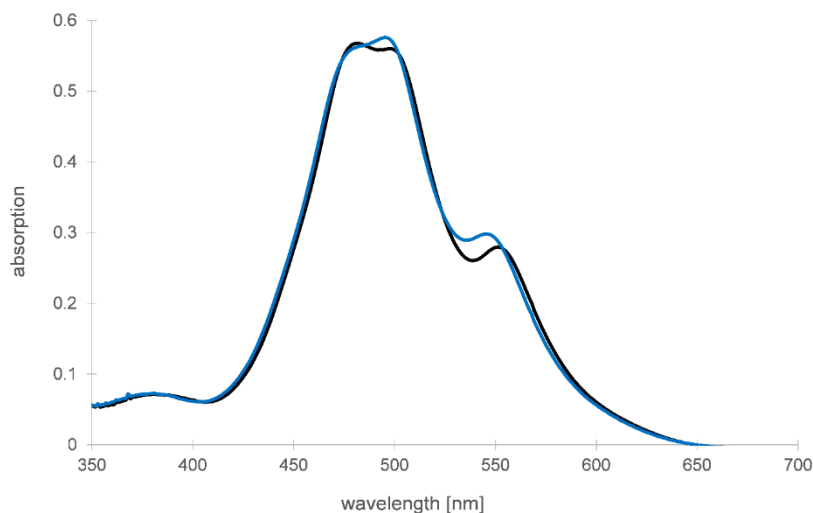


**Figure 5.1** Absorption spectra of 2.5  $\mu\text{M}$  oligomer **I** in 10 mM sodium phosphate buffer and 100 mM NaCl at 20  $^{\circ}\text{C}$  (black) and 90  $^{\circ}\text{C}$  (blue).

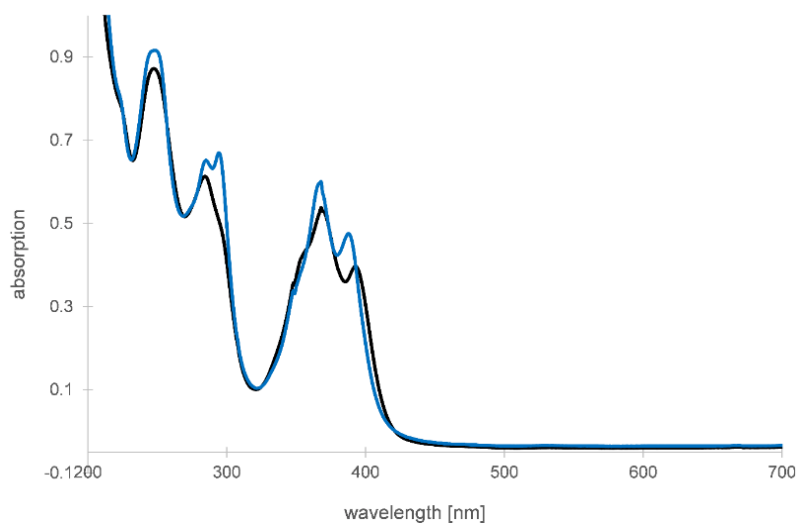


**Figure 5.2** Absorption spectra of 2.5  $\mu\text{M}$  oligomer **III** in 10 mM sodium phosphate buffer and 100 mM NaCl at 20 °C (black) and 90 °C (blue).

### 5.3.2. Time dependent formation of PDI J-aggregates

Addition of 0.2 mM spermine to a solution of molecule **I** or **II** in 10 mM sodium phosphate buffer and 100 mM NaCl induces the formation of a J-aggregate. The characteristic red shifted absorption band of a J-aggregate is visible at 660 nm. Depending on the DNA sequence of the sample the formation of the J-band happens faster or slower. Mixing the two samples with complementary DNA sequence to same amounts still forms a J-aggregate. Thereby it seems that the rate of J-aggregate formation lays in between the rate for the two single strands alone (Figure 5.3).

## 5.0. Report on water-soluble J-aggregate forming PDI-oligomers and their interaction with pyrene-oligomers

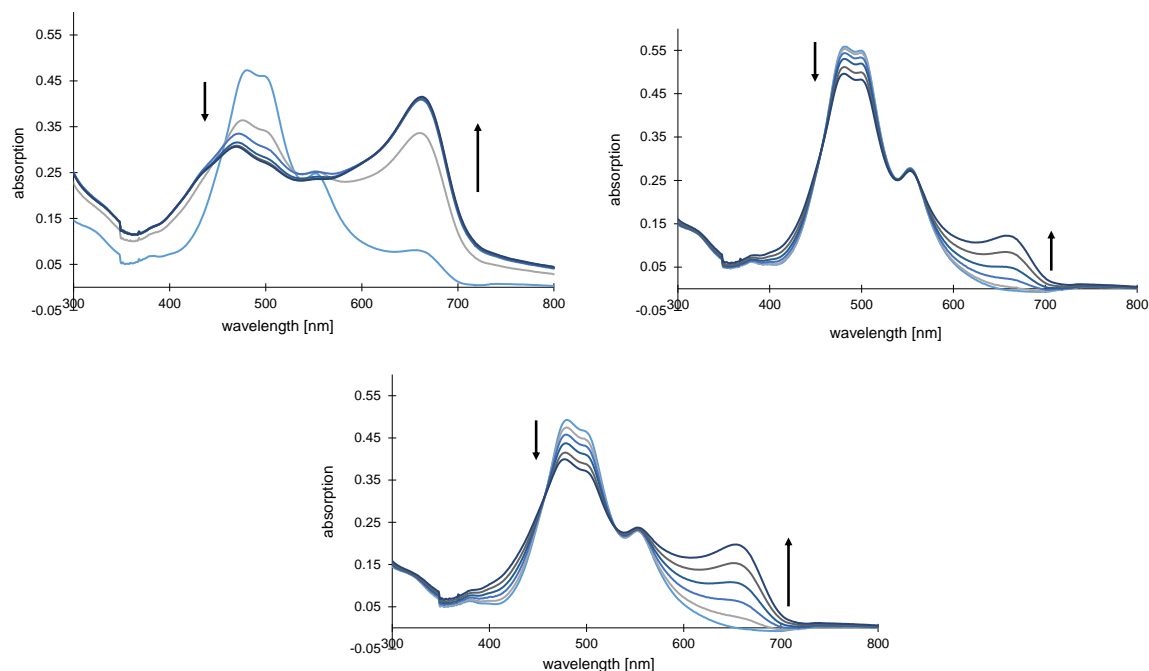


**Figure 5.3** Time dependent absorption of oligomers **I** (top, left), **II** (top, right) and mixture (bottom) at 2.5  $\mu\text{M}$  total oligomer concentration in 10 mM sodium phosphate buffer, pH 7.2, 100 mM NaCl and 0.2 mM spermine tetrahydrochloride. Measurements were performed in 30 min intervals.

### 5.3.3. J-aggregate formation inhibition by PDI-pyrene interaction

Mixing two complementary DNA strands one modified by 6 PDIs and the other with 6 dialkynylpyrene molecules prevents the formation of the previously seen J-aggregate over several hours and days (Figure 5.4). The aligned PDI and pyrene molecules assemble in an aromatic donor-acceptor guided supramolecular stack. The PDI molecules adopt an H-stack like assembly and are prevented from J-aggregate formation. Mixing strand **III** to strand **I** after the formation of the J-aggregate, the J-aggregate remains stable over several hours up to days and could not be destroyed by the added pyrene-hybrids (Figure 5.5). Just after heating and cooling the alternating PDI-pyrene interactions are established. The PDI J-aggregates are the thermodynamically preferred arrangement whereas the alternating pyrene-PDI double strand is the kinetically preferred arrangement.

## 5.0. Report on water-soluble J-aggregate forming PDI-oligomers and their interaction with pyrene-oligomers

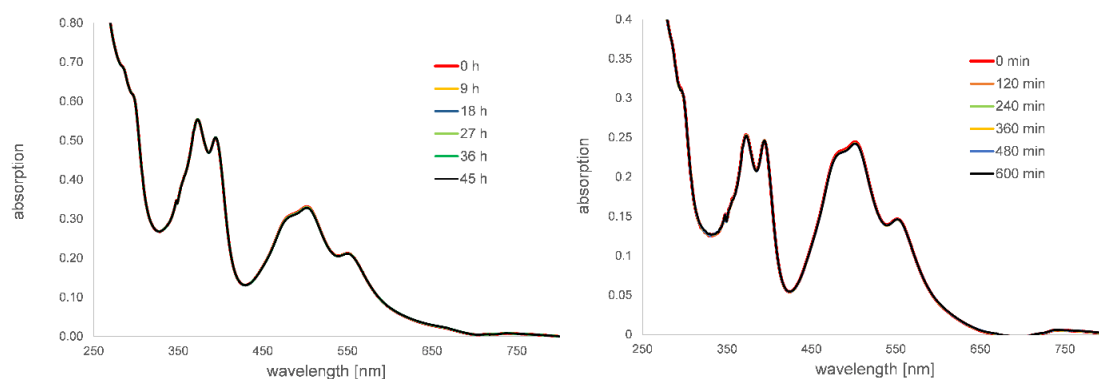


**Figure 5.4** Left side: Oligomers **I\*III** and right side: Oligomers **II\*IX** at 2.5  $\mu\text{M}$  of each single strand. Time interval is indicated in the Figure. Conditions as in Figure 5.3. No formation of PDI J-aggregates is seen.

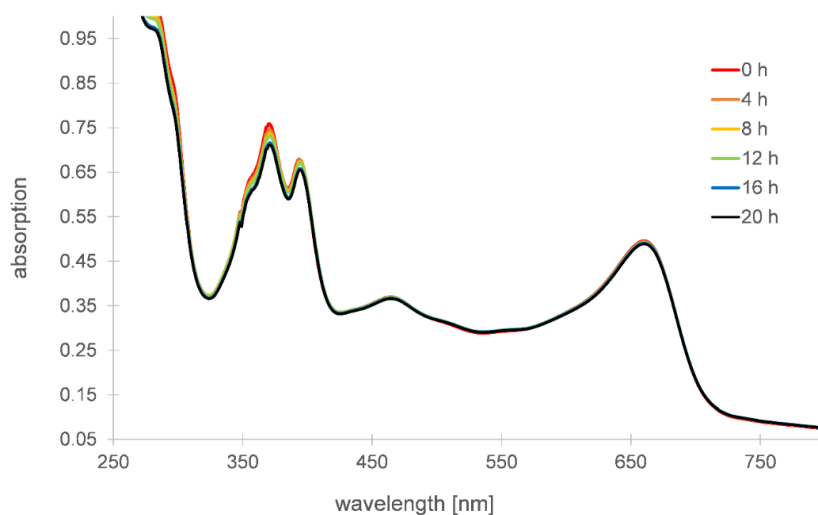


**Figure 5.5** Oligomers **I** and **III** at 2.5 mM each. Oligomer **III** was added after oligomer **I** formed the J-aggregate in 10 mM sodium phosphate buffer, 100 mM NaCl and 0.2 mM spermine tetrahydrochloride. Time steps between the measurements are indicated in the Figure. No destruction of the J-aggregate is visible.

### 5.3.4. Spectroscopic characterization of oligomers with reduced DNA part

Oligomers **V** to **VII** containing 6 PDI molecules and only one of the natural bases form J-aggregates in buffered saline (Figure 5.6). Addition of spermine prevents the formation of the J-aggregate (data not shown). In Figure 5.7 oligomers **VII** and **VIII** as examples are shown to form time dependent J-aggregates. Hybrids with different bases attached show a different kinetic in the formation of the J-band. Increasing salt concentrations or lower temperatures (several h at  $-20\text{ }^{\circ}\text{C}$

## 5.0. Report on water-soluble J-aggregate forming PDI-oligomers and their interaction with pyrene-oligomers

or days at 4 °C) favours the formation of the aggregates. The samples change from a red to a completely black colour upon formation of the J-aggregate (Figure 5.6). The formation of the J-aggregate is reversible upon heating.

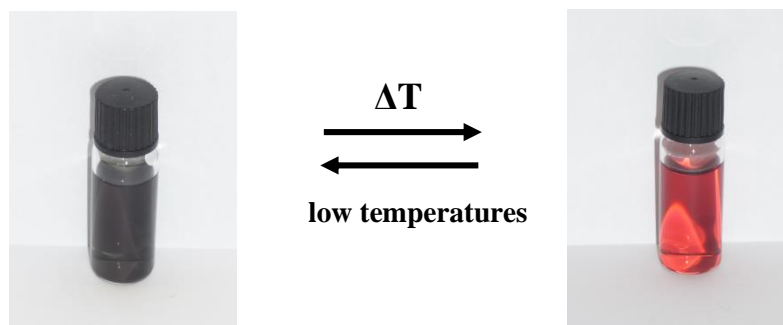


**Figure 5.6** Solution of oligomer **VI** in water after 1 d at -20 °C (left) and few h at 20 °C (right). J-aggregate formation (black sample) is induced at low temperature or high salt concentrations.

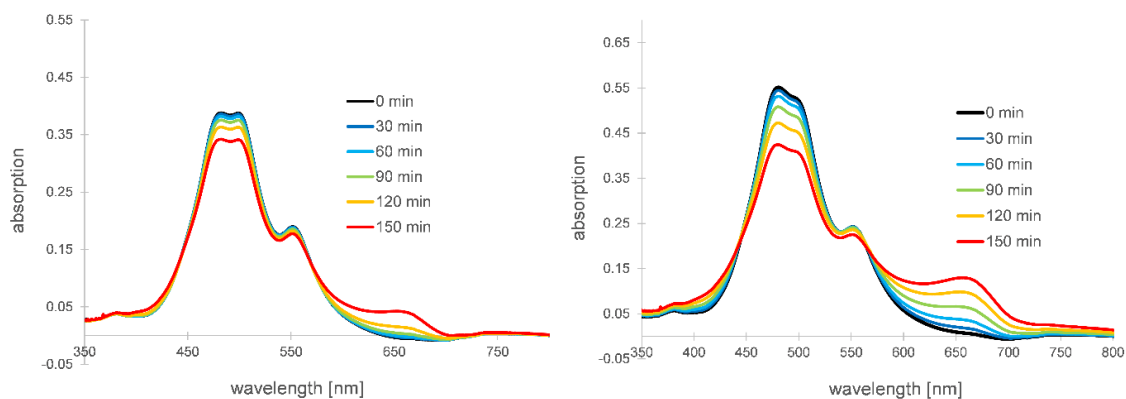


**Figure 5.7** Oligomer **VII** (left) and oligomer **VIII** (right) at 2.5  $\mu\text{M}$  in 10 mM sodium phosphate buffer, pH 7.2 and 70 mM NaCl. Formation of the J-aggregate was induced in absence of the spermine.

After the formation of the J-aggregate a CD spectra of the sample **V** to **VIII** was measured. A normalized absorption trace of the oligomers before and after the formation of the J-aggregate as well as the corresponding CD spectra is shown in Figure 5.8. Differences in the CD spectra are seen dependent of the nucleobase attached to the oligomer. The same behaviour could have been observed in previously described pyrene oligomers<sup>164</sup>. Compared to the previous study, the CD

## 5.0. Report on water-soluble J-aggregate forming PDI-oligomers and their interaction with pyrene-oligomers

signals in this setup is quite pronounced. In the absorption area of the J-aggregate, we see in all cases a pronounced signal which, for oligomer **VI** und **VIII** has a negative sign and for oligomer **V** and **VII** a positive sign. Oligomer **V** and **VIII** show a pronounced induced CD signal. The signals for oligomers **VI** and **VII** seem to have a certain degree of exciton coupled character indicated by a very weak negative signal (at higher wavelength) followed by the pronounced positive peak. A comparison of the four CD spectra can be done by overlaying and normalizing them. Spectra with the negative J-aggregate induced CD signal perfectly overlay (Figure 5.10). The signal of oligomer **VII** is slightly blue shifted compared with the other signals. The exciton character of oligomer **VI** is visible in the overlay. Moreover, at 450 nm a pronounced exciton coupled CD is visible for all oligomers. In all oligomers the spectra shows a positive-negative pattern (from longer wavelength to lower wavelength) except for oligomer **VIII**. The very pronounced exciton signal in the area below 300 nm corresponds again to the sign of the J-band. The oligomers with the positive J-band signal show a positive-negative pattern below 300 nm, whereas the two oligomers with the negative J-band signal show a negative-positive signal below 300 nm. Further studies would be needed to relate the spectral data with proposed structures of the aggregates. Computational studies might give insight in the exact arrangement of the PDI chromophores in the aggregates<sup>168</sup>.

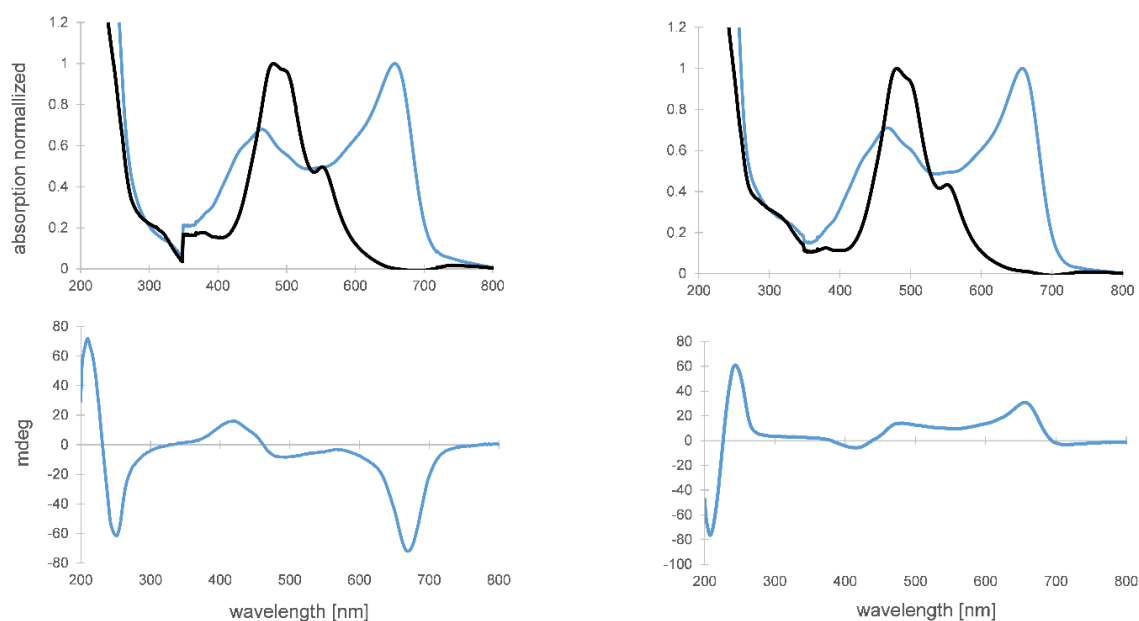


**Figure 5.8** Oligomer **VIII** (left) and oligomer **VII** (right) at 2.5  $\mu\text{M}$  in 10 mM sodium phosphate buffer, pH 7.2 and 30 mM NaCl. Top: absorption before the formation of the J-aggregate (black) and after the formation of the J-aggregate (blue). Bottom: CD spectra of the respective oligomers after the formation of the J-aggregate.



## 5.0. Report on water-soluble J-aggregate forming PDI-oligomers and their interaction with pyrene-oligomers

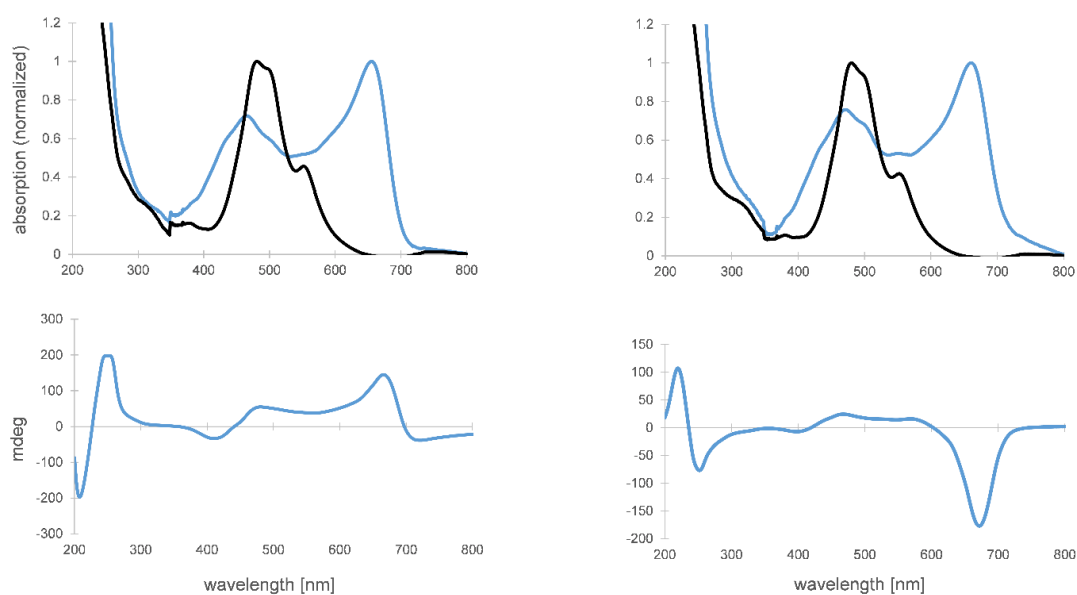


**Figure 5.9** Oligomer VI (left) and oligomer V (right) at 2.5  $\mu\text{M}$  in 10 mM sodium phosphate buffer, pH 7.2 and 30 mM NaCl. Top: absorption before the formation of the J-aggregate (black) and after the formation of the J-aggregate (blue). Bottom: CD spectra of the respective oligomers after the formation of the J-aggregate.

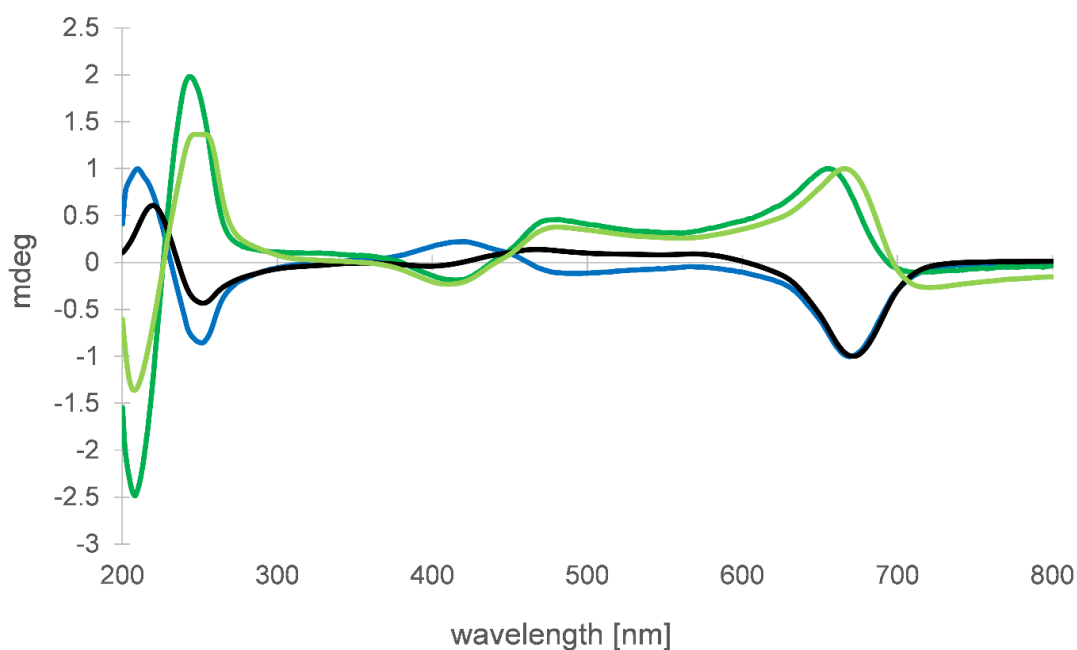


**Figure 5.10** CD spectra overlay (normalized) of the oligomers V (black), VI (light green), VII (green) and VIII (blue) after the formation of the J-aggregate.

The temperature dependent decay of the J-aggregates has been followed by UV/VIS absorption measurements. Absorption was once measured on the J-band (which decreases with increasing temperature) and once at the wavelength of the PDI H-like absorption (which increases with increasing temperature). Only one heating ramp was performed as the kinetics for the formation

## 5.0. Report on water-soluble J-aggregate forming PDI-oligomers and their interaction with pyrene-oligomers

of the J-aggregate is slow. All the oligomers with the different bases show melting temperatures between 65-75 °C.

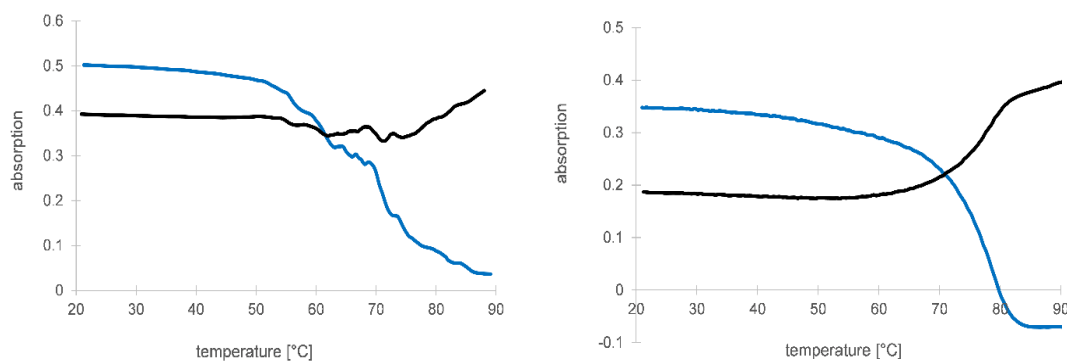


**Figure 5.11** Oligomer **VII** (left) and oligomer **VIII** (right) at 2.5  $\mu\text{M}$  in 10 mM sodium phosphate buffer, pH 7.2, 30 mM NaCl. The melting curve was performed after the J-aggregate was formed. The ramp was 0.5 °C/min.

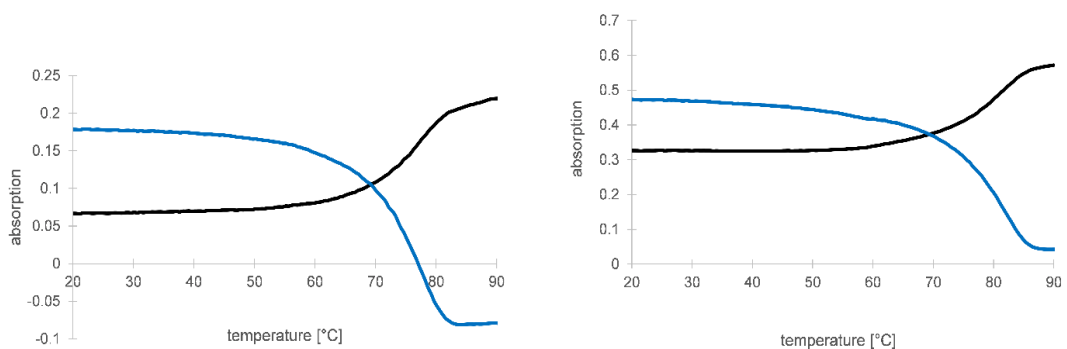


**Figure 5.12** Oligomer **VI** (left) and oligomer **V** (right) at 2.5  $\mu\text{M}$  in 10 mM sodium phosphate buffer, pH 7.2, 30 mM NaCl. The melting curve was performed after the J-aggregate was formed. The ramp was 0.5 °C/min.

In further experiments, the interaction of the oligomers with 6 PDI molecules covalently linked and a corresponding molecule containing 6 pyrene molecules (oligomer **IX**) was tested. Titration of molecule **VI** with oligomer **IX** leads to a decreased absorption of the PDI with a slight red shift of the maximal absorption band at 500 nm (Figure 5.13). The ratio of the absorption at 500 nm and 545 nm decreases as more and more pyrene molecules were added to the solution. This would indicate an H-aggregate destacking by the interacting pyrene molecules. Time dependent UV/VIS measurements of a solution of molecule **VI** at 10 mM sodiumphosphate buffer and 100 mM NaCl and a solution containing equal concentrations of **VI** and **IX** showed that after 10 min the solution with only PDI containing molecules start to form the J-aggregate again whereas in the case of PDI and pyrene compounds in solution the J-aggregate formation is prevented (Figure 5.14). This is most probably due to an alternating face-to-face stacking of the PDIs and pyrenes.

## 5.0. Report on water-soluble J-aggregate forming PDI-oligomers and their interaction with pyrene-oligomers

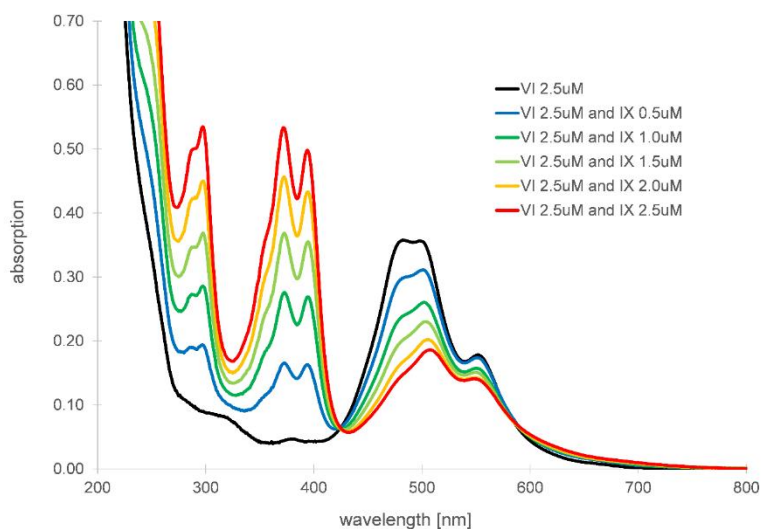


**Figure 5.13** Titration of molecule **IX** at indicated concentrations to a solution containing 2.5 μM of oligomer **VI** in 10 mM sodium phosphate, pH 7.2, 100 mM NaCl.

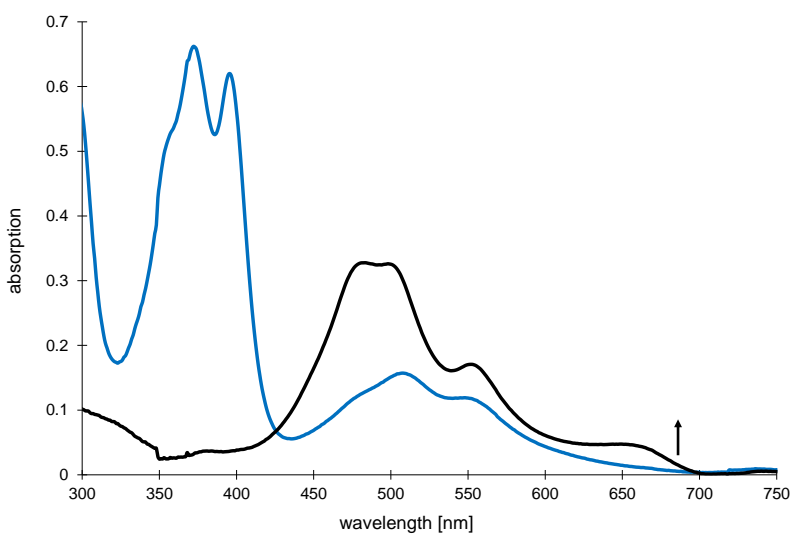


**Figure 5.14** Oligomer **V** (black) and a 1:1 mixture of oligomers **V** and **IX** (blue) in 10 mM sodium phosphate, pH 7.2, 100 mM NaCl. The absorption was measured 10 min after cooling to room temperature. Oligomer **V** starts to form the J-band (indicated by the arrow) whereas the J-band formation in the mixture of oligomer **V** and **IX** is inhibited.

Temperature dependent UV/VIS measurements were performed (Figure 5.16). Hyperchromicity in the area of pyrene and PDI is observed which indicates an unstacking of the compounds at high temperature. The melting curve of the hybrid **V\*IX** shows a DNA like sigmoid cooling and heating behaviour (Figure 5.17). At both wavelength 368 nm and 500 nm the melting behaviour is the same which indicates a coordinated process of the two molecules. At 63 °C a very small kink is present in the cooling curve which is usually seen in nucleation-elongation driven process

## 5.0. Report on water-soluble J-aggregate forming PDI-oligomers and their interaction with pyrene-oligomers

---

in molecular assemblies<sup>204-206</sup>. The transition at 63 °C is very faint thus no further interpretations of the cooling process are done on this state of the experiments. A large hysteresis is seen. The process for the formation of the aggregated structures takes place at lower temperatures than the melting of the previously formed structures.

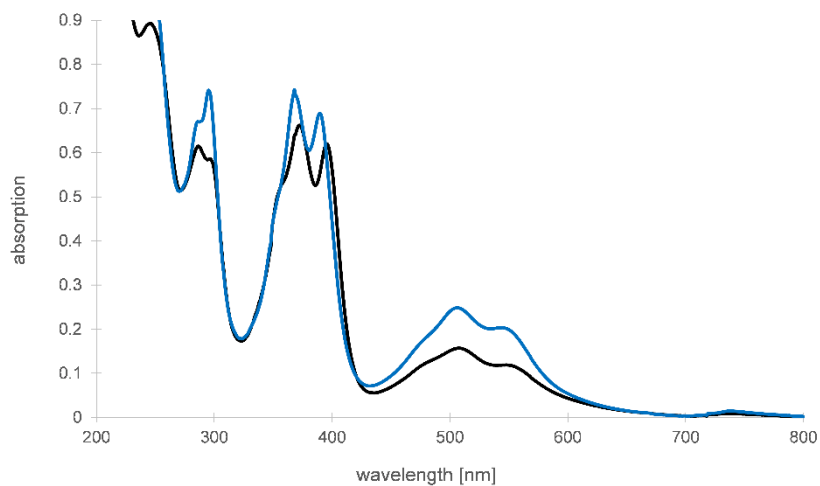


**Figure 5.16** Absorption of a mixture of oligomer **V** and **IX** at 2.5  $\mu\text{M}$  of each single strand in 10 mM sodium phosphate, pH 7.2, 100 mM NaCl at 20 °C (black) and 90 °C (blue).

## 5.0. Report on water-soluble J-aggregate forming PDI-oligomers and their interaction with pyrene-oligomers

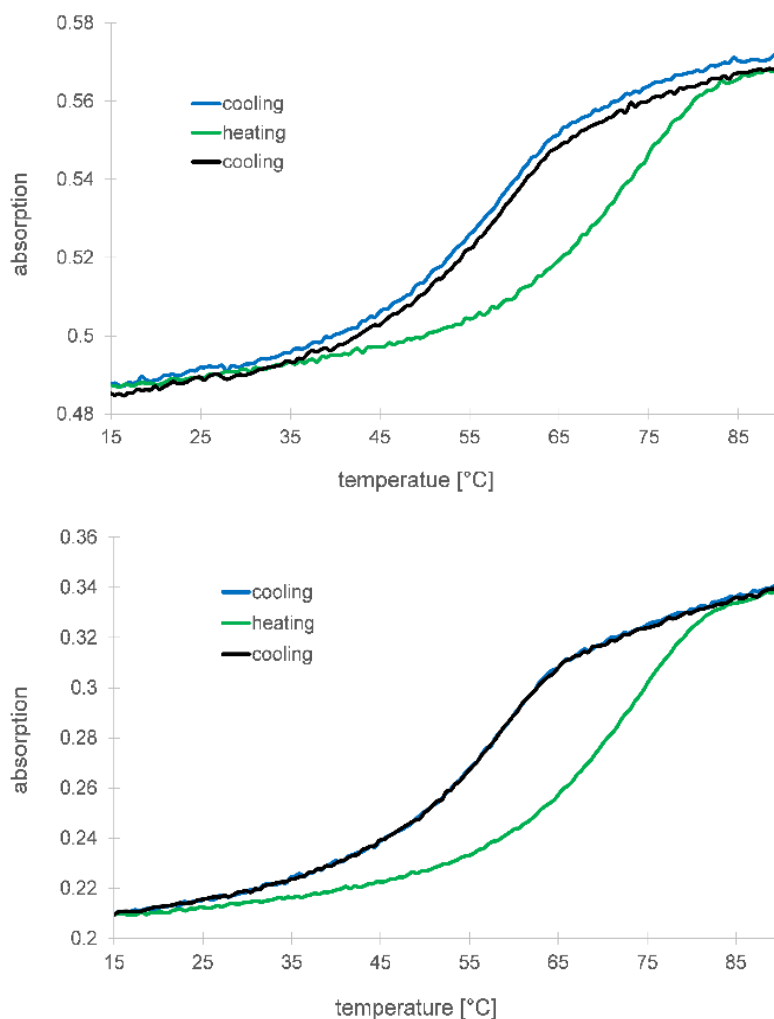


**Figure 5.17** Temperature dependent measurement of a mixture of oligomer **V** and **IX** at 2.5  $\mu\text{M}$  of each single strand in 10 mM sodium phosphate, pH 7.2, 100 mM NaCl. The experiment was performed in cooling-heating-cooling ramps at a rate of 0.5  $^{\circ}\text{C}/\text{min}$ . Top: absorption at the pyrene at 368 nm, bottom: absorption at the PDI at 500 nm.

Atomic force microscopy pictures were taken from the oligomers **V\*IX**. Rod like structures are visible on the mica-sheet with sizes up to 1-2  $\mu\text{m}$  (Figure 5.18). Control experiments with only the oligomer **IX** in solution also forms similar structures. Therefore it is difficult to interpret the AFM pictures of mixtures of **V\*IX**. Either a mixture of the PDI-pyrene oligomers also forms rod like structures or the structures seen are an effect of a too high concentration of molecule **IX** in solution and therefore a self-aggregation of the excess thereof. Spectroscopic measurements above indicate clearly that molecules **V\*IX** interact with each other, therefore a self-aggregation of only **V** and **IX** can be excluded. Interpretable AFM pictures of the J-aggregate forming oligomer **V** were never obtained. From previous studies we know that the kinked 1,8-pyrene is likely to form rod-like polymers (see AFM on top or Ref<sup>167</sup>) whereas the linear 1,6-dialkynylpyrene forms sheet-like polymers<sup>142</sup>. A working hypothesis in our group is that mostly linear molecules form sheet-like polymers. This would indicate that most probably also the PDI-containing hybrids form J-aggregated sheets. Mixtures of the sheet-forming 1,6-dialkynylpyrene

and of the PDI-hybrids would be an interesting study subject. The formation of linear 1D mixed polymers is probable.

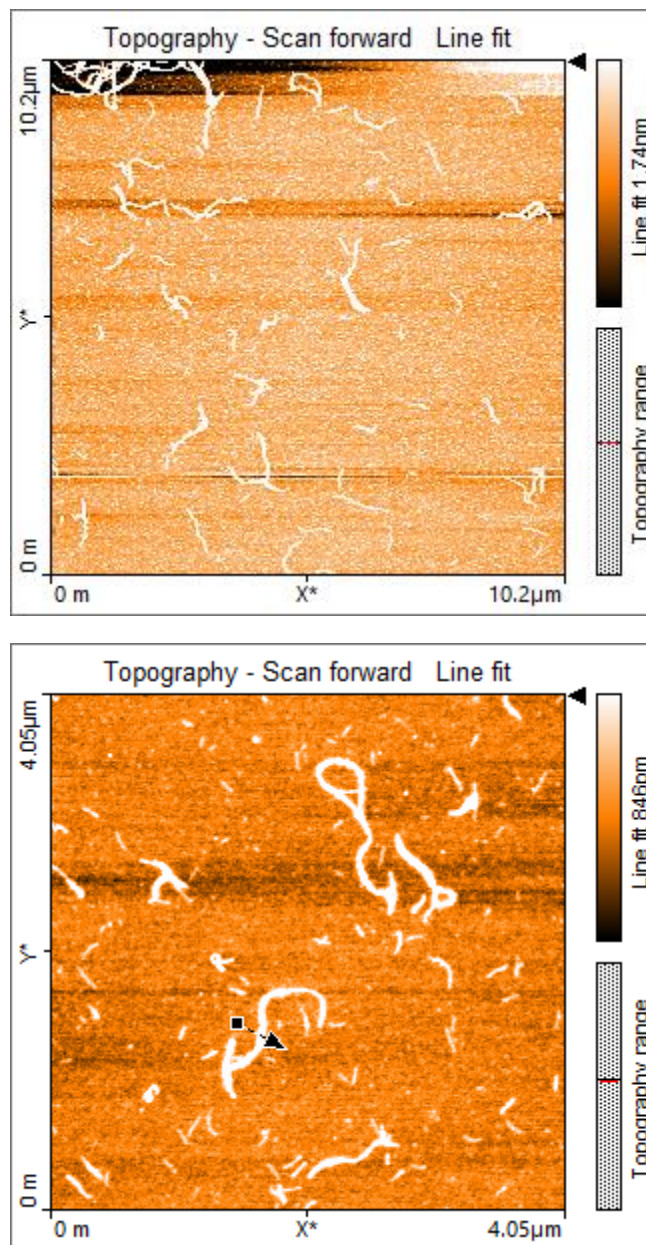


**Figure 5.18** AFM pictures of oligomers **V\*IX** (top) and **IX** (bottom). The samples are prepared 10 mM sodium phosphate, pH 7.2, 100 mM NaCl. Description of the protocol for the preparation of the mica see experimental part.

### 5.3.2. Interaction of PDI- and pyrene 3-mers

Oligomer **X** which consists of three covalently linked PDI molecules shows an absorption trace with an absorption maxima at 480 nm as it is typical for aggregated PDI molecules (Figure 5.19 and chapters above). The concentration of the oligomer **X** in 10 mM phosphate buffer was chosen to be 1  $\mu\text{M}$  in order to generate comparable conditions like in Ref <sup>142</sup> where a 1  $\mu\text{M}$  solution of molecule **XI** was used for the measurements. Addition of up to 100 mM NaCl to oligomer **X** did not induced J-aggregate formation as observed in cases of molecules **V-VIII**. The absorption trace rather shows a pronounced hypochromicity as well as a hypsochromicity (blueshift). This indicates an H-type aggregate. A small shoulder at 590 nm increases which stayed constant over time<sup>207</sup>.

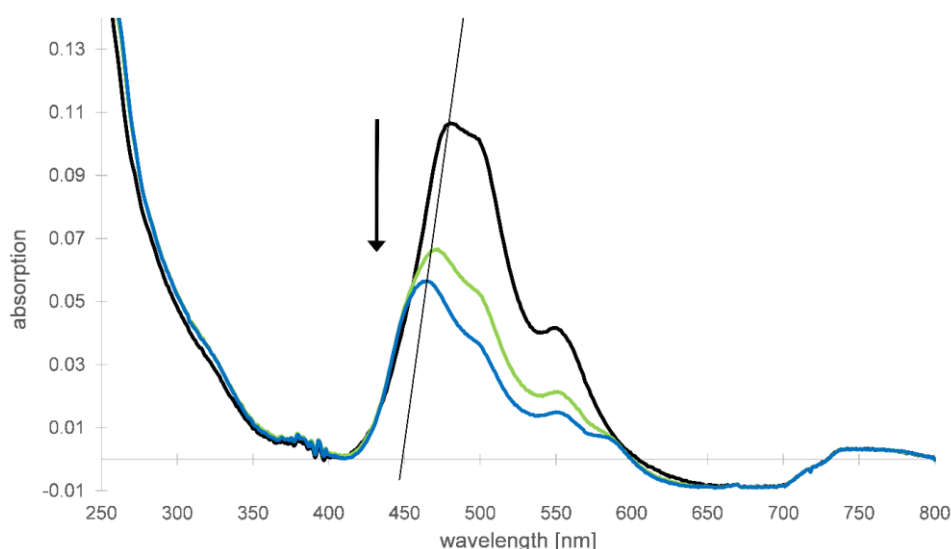


**Figure 5.19** Oligomer **X** at 1  $\mu\text{M}$  in 10 mM sodium phosphate buffer, pH 7.2 and 0 mM NaCl (black), 50 mM NaCl (green) and 100 mM NaCl (blue). A pronounced hypochromicity and a blue-shift of the absorption band is visible.

Mixing the PDI 3 mer **X** with the 1,6-dialkynylpyrene three mer **XI** leads to the absorption spectra depicted in Figure 5.20 at 20 °C and 90 °C. At 20 °C a pronounced pyrene absorption band is visible at 405 nm. This is 15 nm red-shifted compared with the absorption band of the pyrene monomer. At 90 °C the absorption band at 405 nm disappears and the monomeric pyrene absorption is restored. Temperature dependent absorption measurements show the melting of the J-band and the transition to the monomeric pyrene-absorption (Figure 5.21). Comparison of the absorption of the molecules **X** and **XI** and mixtures thereof show the following pattern (Figure

5.22). Molecule **X** shows the causal absorption trace of PDI as seen already in Figure 5.19). Molecule **XI** shows a very pronounced J-band of the vibronic transition  $S_0$ - $S_2$ . This absorption trace and the elucidated underlying structural properties are discussed in great detail in Reference <sup>142</sup>. The newly formed J-band in mixtures of oligomer **X**\***XI** corresponds to the J-band of the  $S_0$ - $S_1$  transition of pyrene. A few dipole moment considerations have to be taken into account to explain the observed behaviour and probably gain insight into possible structural properties of the newly described hetero-aggregates (Scheme 5.3).

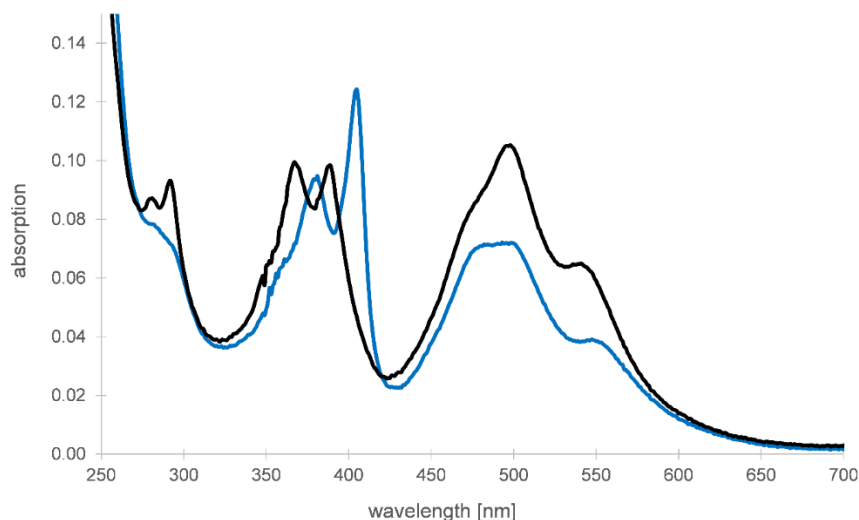


**Figure 5.20** Oligomers **X** and **XI** at 1  $\mu\text{M}$  each in 10 mM sodium phosphate buffer, pH 7.2 at 20  $^{\circ}\text{C}$  (blue) and 90  $^{\circ}\text{C}$  (black).

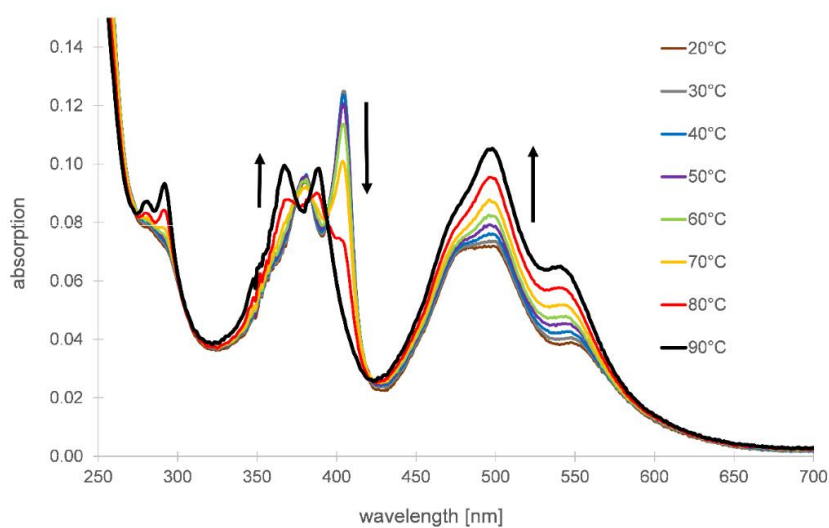


**Figure 5.21** Temperature dependent absorption measurement of a mixture of oligomer **X** and oligomer **XI** at 1  $\mu\text{M}$  of each oligomer in 10 mM sodium phosphate buffer, pH 7.2.



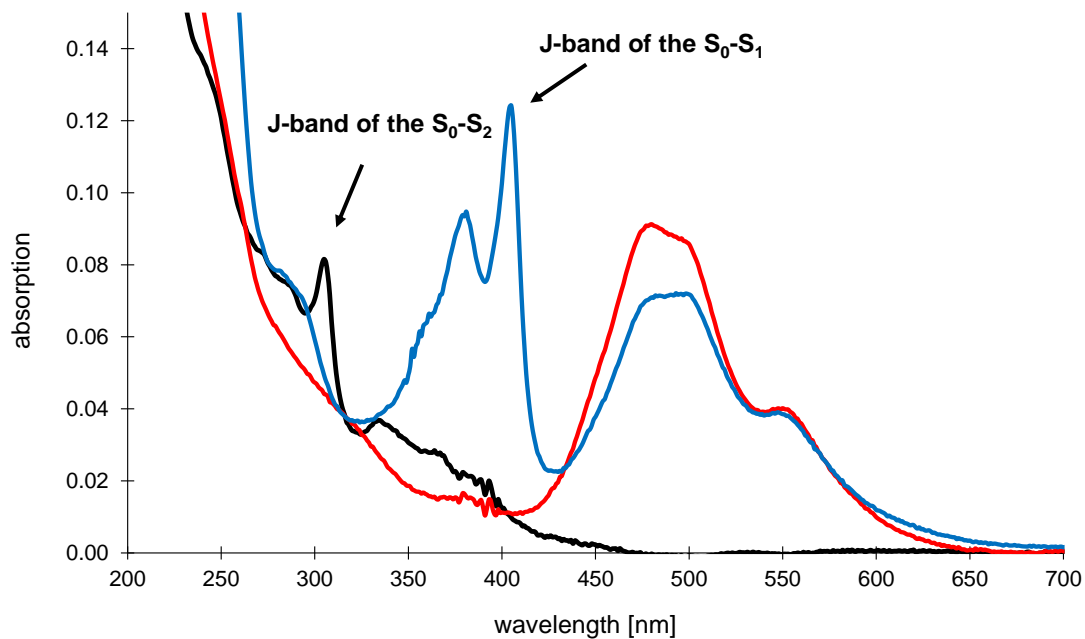
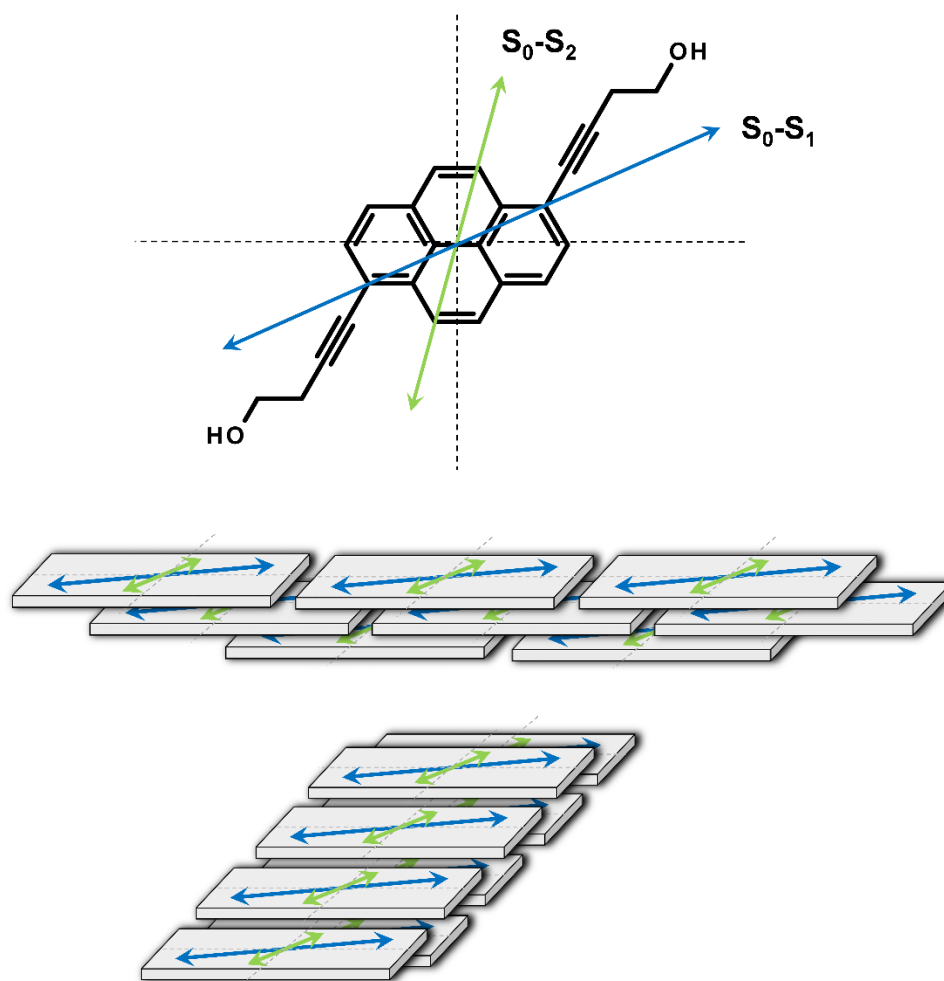
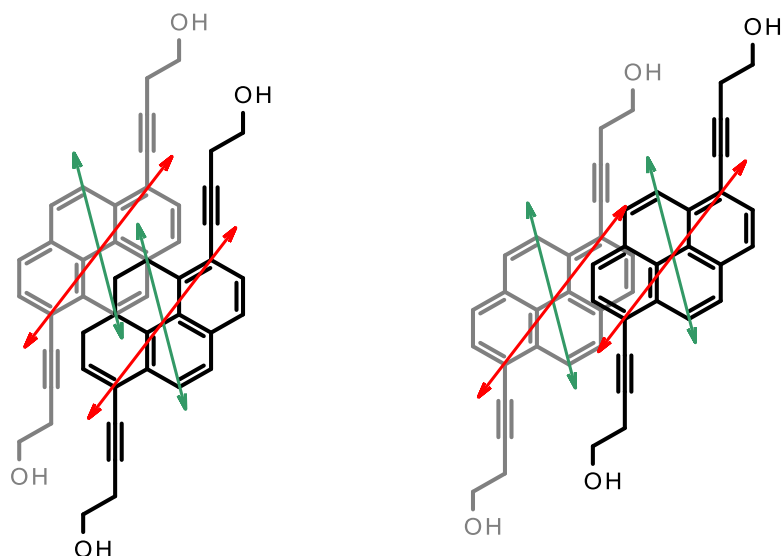


**Figure 5.22** Absorption 1  $\mu\text{M}$  of oligomer **X** (red), **XI** (black) and the mixture of **X** and **XI** (blue) in 10 mM sodium phosphate. The J-bands of the  $S_0$ - $S_1$  and the  $S_0$ - $S_2$  transition of the 1,6-dialkylpyrene are indicated with the arrow.



**Scheme 5.3** Top: 1,6-dialkynylpyrene with the indicated dipole moments of the  $S_0-S_1$  and the  $S_0-S_2$  transition. Middle: Arrangement of the chromophores to form the J-aggregate of the  $S_0-S_1$  transition. Bottom: Arrangement of the chromophores to form the J-aggregate of the  $S_0-S_2$  transition (adapted from Ref<sup>142</sup>).

The dipole moments of the 1,6-dialkynylpyrene are aligned as depicted in Scheme 5.3. The dipole moment of the  $S_0-S_1$  transition are aligned in the long axis of the molecule whereas the dipole moment of the  $S_0-S_2$  transition is aligned along the short axis of the molecule. In case of the molecule **XI** alone a J-arrangement of the  $S_0-S_2$  transition is visible which corresponds to a chromophore arrangement as depicted in Scheme 5.4 left. A schematical representation of the respective chromophore arrangement is seen in Scheme 5.4. When the PDI containing molecule **X** is added to the solution the J-band of the  $S_0-S_1$  is seen. This would account to a chromophore arrangement as depicted in Scheme 5.4 right where the red dipole moments are aligned in a serial manner. On the same time an H-aggregate like stacking of the  $S_0-S_2$  would be visible which in our case is overlaid by the PDI absorption.



**Scheme 5.4** Left: pyrene arrangement in solution without PDI <sup>142</sup>. The S<sub>0</sub>-S<sub>2</sub> transition dipole moment (green) is arranged in a J-aggregate like way, whereas the S<sub>0</sub>-S<sub>1</sub> (red) shows H-aggregate character. Right: upon mixing of the pyrene 3mer with PDI 3mers the transition dipole moments of the S<sub>0</sub>-S<sub>1</sub> and S<sub>0</sub>-S<sub>2</sub> transitions are aligned as shown, forming the S<sub>0</sub>-S<sub>1</sub> J-aggregate and the S<sub>0</sub>-S<sub>2</sub> H-aggregate.

## 5.4. Conclusion and Outlook

In this section of the thesis the discovery of new water-soluble J-aggregate forming PDI-conjugates was described. It was found that oligophosphates containing six PDI molecules form J-aggregated structures. The oligomers were functionalized by either 6 or 1 natural nucleobases. In case that oligomers with complementary DNA strand were mixed, the J-aggregate is still formed. Adding a 1,8-dialkylpyrene 6-mer containing a DNA part which is complementary to the DNA modified PDI oligomers forms alternating PDI-pyrene supramolecular stacks and prevents the PDI from the formation of J-aggregates.

Oligomers which were modified with one of the four natural nucleobases show CD activity.

No structure resolution could have been done so far. To gain information on the morphology of the formed aggregates, AFM or similar techniques would be very desirable and a prerequisite for further investigations. DNA functionalized nanostructures are an interesting starting point for further modification<sup>208-210</sup>. Due to the easy accessibility and the orthogonality of the DNA strands one could well imagine to functionalize the J-forming PDI aggregates by addition of further DNA strands. It has to be taken into account that a double-stranded DNA helix is sterically quite demanding which is a fact that should not be disregarded in the future design of DNA functionalized materials. Furthermore the repulsion of the negatively charged DNA backbone

## 5.0. Report on water-soluble J-aggregate forming PDI-oligomers and their interaction with pyrene-oligomers

---

needs to be considered. A good example therefor is the comparison of J-aggregate forming molecules **I** and **II** and **V-VIII**. Whereas in molecules **I** and **II** the addition of spermine to the sample favours the J-aggregate formation, in samples **V** to **VIII** it prevents the formation. In samples **I** and **II** the negatively charged phosphate backbone is shielded by the positively charged spermine and prevents electrostatic repulsion of the different molecules. For oligomers **V** to **VIII** only one additional base is attached which is sterically not very demanding and does not prevent a proper J-aggregate formation.

## 6.0. Experimental section

**Oligonucleotide synthesis** All chemicals used were purchased from commercial suppliers. Solvents for column chromatography were of technical grade. Purification of the building block phosphoramidites was performed with solvents which were distilled prior to use. The required alkynylpyrene<sup>74</sup> and perylenediimide<sup>211</sup> building blocks were synthesized according to published procedures. The oligomers were prepared on an Applied Biosystems 394 DNA/RNA synthesizer in a 1  $\mu$ mol synthesis. All reagents used for solid phase synthesis were purchased from Proligo®. A standard cyanoethyl phosphoramidite coupling protocol was used beginning with nucleoside-loaded controlled pore glass (CPG) and Universal 3-CPG supports from Glen Research. Commercially available natural nucleoside phosphoramidites were dissolved in CH<sub>3</sub>CN to yield 0.1 M solutions. The 1,8-dialkynylpyrene phosphoramidite was dissolved in 1,2-dichloroethane (0.1 M) and the perylenediimide phosphoramidite in dichloromethane (0.08 M). For the activation of the perylenediimide phosphoramidite a solution of 5-(ethylthio)-1*H*-tetrazole (ETT) in THF (0.3 M) was used. The CPG-bound oligonucleotides were cleaved and deprotected by treatment with 28-30% NH<sub>4</sub>OH at 55 °C for 16 h. The supernatant was collected and the residue was washed three times with 1 ml EtOH/H<sub>2</sub>O 1:1. Oligonucleotides synthesized on the Universal 3-CPG were cleaved using an adapted version (conc. aq. ammonia/methanol 1:2 v/v) of the provided cleavage and deprotection protocol (GlenResearch). After lyophilisation, the crude oligonucleotides were purified by reversed phase HPLC (Merck LiChroCART 250-4; LiChrospher 100, RP-18, 5  $\mu$ m). A gradient starting with 0% up to 100% CH<sub>3</sub>CN in 0.1 M aqueous triethylammonium acetate was set at a flow rate of 1.0 ml/min. The conditions for the HPLC purification are specified in the section below. After purification, samples were lyophilized and redissolved in MilliQ water to yield a 50  $\mu$ M stock solution. Concentration determination was performed using  $\epsilon_{370 \text{ nm}} = 36000 \text{ M}^{-1}\text{cm}^{-1}$  of the pyrene. Concentration determination of the samples containing only PDI was performed as following: concentration of a sample containing two pyrenes and 2 PDI molecules was determined using the absorption of the pyrene. The absorption of the PDI was used as a reference to then adjust the PDI samples with the unknown concentration. The extinction coefficient of dialkynylphenanthrene was determined as  $\epsilon_{326 \text{ nm}} = 35200 \text{ M}^{-1}\text{cm}^{-1}$ .

**Analytical HPCL** The analytical reverse phase HPLC runs of the oligomers were performed using a Merck LiChroCART 250-4; LiChrospher 100, RP-18, 5  $\mu$ m column. A gradient starting with 0% up to 100% CH<sub>3</sub>CN in 0.1 M aqueous triethylammonium acetate was set at a flow rate of 1.0 ml/min. Time program was as specified in Table 6.1. The column was heated to 50 °C. Elution of the sample was detected using a diod-array detector at 260 nm, 370 nm or 505 nm. For analytical HPLC of the compounds consisting of 3 or 4 chromophores a Merck LiChroCART 250-4; LiChrospher 100, RP-8, 5  $\mu$ m column was used. Samples were dissolved in 0.1 M aqueous triethylammonium acetate containing 10 % MeOH and up to 50 % AcN. The HPLC gradient is specified in Table 6.1.

**Table 6.1** Left: Time program for the purification of DNA-oligoarenotide conjugates. Right: Time program for the purification of short, fully modified oligophosphates.

Time (min)	% acetonitrile	Time (min)	% acetonitrile
0.01	0	0.01	50
1.0	0	1.0	50
2.0	0	15	100
22.0	70	16	100
23.0	100	25	100
32.0	100	26	0
33.0	0	31	0
37.0	0		

**Mass-Spectrometry** Mass-spectrometric data of all oligomers were obtained on a Thermo Fisher LTQ Orbitrap XL using Nano Electrospray Ionization (NSI) in a water/acetonitrile/triethylamine solution.

**UV/VIS measurements** UV/VIS measurements were performed on a Varian-Cary-100 Bio spectrophotometer. A Cary-block temperature controller and the Varian Win UV software was used. All specifications like concentration of the oligomers, buffer, pH, salt concentration or temperature are indicated in the respective section.  $T_m$  measurements have been performed measuring the probe temperature in consecutive cooling-heating-cooling ramps at indicated cooling and heating rate.

**Fluorescence measurement** Fluorescence measurement was performed on a Varian-Cary Eclipse fluorescence meter using a Cary Eclipse software. Measurements were performed with 600 V detector voltage, 5 nm excitation slit width and 5 nm emission slit width. Concentration of the oligomers, buffer or salt is indicated in the main text. The samples were excited at the indicated wavelength.  $T_m$  measurements were performed as cooling-heating-cooling ramps with the indicated cooling and heating rate measuring the probe temperature in a cuvette.

**Quantum yield measurement** The quantum yield was determined by integration of the fluorescent area ( $I_c$ ) from 350-600 nm. The absorbance ( $A_c$ ) at the corresponding excitation wavelength was measured<sup>212</sup>. Quinine sulfate in 0.05 M H<sub>2</sub>SO<sub>4</sub> was used as a reference. The absorbance of the quinine sulfate ( $A_R$ ) at 345 nm was around 0.08. Quinine sulfate fluorescence ( $I_R$ ) was integrated from 350-650 nm. The quantum yield was calculated as

$$\phi_c = \frac{I_c * A_R}{A_c * I_R} * \phi_R$$

whereby  $\phi_R$  is the quantum yield of quinine sulfate and corresponds to 0.546.

**AFM measurements** AFM measurements were performed on a Nanoflex AFM (Nanosurf AG, Switzerland) at ambient conditions. 15  $\mu$ l of a solution containing the polymer (0.5  $\mu$ M in 10 mM sodium phosphate buffer, pH 7.2) were incubated on a 3-aminopropyltriethoxy silane modified mica-sheet<sup>213</sup> for 8 min. After incubation the mica sheet was washed with 2 ml MilliQ water and dried under a gentle flow of argon. Measurements were carried out using PPP-NCHR-W cantilevers from Nanosensors (resonance frequency 280 kHz, tip radius 10 nm). Initial scanning area was 10  $\mu$ m x 10  $\mu$ m followed by subsequent reduction of the scanning area to minimal 2.5  $\mu$ m x 2.5  $\mu$ m. Graphical evaluation of the AFM pictures was performed using the Gwyddion Free and Open Source software, covered by GNU General Public License.

**Gel electrophoresis** The PAGE experiments were performed using a 20 % polyacrylamide/Bis solution (19:1, 5% C), prepared from a 40% stock solution (SERVA), and a 10% loading gel. The gel was run for 1 h 40 min at 4 °C, 170 V, 6 mA, 2 W. Around 150 pmol of oligomer was loaded in 10 mM sodium phosphate buffer and 100 mM NaCl. The samples were visualized using a Stains-all solution.

## 7.0. References

- (1) Watson, J. D.; Crick, F. H. C. *Nature* **1953**, *171*, 737.
- (2) Franklin, R. E.; Gosling, R. G. *Nature* **1953**, *171*, 740.
- (3) Wilkins, M. H. F.; Stokes, A. R.; Wilson, H. R. *Nature* **1953**, *171*, 738.
- (4) Matteucci, M. D.; Caruthers, M. H. *Journal of the American Chemical Society* **1981**, *103*, 3185.
- (5) Beaucage, S. L.; Caruthers, M. H. *Tetrahedron Letters* **1981**, *22*, 1859.
- (6) Khakshoor, O.; Kool, E. T. *Chemical Communications* **2011**, *47*, 7018.
- (7) Sacca, B.; Niemeyer, C. M. *Angewandte Chemie-International Edition* **2012**, *51*, 58.
- (8) Michelotti, N.; Johnson-Buck, A.; Manzo, A. J.; Walter, N. G. *Wiley Interdisciplinary Reviews-Nanomedicine and Nanobiotechnology* **2012**, *4*, 139.
- (9) Nangreave, J.; Han, D. R.; Liu, Y.; Yan, H. *Current Opinion in Chemical Biology* **2010**, *14*, 608.
- (10) Seeman, N. C. In *Annual Review of Biochemistry, Vol 79*; Kornberg, R. D., Raetz, C. R. H., Rothman, J. E., Thorner, J. W., Eds. 2010; Vol. 79, p 65.
- (11) Hunziker, J.; Roth, H. J.; Bohringer, M.; Giger, A.; Diederichsen, U.; Gobel, M.; Krishnan, R.; Jaun, B.; Leumann, C.; Eschenmoser, A. *Helvetica Chimica Acta* **1993**, *76*, 259.
- (12) Otting, G.; Billeter, M.; Wuthrich, K.; Roth, H. J.; Leumann, C.; Eschenmoser, A. *Helvetica Chimica Acta* **1993**, *76*, 2701.
- (13) Groebke, K.; Hunziker, J.; Fraser, W.; Peng, L.; Diederichsen, U.; Zimmermann, K.; Holzner, A.; Leumann, C.; Eschenmoser, A. *Helvetica Chimica Acta* **1998**, *81*, 375.
- (14) Uhlmann, E.; Peyman, A. *Chemical Reviews* **1990**, *90*, 543.
- (15) Demesmaeker, A.; Haner, R.; Martin, P.; Moser, H. E. *Accounts of Chemical Research* **1995**, *28*, 366.
- (16) Freier, S. M.; Altmann, K. H. *Nucleic Acids Research* **1997**, *25*, 4429.
- (17) Altmann, K. H.; Dean, N. M.; Fabbro, D.; Freier, S. M.; Geiger, T.; Haner, R.; Husken, D.; Martin, P.; Monia, B. P.; Muller, M.; Natt, F.; Nicklin, P.; Phillips, J.; Pieves, U.; Sasmor, H.; Moser, H. E. *Chimia* **1996**, *50*, 168.
- (18) Matteucci, M.; Lin, K. Y.; Butcher, S.; Moulds, C. *Journal of the American Chemical Society* **1991**, *113*, 7767.
- (19) Stein, C. A.; Cheng, Y. C. *Science* **1993**, *261*, 1004.
- (20) Langkjaer, N.; Pasternak, A.; Wengel, J. *Bioorganic & Medicinal Chemistry* **2009**, *17*, 5420.
- (21) Campbell, M. A.; Wengel, J. *Chemical Society Reviews* **2011**, *40*, 5680.
- (22) Koshkin, A. A.; Singh, S. K.; Nielsen, P.; Rajwanshi, V. K.; Kumar, R.; Meldgaard, M.; Olsen, C. E.; Wengel, J. *Tetrahedron* **1998**, *54*, 3607.
- (23) Singh, S. K.; Nielsen, P.; Koshkin, A. A.; Wengel, J. *Chemical Communications* **1998**, 455.
- (24) Bohringer, M.; Roth, H. J.; Hunziker, J.; Gobel, M.; Krishnan, R.; Giger, A.; Schweizer, B.; Schreiber, J.; Leumann, C.; Eschenmoser, A. *Helvetica Chimica Acta* **1992**, *75*, 1416.
- (25) Tarkoy, M.; Bolli, M.; Schweizer, B.; Leumann, C. *Helvetica Chimica Acta* **1993**, *76*, 481.
- (26) Tarkoy, M.; Bolli, M.; Leumann, C. *Helvetica Chimica Acta* **1994**, *77*, 716.
- (27) Scheidegger, S. P.; Leumann, C. J. *Chemistry-a European Journal* **2006**, *12*, 8014.
- (28) Hikishima, S.; Minakawa, N.; Kuramoto, K.; Fujisawa, Y.; Ogawa, M.; Matsuda, A. *Angewandte Chemie-International Edition* **2005**, *44*, 596.
- (29) Minakawa, N.; Kojima, N.; Hikishima, S.; Sasaki, T.; Kiyosue, A.; Atsumi, N.; Ueno, Y.; Matsuda, A. *Journal of the American Chemical Society* **2003**, *125*, 9970.



- (30) Seela, F.; Becher, G. *Nucleic Acids Research* **2001**, *29*, 2069.
- (31) Piccirilli, J. A.; Krauch, T.; Moroney, S. E.; Benner, S. A. *Nature* **1990**, *343*, 33.
- (32) Switzer, C.; Moroney, S. E.; Benner, S. A. *Journal of the American Chemical Society* **1989**, *111*, 8322.
- (33) Betz, K.; Malyshev, D. A.; Lavergne, T.; Welte, W.; Diederichs, K.; Romesberg, F. E.; Marx, A. *Journal of the American Chemical Society* **2013**, *135*, 18637.
- (34) Li, L. J.; Degardin, M.; Lavergne, T.; Malyshev, D. A.; Dhimi, K.; Ordoukhanian, P.; Romesberg, F. E. *Journal of the American Chemical Society* **2014**, *136*, 826.
- (35) Hirao, I. *Current Opinion in Chemical Biology* **2006**, *10*, 622.
- (36) Malyshev, D. A.; Dhimi, K.; Lavergne, T.; Chen, T.; Dai, N.; Foster, J. M.; Correa, I. R.; Romesberg, F. E. *Nature* **2014**, *509*, 385.
- (37) Kim, H.-J.; Leal, N. A.; Hoshika, S.; Benner, S. A. *Journal of Organic Chemistry* **2014**, *79*, 3194.
- (38) Mitsui, T.; Kimoto, M.; Harada, Y.; Yokoyama, S.; Hirao, L. *Journal of the American Chemical Society* **2005**, *127*, 8652.
- (39) Hirao, I. *Biotechniques* **2006**, *40*, 711.
- (40) Hirao, I.; Kimoto, M.; Mitsui, T.; Fujiwara, T.; Kawai, R.; Sato, A.; Harada, Y.; Yokoyama, S. *Nat. Methods* **2006**, *3*, 729.
- (41) Liu, H. B.; Gao, J. M.; Kool, E. T. *Journal of the American Chemical Society* **2005**, *127*, 1396.
- (42) Liu, H. B.; Gao, J. M.; Maynard, L.; Saito, Y. D.; Kool, E. T. *Journal of the American Chemical Society* **2004**, *126*, 1102.
- (43) Winnacker, M.; Kool, E. T. *Angewandte Chemie-International Edition* **2013**, *52*, 12498.
- (44) Wilson, A.; Gasparini, G.; Matile, S. *Chemical Society Reviews* **2014**, *43*, 1948.
- (45) Lehn, J. M. *Angewandte Chemie-International Edition* **2013**, *52*, 2836.
- (46) Safont-Sempere, M. M.; Fernandez, G.; Wurthner, F. *Chemical Reviews* **2011**, *111*, 5784.
- (47) E., T. L. Z. *Plant Physiology*; 4 th ed.; Sinauer Associates, Inc.: Sunderland, MA, 2006.
- (48) *The term "aromatic chromophore" in the present context describes any type of aromatic molecule other than the canonical nucleobases. This terminology is chosen on the basis of the 2010 Chem Soc Review by Häner and coworkers.*
- (49) Malinovskii, V. L.; Wenger, D.; Haner, R. *Chemical Society Reviews* **2010**, *39*, 410.
- (50) Weisbrod, S. H.; Marx, A. *Chemical Communications* **2008**, 5675.
- (51) Zatspein, T. S.; Stetsenko, D. A.; Gait, M. J.; Oretskaya, T. S. *Bioconjugate Chemistry* **2005**, *16*, 471.
- (52) Malinovskii, V. L.; Wenger, D.; Haener, R. *Chemical Society Reviews* **2010**, *39*, 410.
- (53) Smirnov, S.; Matray, T. J.; Kool, E. T.; de los Santos, C. *Nucleic Acids Research* **2002**, *30*, 5561.
- (54) Brotschi, C.; Mathis, G.; Leumann, C. J. *Chemistry-a European Journal* **2005**, *11*, 1911.
- (55) Nakamura, M.; Murakami, Y.; Sasa, K.; Hayashi, H.; Yamana, K. *Journal of the American Chemical Society* **2008**, *130*, 6904.
- (56) Balaz, M.; Holmes, A. E.; Benedetti, M.; Rodriguez, P. C.; Berova, N.; Nakanishi, K.; Proni, G. *Journal of the American Chemical Society* **2005**, *127*, 4172.
- (57) Mayer-Enthart, E.; Wagner, C.; Barbaric, J.; Wagenknecht, H. A. *Tetrahedron* **2007**, *63*, 3434.
- (58) Nguyen, T.; Brewer, A.; Stulz, E. *Angewandte Chemie-International Edition* **2009**, *48*, 1974.
- (59) Brotschi, C.; Leumann, C. J. *Angewandte Chemie-International Edition* **2003**, *42*, 1655.
- (60) Zahn, A.; Leumann, C. J. *Chemistry-a European Journal* **2008**, *14*, 1087.
- (61) Johar, Z.; Zahn, A.; Leumann, C. J.; Jaun, B. *Chemistry-a European Journal* **2008**, *14*, 1080.
- (62) Letsinger, R. L.; Wu, T. F. *Journal of the American Chemical Society* **1995**, *117*, 7323.

- (63) Lewis, F. D.; Zhang, L. G.; Kelley, R. F.; McCamant, D.; Wasielewski, M. R. *Tetrahedron* **2007**, *63*, 3457.
- (64) Berlin, K.; Jain, R. K.; Simon, M. D.; Richert, C. *Journal of Organic Chemistry* **1998**, *63*, 1527.
- (65) Asanuma, H.; Ito, T.; Yoshida, T.; Liang, X. G.; Komiyama, M. *Angewandte Chemie-International Edition* **1999**, *38*, 2393.
- (66) Bevers, S.; Schutte, S.; McLaughlin, L. W. *Journal of the American Chemical Society* **2000**, *122*, 5905.
- (67) Abdalla, M. A.; Bayer, J.; Radler, J. O.; Mullen, K. *Angewandte Chemie-International Edition* **2004**, *43*, 3967.
- (68) Langenegger, S. M.; Haner, R. *Helvetica Chimica Acta* **2002**, *85*, 3414.
- (69) Christensen, U. B.; Pedersen, E. B. *Nucleic Acids Research* **2002**, *30*, 4918.
- (70) Langenegger, S. M.; Haner, R. *Tetrahedron Letters* **2004**, *45*, 9273.
- (71) Bouquin, N.; Malinovskii, V. L.; Guegano, X.; Liu, S. X.; Decurtins, S.; Haner, R. *Chemistry-a European Journal* **2008**, *14*, 5732.
- (72) Zheng, Y.; Long, H.; Schatz, G. C.; Lewis, F. D. *Chemical Communications* **2005**, 4795.
- (73) Kashida, H.; Tanaka, M.; Baba, S.; Sakamoto, T.; Kawai, G.; Asanuma, H.; Komiyama, M. *Chemistry-a European Journal* **2006**, *12*, 777.
- (74) Bittermann, H.; Siegemund, D.; Malinovskii, V. L.; Haner, R. *Journal of the American Chemical Society* **2008**, *130*, 15285.
- (75) Werder, S.; Malinovskii, V. L.; Haner, R. *Organic Letters* **2008**, *10*, 2011.
- (76) Lehn, J.-M. *Angewandte Chemie International Edition in English* **1990**, *29*, 1304.
- (77) Cockroft, S. L.; Hunter, C. A.; Lawson, K. R.; Perkins, J.; Urch, C. J. *Journal of the American Chemical Society* **2005**, *127*, 8594.
- (78) Hunter, C. A. *Chemical Society Reviews* **1994**, *23*, 101.
- (79) Hunter, C. A.; Sanders, J. K. M. *Journal of the American Chemical Society* **1990**, *112*, 5525.
- (80) Martinez, C. R.; Iverson, B. L. *Chemical Science* **2012**, *3*, 2191.
- (81) Muller, P. *Pure and Applied Chemistry* **1994**, *66*, 1077.
- (82) Petitjean, A.; Cuccia, L. A.; Schmutz, M.; Lehn, J. M. *Journal of Organic Chemistry* **2008**, *73*, 2481.
- (83) Nussbaumer, A. L.; Studer, D.; Malinovskii, V. L.; Haner, R. *Angewandte Chemie-International Edition* **2011**, *50*, 5490.
- (84) Sebaoun, L.; Maurizot, V.; Granier, T.; Kauffmann, B.; Huc, I. *Journal of the American Chemical Society* **2014**, *136*, 2168.
- (85) Khan, A.; Kaiser, C.; Hecht, S. *Angewandte Chemie-International Edition* **2006**, *45*, 1878.
- (86) Delsuc, N.; Kawanami, T.; Lefeuvre, J.; Shundo, A.; Ihara, H.; Takafuji, M.; Huc, I. *ChemPhysChem* **2008**, *9*, 1882.
- (87) Prince, R. B.; Barnes, S. A.; Moore, J. S. *Journal of the American Chemical Society* **2000**, *122*, 2758.
- (88) Tomasini, C.; Huc, I.; Aitken, D. J.; Fuloep, F. *European Journal of Organic Chemistry* **2013**, 3408.
- (89) Lokey, R. S.; Iverson, B. L. *Nature* **1995**, *375*, 303.
- (90) Lista, M.; Orentas, E.; Areephong, J.; Charbonnaz, P.; Wilson, A.; Zhao, Y.; Bolag, A.; Sforazzini, G.; Turdean, R.; Hayashi, H.; Domoto, Y.; Sobczuk, A.; Sakai, N.; Matile, S. *Organic & Biomolecular Chemistry* **2013**, *11*, 1754.
- (91) Bolag, A.; Hayashi, H.; Charbonnaz, P.; Sakai, N.; Matile, S. *Chemistryopen* **2013**, *2*, 55.
- (92) Philp, D.; Stoddart, J. F. *Angewandte Chemie-International Edition* **1996**, *35*, 1155.
- (93) Claessens, C. G.; Stoddart, J. F. *Journal of Physical Organic Chemistry* **1997**, *10*, 254.
- (94) Hof, F.; Craig, S. L.; Nuckolls, C.; Rebek, J. J. *Angewandte Chemie International Edition* **2002**, *41*, 1488.

- (95) Klosterman, J. K.; Yamauchi, Y.; Fujita, M. *Chemical Society Reviews* **2009**, *38*, 1714.
- (96) Misumi, S.; Otsubo, T. *Accounts of Chemical Research* **1978**, *11*, 251.
- (97) Cram, D. J.; Cram, J. M. *Accounts of Chemical Research* **1971**, *4*, 204.
- (98) Cram, D. J.; Cram, J. M. *Accounts of Chemical Research* **1978**, *11*, 8.
- (99) Langenegger, S. M.; Bianké, G.; Tona, R.; Häner, R. *CHIMIA International Journal for Chemistry* **2005**, *59*, 794.
- (100) Langenegger, S. M.; Haner, R. *Chembiochem* **2005**, *6*, 848.
- (101) Langenegger, S. M.; Häner, R. *Helvetica Chimica Acta* **2002**, *85*, 3414.
- (102) Malinovskii, V. L.; Samain, F.; Häner, R. *Angewandte Chemie International Edition* **2007**, *46*, 4464.
- (103) Langenegger, S. M.; Haner, R. *Chemical Communications* **2004**, 2792.
- (104) Khorev, O.; Bosch, C. D.; Probst, M.; Haner, R. *Chemical Science* **2014**, *5*, 1506.
- (105) Trkulja, I.; Haener, R. *Bioconjugate Chemistry* **2007**, *18*, 289.
- (106) Langenegger, S. M.; Haner, R. *Bioorganic & Medicinal Chemistry Letters* **2006**, *16*, 5062.
- (107) Bouquin, N.; Malinovskii, V. L.; Haner, R. *Chemical Communications* **2008**, 1974.
- (108) Biner, S. M.; Haener, R. *Chembiochem* **2011**, *12*, 2733.
- (109) Biner, S. M.; Kummer, D.; Malinovskii, V. L.; Haener, R. *Organic & Biomolecular Chemistry* **2011**, *9*, 2628.
- (110) Haener, R.; Biner, S. M.; Langenegger, S. M.; Meng, T.; Malinovskii, V. L. *Angewandte Chemie-International Edition* **2010**, *49*, 1227.
- (111) Görl, D.; Zhang, X.; Würthner, F. *Angewandte Chemie International Edition* **2012**, *51*, 6328.
- (112) Liu, H.; Cao, X.; Wu, Y.; Liao, Q.; Jimenez, A. J.; Würthner, F.; Fu, H. *Chemical communications (Cambridge, England)* **2014**, *50*, 4620.
- (113) Ghosh, S.; Li, X. Q.; Stepanenko, V.; Würthner, F. *Chemistry-a European Journal* **2008**, *14*, 11343.
- (114) Shao, C. Z.; Stolte, M.; Würthner, F. *Angewandte Chemie-International Edition* **2013**, *52*, 10463.
- (115) Heek, T.; Würthner, F.; Haag, R. *Chemistry-a European Journal* **2013**, *19*, 10911.
- (116) Hariharan, M.; Zheng, Y.; Long, H.; Zeidan, T. A.; Schatz, G. C.; Vura-Weis, J.; Wasielewski, M. R.; Zuo, X. B.; Tiede, D. M.; Lewis, F. D. *Journal of the American Chemical Society* **2009**, *131*, 5920.
- (117) Kaiser, T. E.; Stepanenko, V.; Würthner, F. *Journal of the American Chemical Society* **2009**, *131*, 6719.
- (118) Takada, T.; Yamaguchi, K.; Tsukamoto, S.; Nakamura, M.; Yamana, K. *Analyst* **2014**, *139*, 4016.
- (119) Zeidan, T. A.; Carmieli, R.; Kelley, R. F.; Wilson, T. M.; Lewis, F. D.; Wasielewski, M. R. *Journal of the American Chemical Society* **2008**, *130*, 13945.
- (120) Hariharan, M.; Siegmund, K.; Zheng, Y.; Long, H.; Schatz, G. C.; Lewis, F. D. *Journal of Physical Chemistry C* **2010**, *114*, 20466.
- (121) Kashida, H.; Sekiguchi, K.; Asanuma, H. *Chemistry-a European Journal* **2010**, *16*, 11554.
- (122) Takada, T.; Ashida, A.; Nakamura, M.; Fujitsuka, M.; Majima, T.; Yamana, K. *Journal of the American Chemical Society* **2014**, *136*, 6814.
- (123) Zeidan, T. A.; Hariharan, M.; Siegmund, K.; Lewis, F. D. *Photochemical & Photobiological Sciences* **2010**, *9*, 916.
- (124) Menacher, F.; Stepanenko, V.; Würthner, F.; Wagenknecht, H. A. *Chemistry-a European Journal* **2011**, *17*, 6683.
- (125) Baumstark, D.; Wagenknecht, H.-A. *Chemistry-a European Journal* **2008**, *14*, 6640.
- (126) Li, A. D. Q.; Wang, W.; Wang, L. Q. *Chemistry-a European Journal* **2003**, *9*, 4594.
- (127) Chen, Z. J.; Fimmel, B.; Würthner, F. *Organic & Biomolecular Chemistry* **2012**, *10*, 5845.

- (128) Cozzi, F.; Cinquini, M.; Annunziata, R.; Dwyer, T.; Siegel, J. S. *Journal of the American Chemical Society* **1992**, *114*, 5729.
- (129) Cozzi, F.; Cinquini, M.; Annunziata, R.; Siegel, J. S. *Journal of the American Chemical Society* **1993**, *115*, 5330.
- (130) V. A. Bloomfield, D. M. C., I. Tinoco *Nucleic acids - Structures, Properties and Functions*; University Science Books: Sausalito, 2000.
- (131) Egetenmeyer, S.; Richert, C. *Current protocols in nucleic acid chemistry / edited by Serge L. Beaucage ... [et al.]* **2012**, Chapter 4, Unit4.53.
- (132) Egetenmeyer, S.; Richert, C. *Chemistry-a European Journal* **2011**, *17*, 11813.
- (133) Patra, A.; Richert, C. *Journal of the American Chemical Society* **2009**, *131*, 12671.
- (134) Zhang, L. G.; Zhu, H. H.; Sajimon, M. C.; Stutz, J. A. R.; Siegmund, K.; Richert, C.; Shafirovich, V.; Lewis, F. D. *Journal of the Chinese Chemical Society* **2006**, *53*, 1501.
- (135) Printz, M.; Richert, C. *Chemistry-a European Journal* **2009**, *15*, 3390.
- (136) Guckian, K. M.; Schweitzer, B. A.; Ren, R. X. F.; Sheils, C. J.; Tahmassebi, D. C.; Kool, E. T. *Journal of the American Chemical Society* **2000**, *122*, 2213.
- (137) Scheibe, G.; Schontag, A.; Katheder, F. *Naturwissenschaften* **1939**, *27*, 499.
- (138) Davydov, A. S. *Uspekhi Fizicheskikh Nauk* **1964**, *82*, 393.
- (139) Kasha, M. *Radiation Research* **1963**, *20*, 55.
- (140) Asanuma, H.; Fujii, T.; Kato, T.; Kashida, H. *Journal of Photochemistry and Photobiology C-Photochemistry Reviews* **2012**, *13*, 124.
- (141) Delgado, M. C. R.; Kim, E.-G.; Filho, D. A. d. S.; Bredas, J.-L. *Journal of the American Chemical Society* **2010**, *132*, 3375.
- (142) Vybornyi, M.; Rudnev, A. V.; Langenegger, S. M.; Wandlowski, T.; Calzaferri, G.; Häner, R. *Angewandte Chemie International Edition* **2013**, *52*, 11488.
- (143) Kashida, H.; Asanuma, H.; Komiyama, M. *Angewandte Chemie-International Edition* **2004**, *43*, 6522.
- (144) Fujii, T.; Kashida, H.; Asanuma, H. *Chemistry – A European Journal* **2009**, *15*, 10092.
- (145) Calzaferri, G.; internal report
- (146) *internal report*.
- (147) Neelakandan, P. P.; Zeidan, T. A.; McCullagh, M.; Schatz, G. C.; Vura-Weis, J.; Kim, C. H.; Wasielewski, M. R.; Lewis, F. D. *Chemical Science* **2014**, *5*, 973.
- (148) unpublished data
- (149) Kashida, H.; Higashiyama, N.; Kato, T.; Asanuma, H. *Bioorganic & Medicinal Chemistry* **2013**, *21*, 6191.
- (150) Probst, M.; Langenegger, S. M.; Haner, R. *Chemical Communications* **2014**, *50*, 159.
- (151) Probst, M.; Wenger, D.; Biner, S. M.; Haner, R. *Organic & Biomolecular Chemistry* **2012**, *10*, 755.
- (152) Loll, B.; Kern, J.; Saenger, W.; Zouni, A.; Biesiadka, J. *Nature* **2005**, *438*, 1040.
- (153) Wurthner, F.; Kaiser, T. E.; Saha-Moller, C. R. *Angewandte Chemie-International Edition* **2011**, *50*, 3376.
- (154) Aratani, N.; Kim, D.; Osuka, A. *Accounts of Chemical Research* **2009**, *42*, 1922.
- (155) Olive, A. G. L.; Del Guerso, A.; Schafer, C.; Belin, C.; Raffy, G.; Giansante, C. *Journal of Physical Chemistry C* **2010**, *114*, 10410.
- (156) Calzaferri, G.; Huber, S.; Maas, H.; Minkowski, C. *Angewandte Chemie-International Edition* **2003**, *42*, 3732.
- (157) Calzaferri, G.; Pauchard, M.; Maas, H.; Huber, S.; Khatyr, A.; Schaafsma, T. *Journal of Materials Chemistry* **2002**, *12*, 1.
- (158) Garo, F.; Haner, R. *Angewandte Chemie-International Edition* **2012**, *51*, 916.
- (159) Dutta, P. K.; Varghese, R.; Nangreave, J.; Lin, S.; Yan, H.; Liu, Y. *Journal of the American Chemical Society* **2011**, *133*, 11985.

- (160) Spillmann, C. M.; Buckhout-White, S.; Oh, E.; Goldman, E. R.; Ancona, M. G.; Medintz, I. L. *Chemical Communications* **2014**, *50*, 7246.
- (161) Chen, L.; Honsho, Y.; Seki, S.; Jiang, D. L. *Journal of the American Chemical Society* **2010**, *132*, 6742.
- (162) Sakai, N.; Matile, S. *Journal of the American Chemical Society* **2011**, *133*, 18542.
- (163) Calzaferri, G. In *European Society for Quantum Solar Energy Conversion, Summer School Hirschegg*, 2006.
- (164) Nussbaumer, A. L.; Samain, F.; Malinovskii, V. L.; Haener, R. *Organic & Biomolecular Chemistry* **2012**, *10*, 4891.
- (165) Rudnev, A. V.; Malinovskii, V. L.; Nussbaumer, A. L.; Mishchenko, A.; Haener, R.; Wandlowski, T. *Macromolecules* **2012**, *45*, 5986.
- (166) Malinovskii, V. L.; Nussbaumer, A. L.; Haener, R. *Angewandte Chemie-International Edition* **2012**, *51*, 4905.
- (167) Nussbaumer, A. L.; Studer, D.; Malinovskii, V. L.; Haener, R. *Angewandte Chemie-International Edition* **2011**, *50*, 5490.
- (168) Simona, F.; Nussbaumer, A. L.; Haener, R.; Cascella, M. *Journal of Physical Chemistry B* **2013**, *117*, 2576.
- (169) unpublished work
- (170) Mandelkern, M.; Elias, J. G.; Eden, D.; Crothers, D. M. *Journal of Molecular Biology* **1981**, *152*, 153.
- (171) Arnott, S.; Hukins, D. W. L. *Biochemical and Biophysical Research Communications* **1972**, *47*, 1504.
- (172) Rudnev, A. V.; Malinovskii, V. L.; Nussbaumer, A. L.; Mishchenko, A.; Haner, R.; Wandlowski, T. *Macromolecules* **2012**, *45*, 5986.
- (173) Kumar, G. R.
- (174) Jun, E. J.; Won, H. N.; Kim, J. S.; Lee, K. H.; Yoon, J. *Tetrahedron Letters* **2006**, *47*, 4577.
- (175) It has to be mentioned that it can not be excluded that the fluorescence signal in Figure 4.33 could also be influenced by very small contaminations of pyrene monomer molecule which than acts as an energy acceptor.
- (176) Studying the polymers with AFM it was found that the morphology of the polymers did not change whether the samples were cooled very fast (up to 5 °C per min or slowly 0.2 °C per min). Fluorescence studies revealed that upon fast cooling of the samples a higher content of phenanthrene fluorescence remains, whereas after slow cooling the phenanthrene fluorescence is less pronounced. This could probably be explained with a more uniform and alternating distribution of phenanthrene and pyrene molecules in the polymer upon slow cooling and avoiding the formation of homoaggregates of the one or other molecule.
- (177) Forster, T. *Annalen Der Physik* **1948**, *2*, 55.
- (178) Collini, E. *Chemical Society Reviews* **2013**, *42*, 4932.
- (179) Schaufele, F.; Demarco, I.; Day, R. N. In *Molecular Imaging*; Periasamy, A., Day, R. N., Eds.; American Physiological Society: San Diego, 2005, p 72.
- (180) Strumpfer, J.; Sener, M.; Schulten, K. *Journal of Physical Chemistry Letters* **2012**, *3*, 536.
- (181) Fassioli, F.; Dinshaw, R.; Arpin, P. C.; Scholes, G. D. *Journal of the Royal Society Interface* **2014**, *11*.
- (182) Andrea Rozzi, C.; Maria Falke, S.; Spallanzani, N.; Rubio, A.; Molinari, E.; Brida, D.; Maiuri, M.; Cerullo, G.; Schramm, H.; Christoffers, J.; Lienau, C. *Nat Commun* **2013**, *4*, 1602.
- (183) Cheng, Y.-C.; Fleming, G. R. *Annual Review of Physical Chemistry* **2009**, *60*, 241.
- (184) Engel, G. S.; Calhoun, T. R.; Read, E. L.; Ahn, T.-K.; Mancal, T.; Cheng, Y.-C.; Blankenship, R. E.; Fleming, G. R. *Nature* **2007**, *446*, 782.
- (185) Lee, H.; Cheng, Y.-C.; Fleming, G. R. *Science* **2007**, *316*, 1462.

- (186) *Chrysene-diol was a kind gift from C. D. Bösch.*
- (187) Scheibe, G. *Angewandte Chemie* **1937**, *50*, 0212.
- (188) Scheibe, G.; Kandler, L.; Ecker, H. *Naturwissenschaften* **1937**, *25*, 75.
- (189) Jelley, E. E. *Nature* **1936**, *138*, 1009.
- (190) Mobius, D. *Advanced Materials* **1995**, *7*, 437.
- (191) Markova, L. I.; Malinovskii, V. L.; Patsenker, L. D.; Haner, R. *Chemical Communications* **2013**, *49*, 5298.
- (192) Cogdell, R. J.; Gall, A.; Kohler, J. *Quarterly Reviews of Biophysics* **2006**, *39*, 227.
- (193) Koepke, J.; Hu, X. C.; Muenke, C.; Schulten, K.; Michel, H. *Structure* **1996**, *4*, 581.
- (194) Hu, X. C.; Schulten, K. *Physics Today* **1997**, *50*, 28.
- (195) Hu, X. C.; Damjanovic, A.; Ritz, T.; Schulten, K. *Proceedings of the National Academy of Sciences of the United States of America* **1998**, *95*, 5935.
- (196) Pullerits, T.; Sundstrom, V. *Accounts of Chemical Research* **1996**, *29*, 381.
- (197) Tamiaki, H.; Amakawa, M.; Shimono, Y.; Tanikaga, R.; Holzwarth, A. R.; Schaffner, K. *Photochemistry and Photobiology* **1996**, *63*, 92.
- (198) Oostergetel, G. T.; Reus, M.; Chew, A. G. M.; Bryant, D. A.; Boekema, E. J.; Holzwarth, A. R. *Febs Letters* **2007**, *581*, 5435.
- (199) Ganapathy, S.; Oostergetel, G. T.; Wawrzyniak, P. K.; Reus, M.; Chew, A. G. M.; Buda, F.; Boekema, E. J.; Bryant, D. A.; Holzwarth, A. R.; de Groot, H. J. M. *Proceedings of the National Academy of Sciences of the United States of America* **2009**, *106*, 8525.
- (200) Kaiser, T. E.; Wang, H.; Stepanenko, V.; Wurthner, F. *Angewandte Chemie-International Edition* **2007**, *46*, 5541.
- (201) Thalacker, C.; Wurthner, F. *Advanced Functional Materials* **2002**, *12*, 209.
- (202) I.G, W. F. S. *J-Aggregates of perylene dyes*; World Scientific Publishing Co. Pte. Ltd, 2012; Vol. 2.
- (203) Häner, R.; Samain, F.; Malinovskii, V. L. *Chemistry – A European Journal* **2009**, *15*, 5701.
- (204) Zhao, D. H.; Moore, J. S. *Organic & Biomolecular Chemistry* **2003**, *1*, 3471.
- (205) Korevaar, P. A.; George, S. J.; Markvoort, A. J.; Smulders, M. M. J.; Hilbers, P. A. J.; Schenning, A.; De Greef, T. F. A.; Meijer, E. W. *Nature* **2012**, *481*, 492.
- (206) Smulders, M. M. J.; Nieuwenhuizen, M. M. L.; de Greef, T. F. A.; van der Schoot, P.; Schenning, A.; Meijer, E. W. *Chemistry-a European Journal* **2010**, *16*, 362.
- (207) It could be discussed whether this band indicates a J-aggregate. The absorption band is very faint and could not be evolved by adding salt like in previous cases. The stock solution (20  $\mu$ M) of molecule X however formed black aggregates at -20 °C over several days. Increase of concentration could probably result in the formation of J-aggregates. .
- (208) Clave, G.; Chatelain, G.; Filoramo, A.; Gasparutto, D.; Saint-Pierre, C.; Le Cam, E.; Pietrement, O.; Guerineau, V.; Campidelli, S. *Organic & Biomolecular Chemistry* **2014**, *12*, 2778.
- (209) Jakobsen, U.; Simonsen, A. C.; Vogel, S. *Journal of the American Chemical Society* **2008**, *130*, 10462.
- (210) Pinheiro, A. V.; Han, D. R.; Shih, W. M.; Yan, H. *Nature Nanotechnology* **2011**, *6*, 763.
- (211) Rahe, N.; Rinn, C.; Carell, T. *Chemical Communications* **2003**, 2120.
- (212) Crosby, G. A.; Demas, J. N. *The Journal of Physical Chemistry* **1971**, *75*, 991.
- (213) Lyubchenko, Y. L.; Jacobs, B. L.; Lindsay, S. M. *Nucleic Acids Research* **1992**, *20*, 3983.

## 8.0. Appendix

Table APP 1 MS and sequence of the described oligomers.

Oligomer name	Sequence	Calculated Mass	Measured Mass	Comments
1	5' GCG TTA <b>YYY Y</b>	3407.6	3405.7	
2	5' <b>YYYY</b> TAACGC	3376.6	3374.7	
3	5' <b>Y EY</b> YTA ACG C	3544.6	3545.0	
4	5' <b>EYE</b> YTA ACG C	3712.6	3714.0	
5	5' <b>EEE</b> YTA ACG C	3880.7	3880.7	
6	5' GCG TTA <b>EEE E</b>	4079.7	4080.0	
7	5' <b>EEE</b> ETA ACG C	4048.7	4050.0	
8	5' <b>YYY</b> ETA ACG C	3544.1	3544.7	
9	5' <b>Y EY</b> ETA ACG C	3712.6	3713.7	
10	5' <b>EYE</b> ETA ACG C	3880.7	3881.7	
11	ordered Reference			
12	5' YTA ACG C	2176.3	2175.4	
13	5' ETA ACG C	2344.3	2344.4	
14	5' <b>Y YE</b> ETA ACG C	3712.6	3714.0	
15	5' <b>EEY</b> YTA ACG C	3712.6	3714.0	
16	5' GCG TTA <b>XXX X</b>	3407.6	3408.0	
17	5' <b>XXX</b> XTA ACG C	3376.1	3376.0	
18	5' <b>XXX</b> ETA ACG C	3544.6	3544.0	
19	5' <b>X EX</b> XTA ACG C	3544.6	3544.0	
20	5' <b>X EX</b> ETA ACG C	3712.6	3712.0	
21	5' <b>EXE</b> XTA ACG C	3712.6	3713.0	
22	5' <b>EXE</b> ETA ACG C	3880.7	3880.0	
23	5' <b>EEE</b> XTA ACG C	3880.7	3880.0	
24	5' <b>Y YE</b> EAT TGC G	3743.7	3745.0	
25	5' <b>EEY</b> YAT TGC G	3743.7	3744.9	
Oligomer a	5' <b>ααα</b>	1066.3	1066.3	
Oligomer b	5' <b>αααY</b>	1466.3	1466.4	
Oligomer c	5' <b>YYY</b>	1138.0	1137.3	
I	5' GCG TTA <b>EEE EEE</b>	5215.9	5217.92	
II	5' <b>EEE EEE</b> TAA CGC	5184.9	5184.0	side product – 1 PDI
III	5' <b>YYY YYY</b> TAA CGC	4176.7	4176.8	
IV	5' GCG TTA <b>YYY YYY</b>	4207.8	4209.0	

## 8.0. Appendix

V	5' <b>EEE EEE</b> G	3675.9	3677.7	MS: major contaminations
VI	5' <b>EEE EEE</b> C	3635.9	3637.7	MS: major contaminations
VII	5' <b>EEE EEE</b> T	3650.9	3652.7	MS: major contaminations
VIII	5' <b>EEE EEE</b> A	3659.9	3661.7	MS: major contaminations
IX	5' <b>YYY YYY</b> C	2627.8	2627.8	
X	5' <b>EEE</b>	1642.0	1642.4	

oligomer	sequence	mass calc.	mass found
P( $\alpha$ 5)	5' CTG CGA GTG T $\alpha\alpha\alpha\alpha$ ACG TTC CTT C 3'	7955.5	7955.3
A(E5)	5' GAA GGA ACG TEE EEE ACA CTC GCA G 3'	9000.0	9001.4
A(Y5)	5' GAA GGA ACG TYY YYY ACA CTC GCA G 3'	8160.0	8160.5



### HPLC Trace of oligomers and elution times

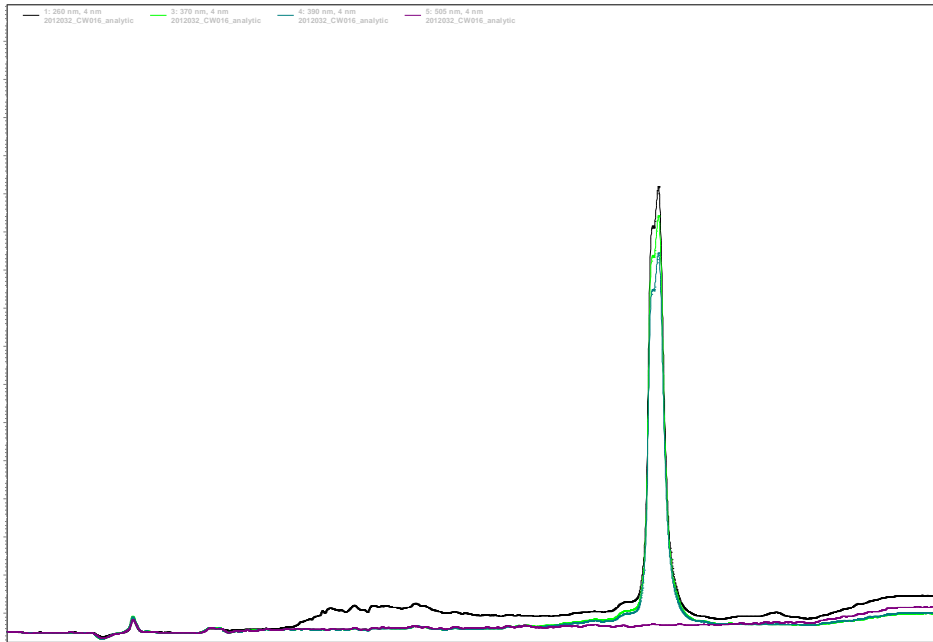


Figure APP 1 HPLC trace of oligomer 1 eluting at 20.9 min.

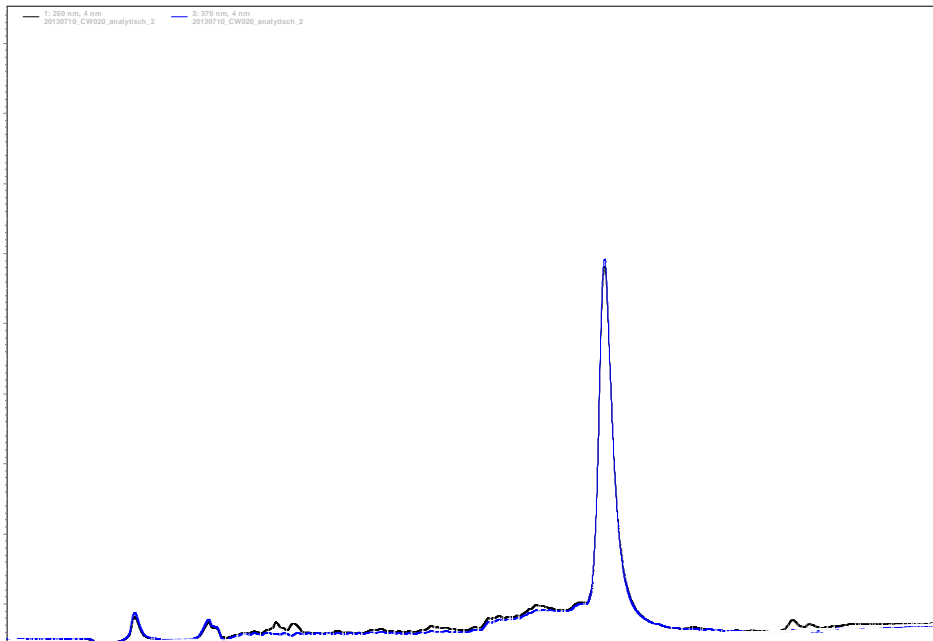


Figure APP 2 HPLC trace of oligomer 2 eluting at 21.1 min

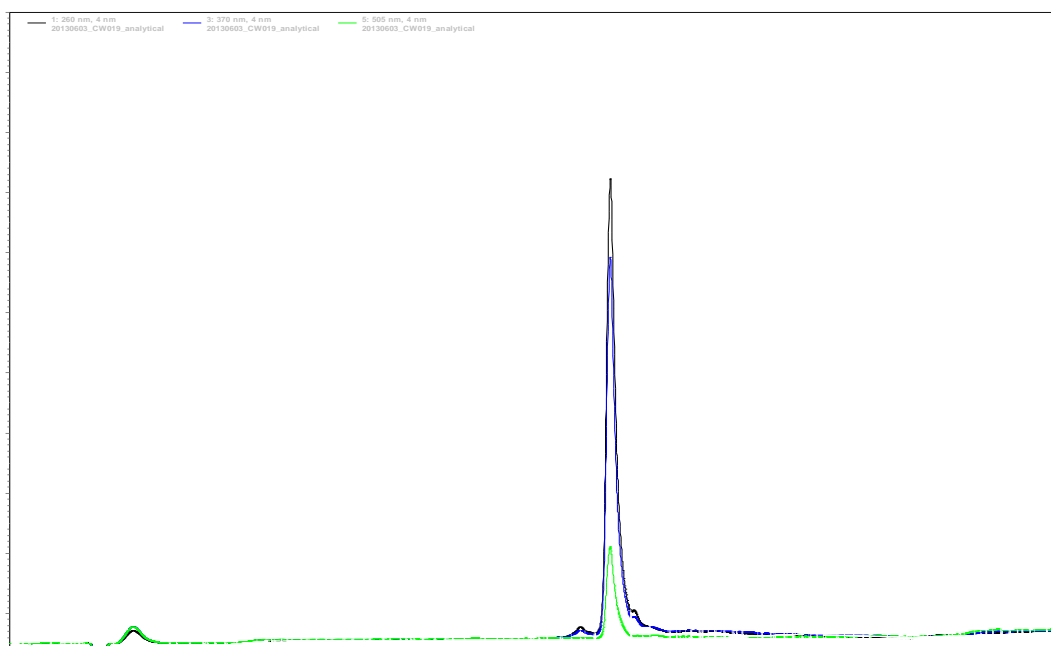


Figure APP 3 HPLC trace of oligomer 3 eluting at 17.0 min.

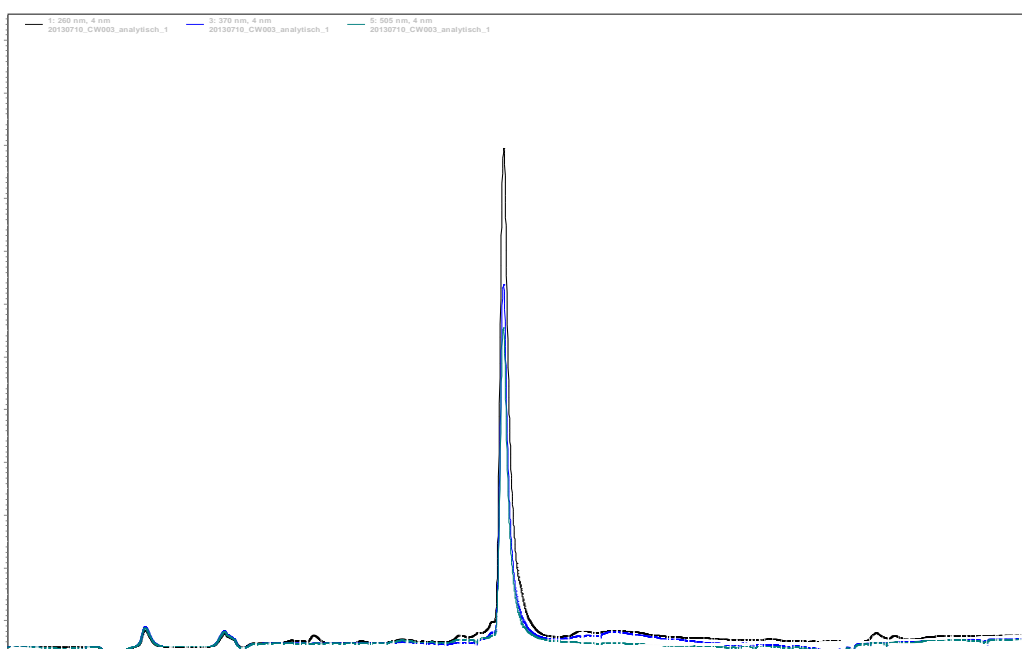
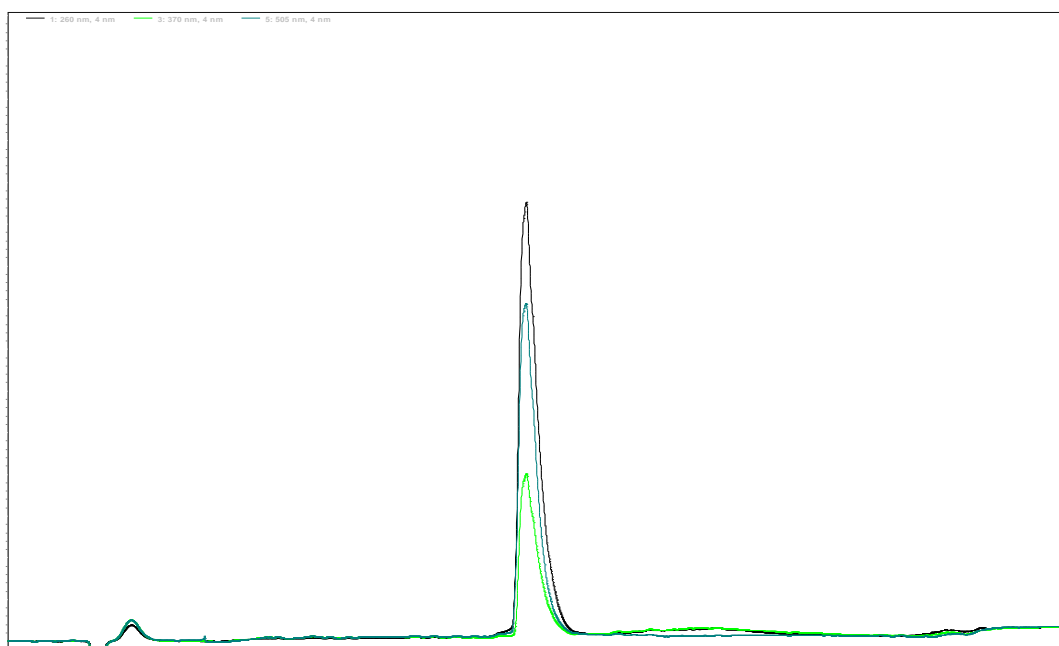
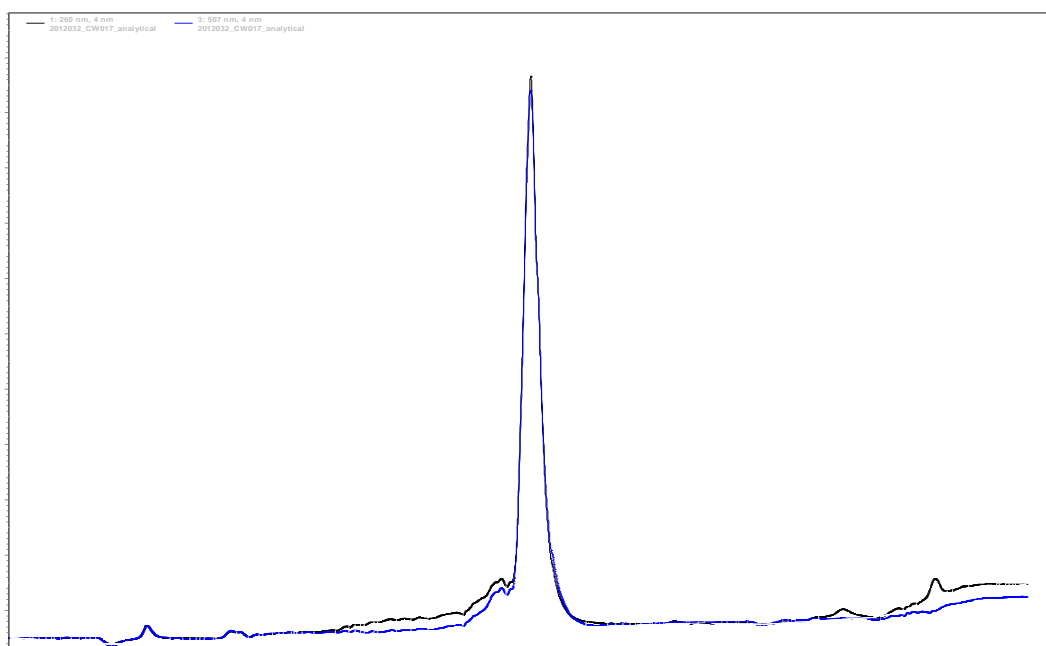


Figure APP 4 HPLC trace of oligomer 4 eluting at 15.0 min.



**Figure APP 5** HPLC trace of oligomer **5** eluting at 14.62 min.



**Figure APP 6** HPLC trace of oligomer **6** eluting at 15.4 min.

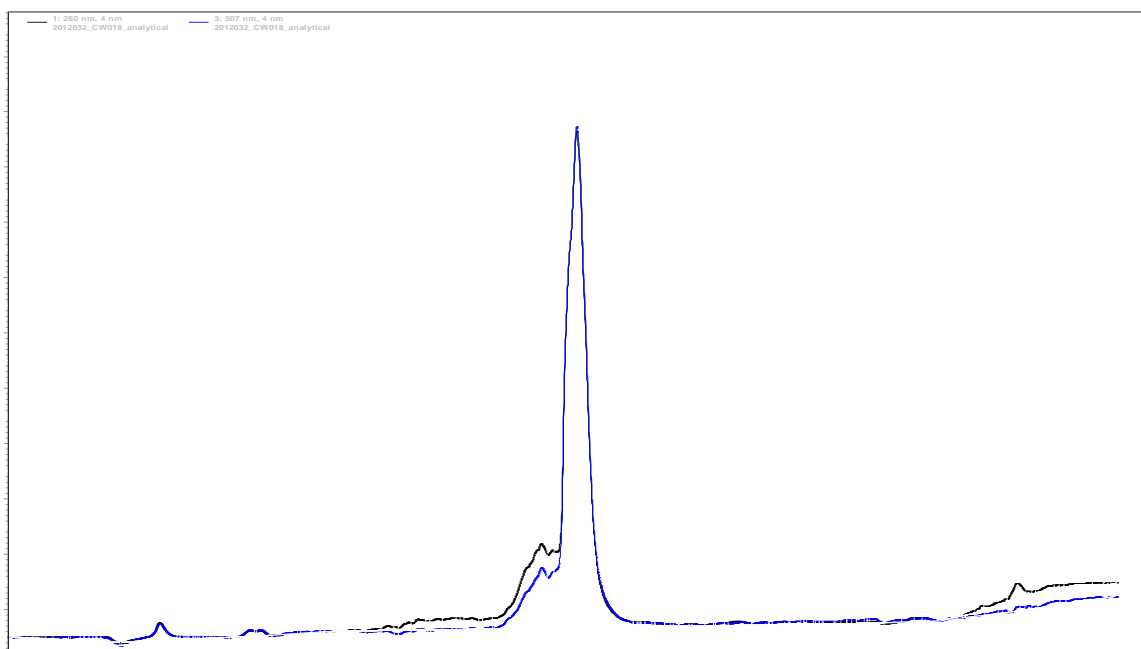


**Figure APP 7** HPLC trace of oligomer **7** eluting at 15.3.

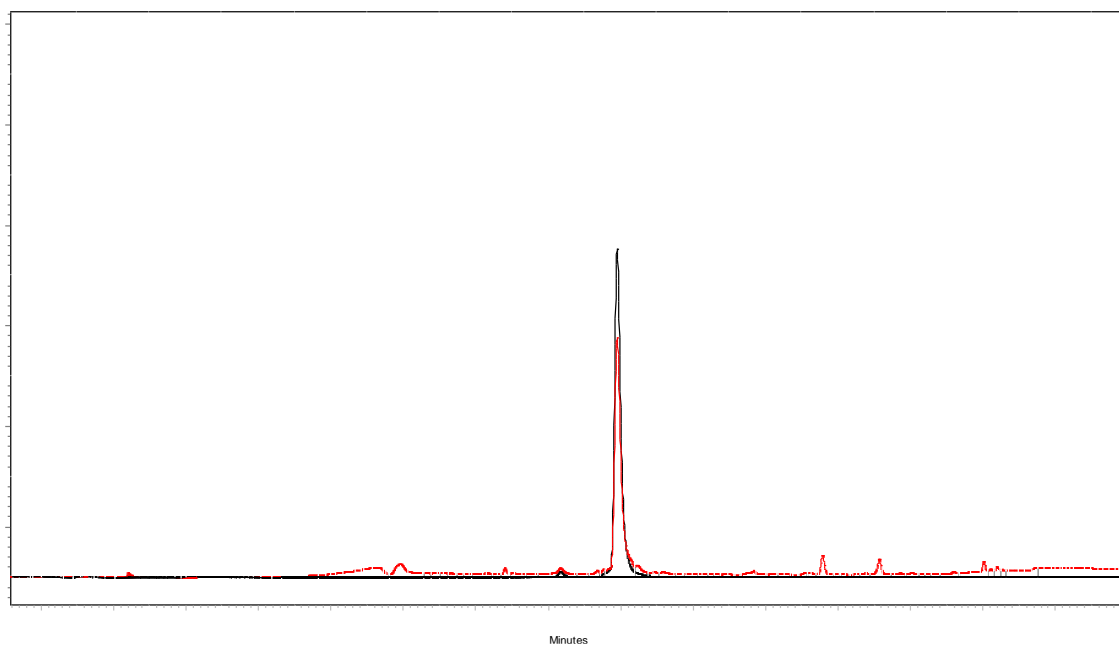


**Figure APP 8** HPLC trace of oligomer **8** eluting at 16.9 min

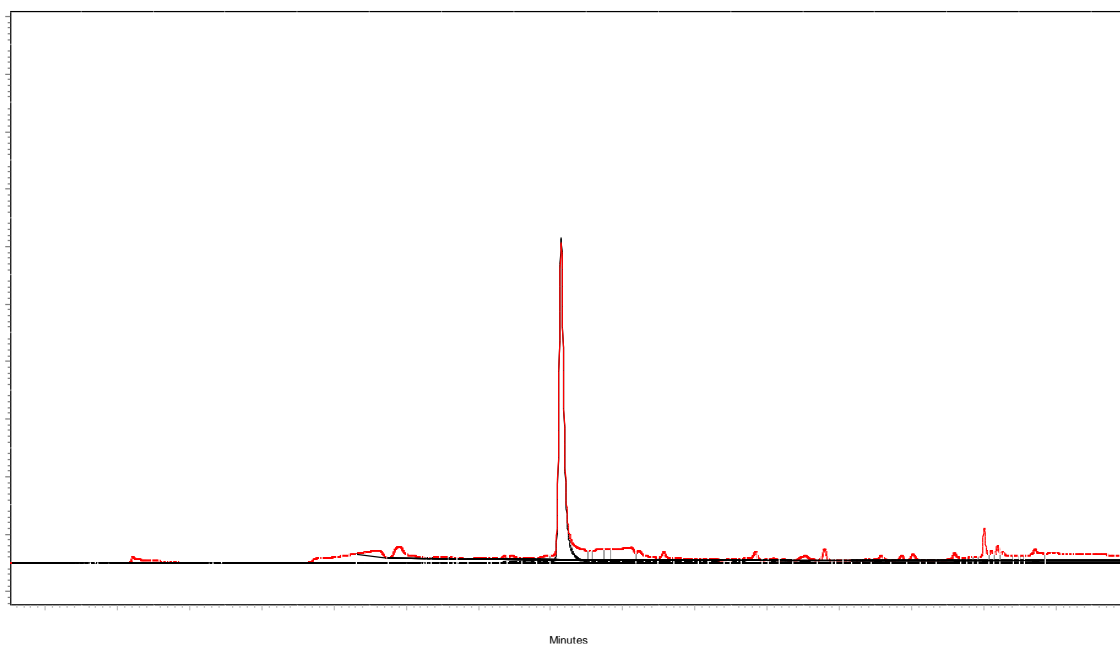


**Figure APP 9** HPLC trace of oligomer **9** eluting at 15.2 min

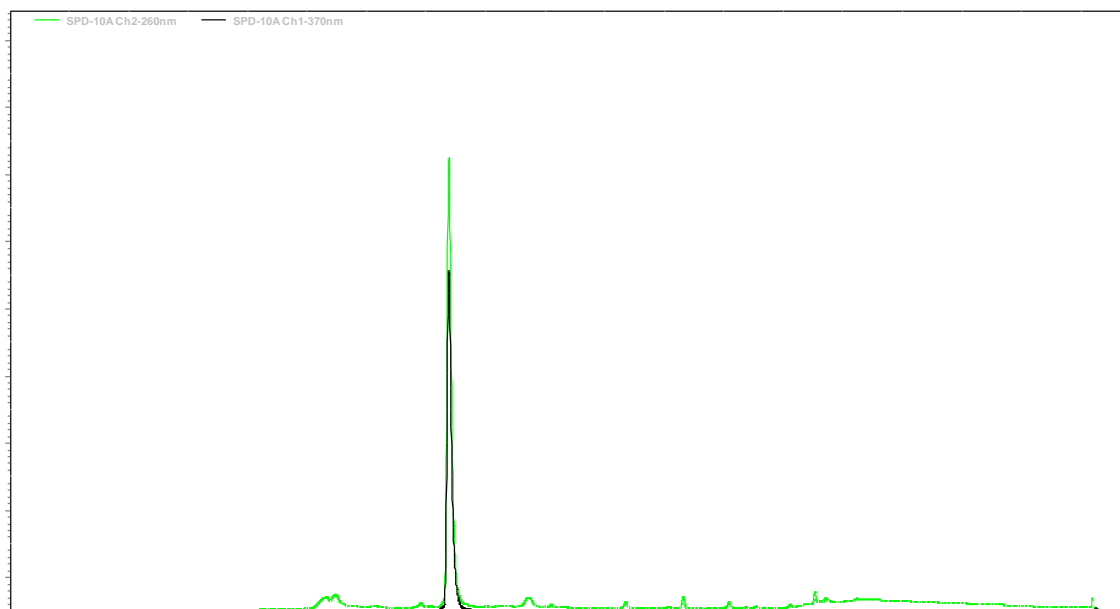


**Figure APP 10** HPLC trace of oligomer **10** eluting at 14.75 min

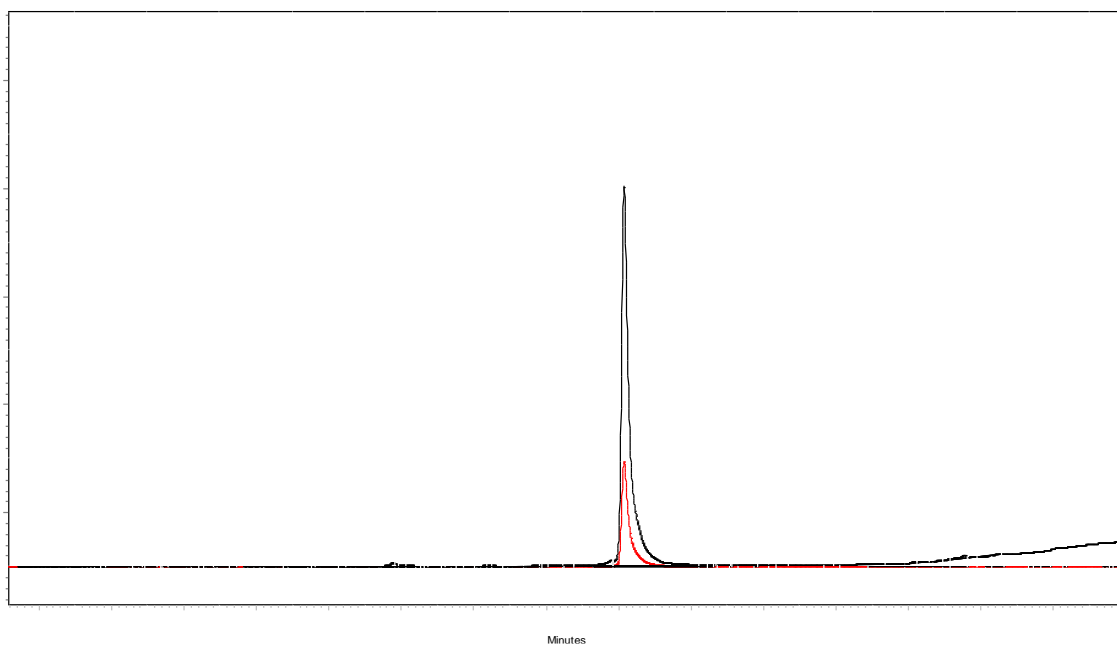


**Figure APP 11** HPLC trace of oligomer **14** eluting at 17.13 min

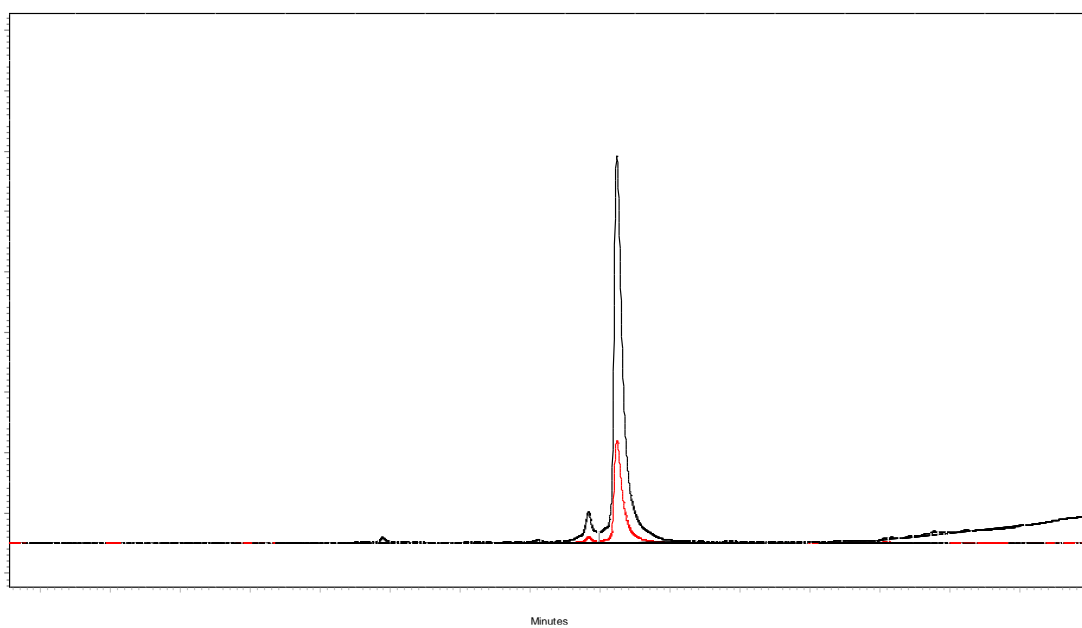


**Figure APP 12** HPLC trace of oligomer **15** eluting at 17.5 min

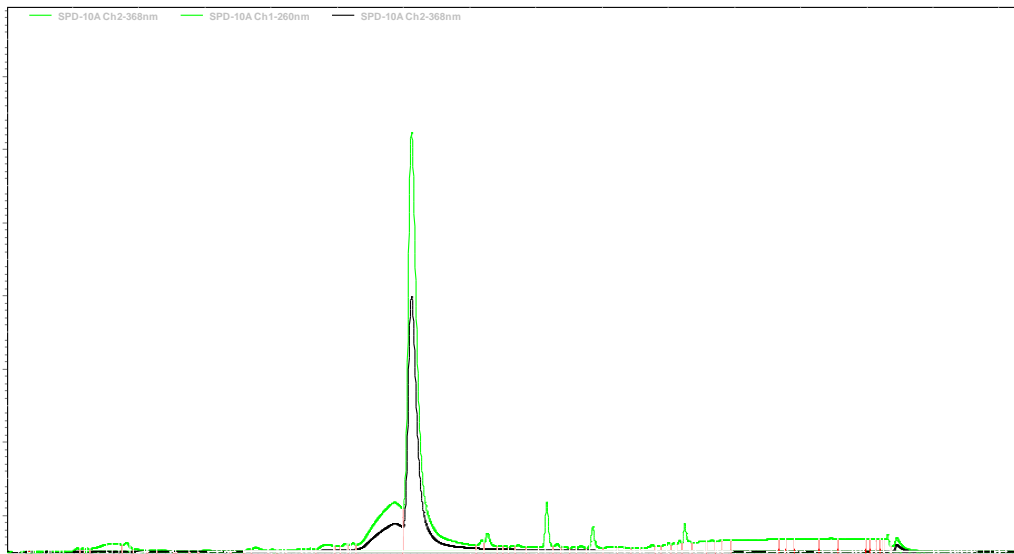


**Figure APP 13** HPLC trace of oligomer 16.

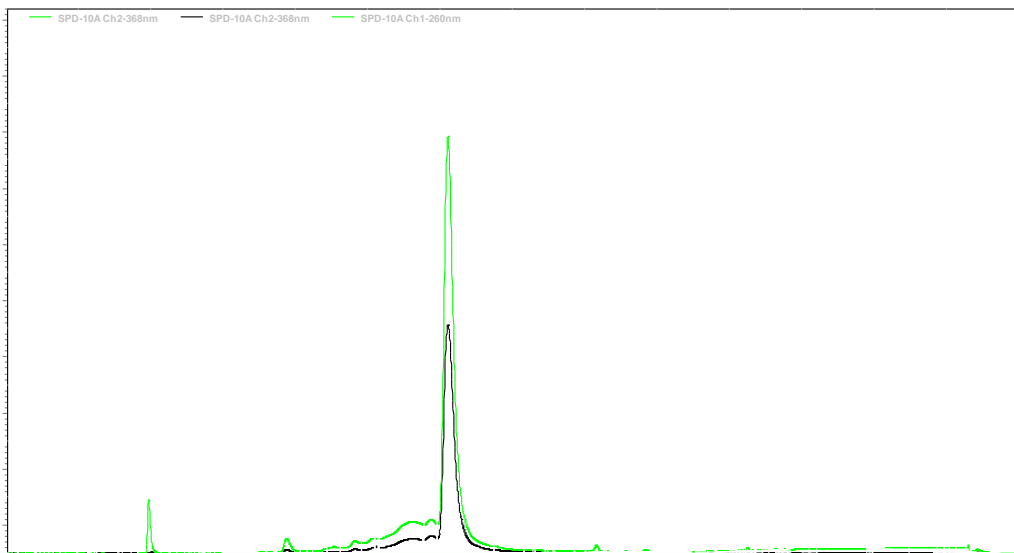


**Figure APP 14** HPLC trace of oligomer 17.

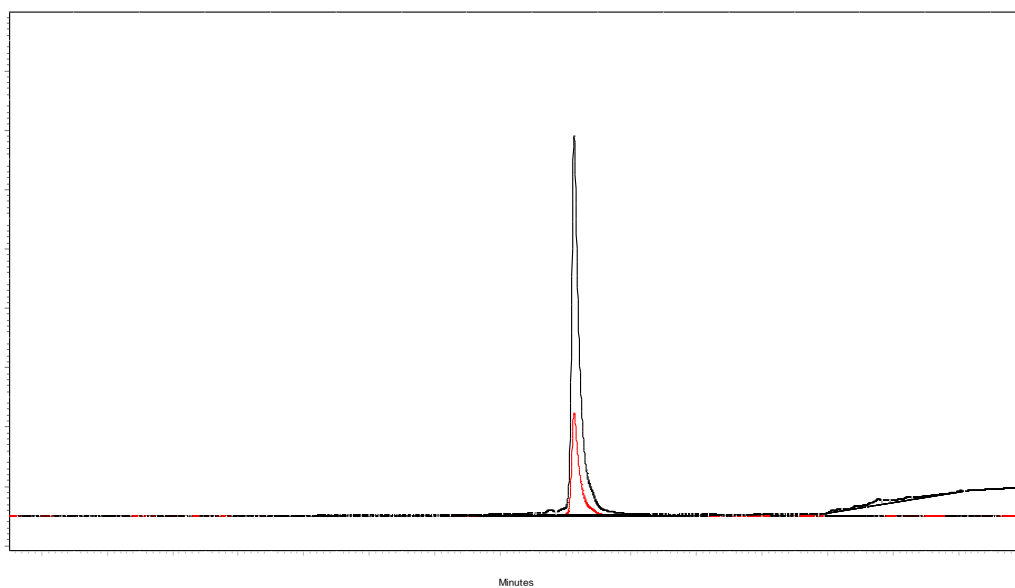


**Figure APP 15** HPLC trace of oligomer **24** eluting at 17.27 min

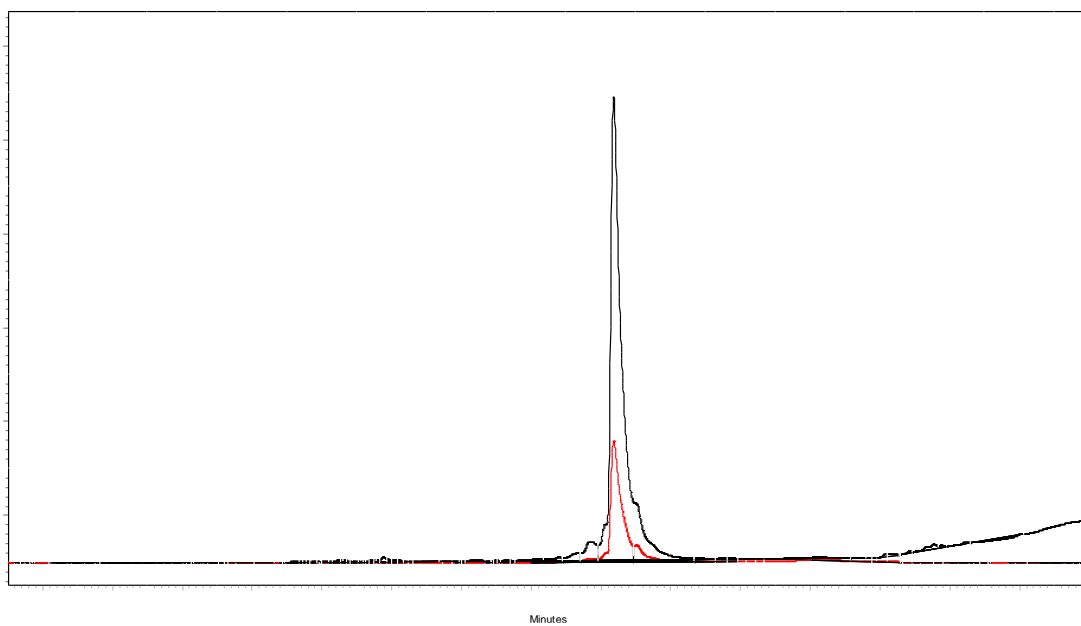


**Figure APP 16** HPLC trace of oligomer **25** eluting at 17.34 min



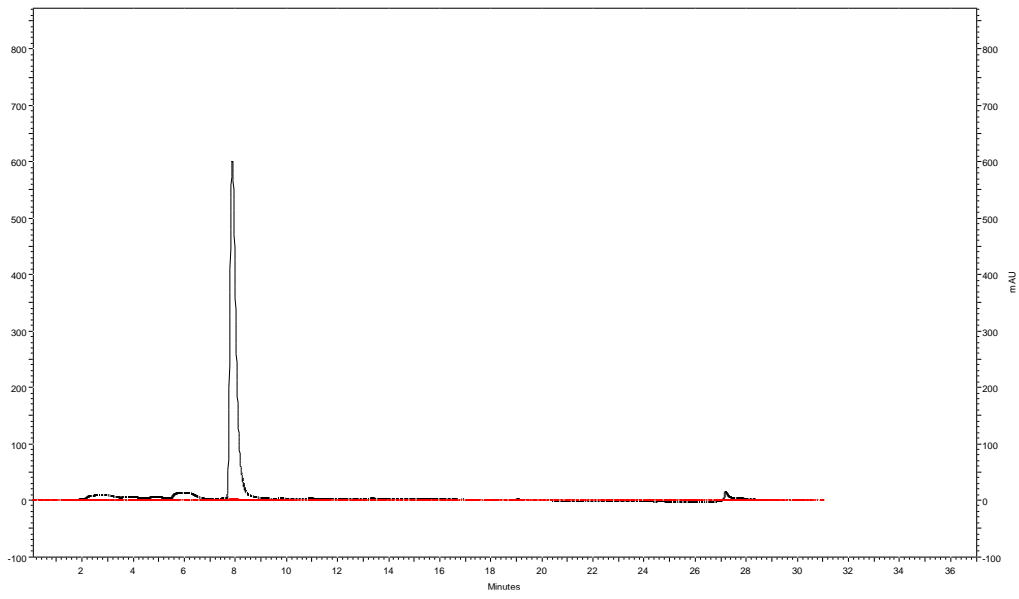


Figure APP 17 HPLC trace of oligomer **a** eluting at 7.9 min

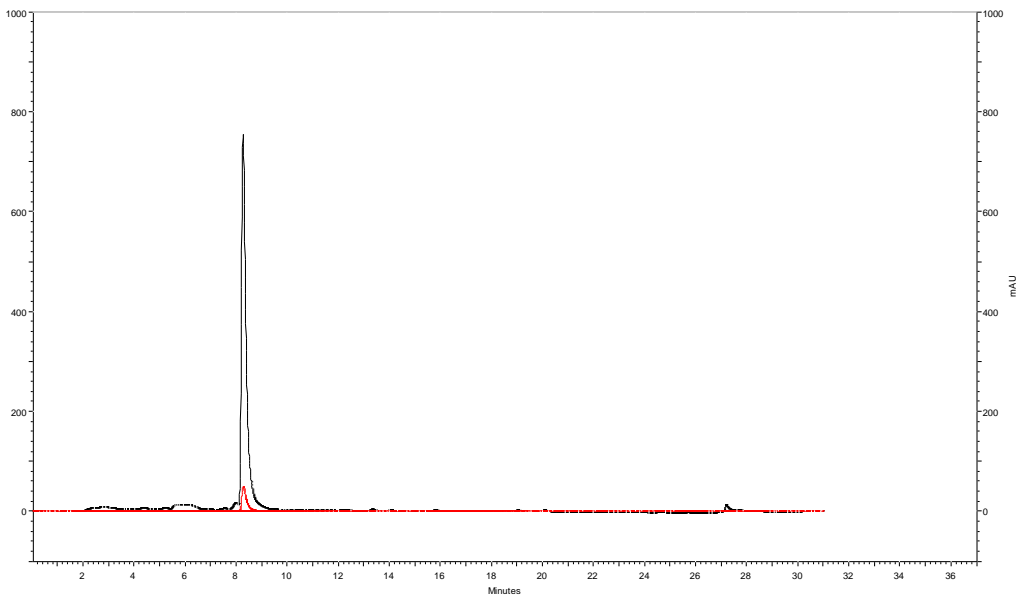
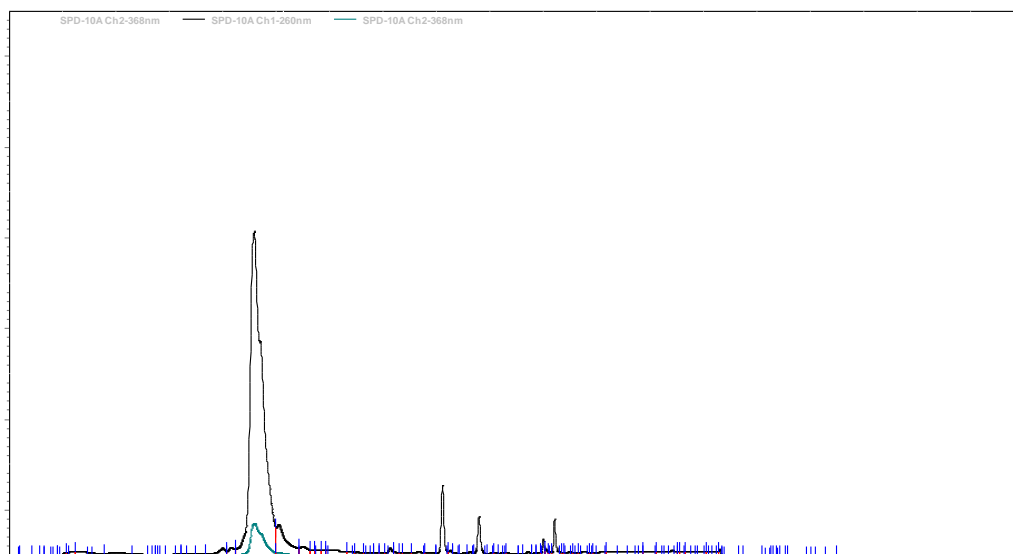
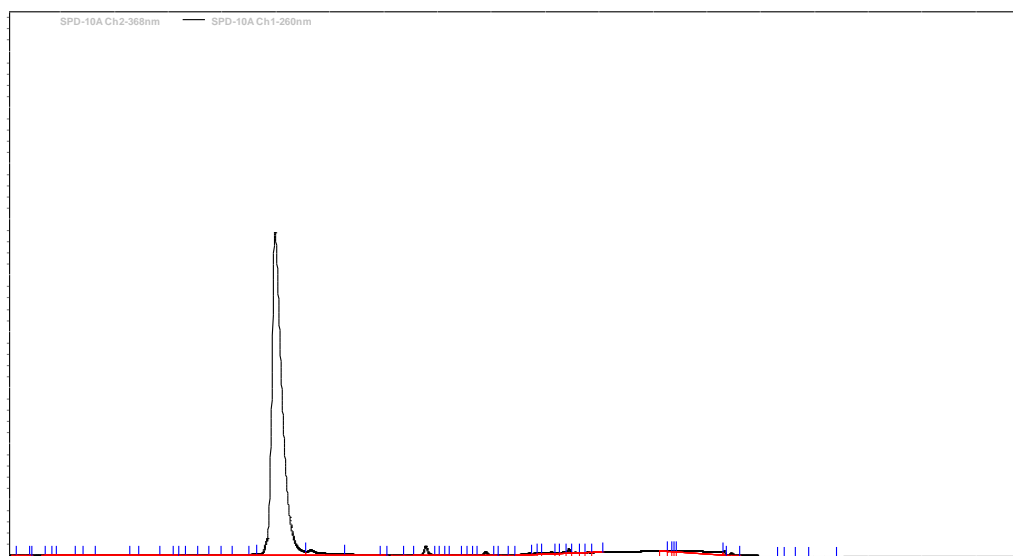


Figure APP 18 HPLC trace of oligomer **b** eluting at 8.3 min



**Figure APP 19** HPLC trace of oligomer **V** eluting at 9.5 min



**Figure APP 20** HPLC trace of oligomer **VI** eluting at 9.92 min

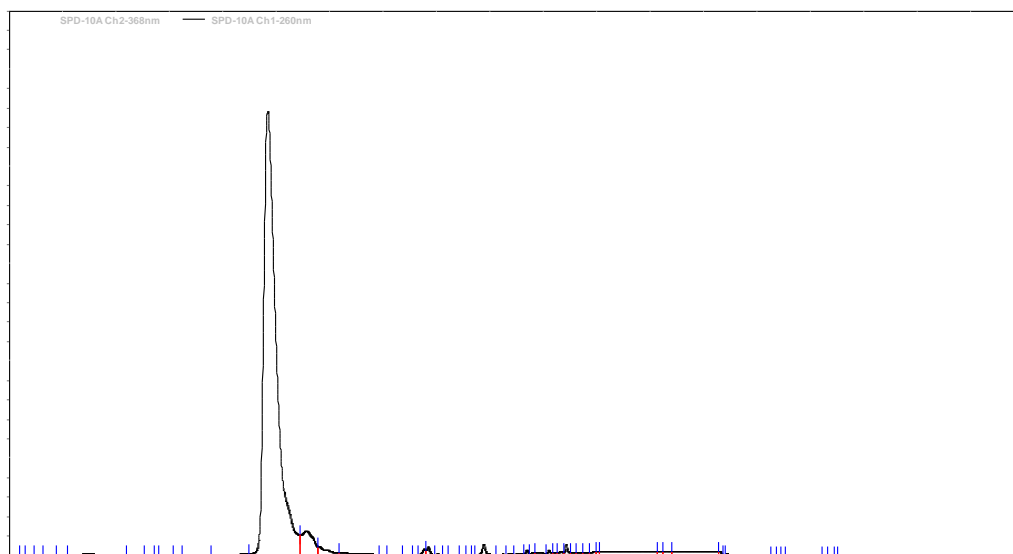


**Figure APP 21** HPLC trace of oligomer **VII** eluting at 9.8 min

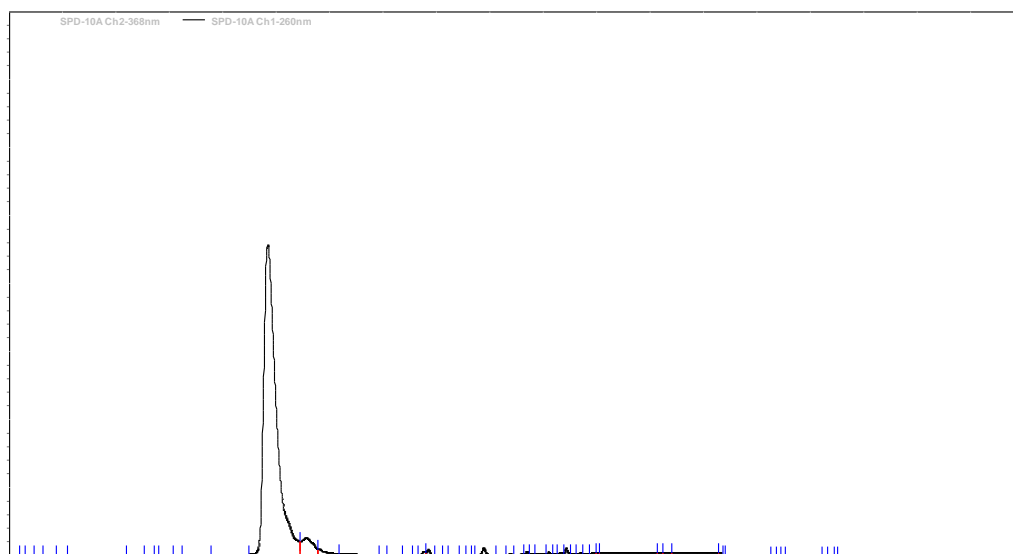


**Figure APP 22** HPLC trace of oligomer **VIII** eluting at 9.9 min.

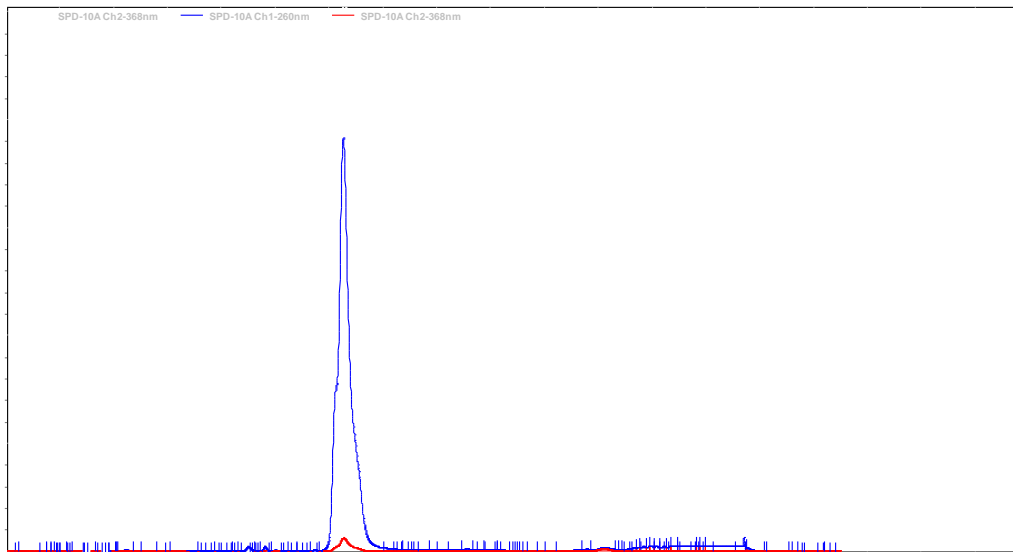


**Figure APP 23** HPLC trace of oligomer **A(E5)** eluting at 12.5 min (Gradient in 2 min - 15 min from 5 % AcN to 50 % AcN).

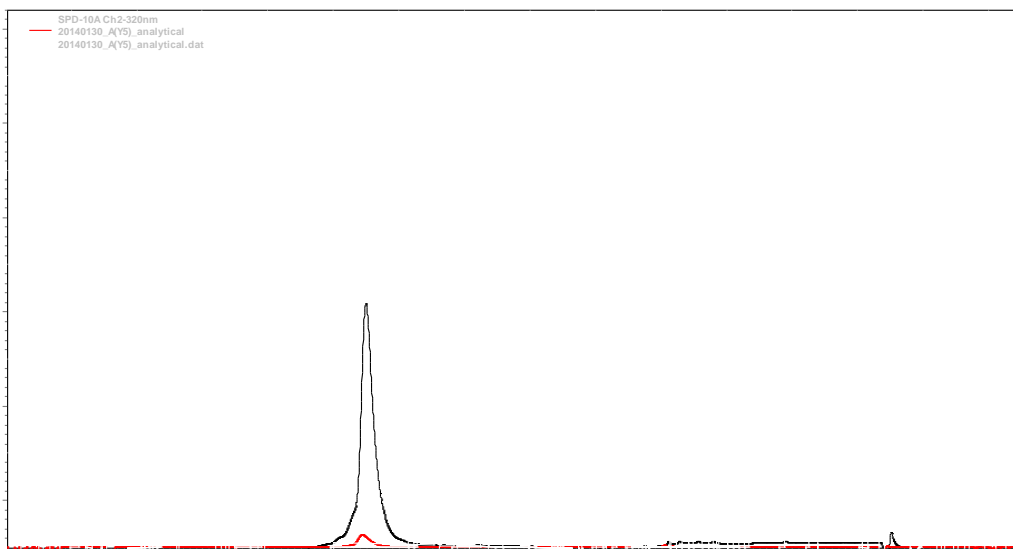


**Figure APP 24** HPLC trace of oligomer **A(Y5)** eluting at 10.8 min (gradient in 2 min - 15 min from 20 % AcN to 70 % AcN)

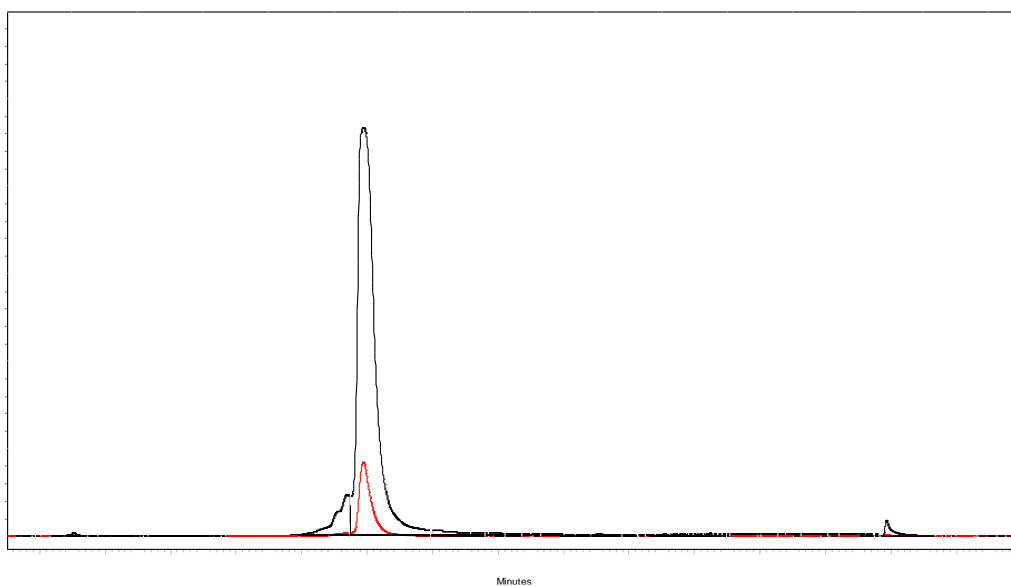


**Figure APP 25** HPLC trace of oligomer **P( $\alpha$ 5)** eluting at 10.8 min (gradient in 2 min -15 min from 20 % AcN to 70 % AcN)

**Crystal structure of 3,6-dialkynylphenanthrene and naphthalendiimide (mentioned in Chapter 4 as quencher molecule but not further discussed in the thesis)**

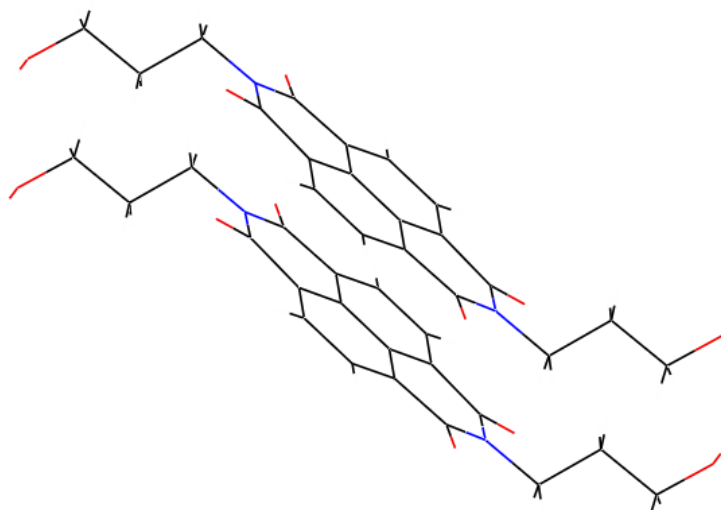


**Figure APP 23** Unit cell of a crystal of naphthalenediimide-diol. Two naphthalene are packed in a slipped face-to-face stacking.

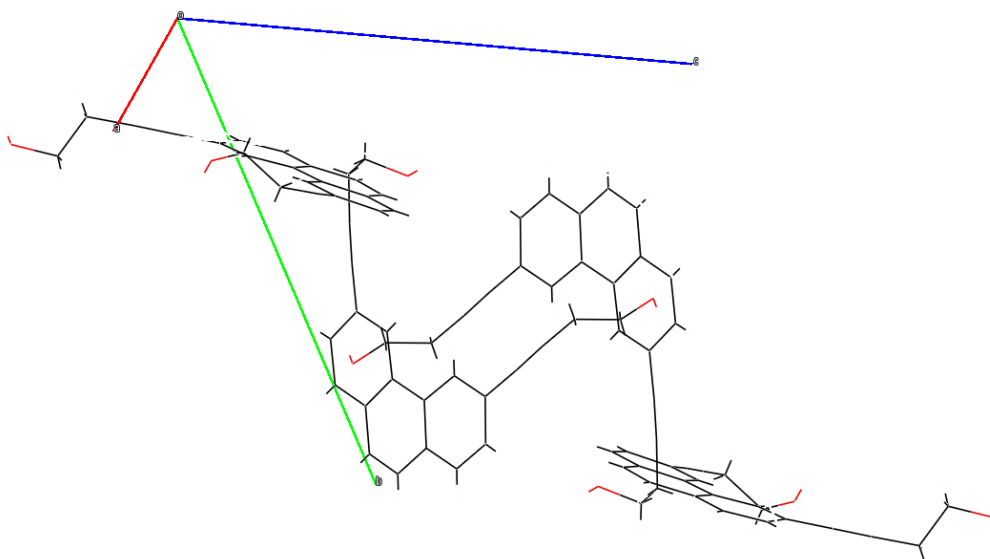


**Figure APP 24** Unit cell of a crystal of 3,6-dialkynylphenanthrene. Phenanthrenes are stacked in a Herring-bone type like arrangement.

## 9.0. Curriculum Vitae

### Personal Data

---

Name	Christian Bernhard Winiger
Date of birth	08.07.1985
Place of birth	Wil (SG)
Address	Talweg 19 CH-3063 Ittigen Switzerland
e-Mail	christian.winiger@dcb.unibe.ch
Mobile	0041 79 742 88 13
Marital status	single



### Research/Education

---

Research	PhD candidate at the department of chemistry and biochemistry at the University of Bern under supervision of Professor Häner (Thesis title: From DNA-guided Chromophore Arrays to Light-Harvesting Polymers)
2010	Research internship at Roche Kulmbach GmbH (now Axolab)
2008-2010	Master studies in „Biological Chemistry“ at the Swiss Federal Institute of Technology in Zurich (ETH) under supervision of Professor Hilvert <ul style="list-style-type: none"><li>- Semester work in the laboratory of Prof. D. Hilvert, ETH, Zurich (Title: scFv 1E9 – A Catalytic Antibody for a Diels-Alder Reaction)</li><li>- Semester work in the laboratory of Prof. J.J. Toulmé, Bordeaux, France (Title: Functional SELEX – Aptabeacons for molecular detection)</li><li>- Master thesis in the laboratory of Prof. R. Schibli, ETH, Zurich (Title: Synthesis and Evaluation of Novel <sup>67</sup>Ga- and <sup>177</sup>Lu-DOTA-Folate Radiopharmaceuticals for Potential Application in Folate Receptor Targeted Radionuclide Cancer Therapy)</li></ul>
2005-2008	Bachelor studies in Biology and Chemistry at the Swiss Federal Institute of Technology in Zurich (ETH)
2000-2004	School of higher Education, Biology and Chemistry

## 10.0. List of Publications

- Published**
- DOTA Conjugate with an Albumin-Binding Entity Enables the First Folic Acid-Targeted Lu-177-Radionuclide Tumor Therapy in Mice  
Dr. C. Mueller\*; Dr. H. Struthers; C. Winiger; Dr. K. Zhernosekov; Prof. Dr. R. Schibli  
JOURNAL OF NUCLEAR MEDICINE, **2013**, 54, Pages: 124-131  
DOI: 10.2967/jnumed.112.107235
- Influence of perylenediimide-pyrene supramolecular interactions on the stability of DNA-based hybrids: Importance of electrostatic complementarity  
C.B. Winiger; Dr. S.M. Langenegger; Dr. O. Khorev; Prof. Dr. R. Häner\*  
BEILSTEIN JOURNAL OF ORGANIC CHEMISTRY, **2014**, 10, Pages 1589-1595  
DOI: 10.3762/bjoc.10.164
- Long Distance EET in Light-Harvesting Supramolecular Polymers  
C.B. Winiger; Dr. S. Li; Dr. G.R. Kumar; Dr. S.M. Langenegger; Prof. Dr. R. Häner\*  
Angewandte Chemie Int. Ed, **2014**, 53, DOI:10.1002/anie.201407968
- Submitted**
- Co-existing excitonic states in alternating, DNA-assembled chromophore stacks  
C.B. Winiger; Dr. S.M. Langenegger; Prof. Dr. G. Calzaferri\*; Prof. Dr. R. Häner\*
- Oral presentations**
- “Aromatic donor-acceptor interactions in DNA-guided  $\pi$ -stacks” Snow Symposium 2014 of the Swiss Chemical Society
- “Investigation of Selectivity of Aromatic Stacking Interactions in Polar Media” Villars Summer School 2012 (awarded)
- “Investigation of Selectivity of Aromatic Stacking Interactions in DNA-guided hybrids”, DCB Graduate Symposium 2011